Validating the Fatigue Endurance Limit for Hot Mix Asphalt

DETAILS

128 pages | | PAPERBACK
ISBN 978-0-309-11821-7 | DOI 10.17226/14360

AUTHORS

R Michael Anderson; Samuel H Carpenter; Jo Sias Daniel; Brian D Prowell; Shihui Shen; Sudip Bhattacharjee; Aravind Krishna Swamy; E Ray Brown; Harold Von Quintus; Saeed Maghsoodloo; Transportation Research Board

NATIONAL COOPERATIVE HIGHWAY RESEARCH PROGRAM

NCHRP REPORT 646

Validating the Fatigue Endurance Limit for Hot Mix Asphalt

Brian D. Prowell
Advanced Materials Services, LLC[1]
Auburn, AL

E. Ray Brown
U.S. Army Corps of Engineers[1]
Vicksburg, MS

R. Michael Anderson
Asphalt Institute
Lexington, KY

Jo Sias Daniel
Aravind Krishna Swamy
University of New Hampshire
Durham, NH

Harold Von Quintus
Applied Research Associates, Inc.
Austin, TX

Shihui Shen[2]
Washington State University
Pullman, WA

Samuel H. Carpenter
University of Illinois
Urbana-Champaign, IL

Sudip Bhattacharjee[3]
Alabama A&M University
Huntsville, AL

Saeed Maghsoodloo
National Center for Asphalt Technology
Auburn, AL

Formerly [1]National Center for Asphalt Technology, [2]University of Illinois, and [3]University of New Hampshire, respectively.

Subscriber Categories
Materials • Pavements

Research sponsored by the American Association of State Highway and Transportation Officials
in cooperation with the Federal Highway Administration

TRANSPORTATION RESEARCH BOARD

WASHINGTON, D.C.
2010
www.TRB.org

NATIONAL COOPERATIVE HIGHWAY RESEARCH PROGRAM

Systematic, well-designed research provides the most effective approach to the solution of many problems facing highway administrators and engineers. Often, highway problems are of local interest and can best be studied by highway departments individually or in cooperation with their state universities and others. However, the accelerating growth of highway transportation develops increasingly complex problems of wide interest to highway authorities. These problems are best studied through a coordinated program of cooperative research.

In recognition of these needs, the highway administrators of the American Association of State Highway and Transportation Officials initiated in 1962 an objective national highway research program employing modern scientific techniques. This program is supported on a continuing basis by funds from participating member states of the Association and it receives the full cooperation and support of the Federal Highway Administration, United States Department of Transportation.

The Transportation Research Board of the National Academies was requested by the Association to administer the research program because of the Board's recognized objectivity and understanding of modern research practices. The Board is uniquely suited for this purpose as it maintains an extensive committee structure from which authorities on any highway transportation subject may be drawn; it possesses avenues of communications and cooperation with federal, state and local governmental agencies, universities, and industry; its relationship to the National Research Council is an insurance of objectivity; it maintains a full-time research correlation staff of specialists in highway transportation matters to bring the findings of research directly to those who are in a position to use them.

The program is developed on the basis of research needs identified by chief administrators of the highway and transportation departments and by committees of AASHTO. Each year, specific areas of research needs to be included in the program are proposed to the National Research Council and the Board by the American Association of State Highway and Transportation Officials. Research projects to fulfill these needs are defined by the Board, and qualified research agencies are selected from those that have submitted proposals. Administration and surveillance of research contracts are the responsibilities of the National Research Council and the Transportation Research Board.

The needs for highway research are many, and the National Cooperative Highway Research Program can make significant contributions to the solution of highway transportation problems of mutual concern to many responsible groups. The program, however, is intended to complement rather than to substitute for or duplicate other highway research programs.

NCHRP REPORT 646

Project 09-38
ISSN 0077-5614
ISBN 978-0-309-11821-7
Library of Congress Control Number 2010921174

COPYRIGHT INFORMATION

NOTICE

The project that is the subject of this report was a part of the National Cooperative Highway Research Program conducted by the Transportation Research Board with the approval of the Governing Board of the National Research Council. Such approval reflects the Governing Board's judgment that the program concerned is of national importance and appropriate with respect to both the purposes and resources of the National Research Council.

The members of the technical committee selected to monitor this project and to review this report were chosen for recognized scholarly competence and with due consideration for the balance of disciplines appropriate to the project. The opinions and conclusions expressed or implied are those of the research agency that performed the research, and, while they have been accepted as appropriate by the technical committee, they are not necessarily those of the Transportation Research Board, the National Research Council, the American Association of State Highway and Transportation Officials, or the Federal Highway Administration, U.S. Department of Transportation.

Each report is reviewed and accepted for publication by the technical committee according to procedures established and monitored by the Transportation Research Board Executive Committee and the Governing Board of the National Research Council.

The Transportation Research Board of the National Academies, the National Research Council, the Federal Highway Administration, the American Association of State Highway and Transportation Officials, and the individual states participating in the National Cooperative Highway Research Program do not endorse products or manufacturers. Trade or manufacturers' names appear herein solely because they are considered essential to the object of this report.

Published reports of the

NATIONAL COOPERATIVE HIGHWAY RESEARCH PROGRAM

are available from:

Transportation Research Board
Business Office
500 Fifth Street, NW
Washington, DC 20001

and can be ordered through the Internet at:

http://www.national-academies.org/trb/bookstore

Printed in the United States of America

THE NATIONAL ACADEMIES

Advisers to the Nation on Science, Engineering, and Medicine

The **National Academy of Sciences** is a private, nonprofit, self-perpetuating society of distinguished scholars engaged in scientific and engineering research, dedicated to the furtherance of science and technology and to their use for the general welfare. On the authority of the charter granted to it by the Congress in 1863, the Academy has a mandate that requires it to advise the federal government on scientific and technical matters. Dr. Ralph J. Cicerone is president of the National Academy of Sciences.

The **National Academy of Engineering** was established in 1964, under the charter of the National Academy of Sciences, as a parallel organization of outstanding engineers. It is autonomous in its administration and in the selection of its members, sharing with the National Academy of Sciences the responsibility for advising the federal government. The National Academy of Engineering also sponsors engineering programs aimed at meeting national needs, encourages education and research, and recognizes the superior achievements of engineers. Dr. Charles M. Vest is president of the National Academy of Engineering.

The **Institute of Medicine** was established in 1970 by the National Academy of Sciences to secure the services of eminent members of appropriate professions in the examination of policy matters pertaining to the health of the public. The Institute acts under the responsibility given to the National Academy of Sciences by its congressional charter to be an adviser to the federal government and, on its own initiative, to identify issues of medical care, research, and education. Dr. Harvey V. Fineberg is president of the Institute of Medicine.

The **National Research Council** was organized by the National Academy of Sciences in 1916 to associate the broad community of science and technology with the Academy's purposes of furthering knowledge and advising the federal government. Functioning in accordance with general policies determined by the Academy, the Council has become the principal operating agency of both the National Academy of Sciences and the National Academy of Engineering in providing services to the government, the public, and the scientific and engineering communities. The Council is administered jointly by both the Academies and the Institute of Medicine. Dr. Ralph J. Cicerone and Dr. Charles M. Vest are chair and vice chair, respectively, of the National Research Council.

The **Transportation Research Board** is one of six major divisions of the National Research Council. The mission of the Transportation Research Board is to provide leadership in transportation innovation and progress through research and information exchange, conducted within a setting that is objective, interdisciplinary, and multimodal. The Board's varied activities annually engage about 7,000 engineers, scientists, and other transportation researchers and practitioners from the public and private sectors and academia, all of whom contribute their expertise in the public interest. The program is supported by state transportation departments, federal agencies including the component administrations of the U.S. Department of Transportation, and other organizations and individuals interested in the development of transportation. **www.TRB.org**

www.national-academies.org

COOPERATIVE RESEARCH PROGRAMS

CRP STAFF FOR NCHRP REPORT 646

Christopher W. Jenks, *Director, Cooperative Research Programs*
Crawford F. Jencks, *Deputy Director, Cooperative Research Programs*
Edward T. Harrigan, *Senior Program Officer*
Melanie Adcock, *Senior Program Assistant*
Eileen P. Delaney, *Director of Publications*
Hilary Freer, *Senior Editor*

NCHRP PROJECT 09-38 PANEL
Field of Materials and Construction—Area of Bituminous Materials

Linda M. Pierce, *Applied Pavement Technology, Inc., Santa Fe, NM* (Chair)
Steven W. Krebs, *Wisconsin DOT, Madison, WI*
Allen Cooley, *Burns Cooley Dennis, Inc., Ridgeland, MS*
G. William Maupin, Jr., *Virginia DOT, Charlottesville, VA*
Richard W. May, *SemMaterials, LP, Tulsa, OK*
Leslie Ann McCarthy, *Villanova University, Villanova, PA*
Carl L. Monismith, *University of California - Berkeley, Berkeley, CA*
Amy M. Schutzbach, *Illinois DOT, Springfield, IL*
Gregory A. Sholar, *Florida DOT, Gainesville, FL*
Linbing Wang, *Virginia Polytechnic Institute and State University, Blacksburg, VA*
Travis M. Wombwell, *Missouri DOT, Macon, MO*
Wei-Shih "Wes" Yang, *New York State DOT, Albany, NY*
Ernest Bastian, *FHWA Liaison*
John "Jack" Youtcheff, *FHWA Liaison*
Frederick Hejl, *TRB Liaison*

FOREWORD

By Edward T. Harrigan
Staff Officer
Transportation Research Board

This report presents the findings of research performed to investigate the existence of a fatigue endurance limit for hot mix asphalt (HMA) mixtures, the effect of HMA mixture characteristics on the endurance limit, and the potential for the limit's incorporation in structural design methods for flexible pavements. The report describes the research performed and includes proposed standard practices using various experimental and analytical procedures for determining the endurance limit of HMA mixtures. Thus, the report will be of immediate interest to materials and structural design engineers in state highway agencies and engineers in the HMA construction industry.

Many well-constructed flexible pavements with a thick HMA structure have been in service for 40 or more years without any evidence of bottom-up fatigue cracking. This field experience suggests that an endurance limit, that is, a level of strain below which fatigue damage does not occur for any number of load repetitions, is a valid concept for HMA mixtures.

The concept of an endurance limit is widely recognized in many areas of materials science, especially that of ferrous metals. The endurance limit is usually calculated from the relationship of strain to load repetitions to failure. Defining an endurance limit for HMA mixtures will result in more efficient structural design of flexible pavements built with mixtures of varying properties. For instance, small increases in the binder content of HMA mixtures provide longer fatigue lives (presumably because of a higher strain level for the endurance limit of these mixtures). Other factors likely to determine the value of the fatigue endurance limit for a given HMA mixture are the incorporation of a modifier in the asphalt binder, the aggregate type and gradation, the asphalt binder grade, and the mixture's volumetric properties.

Previous research suggested that the fatigue behavior of flexible pavements is consistent with the existence of an endurance limit with an approximate value of 70 microstrains. However, few laboratory studies corroborate this value. Moreover, pavement design approaches, including the Mechanistic-Empirical Pavement Design Guide (MEPDG) developed in NCHRP Projects 1-37A and 1-40, do not fully incorporate the endurance limit concept. This is because, to date, research into the fatigue of HMA mixtures has been limited to strain levels well above the hypothesized value of 70 microstrains.

The objectives of this research were to (1) test the hypothesis that there is an endurance limit in the fatigue behavior of HMA mixtures, (2) measure the value of the endurance limit for a representative range of HMA mixtures, and (3) recommend a procedure to incorporate the effects of the endurance limit into mechanistic pavement design methods. The research was performed by the National Center for Asphalt Technology, Auburn University, Auburn, AL, with the assistance of the following organizations: Applied Research Associates,

Inc., Round Rock, TX; the Asphalt Institute, Lexington, KY; the University of Illinois, Urbana-Champaign, IL; and the University of New Hampshire, Durham, NH.

The report fully documents the design and conduct of an extensive laboratory program of beam fatigue and uniaxial tension testing that experimentally confirmed the existence of an HMA fatigue endurance limit and quantified how the value of the limit is influenced by HMA mixture and binder properties. Based on these results, a practical definition of the endurance limit was developed, along with a methodology to estimate the endurance limit in the laboratory. Analysis of in-service pavements by the research team also demonstrated the existence of the endurance limit and indicated that polymer modification of asphalt binders improves the fatigue performance of HMA mixtures and flexible pavements. Finally, sensitivity analyses were conducted that indicated that the value of the endurance limit can affect the recommended thickness of perpetual pavements designed with the MEPDG and PerRoad methodologies significantly.

This report includes six appendices as follows:

- Appendix A: A Proposed Standard Practice for Predicting the Endurance Limit of Hot Mix Asphalt (HMA) for Long-Life Pavement Design;
- Appendix B: A Proposed Standard Practice for Predicting the Endurance Limit of Hot Mix Asphalt (HMA) by Pseudo Strain Approach;
- Appendix C: A Proposed Standard Practice for Extrapolating Long-Life Beam Fatigue Tests Using the Ratio of Dissipated Energy Change (RDEC);
- Appendix D: A summary of results of the beam fatigue testing accomplished during the project;
- Appendix E: An analytical method for construction of a damage characteristic curve through calculation of pseudo strains; and
- Appendix F: A proposed design for an interlaboratory study to develop a precision statement for AASHTO T321, Standard Method of Test for Determining the Fatigue Life of Compacted Hot-Mix Asphalt (HMA) Subjected to Repeated Flexural Bending.

The proposed standard practices are under consideration for possible adoption by the AASHTO Highway Subcommittee on Materials and the AASHTO Joint Technical Committee on Pavements.

CONTENTS

AUTHOR ACKNOWLEDGMENTS

The research described herein was performed under NCHRP Project 9-38 by the National Center for Asphalt Technology (NCAT) at Auburn University. Ray Brown served as the Principal Investigator and Brian Prowell and Michael Anderson served as Co-Principal Investigators. Brown and Prowell were employed by NCAT when this research began.

The research team included the Asphalt Institute; the University of New Hampshire; Applied Research Associates, Inc.; the University of Illinois, and, later, Advanced Materials Services, LLC. The Asphalt Institute assisted in beam fatigue testing in Phases I and II of the project. Jo Daniel oversaw uniaxial tension testing and analyses at the University of New Hampshire. Harold Von Quintus with Applied Research Associates, Inc., performed survival analyses of in-service pavements and provided guidance on the MEPDG. Samuel Carpenter oversaw beam fatigue testing in Phase II of the study with Shihui Shen at the University of Illinois and provided expertise on analyses using the ratio of dissipated energy. Brian Prowell was primarily responsible for the technical content of the remaining sections and for assembling the final report. Pamela Turner supervised laboratory testing at NCAT.

The project team appreciates the support and technical assistance of Bor-Wen Tsai of the University of California, Berkeley; Rich May of SEM Materials; and Bill Maupin, Jr., of the Virginia Transportation Research Council. These three agencies volunteered to participate in the beam fatigue mini round-robin to help develop a better understanding of the variability of beam fatigue tests. They also assisted in the evaluation of the draft protocols for determining the endurance limit.

Other individuals provided invaluable assistance to the project. Bor-Wen Tsai provided significant technical assistance with the single- and three-stage Weibull method. Chris Wagner (FHWA) assisted with the MEPDG. Buzz Powell provided technical data from the NCAT Test Track. David Timm and Richard Willis provided advice and guidance for calculating shift factors based on field strain measurements and incorporating the endurance limit into M-E pavement design.

SUMMARY

Validating the Fatigue Endurance Limit for Hot Mix Asphalt

Hot-mix asphalt (HMA) pavements have been designed primarily to resist rutting of the subgrade and bottom-up fatigue cracking. In classical pavement design, as design load applications increase, pavement thickness also must increase. There is a growing belief that bottom-up fatigue cracking does not occur for thick pavements. The concept of the HMA fatigue endurance limit—a level of strain below which there is no cumulative damage over an indefinite number of load cycles—is proposed to explain this occurrence. Therefore, additional pavement thickness, greater than that required to keep strain levels at the bottom of the HMA layer below the endurance limit, would not provide additional life. This concept has significant design and economic implications.

Research in the 1970s observed that the log-log relationship between strain and bending cycles for a number of HMA mixes converged below 70 micro-strain (ms) at a high number of loading cycles. Field studies in the United Kingdom recommended an HMA thickness range between 7.9 in. and 15.4 in. for a long-life pavement depending on such factors as binder stiffness. The stiffness of thick pavements was observed to increase with time, most likely due to binder aging. Other studies have documented the absence of bottom-up fatigue cracking in thick pavements and the common occurrence of top-down cracking.

In theory, samples tested at a strain level below the endurance limit should last for an indefinite or infinite number of loading cycles. It is impossible to test samples to an infinite number of cycles. Therefore, a practical definition of the endurance limit, or a laboratory life representative of the endurance limit was needed. A capacity analysis indicated that at minimum safe spacing, a lane carrying 100% trucks 24 hours a day, 7 days a week for 40 years could carry a maximum of 329,376,000 trucks that would produce 1,317,504,000 axle repetitions (neglecting the steer axle). However, a more likely traffic stream would produce a maximum of approximately 500 million axle load repetitions.

Studies have indicated that a shift factor, ranging from 4 to 100, must be applied to relate laboratory and field fatigue performance. There are many reasons that probably lead to the need for a shift factor with two primary factors being rest periods and healing. A shift factor of 10 was recommended in the Strategic Highway Research Program (SHRP) by Leahy et al. (*46*). Considering this shift factor, laboratory testing to 50 million cycles would equate to approximately 500 million loading cycles in the field or approximately the maximum probable loading in a 40-year period. This was considered a practical target for evaluating parameters indicating an endurance limit.

An experimental plan was developed using a single aggregate gradation, two levels of binder content (optimum and optimum plus 0.7%), and two binder grades (PG 67-22 and PG 76-22). The aggregates, gradations, optimum binder content, and binder grades/sources matched those used in the base layers of the 2003 National Center for Asphalt Technology (NCAT) Test Track structural sections. Using the same mixtures as the NCAT Test Track

allowed calibration of the fatigue shift factor. Samples at optimum asphalt content were compacted to $7 \pm 0.5\%$ air voids while samples at optimum plus asphalt content were compacted to $3.3 \pm 0.5\%$ air voids. Beam fatigue and uniaxial tension testing were performed on the four mixtures. In Phase II, beam fatigue tests were performed on two additional mixes at optimum asphalt content using a PG 58-28 and PG 64-22.

Beam fatigue testing was conducted according to AASHTO T321. At least two replicates were tested at 800, 400, 200, or 100 ms until the fatigue lives of two replicates at a given strain level exceeded 50 million cycles. The time to test a single sample to 50 million load cycles is approximately 50 days. At this point, a log-log regression was performed between strain and fatigue life using all of the data for which samples failed in less than 50 million cycles. The strain level that corresponded to a fatigue life of 50 million cycles was predicted. Two additional beams were tested at this strain level.

A number of extrapolation techniques were considered to predict the number of cycles to failure (N_f) for beams that are not tested to failure, including the exponential model described in AASHTO T321, a logarithmic regression, ratio of dissipated energy change, and single- and three-stage Weibull models. The extrapolations were evaluated using samples that had long fatigue lives—in excess of 12 million cycles—but failed before 50 million cycles. The logarithmic regression and ratio of dissipated energy change consistently overestimated N_f, often by several orders of magnitude. The exponential model consistently underestimated N_f if the entire loading history to failure was not used in the calculation. This suggested the exponential model was not a good technique for extrapolation from a number of loading cycles less than N_f. Extrapolations using the single-stage Weibull model were generally distributed around the line of equality and provided the best prediction. In one case, the three-stage Weibull model provided a more accurate prediction of N_f and it always provided a better fit to the stiffness versus loading cycle data.

For each mixture, log-log regression plots were created using the data for samples that failed in less than 50 million cycles. Prediction limits were determined for lower strain levels. The extrapolated N_f for samples that did not fail within 50 million cycles indicated fatigue lives that were longer than those indicated by the prediction limits from the regression of samples tested at "normal" strain levels. This deviation indicates the existence of an endurance limit for HMA.

A standard practice was developed to predict the endurance limit based on tests conducted at normal strain levels (above the endurance limit) based on statistical prediction limits. The estimate of the endurance limit is the one-sided, 95% confidence lower prediction limit for the strain level that produces a fatigue life of 50 million cycles. Confirmation tests at the predicted strain level are recommended. The predicted endurance limits determined using this methodology ranged from 75 to 200 ms. Stiffer binders tended to produce higher endurance limits. Optimum plus binder content combined with lower sample air voids produced a slight increase in the endurance limit.

A mini round-robin was conducted to assess the variability of beam fatigue tests at normal strain levels and extrapolations at low strain levels. N_f varies significantly depending on the strain level at which the samples are tested. The log base 10 transformation of N_f was used in the round robin analyses to produce a relatively constant variability across the range of strain levels evaluated. On a log basis for normal strain fatigue tests, the repeatability (within-lab) standard deviation was determined to be 0.248 and the reproducibility (between-lab) standard deviation was determined to be 0.318. This results in within- and between-lab coefficients of variation of 5.4% and 6.8%, respectively. The single-stage Weibull extrapolations had the lowest variability within and between labs.

Uniaxial tension tests were performed on cylindrical samples cored and sawed from specimens compacted in the Superpave gyratory compactor. Testing included complex modulus, monotonic, and fatigue tests in uniaxial tension. Analysis of these data was done using viscoelastic and continuum damage mechanics principles to identify the fatigue endurance limit

of the PG 67-22 optimum, PG 67-22 optimum plus, PG 76-22 optimum, and PG 76-22 optimum plus mixtures. Frequency sweeps at various temperatures were run to measure the complex dynamic modulus of each mix. The dynamic modulus and phase angle master curves were constructed from these data and the relaxation master curve obtained through linear viscoelastic conversion. The damage characteristic curve of each mix was obtained by running uniaxial monotonic tests to failure or by running constant amplitude fatigue tests to failure. The characteristic damage curve was used to predict the number of cycles to failure at different strain amplitudes to determine the fatigue endurance limit of the mixture. The estimated endurance limits from this method varied depending on whether the generalized power law or exponential model was used to fit the data in the characteristic curve. The estimated endurance limits for the generalized power law ranged from 164 to 261 ms, while those for the exponential model ranged from 47 to 96 ms. The relative rankings of the binders evaluated in Phase I appeared to be reversed from the beam fatigue tests.

A second methodology was employed where fatigue tests with increasing strain amplitude were run in uniaxial tension to directly identify the fatigue endurance limit of the mixtures. The stress versus strain loading history forms a hysteresis loop, the area of which is the dissipated energy per cycle. The use of pseudo strain instead of engineering strain in constitutive analysis removes the hysteretic effect of viscoelasticity. If the induced strain levels are low enough not to induce damage (e.g., below the endurance limit) then the hysteresis loop collapses since the dissipated energy is only due to the viscoelastic response of the material. The estimated endurance limit using this methodology ranged from 115 to 250 ms. However, differences were observed between the strain applied through the cross head and the induced strain measured on the samples. These differences made it difficult to precisely increment the induced strain in order to accurately determine the endurance limit.

Analyses were performed of LTPP data for indications of the endurance limit. A 1995 survivability analysis of data from the general pavement studies (GPS) experiments known as GPS-1 and GPS-2 indicated an endurance limit of approximately 65 ms. However, when the analysis was updated, and LTPP special pavement studies (SPS) data were added from SPS-1, no endurance limit was indicated. During the period between the original and updated analyses, LTPP changed the definition of longitudinal cracking in the wheel path. This may have resulted in cracks previously identified as top-down cracking to be reclassified as bottom-up fatigue cracks. Forensic investigations on the thicker pavements in the study, exhibiting cracking, are required to identify the type of cracking. Still, separation was indicated between the survivability of pavements with tensile strains at the bottom of the HMA layer less than 150 ms and those equal to or greater than 150 ms. This may indicate that neglecting top-down cracking, the endurance limit may be less than 150 ms. Additional cracking data were presented, which demonstrates the improved fatigue performance of mixes containing polymer modified binders, similar to that indicated in the beam fatigue testing program.

Analyses were conducted on data from the structural sections of the 2003 NCAT Test Track to estimate the shift factor between laboratory and field performance. Three of the eight structural sections exhibited fatigue cracking in excess of 40% of the wheel-path area or approximately 20% of the total lane area during the test track loading cycle (application of 10 million equivalent single-axle loads [ESALs]). Forensic investigations indicated that the cracking in one of these sections resulted from debonding of the HMA layers. A fourth section had limited cracking and cumulative damage was estimated at 0.7 at the end of the loading cycles.

All of the structural sections were instrumented to measure strain at the bottom of the HMA layer. The measured strain data, pavement temperatures, and axle repetitions were used with the fatigue transfer functions developed as part of the beam fatigue testing to calculate incremental damage on an hourly basis. Shift factors between 4.2 and 75.8 were calculated between laboratory and field performance. The shift factor of 4.2 was determined

for a polymer modified section with a total asphalt thickness of only 4.8 in. Similar calculations were performed with PerRoad and the Mechanistic-Empirical Pavement Design Guide (MEPDG). The shift factors determined using PerRoad ranged from 6.7 to 45.0. Damage in the MEPDG was calculated using the nationally calibrated fatigue model, not the transfer function developed as part of the beam fatigue testing. Shift factors for two sections analyzed with the MEPDG ranged from 0.7 to 1.0. The predicted cracking based on 90% reliability was much higher. Overall, it was concluded that the assumption of a shift factor of 10 between laboratory and field performance was reasonable.

Analyses were conducted using the MEPDG and PerRoad to determine their sensitivity to the measured fatigue endurance limit. Analyses were conducted with both the NCAT Test Track traffic (very limited range of axle weights) and the MEPDG default truck traffic classification No. 1 for principal arterials. The perpetual pavement thickness determined with both programs was sensitive to the measured endurance, a 50 ms change in the endurance limit resulted in approximately a 7- to 8-in. change in pavement thickness for the MEPDG or a 4-in. change in pavement thickness for PerRoad.

Using the endurance limits predicted from beam fatigue tests conducted as part of the study and the default traffic classification, the perpetual pavement thickness determined with PerRoad was approximately the same as the 20- and 40-year conventional (no endurance limit) MEPDG or 1993 AASHTO Pavement Design Guide pavement thicknesses. The MEPDG perpetual thickness was approximately 50% thicker. The overall conclusions at the end of a 20- or 40-year period were significantly different. With the conventional designs, the pavements would have failed in bottom-up fatigue with cracking over 20% of the lane area at 90% reliability while no cracking would be expected if the endurance limit was considered.

The implementation of the endurance limit as a single value for a given mix appears reasonable for M-E design programs that use equivalent temperature concepts, such as PerRoad. For the MEPDG, however, temperature as a function of depth is calculated on an hourly basis throughout the design life or analysis period. This can result in higher peak temperatures, with corresponding higher strains at the bottom of the asphalt layer, than equivalent temperature methods.

Research conducted outside this study indicates that the endurance limit based on laboratory testing varies as a function of temperature. One interpretation of this may be that a mix's ability to heal and therefore its fatigue "capacity" are greater at higher temperatures. A field study of data from the NCAT Test Track indicates pavements can withstand a distribution of strains without incurring cumulative damage. Both of these concepts have merit and both are recommended for future research aimed at better implementing the endurance limit in the MEPDG.

CHAPTER 1

Introduction and Research Approach

Introduction

Fatigue cracking has been an issue in the design and performance of hot mix asphalt (HMA) pavements ever since hot mix asphalt pavements began to be used. It has long been understood that pavement structures that are too thin fail in fatigue under repeated loads. This type of structural failure results from fatigue of the HMA mixtures and results in the formation of alligator cracking.

There are a number of properties in the mixture that can be adjusted to improve the resistance to fatigue but the most important property by far is the thickness of the HMA and its resulting effect on the tensile strain at the bottom of the HMA. It is this strain at the bottom of the asphalt that is the primary cause of the bottom-up fatigue cracking. Ultimately, a method is needed to determine the expected strain at the bottom of the asphalt layer more accurately and to determine the effect of this expected strain on the fatigue resistance of the mixture. Determination of fatigue life based on laboratory tests generally does not provide an accurate predictor of what is observed in the field and a shift factor must be applied. There are many reasons that probably lead to the need for a shift factor, including: aging, rest periods, healing, densification under traffic, temperature fluctuations, concept of constant stress versus constant strain, simulation of field compaction versus laboratory compaction, and property changes due to other environmental conditions such as aging of the binder and moisture damage. The shift factor can be significant (e.g.,15 to 20 times or more of the laboratory estimate of the fatigue life).

Much research was performed in the 1960s and 1970s to study fatigue of HMA. Until recent years it was believed that fatigue cracking always started at the bottom of the HMA layers and propagated up through the HMA layers, eventually reaching the surface. However, recently there is evidence that some projects have exhibited fatigue failure due to top-down cracking. Generally, it is believed that any modification to the mix properties that will improve the resistance to bottom-up cracking will also improve the resistance to top-down cracking. Whether it is top-down cracking or bottom-up cracking, the likely cause of fatigue distress is tensile strains in the HMA at critical points in the pavement structure.

There is now a much wider use of polymer modified asphalts than in past years. There have been very few fatigue studies on mixtures containing modified asphalts, and it is not clear how much improvement, if any, can be obtained from modified mixtures.

Typically, fatigue data are analyzed by plotting the number of cycles to failure versus the maximum tensile strain or stress in the HMA specimens. It has been shown that plotting these data on a log-log (log of cycles to failure versus log of applied stress or strain) plot will provide approximately a straight line. It is very time consuming to conduct fatigue tests at very high numbers of cycles so, generally, researchers have applied fairly high stress or strain values so that the number of cycles to failure will not be so high as to provide excessive test time. It is generally believed that approximately 10 specimens must be tested for each mixture being evaluated to provide a suitable relationship between applied stress or strain and number of cycles to failure.

Since most of the testing has been done at higher stress or strain levels, there has not been much work to look at the expected performance at lower stress or strain levels even though these lower stress levels are typical in the field. Generally, a best-fit line is determined for the data at these relatively high strain or stress levels and the performance of mixtures at lower stress or strain levels is extrapolated from the data. Hence, there is very little understanding of the actual performance that would be expected at these lower levels.

Some work has indicated that there might be a level of stress or strain below which no damage occurs to the test specimen. The stress or strain level below which no fatigue damage originating from the bottom of the pavement structure occurs has

been termed *fatigue endurance limit.* If a pavement is designed and constructed so that under repeated traffic loads no damage occurs, then that pavement should last indefinitely without a structural failure. This pavement will still require overlays on some regular basis to maintain the surface in good operating condition, but the pavement structure should provide a very long life.

Research Problem Statement

Work is needed to determine if there is an endurance limit for HMA and, if so, how this information should be used in pavement design. One would not want to design all pavements, regardless of traffic level, so that the endurance limit is not exceeded since this would result in the same design thickness regardless of traffic level. For very high traffic levels it might be desirable to design the pavement so that the endurance limit is not exceeded, but for low traffic levels it is likely that this approach would be too expensive. However, a similar concept could be employed for pavements subject to very low traffic levels to ensure a long life. As always, the pavement should be designed to provide the lowest life-cycle costs.

Hence, there is a need first of all to determine if there is an endurance limit for HMA. Once the endurance limit is determined it is important to determine how this endurance limit would fit into the new mechanistic pavement design procedures.

Objectives

The objectives of this study are to

1. Test the hypothesis that there is an endurance limit in the fatigue behavior of HMA mixtures and measure its value for a representative range of HMA mixtures.
2. Recommend a procedure to incorporate the effects of the endurance limit into mechanistic pavement design methods.

Scope

This study included a literature review, laboratory testing, and analysis of field data. A mix design, used to construct structural sections at the 2003 National Center for Asphalt Technology (NCAT) Test Track, was replicated. Four versions of the mix design were evaluated encompassing the effect of increased asphalt binder content and polymer modification. The mixtures with higher asphalt binder contents were prepared at higher densities to simulate the improvement in compaction expected in the field. Beam fatigue and uniaxial tension testing were conducted to determine fatigue life. Beam fatigue testing was conducted at progressively lower strain levels until a fatigue life in excess of 50 million cycles was achieved. Data from the Long-Term Pavement Performance (LTPP) study were analyzed to determine if they supported the endurance limit concept.

CHAPTER 2

State of Practice

A review of the existing literature was conducted to answer the following specific questions:

1. What is an endurance limit?
2. What field or laboratory studies support the existence of an endurance limit?
3. What HMA material factors affect fatigue life and consequently might affect the endurance limit for different materials?
4. What are the best methods of measuring fatigue life in the laboratory?
5. What analysis methods should be used to analyze fatigue data in order to identify the endurance limit for a given mixture?

A tremendous volume of literature was identified related to the factors affecting fatigue life, methods of measuring fatigue life, and analyzing fatigue data. Three very good summaries of this literature were identified, one by Epps and Monismith (*1*) produced in the early 1970s and two additional summaries produced as part of the Strategic Highway Research Program (SHRP) (*2, 3*). Therefore, an attempt was not made to summarize all of the references related to factors affecting fatigue life and fatigue measurement.

Arguments for the Existence of the Endurance Limit

Pavements have been designed primarily to resist rutting of the subgrade and bottom-up fatigue cracking. In classical pavement design, as design load applications increase, pavement thickness must also increase. There is a growing belief that for thick pavements, bottom-up fatigue cracking does not occur. The concept of an endurance limit has been developed, representing a strain level resulting from a combination of HMA stiffness and thickness, below which bottom-up cracking will not initiate. Therefore, additional pavement thickness, greater than that required to keep strains below the endurance limit, would not provide additional life. This concept has significant design and economic implications.

The concept of the endurance limit was originally developed for metals (*4, 5*). Barret et al. (*5*) describe the endurance limit for metals as being a stress below which, for uncracked materials, the plot of stress versus cycles to failure becomes essentially horizontal and fatigue does not occur. Figure 2.1 illustrates the theoretical concept of the endurance limit, as it would be applied to HMA.

The concept of the endurance limit was first implemented for paving materials by the Portland Cement Association. An examination of fatigue tests conducted by various researchers on Portland cement concrete beams, discussed in Baladi and Snyder (*6*) and Huang (*7*), indicated that if the stress ratio is kept below 0.45, the concrete will have an essentially infinite fatigue life. The stress ratio was defined as the ratio of stress induced in the concrete pavement to the concrete's modulus of rupture. A maximum of 10 million cycles to failure was used for the majority of this testing (one sample was tested to approximately 20 million cycles) (Figure 2.2).

Monismith and McLean (*8*) first proposed an endurance limit of 70 micro-strain (ms) for asphalt pavements. It was observed that the log-log relationship between strain and bending cycles converged below 70 ms at approximately 5 million cycles. Maupin and Freeman (*9*) noted a similar convergence. Using low-strain design principles, Monismith and McLean (*8*) designed a pavement structure that increased the fatigue life of the pavement from 12 to approximately 19-plus years.

In the field, Nunn (*10*) in the United Kingdom (UK) and Nishizawa et al. (*11*) in Japan proposed concepts for long-life pavements for which classical bottom-up fatigue cracking would not occur. Nunn (*10*) defines long-life pavements as those that last at least 40 years without structural strengthen-

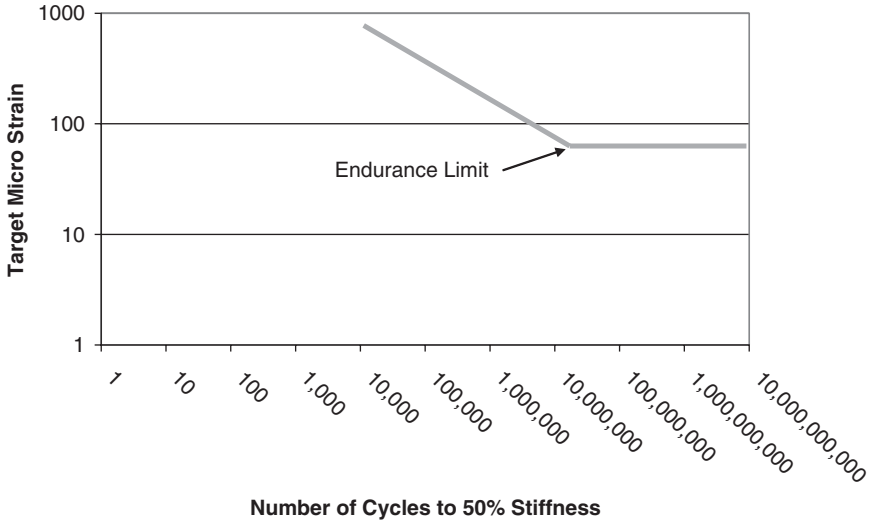

Figure 2.1. Idealized concept of the endurance limit.

ing. The UK's pavement design system was based on experimental roads that had carried up to 20 million standard axles. When this study was conducted, these relationships were being extrapolated to more than 200 million standard axles. Nunn (*10*) evaluated the most heavily traveled pavements in the UK, most of which had carried in excess of 100 million standard axles to evaluate the then current design system. Nunn (*10*) concluded the following:

- For pavements in excess of 7.1 in. (180 mm) thick, rutting tended to occur in the HMA layers.
- Surface initiated cracking was common in high-traffic pavements, but there was little evidence of bottom-up fatigue. Surface initiated cracks tended to stop at a depth of 4 in. (100 mm).
- It was observed that the stiffness of thick pavements was increasing with time, most likely due to binder aging. This would not tend to occur if the pavement was weakening due to accumulated damage.
- A minimum thickness for a long-life pavement was recommended as 7.9 in. with a maximum thickness of 15.4 in. This range is based on a variety of factors such as binder stiffness.

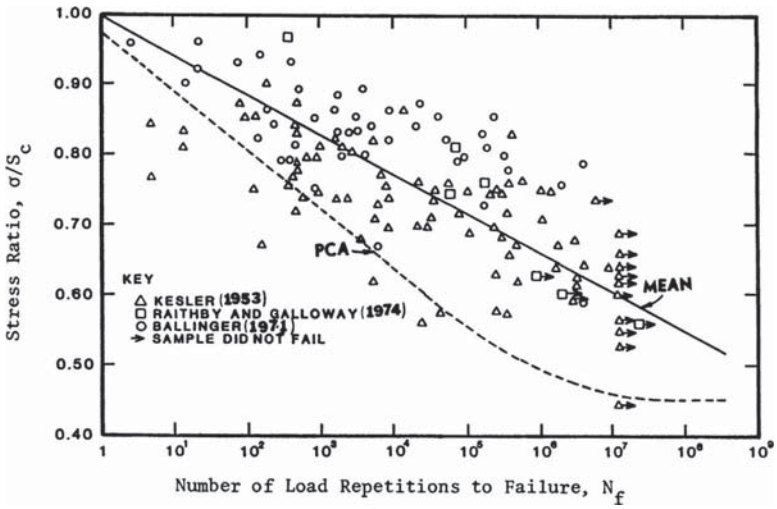

Source: Huang, Yang, H., *Pavement Analysis and Design,* 2nd ed., © 2004, p. 317. Reprinted by permission of Pearson Education, Inc. Upper Saddle River, NJ.

Figure 2.2. Illustration of endurance limit for concrete pavements (7).

Nishizawa et al. (*11*) reported an endurance limit of 200 ms based on the analysis of in-service pavements in Japan. Similarly, strain levels at the bottom of the asphalt layer of between 96 and 158 ms were calculated based on back-calculated stiffness data from the falling-weight deflectometer for a long-life pavement in Kansas (*12*). Others (*13, 14*) report similar findings, particularly, the absence of bottom-up fatigue cracking in thick pavements and the common occurrence of top-down cracking.

Factors Affecting Fatigue Life

A significant amount of fatigue research was conducted in the 1960s and 1970s. Epps and Monismith (*1*) provide a summary of the effects resulting from binder stiffness, asphalt content, aggregate type, aggregate gradation, and air void content. Table 2.1 indicates the relative affects of these components. The authors conclude that binder stiffness and air void content have a larger influence on fatigue life than aggregate type and gradation. The SHRP A-404 research (*3*) noted that angular aggregates tended to produce both stiffer mixes and longer fatigue lives. Harvey and Tsai (*15*) evaluated the effect of air voids and asphalt content on fatigue life. In most previous evaluations, a constant compaction effort was used to produce samples. This results in air voids being highly correlated with the asphalt content of a given mix in which case there is little relationship between asphalt content and fatigue life. In this instance, specific air void levels were targeted, resulting in relationships between fatigue life and both air void content and asphalt content. Voids filled with binder (VFB) have been a typical parameter used in fatigue life prediction equations. Harvey and Tsai (*15*) caution against the use of VFB since various combinations of air voids and asphalt content will produce the same VFB. Maupin and Freeman (*9*) note that there was little increase in fatigue life resulting from an increase of 0.5% binder, but significant increases were seen with an increase of 1.0% binder.

Strategies to Produce Long-Life Pavements

A number of strategies have been put forth to promote the likelihood of constructing a long-life pavement, including: polymer modification, rich bottom layers, and high-modulus asphalt bases.

Polymer Modification

Fatigue testing and analyses of asphalt mixtures made with modified asphalt binders has been performed in several studies. In 1988, Goodrich presented an early study on the fatigue performance of polymer modified mixes (*17*). In this study, three unmodified asphalt binders with different temperature susceptibilities and two modified asphalt binders—produced using one base asphalt and two levels of modification

Table 2.1. Factors affecting the stiffness and fatigue behavior of hot mix asphalt (*16 in 1*).

Factor	Change in Factor	Effect of Change in Factor		
		On Stiffness	On Fatigue Life in Controlled Stress Mode of Test	On Fatigue Life in Controlled Strain Mode of Test
Asphalt Penetration	decrease	increase	increase	decrease
Asphalt Content	increase	increase[a]	increase[a]	increase[b]
Aggregate Type	increase in rough texture and angularity	increase	increase	decrease
Aggregate Gradation	open to dense	increase	increase	decrease[d]
Air Void Content	decrease	increase	increase	increase[d]
Temperature	decrease	increase[c]	increase	decrease

Notes:
[a]Reaches optimum level above that required by stability considerations.
[b]No significant amount of data; conflicting considerations of increase in stiffness and reduction of strain in asphalt make this speculative.
[c]Approaches upper limit at temperature below freezing.
[d]No significant amount of data.

(not identified)—were evaluated using mixture fatigue tests. The intent was to correlate binder properties with mixture fatigue performance. Laboratory testing was conducted using flexural beam fatigue at 25°C and 1.67 Hz loading frequency in controlled stress mode. Tests were conducted at an initial strain level of 400 ms, and findings indicated that the fatigue lives of the two modified asphalt binders were an order of magnitude greater than the fatigue life of one of the unmodified asphalt binders (produced from the same source as the base asphalt used to create the modified asphalt binders). The base asphalt properties appear to be important in the performance of the modified asphalt binders. Mixtures made with one unmodified asphalt binder with low temperature susceptibility, had approximately two to three times the fatigue life of the polymer modified mixtures.

During the Strategic Highway Research Program (SHRP), the A-003A contractor evaluated the use of the flexural beam fatigue test as a mixture performance test for fatigue. The modified asphalt mixtures experiment (MAME), described in SHRP Report A-404, was performed to determine if the fatigue characteristics of modified mixtures could be evaluated using the flexural beam fatigue test (*18*). Asphalt mixtures were made using one aggregate source, three asphalt binders (AAF-1, AAG-1, and AAK-1), and three modifiers (identified as M-405, M-415, and M-416). Test results indicated that the addition of modifier M-405 to each of the three asphalt binders decreased the fatigue life compared to the unmodified asphalt mixes. The addition of modifiers M-415 and M-416 had a negative effect on the fatigue life of mixes made with AAG-1, but substantially increased the fatigue life (by approximately three to five times) of mixtures made with AAK-1 compared to the unmodified mixtures. A validation study was performed using slab wheel track tests on mixtures made with AAG-1 and the three modifiers. Although the results were similar for the M-405 modifier (decrease in fatigue life), the M-415 and M-416 modifiers resulted in an increase in fatigue life from the slab wheel track test. This was contrary to the findings of the flexural beam fatigue tests.

Shortly after the implementation of the Superpave performance-graded asphalt binder tests and specification, users recognized that the properties of modified asphalt binders may not be characterized properly using the Superpave binder tests. This led to the funding of NCHRP Project 9-10, "Superpave Protocols for Modified Asphalt Binders," in 1996. The research (*19*) was conducted by the University of Wisconsin-Madison, Asphalt Institute, and NCAT, under the direction of Hussain Bahia.

The NCHRP 9-10 research evaluated the effectiveness of the intermediate temperature stiffness requirement ($G^*\sin\delta \leq 5000$ kPa) by performing flexural beam fatigue tests on four aggregate structures (gravel and limestone, coarse and fine gradation) using nine different modified asphalt binders. Testing was conducted on mixtures using 10 Hz sinusoidal loading with a peak-to-peak strain of 800 ms. The test temperature was selected for each mixture as the temperature where the intermediate temperature requirement was met ($G^*\sin\delta = 5000$ kPa). So, unlike other studies in which the temperature was fixed (usually at 20°C), the viscous component of the shear modulus was fixed.

A brief examination of the data in the report indicates that the fatigue lives of the modified mixtures could be significantly different. Mixtures made with a PG 82-22 asphalt binder produced using a radial styrene-butadiene-styrene (SBS) modifier had fatigue lives at 24°C that were two to five times the fatigue lives (tested at 32°C) of mixtures made with an unmodified (oxidized) PG 82-22 asphalt binder. Since the $G^*\sin\delta$ value was the same for each of these mixtures at their respective test temperatures, the researchers considered the intermediate temperature criterion in the PG binder specification to be inadequate for assessing the fatigue characteristics of asphalt binders.

A temperature equivalency experiment conducted during SHRP (*18*) indicated a strong relationship between temperature and fatigue life at a given strain level, with fatigue life decreasing as the temperature decreased. Thus, it could be hypothesized that the difference in fatigue life between the SBS-radial modified PG 82-22 mixtures and the oxidized PG 82-22 mixtures would be greater if the test temperatures had been equal.

Monismith et al. (*20*) reported on the development of the design and specifications for the California I-710 rehabilitation. In the study, AR-8000 (roughly equivalent to a PG 64-10 or PG 64-16) and PBA-6a (PG 64-40) asphalt binders were used to prepare mixtures for testing. When tested at 20°C using the procedure described in AASHTO T321, the measured fatigue life of the PBA-6a mixtures was approximately an order of magnitude (10 times) greater than the fatigue life of the AR-8000 mixtures. This relationship seemed to be affected by the applied strain resulting in an increased difference between the two sets of fatigue lives at higher strain levels.

Lee et al. (*21*) reported on a laboratory evaluation of the effects of aggregate gradation and binder type on mixture fatigue life. Using uniaxial tension fatigue test results (conducted at 25°C) and a viscoelastic fatigue model, the authors calculated that mixtures made with an SBS-modified PG 76-22 asphalt binder had 10 times greater fatigue life than mixtures made with an unmodified asphalt binder, regardless of aggregate gradation.

Research performed in 2002 by the Asphalt Institute for the Asphalt Pavement Alliance evaluated the possibility of a fatigue endurance limit by testing mixtures made with two asphalt binders (PG 64-22 and PG 76-22) and two asphalt binder contents at various strain levels. The results, shown in

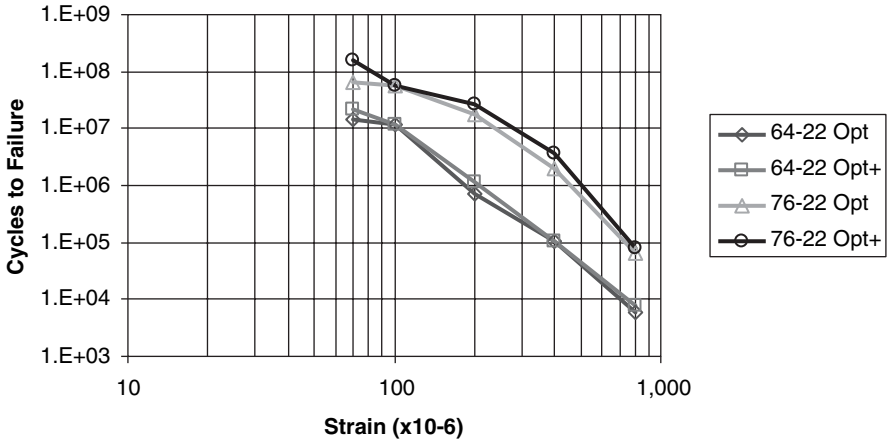

Figure 2.3. Fatigue life comparison for modified and unmodified mixes (22).

Figure 2.3, indicate that the mixtures made with the PG 76-22 asphalt binder have approximately an order of magnitude (i.e., 10 times) greater fatigue life than the mixtures made with the PG 64-22 asphalt binder.

Von Quintus (*23*) conducted a study to quantify the effects of polymer modified asphalts. Based on a literature review, Von Quintus reported that PMA mixtures generally last about 25% longer than conventional mixtures. Some premature failures caused concern. However, most of the failures were " . . . found to occur prior to the adoption of the Performance Graded (PG) binder specification and can be traced back to inferior construction (for example, high air voids), inferior materials, and/or inadequate design thickness." The study also notes "One of the more important findings from the recent field experiments is that many of the PMA pavements are not exhibiting fatigue cracking or have less load-related cracking than the control sections (unmodified mixtures)."

In summary, there appears to be significant historical data indicating that the laboratory fatigue performance of modified asphalt mixtures is greater than mixtures made with unmodified asphalt binders. In some reported cases, modified asphalt mixtures have exhibited an order of magnitude greater fatigue life compared to unmodified asphalt mixtures. The fatigue characteristics appear to be dependent on the base asphalt binder used for modification.

Rich Bottom Layers

The concept of a rich bottom layer originated from the Australian experience (*24*) and was explored during SHRP experiments. Two potential benefits are created through the use of a rich bottom layer: increased asphalt binder content and decreased air voids in the bottom layer (as a result of easier compaction created by the additional asphalt binder).

Several known literature sources confirm the rationale for these concepts. In the mix design fatigue experiment reported in SHRP Report A-404, one asphalt-aggregate mixture (RB aggregate and AAG-1 asphalt binder) was used to prepare specimens at three different levels of air voids and two different levels of asphalt binder content (4.5 and 6.0%). The effect of asphalt binder content on fatigue life was a primary focus of this study since the 8 × 2 expanded test program experiment did not evaluate asphalt binder content as a variable. A separate 2 × 2 pilot test program used two asphalt binder contents defined as *optimum* and *high*—with the high asphalt binder content established as 0.6% higher than the optimum asphalt binder content. For the 2 × 2 pilot test program, a statistical analysis of results from flexural beam fatigue (controlled stress and controlled strain) and other tests indicated that asphalt content did not significantly affect fatigue life (*18*).

The results of the mix design fatigue experiment indicate that asphalt binder content significantly affected flexural stiffness (decreasing by 8% as asphalt binder content increased) and fatigue life—increasing the fatigue life by 67% as the asphalt binder content increased from 4.5% to 6%. As in other experiments, increasing the air void content resulted in a decrease in flexural stiffness of 33% and a decrease in fatigue life by 45% as air voids increased from 4% to 8% (*18*).

Harvey and Tsai (*25*) conducted a study on the effects of asphalt content and air void content on mixture fatigue and stiffness. Samples were produced at five asphalt contents: 4.0%, 4.5%, 5.0%, 5.5%, and 6.0% by weight of aggregate and three ranges of air voids: 1% to 3%, 4% to 6%, and 7% to 9%. In this experiment, a constant compaction effort was not used, so air voids were independent of asphalt content. Constant strain tests were performed at two strain levels: 300 and 150 ms. Analysis of the data indicated that higher asphalt content and lower air voids resulted in longer fatigue lives. Lower asphalt content and lower air voids resulted in higher initial stiffness. Instead of using stiffness in mixture fatigue life prediction models, the authors recommended evaluating the

laboratory fatigue life and then predicting pavement performance by incorporating the effect of mixture stiffness on the predicted pavement strains resulting from layered elastic analysis. Using this methodology, the authors show the potential benefits of a rich bottom layer. It is also important to recognize that lower in-place air voids increase stiffness while resulting in longer fatigue lives, opposite conventional wisdom that suggests that stiffer mixes have shorter fatigue lives.

Monismith et al. (*20*) reported on the development of the design and specifications for the California I-710 rehabilitation. In their study, AR-8000 (roughly equivalent to a PG 64-10 or PG 64-16) and PBA-6a (PG 64-40) asphalt binders were used to prepare mixtures for testing at two combinations of asphalt binder content and air void content. Mixes were prepared with 0.5% higher asphalt binder content and 3% lower air voids. When tested at 20°C using the procedure described in AASHTO T321, the measured fatigue life of the mixes with 0.5% higher asphalt binder content (and lower air void contents) was approximately two times the fatigue life of mixes prepared at lower asphalt binder content.

Anderson and Bentsen (*26*) reported on a study evaluating the influence of voids in mineral aggregate (VMA) on mixture performance. Since VMA is related to asphalt binder content, mixtures with high VMA had asphalt binder contents that were approximately 1.0% higher than the low VMA mixtures. Flexural beam fatigue testing conducted at 20°C and 500 ms indicated that the mixes with the higher asphalt binder contents had two times greater laboratory fatigue life than the low asphalt binder content mixes.

Harvey et al. (*24*) reported on California's experiences with the design and construction of long-life asphalt pavements. The authors reported that most full-depth asphalt long-life designs will include a stiff, fatigue-resistant bottom layer. This layer, termed *a rich bottom layer,* is designed to have a very low air void content (approximately 0% to 3%). Stiffness of the layer is a consideration since it is intended to reduce the overall thickness of the HMA layers. The low air void content also reduces permeability and improves moisture resistance. The benefit of rich bottom layers is maximized with a thickness range of 50 mm to 75 mm. Illinois has also adopted this concept (*14*).

Generally the stiffness of a mix can be increased with increased compaction. Further, increased compaction generally increases fatigue life at the same strain level. Thus, increased compaction specifications for lower lifts result in both lower strains due to increased stiffness and also increased fatigue life for a given strain level, producing a more economical pavement. The unbound layers must be sufficiently stiff to allow a high degree of compaction in the bottom HMA layers.

A study conducted by Maupin (*27*) examined the impact of asphalt content on durability of Virginia surface mixtures. Testing was conducted on 9.5-mm and 12.5-mm nominal maximum aggregate size (NMAS) mixtures to examine the effect of increasing asphalt binder content. Flexural beam fatigue tests conducted at 600 ms indicated a slight increase in fatigue life with the 0.5% higher asphalt content. A substantial increase in fatigue life was noted with 1.0% higher asphalt content.

High Modulus Base

Europeans have used stiff binders to produce high modulus base layers (*10, 14, 28, 29*). Corte (*28*) reported on the use of high modulus asphalt mixtures in France. The first use of high-modulus asphalt concrete (HMAC) occurred around 1980. Initially, these mixtures were used for strengthening or rehabilitation where pavement thickness was constrained (for instance by bridge clearance). The use increased in 1985. It was found that locally available weak aggregates could be used with stiff binders. These mixtures were designed with relatively high asphalt binder content and low voids (less than 6%). Constant strain fatigue tests indicate that HMAC mixes are more fatigue resistant than conventional base mixtures. This is believed to be due to the higher asphalt content and lower voids found in the HMAC mixtures. Corte's findings match the findings in similar studies where lower air voids increase stiffness, but also appear to increase fatigue life (*20, 21*). The stiffness of these layers reduce the strain at the bottom of the asphalt layer using less thickness than conventional asphalts. Cracking can be a problem with these mixes. Corte (*28*) discusses binder tests to minimize the likelihood of cracking.

Laboratory Fatigue Tests and Analysis Methods

The SHRP A003-A project (*2, 3*) evaluated seven methods of measuring laboratory fatigue life. Repeated load flexure and direct tension tests received the highest rankings. A methodology was developed to evaluate fatigue life using flexural beam fatigue tests conducted in constant strain mode at 10 Hz. Thin pavements are generally subjected to a mode of loading best represented by constant strain. Thick pavements are generally represented by a mode of loading most closely represented by constant stress. However, the SHRP A003-A researchers recommended constant strain tests for all pavement loading conditions. This recommendation was based upon the fact that if fatigue evaluations are made in the context of the pavement structure (e.g. by calculating expected strains at the bottom of a given pavement structure), then constant stress and constant strain tests give similar rankings (*3, 25, 30*). AASHTO T321 is the current standard for beam fatigue tests.

The direct tension test was eliminated early in the SHRP A003-A research due to difficulties aligning and gripping the specimens (*2*). However, research under the direction of Kim appears to have improved this technique (*31–33*). Previous researchers noted that only a portion of a sample's dissipated energy is most likely causing damage (*34, 35*). Daniel and Kim (*32*) developed a method using a characteristic curve from which fatigue life can be predicted rapidly from monotonic uniaxial tension tests. A characteristic curve is generated by modeling viscoelastic material behavior using Schapery's correspondence principle, continuum damage mechanics, and work potential theory. This method may be used to more rapidly determine the endurance limit of a mixture. Uniaxial tension testing would not require the production of an HMA beam and instead would use a sample more closely related to those being contemplated for simple performance tests related to rutting.

Maupin and Freeman (*9*) evaluated five simple tests to predict fatigue life. Indirect tensile test results were found to be correlated to the coefficients used in standard equations to predict fatigue life in both constant stress and constant strain modes of testing. Von Quintus has indicated that a long-life pavement may be designed where the strain at the bottom of the asphalt layer is less than 1.0% of the indirect tensile strength failure strain. Thus, indirect tensile strength may also provide a rapid screening tool to evaluate the endurance limit of a given mixture.

Laboratory Studies to Quantify the Endurance Limit

As interest in long-life pavements grew, laboratory studies began to try to validate the existence of the endurance limit and develop methods of determining it for a given mixture. Ghuzlan and Carpenter (*34*) proposed the use of the dissipated energy ratio (DER) to define the existence of an endurance limit. The dissipated energy for a given fatigue cycle is calculated as the area of the stress-strain hysteresis loop (*3, 35*). DER is simply the ratio of dissipated energy from one cycle to the next. During the course of a fatigue test, three regions of the DER curve versus loading cycles may be identified: an initial downward trend, a plateau with a nearly constant energy input, and a failure region where the dissipated energy rapidly increases which occurs at approximately 40% of the initial stiffness (*34, 35*). Carpenter et al. (*36*) conducted additional beam fatigue tests in the range of 70 to 100 ms with samples being tested to between 38 and 46 million cycles. They concluded that low strain testing in the range of 70 ms resulted in "extraordinarily long fatigue life." Researchers at the University of Illinois, under the direction of Carpenter, have conducted a number of low strain beam fatigue tests that indicated a break in fatigue life behavior for samples with fatigue lives in excess of 11 million cycles (*37*). Tests were also conducted that indicated that periodic overloads (loads creating strain levels in excess of the endurance limit) would not substantially reduce the fatigue life where the majority of the load cycles were less than the endurance limit (*37*). The Asphalt Institute conducted a study to identify the endurance limit for the Asphalt Pavement Alliance (*38, 39*). Beam samples were tested to a maximum of 4 million cycles. Extrapolations support the presence of an endurance limit between 70 and 100 ms.

Shen and Carpenter (*40*) developed a new method for determining/predicting the endurance limit. Their research indicated a linear relationship between the log of the plateau value of the ratio of dissipated energy curve (previously called DER) and the log of cycles to 50% initial stiffness for both normal and low (below the endurance limit) strain levels. Further, they believe this methodology can be used to extrapolate the failure point for tests conducted in as little as 500,000 cycles. A tentative plateau value of 8.57E-9 was identified as indicating the endurance limit. This appears to be a promising technique for analyzing the endurance limit.

Modeling Fatigue and Relationship to Field Performance

The NCHRP 1-37A Design Guide has instituted an enhanced version of the Asphalt Institute Model for fatigue life (*41*). The enhancements were developed to better predict the performance of thin pavements in a constant strain mode of loading. With this model, pavement thickness will continually increase with increasing design traffic loads. The literature indicates a number of factors that must be accounted for if an alternate approach for fatigue life determination, which incorporates the endurance limit, is developed.

Previous studies indicate a coefficient of variation of approximately 40% for beam fatigue tests (*3, 30*). This variability must be accounted for when making fatigue life predictions and extrapolations. Several methods for accounting for this variability have been proposed (*30, 42–44*). For fatigue-life predictions below the endurance limit, variability of design traffic estimates should also be considered (*30, 43*). However, if a truly infinite fatigue life is estimated by the endurance limit, design traffic reliability may be of lesser importance. Harvey et al. (*43*) developed a method that incorporates the variability from laboratory fatigue tests, materials production, and construction. Material production variability includes asphalt content and in-place air voids. Construction variation is represented by variation in pavement thickness and subgrade support. Monte Carlo simulation is used to estimate the combined affect of material and construction variation. Savard et al. (*44*) report on a French methodology to determine an acceptable strain limit

based on variability in the fatigue tests and subgrade support. This methodology could be used to shift the measured endurance limit for a mixture from a 50% reliability of the laboratory test data to an acceptable level of reliability for the constructed pavement.

Fatigue tests are typically conducted at 20°C. However, pavement damage varies with temperature and the resulting changes in stiffness of the HMA layers. Methodologies have been developed to shift fatigue life results at 20°C to an equivalent annual or monthly temperature (*30, 43–45*). Overloads, or strain levels exceeding the endurance limit, are most likely to occur either in the warmest summer months (*37*) or when the spring thaw occurs, depending on environmental conditions.

Finally, in-service pavements tend to have longer fatigue lives than those indicated by laboratory tests. Thus, a shift factor is applied to laboratory fatigue life to predict field fatigue life (*41, 43–44, 46–47).* The shift factor is believed to account for such things as the affect of rest periods and healing. Shift factors may range from 10 to 100 (*43*). Leahy et al. (*46*) recommended a shift factor of 10 for up to 10% fatigue cracking in the wheel path. Harvey et al. (*43*) calibrated shift factors for California conditions. The shift factor calculated with their equation increases with decreasing strain levels. A shift factor of 16.6 would be calculated for 70 ms. Pierce and Mahoney (*47*) note that Washington State uses shift factors between 4 and 10. Smaller shift factors are used for thicker pavements.

CHAPTER 3

Research Plan

Introduction

Based upon the review of the literature, a controlled laboratory experimental plan was developed. The experimental plan was developed with the primary objective of testing the hypothesis that there is an endurance limit for HMA mixtures. As a secondary objective, some of the HMA material properties that affect the endurance limit were investigated.

A working definition of the endurance limit was developed as a framework for testing within the experimental plan. Although the endurance limit is defined as an essentially infinite fatigue life for metal alloys, testing for an infinite life is impractical. The endurance limit must be defined in practical, usable terms if it is to have meaning. For example, the literature has defined 40 to 50 years as a reasonable lifetime to be considered as a long lasting, or perpetual, pavement. Hence, determining a strain level that results in 40 to 50 years (or even more) of pavement life is a very practical way to identify the endurance limit.

The *Highway Capacity Manual* states that the maximum number of passenger cars per hour per lane for a freeway at a free flow speed of 65 mph is 2,350 (*48*). In rolling terrain, a single truck or bus would replace 2.5 passenger cars (*48*). Thus, one would expect a maximum of 940 trucks per hour, 22,560 trucks per day, or a maximum of 329,376,000 trucks in a 40-year period. Such a case might represent a dedicated truck lane running at capacity 24 hours a day, 7 days a week, 365 days a year, an unlikely occurrence. By comparison, the very heavily traveled section of Interstate 710 in California carried a maximum of 9,650 trucks per day in the design lane (*20*). By calculating the appropriate heavy-vehicle adjustment factor and determining its impact on traffic flows (*48*), mixed traffic streams with 25% and 50% trucks would produce a maximum of 148,219,200 (10,152 trucks per day) and 235,118,400 trucks in a 40-year period, respectively.

Consider, for example, an FHWA Class 9 vehicle or five-axle single trailer, which typically consists of two tandem axles and a single steering axle (three axle groups). Strain traces indicate that the tandem axle results in two distinct load repetitions (*49*). Assuming that one is designing a perpetual pavement for the tandem axle load, the steering axles would have a lower loading so, theoretically, in a perpetual pavement design they would do no damage to the pavement. Thus, each Class 9 vehicle would provide four load repetitions to the pavement for a maximum total of 1,317,504,000 axle load repetitions in a 40-year period. This represents a theoretical maximum loading where every truck is fully loaded and the design lane is at maximum capacity for 24 hours a day, 7 days a week, for a 40-year period. This loading condition would be expected to be even more severe than a dedicated truck lane. A similar methodology was used by Mahoney to calculate the maximum number of ESALs expected in a 40-year period (unpublished data).

In actual mixed traffic streams, the highest percentage of trucks tends to be about 50%, which would reduce the maximum number of load repetitions to 940,473,600 or a maximum number of load repetitions of 592,876,800 for 25% trucks. Even the most heavily traveled highways do not maintain traffic streams at capacity 24 hours a day and not all trucks are loaded. The fact that all trucks are not fully loaded is illustrated by a Washington DOT study of 10 weigh-in-motion sites over a one-year period, which indicated that the typical number of ESALs for a Class 9 vehicle was 1.2 (*50*). If 1.2 "design load" axles were applied per truck for the maximum number of trucks per lane in a 40-year period (329,376,000), a total of 395,251,200 load repetitions would be applied. Also, in winter months in many parts of the country, the pavement stiffness is very high, and this results in significantly lower strains. Therefore, it is a reasonable assumption that the maximum possible number of load repetitions expected in a 40-year period is approximately 500 million. This could be considered as a practical target for evaluating parameters (strain or energy) indicating an endurance limit.

Research conducted during the SHRP recommended a shift factor of 10 between laboratory beam fatigue results and field performance, equating to 10% cracking in the wheel-path (*46*). Considering this shift factor, laboratory testing to 50 million cycles would equate to approximately 500 million loading cycles in the field or approximately the maximum possible loading in a 40-year period. Based on these analyses, a mix that provided 50 million cycles or more of fatigue life in the laboratory was considered to be indicative of a long-life pavement.

If pavements were designed to have a strain level at the endurance limit, then all pavements, regardless of traffic, would be designed with approximately the same thickness of HMA (assuming the same underlying support). This approach is contrary to the way pavements have been designed in the past and is unlikely to be cost effective for future designs. Hence, it is more reasonable, especially for highways with low to medium traffic, to design a pavement for the expected traffic during an extended period of years (e.g., 40 to 50) than to simply design at the endurance limit.

Practically speaking, highways with lower traffic levels can be designed with less pavement structure and still have long lives. Hence, the amount of traffic has to be a critical element in the design process. In the past there has been very little fatigue testing at low strains (very high cycles to failure) and this study was designed to identify the relationship between strain and cycles to failure at these very low strains (high cycles to failure). In the process of evaluating low strains, it was felt that the "endurance limit" would be better identified.

Two test procedures were utilized to evaluate the existence of the endurance limit: beam fatigue tests and uniaxial tension tests. Beam fatigue tests have been the most widely used method for testing fatigue in the United States. Uniaxial tension tests have provided an alternative that allowed a more fundamental analysis by modeling the viscoelastic material behavior using Schapery's correspondence principle, continuum damage mechanics, and work potential theory.

Materials

The literature indicated that the primary material properties affecting fatigue life are binder content, binder stiffness, and air void content. The literature indicated that aggregate gradation, type, shape, and angularity have more limited effects. Different nominal maximum aggregate sizes, with their corresponding differing minimum VMA requirements, will tend to produce differing volumes of asphalt binder.

Phase I

A full-factorial experiment was conducted to evaluate the existence of an endurance limit and to identify factors affecting the endurance limit. Two main factors were included in the experiment. Two additional factors were fixed. These factors along with their levels are as follows:

- Nominal maximum aggregate size (NMAS)—19.0 mm
- Aggregate type—granite
- Asphalt content—optimum and optimum + 0.7%
- Binder stiffness—PG 67-22 and PG 76-22

The lower lifts of part of the structural experiment from the 2003 NCAT Test Track were replicated to provide two of the mixes for the experiment. The mixes were a 19.0 mm NMAS granite mixture at optimum asphalt content with both neat PG 67-22 and SBS modified PG 76-22 binder. The average field gradations, shown in Table 3.1, were used as the target gradation for the laboratory study. Previous research on fatigue has indicated that fatigue results are relatively insensitive to gradation. Therefore, it was felt that the use of the average gradation would be appropriate.

The base mix was placed in four lifts for sections N3 and N4 and two lifts in the other sections. The asphalt content of the base layer for section N8 was intentionally set at 0.5% above optimum. Therefore, it was not included in the average.

Table 3.1. Production gradations for base layers of 2003 NCAT Test Track structural experiment.

Sieve Size	N1	N2	N3 - Upper	N3 - Lower	N4 - Upper	N4 - Lower	N5	N6	N7	N8	Average
1"	100	100	100	100	100	100	100	100	100	100	100
3/4"	92	93	100	90	92	88	92	90	90	92	92
1/2"	80	84	84	79	79	77	79	78	78	83	80
3/8"	71	74	75	68	66	66	66	71	71	73	70
No. 4	49	53	57	50	49	49	49	53	53	54	52
No. 8	40	43	48	44	43	42	43	44	44	45	44
No. 16	33	35	42	39	36	36	36	36	36	37	37
No. 30	24	24	33	30	26	28	26	27	27	26	27
No. 50	13	14	20	16	14	16	14	15	15	14	15
No. 100	8	9	11	9	8	9	8	9	9	9	9
No. 200	5.5	5.5	6.7	5.6	5.5	5.5	5.5	5.7	5.7	5.5	6
Asphalt Content	4.3	4.5	4.3	4.6	4.7	4.4	4.7	5.0	5.0	5.2	4.7

Table 3.2. High and intermediate temperature test data for PG 64-22 binder.

Test	Value, kPa	Failure Temperature, °C
DSR G*/sin δ, original binder at 64°C	1.702	68.4
DSR G*/sin δ, RTFO residue at 64°C	4.268	69.1
DSR G* (sin δ), PAV residue at 25°C	2805	20.4

The PG 67-22 used at the 2003 NCAT Test Track is a non-standard grade used in the southeastern United States. The high temperature and intermediate temperature binder test data for the neat binder used in the 2003 NCAT Test Track are shown in Table 3.2. The data indicates that the PG 67-22 used at the NCAT Test Track also meets the properties of a PG 64-22.

Following the procedures developed during SHRP and described in AASHTO R30, all mixtures underwent short-term aging for 4 h at 135°C before compaction. This short-term aging procedure allows for absorption of the asphalt binder into the aggregate and simulates the aging that occurs during production at an HMA facility.

Sample preparation affects the measured fatigue life. To reduce variability, all of the samples tested in the study were mixed and compacted by NCAT. Individual beams were compacted using a linear kneading compactor for beam fatigue testing. Samples were then wet sawed to specified dimensions. Cylindrical samples were compacted using the Superpave gyratory compactor for uniaxial tension testing. These samples were later cored and sawed to size once they reached the University of New Hampshire's laboratory. Samples were carefully packed for shipping to other laboratories.

The air void contents of the optimum asphalt content samples were targeted at 7 ± 0.5%. An experiment was conducted to assess the expected reduction in air voids, using the same constant stress compaction effort that would result from the optimum plus asphalt content. A 3.7% reduction in air voids was observed, resulting in a target air voids content of 3.3 ± 0.5% for the optimum plus asphalt content samples.

Phase II

Additional testing was completed at the end of Phase I to examine the variability of beam fatigue testing and calculation of the endurance limit and the affect of binder grade on the endurance limit. Two additional binder grades, PG 58-28 and PG 64-22, were utilized in the previously described mixture at optimum asphalt content.

To date, a precision statement has not been developed for beam fatigue testing. A full round-robin according to ASTM C802 is beyond the scope of this project. A smaller scale round-robin was conducted to provide an estimate of the variability of beam fatigue testing.

Test Methods

Flexural Beam Fatigue Testing

Four-point beam fatigue testing was conducted according to AASHTO T321, "Determining the Fatigue Life of Compacted Hot-Mix Asphalt (HMA) Subjected to Repeated Flexural Bending." In this procedure, beam specimens (380-mm length, 63-mm width, 50-mm height) are loaded under strain-controlled conditions using sinusoidal loading at 10 Hz. The literature indicated that beam fatigue tests were the most commonly used form of fatigue test in the United States. The literature also indicated that beam fatigue tests were sensitive to material properties.

Testing was conducted in constant strain mode. Although the literature indicated that constant stress tests may be more appropriate for thick pavements, it also indicated that pavements never perform in a true constant stress manner, whereas the performance of thick pavements can be approximated by constant strain tests. Further, the stiffest mix performs the best in constant stress testing, but this is usually not the case in the field. It is felt that mixture stiffness is accounted for in the analysis when calculating the strain at the bottom of the HMA layer.

Each of the cells in the experimental plan (Table 3.1) was to be tested at six strain levels beginning on the high end of the range, as follows:

- 800 ms,
- 400 ms,
- 200 ms,
- 100 ms,
- 70 ms, and
- 50 ms.

At least two replicates were tested for each cell. Once the fatigue lives of both replicates at a given strain level exceeded 50 million cycles, the next lower strain level was not tested. AASHTO T321 indicates typical strain levels between 250 and 750 ms. The literature suggests that the endurance limit in the laboratory is on the order of 70 ms (*8, 36*) and possibly up to 200 ms in the field (*11*). The 50 ms strain level was added so that at least one strain level would be investigated that was believed to be below the endurance limit.

Two replicate tests were performed at each strain level. This provided a maximum total of 12 data points to fit the relationship between strain and cycles to failure. Ideally, the research team would have tested three replicates at each strain level. However, there was concern over the additional time this would take at low strain levels. If the research team were assured that the log-log relationships for strain or energy concepts remained a straight line at low strain levels, three replicates would have been preferable (*51*). However, since this

study was trying to identify a break or curve in those relationships, it was felt that fewer points at more levels provided more information.

Testing was conducted to failure (a reduction in stiffness of 50%) or a minimum of 50 million cycles. Since the goal of this study was to determine the existence of an endurance limit, the strain levels were being altered to better define the endurance limit. For instance, the PG 64-22 mix at optimum asphalt content tested at 100 ms had fatigue lives in excess of 50 million cycles, but when tested at 200 ms, failed prior to 50 million cycles (average 20,445,922 cycles). Therefore, it was decided that it was more informative to perform tests at an intermediate strain level between 100 and 200 ms instead of conducting tests at strain levels less than 100 ms. In this example, 170 ms was selected as the point where the log-log relationship between strain and cycles to failure, developed at higher strain levels (800 to 200 ms), predicted a fatigue life of 50 million cycles.

Three beam fatigue devices were used to conduct the testing. The study began with NCAT using a single IPC Global beam fatigue device and the Asphalt Institute using a Cox & Sons beam fatigue fixture in an Interlaken hydraulic load frame. NCAT later added a second IPC Global beam fatigue device. The Asphalt Institute had some difficulties testing at low strain levels and testing to greater than 10 million cycles to failure with their Interlaken hydraulic load frame. Consequently, the Asphalt Institute also obtained an IPC Global beam fatigue device. Rutgers University also tested a PG 67-22 at optimum plus asphalt content beam at 200 ms using an IPC Global beam fatigue device.

In Phase II, two of the labs used a Cox & Sons fixture in a servo-hydraulic frame and the remaining four labs used IPC Global's pneumatic system to conduct the beam fatigue tests. Testing in Phase II was conducted at 800 and 400 ms and the strain level representing the average of the predicted endurance limit for all of the labs testing a given mix.

Uniaxial Testing

A methodology by which the material response under various uniaxial tensile testing conditions (type of loading and temperature) can be predicted from the material response obtained from a single testing condition has been proposed by Daniel and Kim (*32*). The basis of this methodology is in a characteristic curve that describes the reduction in material integrity as damage increases. The characteristic curve is generated by modeling the viscoelastic material behavior using Schapery's correspondence principle, continuum damage mechanics, and work potential theory. The characteristic curve at any combination of temperature and loading conditions (cyclic versus monotonic, amplitude/rate, frequency) where viscoelastic behavior dominates the material response can be found by utilizing the time-temperature superposition principle and the concept of reduced time.

Chehab et al. (*33*) demonstrated that the viscoelastic time-temperature shift factors are applicable to mixtures with growing damage. Therefore, the shift factors determined from complex modulus master curve construction can be used to shift the characteristic curves at various temperatures to a single reference temperature. Complex modulus (frequency sweep) testing was conducted at five temperatures, −10°C, 0°C, 10°C, 20°C, and 30°C to develop the master curve. Uniaxial frequency sweep testing was conducted with a mean stress of zero to prevent the accumulation of permanent deformation. It is interesting to note that Daniel and Kim (*32*) recommend the following for testing:

> Ms levels of 50–70 should be targeted at each frequency-temperature combination to ensure that the linear viscoelastic response is measured and that damage is not induced in the specimens.

The ms levels noted by Daniel and Kim correspond to the anticipated level of the endurance limit. Following the frequency sweep tests, the same samples were loaded in monotonic tension to failure. The strain rate will be chosen to prevent the occurrence of a brittle failure. The monotonic tension tests will be used to develop the characteristic curve.

Once the characteristic curve and viscoelastic shift factors are known, the behavior of the mix at other temperatures and loading rates/amplitudes can be predicted. The number of cycles to failure for different amplitudes and temperatures were then predicted using the characteristic curve, and the shift factors were determined from complex modulus testing. Selected continuous cycles to failure tests were performed to verify the predicted values. The continuous cycles to failure test consists of a constant crosshead strain amplitude haversine loading applied continuously to the specimen in the tensile direction until failure occurs. Frequencies of 1 Hz and 10 Hz are used for the fatigue testing. The amplitude is chosen to achieve failure of the specimen at a desired number of cycles based on the fact that the higher the amplitude, the faster the specimen will fail. For this study, tests at 10 Hz were used for the verification fatigue tests to allow comparison with the beam fatigue results. Because of machine compliance, even when constant strain tests are conducted, the sample receives a mixed mode of loading comparable to real pavements.

Due to limitations in computer memory, and the need for a reasonably fast data acquisition rate to capture the necessary information, only snapshots of data can be acquired during the damage tests. In the continuous cyclic fatigue tests, one-second snapshots of data at a rate of 100 points per cycle (1,000 points per second for the 10 Hz loading frequency) were collected on a logarithmic scale up to a time increment of 2 to 10 minutes, depending upon the projected failure time

of the specimen. If specimens are expected to fail in a shorter amount of time, the time between successive snapshots was reduced in an attempt to acquire data close to the actual failure point and to adequately describe the changing material behavior as damage grows in the specimen.

Samples 150 mm tall by 75 mm in diameter were cored from gyratory samples for testing. Prior to testing, steel end plates were glued to the specimen using Devcon Plastic Steel epoxy. A gluing jig was used to minimize any eccentricities due to unparallel specimen ends. Four loose core type linear variable differential transformers (LVDTs) were mounted to the specimen surface at 90° radial intervals using a 100-mm gage length. Additionally, two spring-loaded LVDTs were mounted 180° apart to measure the plate-to-plate deformations. The ram and LVDT deformations and load cell measurements were collected using a National Instruments data acquisition board and Labview software.

Testing was performed using a closed-loop servo-hydraulic testing system. A 8.9 kN (2,000-lb) or 89 kN (20,000-lb) load cell was used depending upon the anticipated testing loads. The temperature was controlled with an environmental chamber that uses liquid nitrogen for cooling and a feedback system that maintains the temperature during testing. An example of a failed uniaxial tension fatigue sample is shown in Figure 3.1.

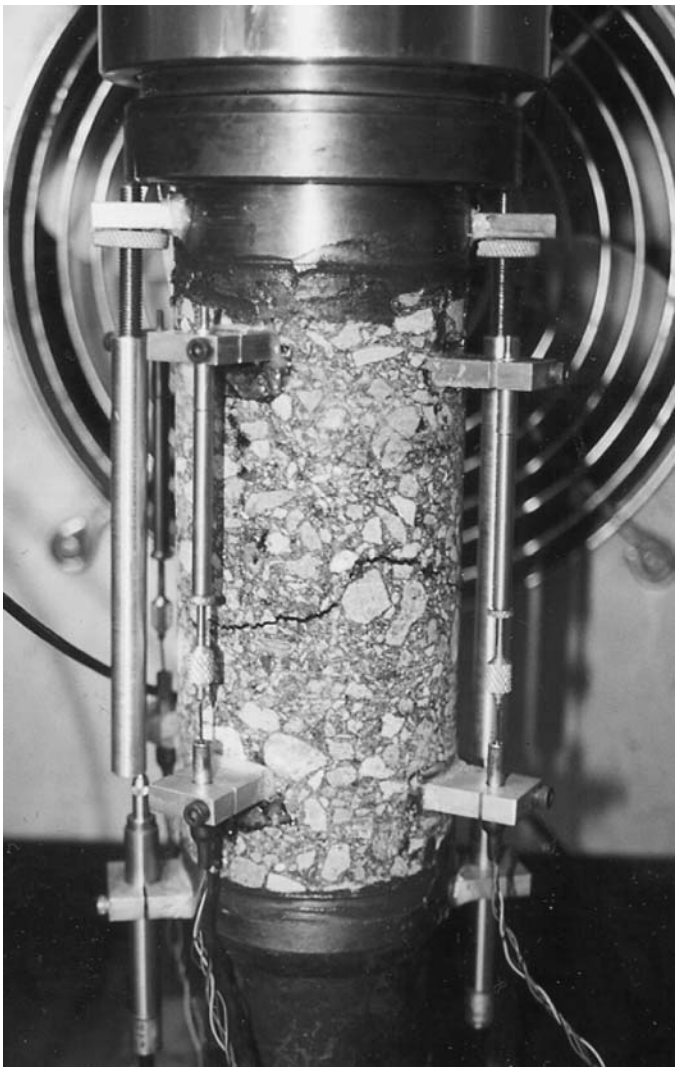

Figure 3.1. Uniaxial tension fatigue sample.

Indirect Tensile Testing

The literature indicates that parameters from the indirect tensile strength test, AASHTO T322, may be correlated with parameters related to the endurance limit. This test was considered as a possible surrogate test, which could be conducted more expediently, than the long-duration beam fatigue tests. Indirect tensile tests were conducted on the Phase I mixes.

CHAPTER 4

Beam Fatigue Test Results and Analyses

This chapter describes the beam fatigue testing conducted to confirm the existence of the endurance limit. One of the most important aspects of this research is a practical definition for the endurance limit. Asphalt mixtures simply cannot be tested for an infinite fatigue life in the laboratory. Testing at 10 Hz, approximately one million load repetitions can be applied to a beam fatigue sample in a given day. The primary goal of this testing was to confirm the existence of a fatigue endurance limit. In order to accomplish this goal, it was necessary to develop a method for estimating the endurance limit through accelerated testing in a reasonable period of time. A secondary goal was an estimate of the variability associated with beam fatigue testing and its potential impact on pavement thickness design.

The first portion of Chapter 4 discusses methods for extrapolating the fatigue failure point for strain levels that did not result in failure in less than 50 million loading cycles. The methods were applied to samples that had fatigue lives in excess of 10 million, but less than 50 million loading cycles. The second portion of the chapter presents the data collected in Phase I, as well as additional binder grades tested with the same mixture in Phase II. Evidence of the existence of a fatigue endurance limit is presented for each of these mixtures. The third portion of the chapter describes a limited round-robin conducted to assess the variability of fatigue testing and the prediction of the endurance limit. Finally, indirect tensile tests were investigated as a surrogate for beam fatigue tests.

As discussed in Chapter 3, a single gradation and aggregate type was used for all of the testing. A full-factorial experiment, shown in Table 4.1, was conducted in Phase I to evaluate the existence of an endurance limit and to identify factors affecting the endurance limit. Two main factors were included in the experiment—binder grade and asphalt content. Binder grade was varied at two levels: PG 67-22 and PG 76-22. As noted previously, the PG 67-22 also met the requirements of a PG 64-22. Asphalt content was varied at two levels: optimum and optimum plus 0.7%. Optimum asphalt content was determined at N_{design} = 80 gyrations. In addition, the samples' air void contents were reduced from 7.0 ± 0.5% to 3.3 ± 0.5% for the optimum plus samples. The voids for the optimum plus samples were reduced to simulate the expected improved densification in the field. Advantages of optimum plus or rich bottom layers are believed to include better compactability, greater resistance to fatigue damage, and improved moisture susceptibility.

Extrapolation Methods to Predict Fatigue Life

As discussed previously, it was decided prior to the start of testing that beam fatigue tests would be terminated at 50 million cycles. If a shift factor of 10 was applied to the test results from a sample tested to 50 million cycles, it would then be estimated that the pavement could withstand 500 million loading cycles at the corresponding strain level. Based on capacity analysis of a lane, this then represents a reasonable maximum number of loading cycles that might occur in a 40-year period. For the practical definition of the endurance limit, a 40-year life was considered to be indicative of a long-life pavement. It takes approximately 50 days to test a single sample to 50 million cycles. Additional analyses will be discussed later to evaluate the existence of a theoretical or truly infinite life endurance limit.

For samples that failed in less than 50 million cycles at 50% of initial stiffness, the number of cycles to failure was determined from the data acquisition software controlling the test. However, if the test was terminated prior to reaching 50% of initial stiffness, either due to an equipment problem or to reaching 50 million cycles, an extrapolation procedure was used to estimate the number of loading cycles, N_f, corresponding to 50% of initial stiffness. Ideally, a method of extrapolation would be identified that could be used to shorten the beam fatigue testing procedure used to determine the endurance limit. Then, samples could be tested to 4 million

Table 4.1. Experimental design.

NMAS (mm)	Binder Content	Granite	
		PG 67-22	PG 76-22
19.0	Optimum	X	X
	Optimum +	X	X

cycles as done in the Asphalt Institute study (*38, 39*) or possibly 10 million cycles and the fatigue life at, or close to, the endurance limit predicted.

In Phase I, testing was conducted at progressively lower strain levels until two samples at a given strain level reached 50 million cycles without reaching 50% of their initial stiffness (failure). Instead of testing at a lower strain level below that providing a fatigue life of at least 50 million cycles, samples were tested at the strain level predicted to provide a fatigue life of 50 million cycles. The goal of this additional point was to help define the transition from "normal" strain test to tests below the apparent fatigue endurance limit or "low" strain tests.

For the PG 67-22 mix at optimum asphalt content, the data from 800 through 200 ms were used to estimate the strain level that would result in a fatigue life of 50 million cycles. A linear regression was performed between the Log_{10} of ms and the Log_{10} of loading cycles to 50% initial stiffness. The $R^2 = 99.6$ for Equation 1. Using Equation 1, it was determined that a strain level of 166 ms should produce a fatigue life of 50 million cycles. This was rounded to 170 ms for testing purposes. Testing was conducted at this strain level to better define the endurance limit.

$$N_f = 10^{20.6} \times \varepsilon^{-5.81} \quad (1)$$

where,

N_f = number of cycles to 50% of initial stiffness and
ε = constant strain used in beam fatigue test (ms).

When testing the PG 67-22 mix at optimum asphalt content at 170 ms, the first replicate failed in 34.7 million cycles. The second replicate was at 55% of its initial stiffness at 50 million cycles. Therefore, testing was extended to see if the failure point could be determined. However, at 60 million cycles, Sample 23 still retained 53% of its initial stiffness. Therefore, testing was suspended at 60 million cycles.

For the PG 67-22 mix at optimum asphalt content, samples tested at 200 and 170 ms were used to investigate extrapolation techniques. These strain levels and similar strain levels for the other mixes used in Phase I provided long fatigue lives (in excess of 10 million cycles) while still having a defined failure point that could be used to investigate the accuracy of the extrapolation. Five techniques were investigated for extrapolation: exponential model, logarithmic model, Weibull function, three-stage Weibull function, and ratio of dissipated energy change (RDEC). Each of these is discussed below, and examples are provided of the predicted fatigue lives.

Fatigue Life Extrapolation Using AASHTO T321 Exponential Model

AASHTO T321 specifies an exponential model (Equation 2) for the calculation of cycles to 50% initial stiffness, as follows:

$$S = Ae^{bn} \quad (2)$$

where,

S = sample stiffness (MPa),
A = constant,
b = constant, and
n = number of load cycles.

The constants are determined by regression analysis of loading cycles versus the natural logarithm of the flexural stiffness. The number of cycles to failure is determined by solving Equation 2 for 50% of initial stiffness. In this study, for samples tested to less than 50 million cycles, the number of cycles reported to reach 50% of the initial stiffness are the actual number of cycles recorded by the test equipment, not the number of cycles determined using Equation 2. No discussion is provided in AASHTO T321 regarding whether or not all of the data (particularly the initial data) should be used when solving for the constants in Equation 2 (*52*).

Sample 5 of the PG 67-22 mix at optimum asphalt content, which was tested at 170 ms, was selected as an example. It was desirable to select a sample that had as long a fatigue life as possible and had reached 50% of initial stiffness within 50 million cycles. It was felt that an extrapolation method that worked well at high strain levels may not prove to be as accurate at strain levels closer to the anticipated endurance limit. Figure 4.1 shows fits to the loading cycle versus sample stiffness data determined using Equation 2. The coefficients for Equation 2 were fit using the data up to 4 million cycles, 10 million cycles, and failure (34.7 million cycles). As can be seen from Figure 4.1, when all of the data up to failure was used to fit the model, the model provides a reasonable estimate of fatigue life.

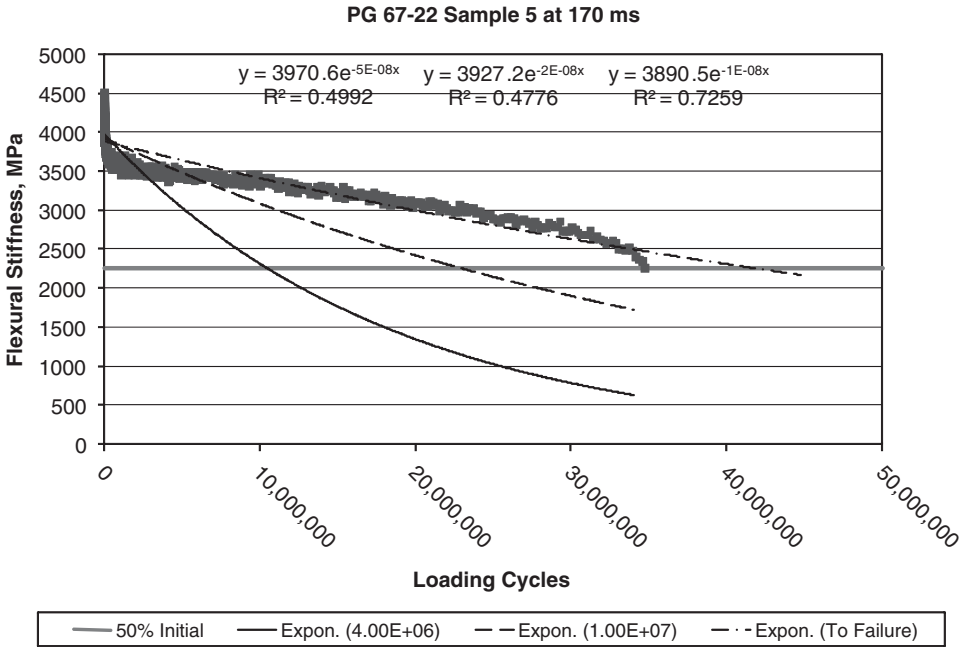

Figure 4.1. Examples of fatigue life estimates using the exponential model.

Fatigue Life Extrapolation Using Natural Logarithm of Loading Cycles versus Stiffness

A logarithmic model (Equation 3) using the natural logarithm of loading cycles versus stiffness was evaluated as one alternative to the exponential model.

$$S = \alpha + \beta \times \ln(n) \tag{3}$$

where,

S = the sample stiffness at loading cycle n, and
α and β are regression constants.

When all of the fatigue data are used to fit a logarithmic model, the slope of the fitted line at higher numbers of loading cycles may be flatter than the actual data. This leads to an overestimation of the fatigue life. This is illustrated in Figure 4.2 for Sample 5 of the PG 67-22 mix at optimum asphalt content. The fits to the logarithmic model using just the first 10 million cycles and using all of the data are indistinguishable on the plot. Note that in Figure 4.2 the logarithmic model provides very high R^2 values, but the fitted model does not match the experimental data at a high number of cycles.

However, by eliminating a portion of the early loading cycles, a good match to the data can generally be obtained,

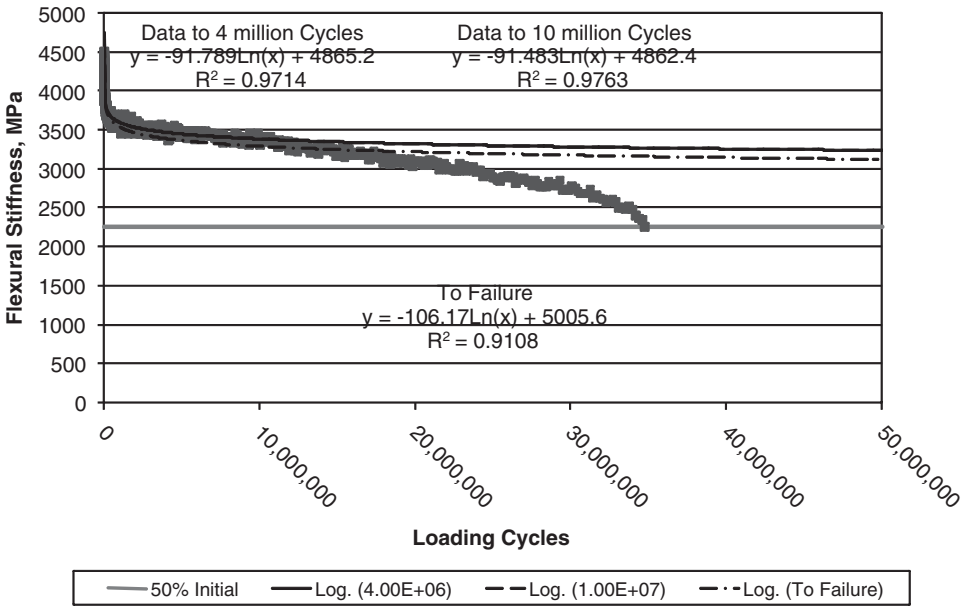

Figure 4.2. Logarithmic model fits for PG 67-22 at optimum, Sample 5.

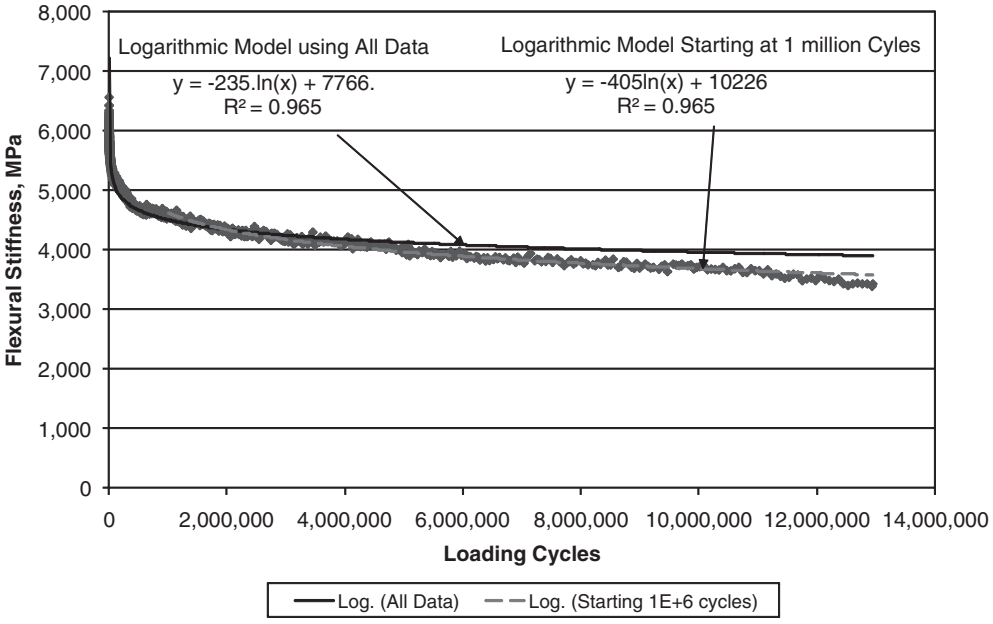

Figure 4.3. Logarithmic model fits for PG 67-22 at optimum, Sample 6.

particularly at low strain levels. In Figure 4.3, logarithmic models were fit to the data from Sample 6 of the PG 67-22 mix at optimum asphalt content, which was tested at 200 ms. In Figure 4.3, logarithmic models are shown including all of the initial loading cycles and excluding the first million loading cycles. This provides a better fit to data, but still would tend to overestimate the fatigue life. Further, the number of early loading cycles that are not included must be determined by trial and error. Note that all of the logarithmic models shown in Figures 4.2 and 4.3 provide high R^2 values, even when the fit to the data at a high number of cycles is not very good. This suggests that R^2 values alone are not adequate to evaluate extrapolation models. It is believed that the poor fit at a high number of cycles results from the fact that the data are collected using a logarithmic progression. That is, the sampling rate is high, every 10 cycles, when the test is initiated but may be every million cycles at a high number of cycles. Thus, there are more data points to fit in the early portion of the curve. Rowe and Bouldin (*53*), when examining fits from the exponential model, concluded that fatigue data should be taken with every 5% reduction in stiffness.

Fatigue Life Extrapolation Using the Power Model

The ratio of dissipated energy, developed by Shen and Carpenter (*40*) also requires that the number of cycles to 50% of initial stiffness be calculated in order to determine the plateau values. Shen (*54*) recommends a power model (Equation 4) for the extrapolation of stiffness versus loading cycles, as follows:

$$S = \alpha + n^{\beta} \tag{4}$$

where,

α = 10 raised to the power of the intercept from regression of log (S) versus log (n), and

β = the slope from regression of log (S) versus log (n).

The power model has a similar shape to the logarithmic model. Shen (*54*) also reported the need to eliminate a number of initial cycles to obtain a good fit to the slope at high numbers of cycles. Failure to eliminate some of the initial cycles results in an overestimation of the fatigue life. Additional discussion on the use of the power model and its application to the ratio of dissipated energy will be provided later in this report.

Fatigue Life Extrapolation Using the Weibull Survivor Function

Often, failure data can be modeled using a Weibull distribution. The Weibull function is commonly used in reliability engineering to estimate survival life. Tsai et al. (*55*) applied the Weibull survivor function to HMA beam fatigue data. The generalized equation for the Weibull function is given by Equation 5.

$$R(t) = \exp -\left(\frac{t-\delta}{\theta-\delta}\right)^{\gamma} \tag{5}$$

where,

$R(t)$ = the reliability at time t where t might be time or another life parameter such as loading cycles,

γ = the slope,

δ = the minimum life, and

θ = the characteristic life.

Tsai et al. (*55*) applied a specialized case of the Weibull function where the minimum life, δ, was assumed to be 0. In this case, the characteristic life = 1/λ and the Weibull function simplifies to Equation 6. Since the beam fatigue loading cycles are applied at a constant frequency of 10 Hz, loading cycles, n, can be substituted for time, t.

$$S(t) = \exp(-\lambda \times n^{\gamma}) \quad (6)$$

where,

$S(t)$ = probability of survival until time t,
λ = scale parameter (intercept), and
γ = shape parameter (slope).

The stiffness ratio can be used to characterize fatigue damage. The stiffness ratio is the stiffness measured at cycle n, divided by the initial stiffness, determined at the 50th cycle. Tsai (*56*) states that at a given cycle n, the beam being tested has a probability of survival past cycle n equal to the SR times 100%. Thus, SR(n) can be substituted for S(t). Tsai (*56*) presents the derivation of Equation 7, which allows the scale and shape parameters for laboratory beam fatigue data to be determined by linear regression.

$$\ln(-\ln(SR_n)) = \ln(\lambda) + \gamma \times \ln(n) \quad (7)$$

where,

SR_n = stiffness ratio or stiffness at cycle n divided by the initial stiffness.

Figure 4.4 shows an example of the data from the two 100 ms samples from the PG 67-22 at optimum mixture in the form of Equation 7. Tsai et al. (*55*) observed that the concave down shape, exhibited by Sample 13, "implied that the fatigue damage rate is slowed down and flattens out with increased repetitions and thus causes no further damage after a certain number of repetitions." This behavior is believed to be indicative of the endurance limit.

Fatigue Life Extrapolation Using Three-Stage Weibull Function

In the previous section, the Weibull survivor function was presented as a method for modeling the fatigue life of beam fatigue tests. In later sections, it will be demonstrated that the single-stage Weibull function generally provides a good estimate of a sample's fatigue life and is reproducible when calculated by different laboratories. There are, however, cases for which the single-stage Weibull function apparently underpredicts fatigue life. Sample 13 in Figure 4.4 is one such example (but Sample 13 is not specifically labeled on the plot). It should be noted that with the exception of two examples analyzed by Tsai, the three-stage Weibull analyses were not conducted until after the completion of all of the Phase I and II testing.

To improve upon the accuracy of the single-stage Weibull function, Tsai et al. (*57*) developed a methodology for fitting a three-stage Weibull curve. Tsai et al. (*57*) theorized that a

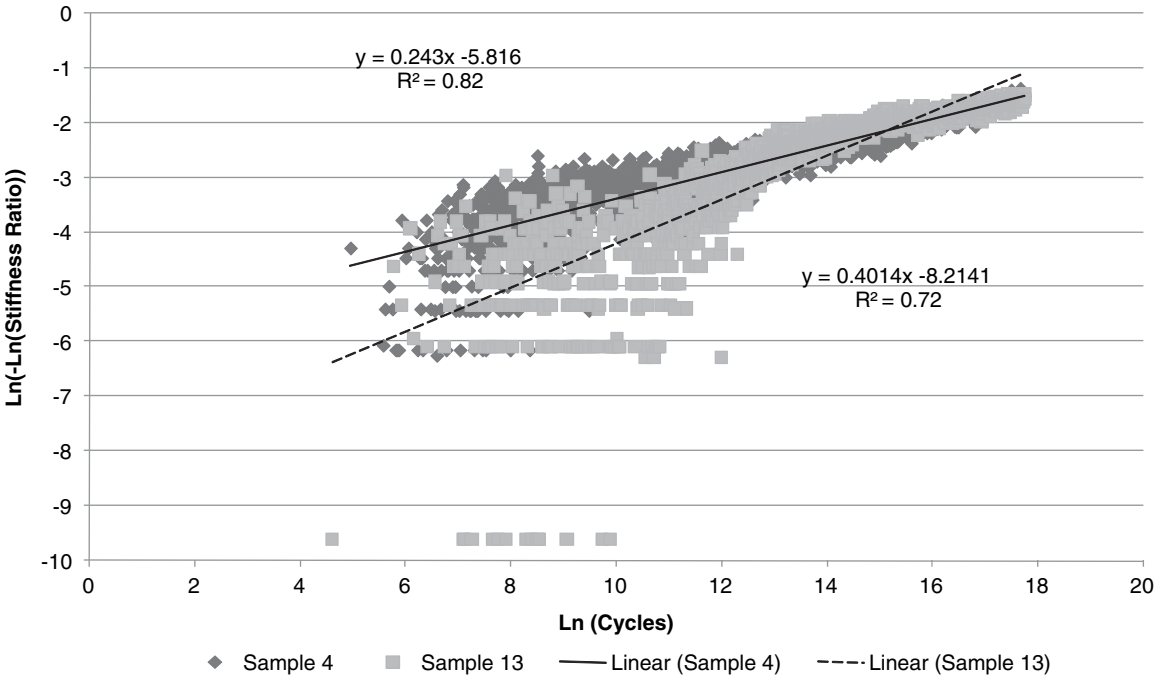

Figure 4.4. Weibull survivor function for PG 67-22 at optimum 100 ms samples.

plot of loading cycles versus stiffness ratio could be divided into three stages: initial heating and temperature equilibrium, crack initiation, and crack propagation. In the case of low strain tests (below the endurance limit), the third stage does not appear to represent crack propagation, but rather concave down stage with a reduced rate of damage.

A Weibull function is fit to each of these stages as shown in Equation 8:

$$\begin{aligned} SR_1 &= e^{\left(-\alpha_1 \times n^{\beta_1}\right)} && \text{for } 0 \le n < n_1 \\ SR_2 &= e^{\left(-\alpha_2 \times (n-\gamma_1)^{\beta_2}\right)} && \text{for } n_1 \le n < n_2 \\ SR_3 &= e^{\left(-\alpha_3 \times (n-\gamma_2)^{\beta_3}\right)} && \text{for } n_2 \le n < n_3 \end{aligned} \quad (8)$$

Coefficients α_1, α_2, α_3, β_1, β_2, β_3, n_1, and n_2 are illustrated in Figure 4.5.

Using a series of mathematical manipulations (*57*), n_1, γ_1, n_2, and γ_2 can be calculated sequentially as follows:

$$n_1 = \left[\frac{\alpha_2}{\alpha_1} \times \left(\frac{\beta_2}{\beta_1} \right)^{\beta_2} \right]^{\frac{1}{\beta_2 - \beta_1}} \quad (9)$$

$$\gamma_1 = \left(1 - \frac{\beta_2}{\beta_1} \right) \times n_1 \quad (10)$$

$$n_2 = \gamma_1 + \left[\frac{\alpha_3}{\alpha_2} \times \left(\frac{\beta_3}{\beta_2} \right)^{\beta_3} \right]^{\frac{1}{\beta_2 - \beta_3}} \quad (11)$$

$$\gamma_2 = \left(1 - \frac{\beta_3}{\beta_2} \right) \times n_2 + \frac{\beta_3}{\beta_2} \times \gamma_1 \quad (12)$$

Tsai et al. (*57*) applied a genetic algorithm to resolve the six unknown parameters. A genetic algorithm requires a parameter definition, in this case Equations 8 through 12, and a fitness function. Residual sum of squares between the measured and fitted ln(-ln(SR)) for each cycle is used as the fitness function. A "good gene" is defined as an optimum set of parameters to minimize the fitness function. A set of input ranges is first determined for α_1, α_2, α_3, β_1, β_2, and β_3. The input ranges are determined by visual inspection of the data. Simple linear regressions are performed for each stage to determine slopes and offsets. An example is shown in Figure 4.5. Tolerances are applied to the parameters determined by inspection to set initial ranges for each coefficient. The input ranges and test data are entered into a FORTRAN program, N3stage.exe, developed by Tsai. The program randomly generates a set of parameters or "genes" within the input ranges. The fitness parameter is calculated for each set of genes and the sets of genes are ranked. Good genes are mated and bad genes are discarded and replaced with new genes. The cycle of producing genes, ranking genes by the residual sum of squares, mating and

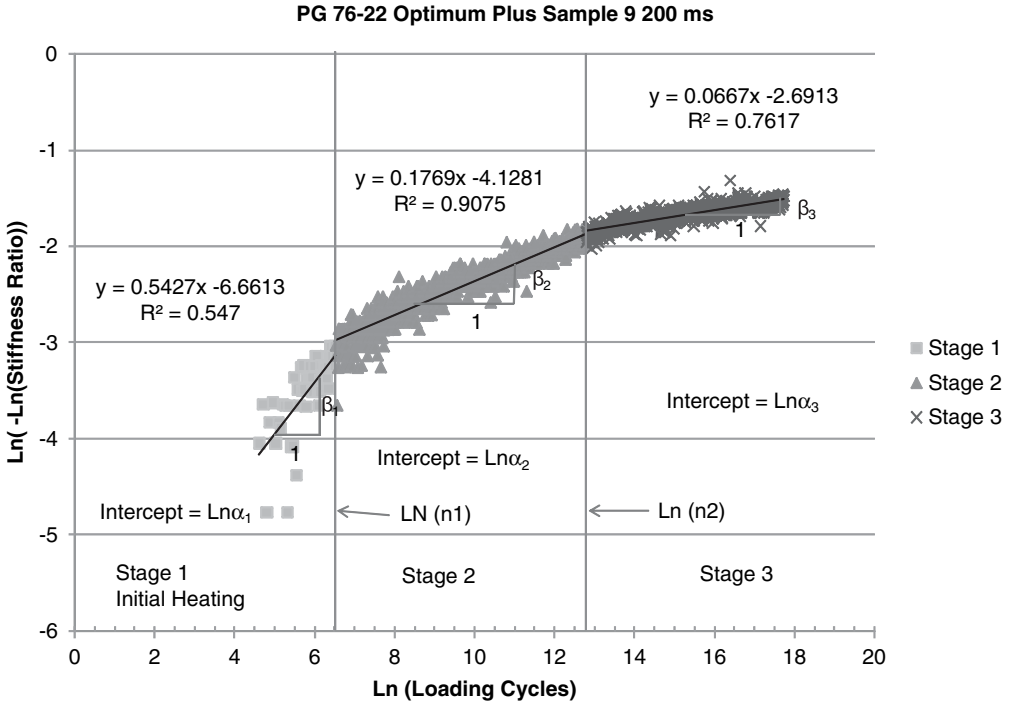

Figure 4.5. Three-stage Weibull curve definitions.

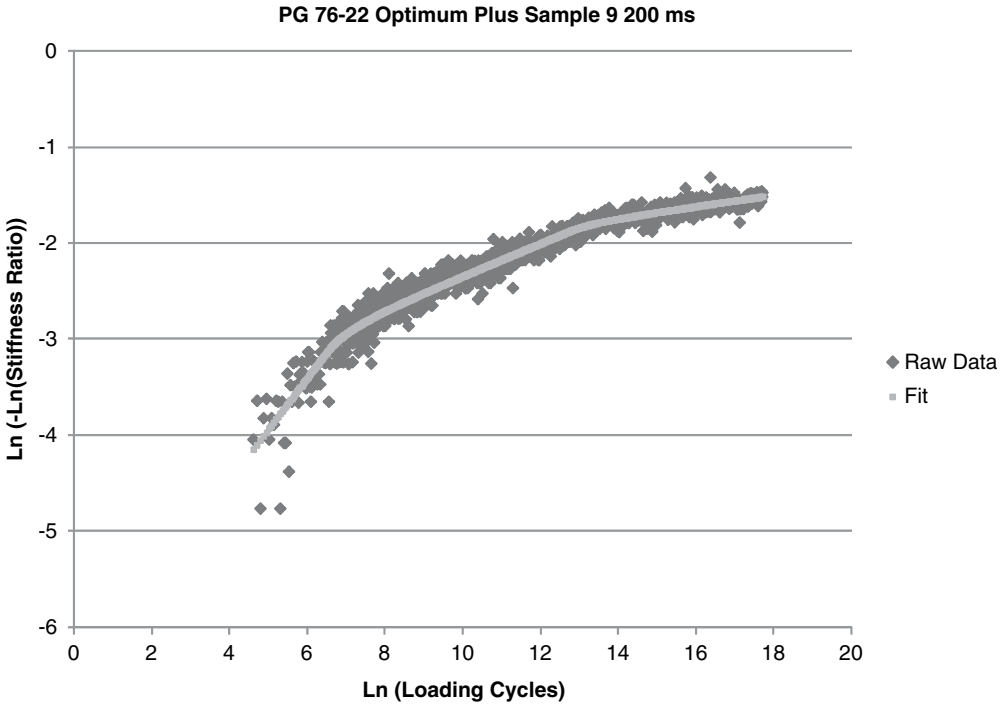

Figure 4.6. Three-stage Weibull fit to transformed data.

replacing genes, continues until the specified number of generations is complete (*58*). The N3stage program typically takes 30 to 60 minutes to complete 750 generations, depending on the size of the data set. The complete calculation procedure is described in Appendix A, Proposed Standard Practice for Predicting the Endurance Limit of Hot Mix Asphalt (HMA) for Long-Life Pavement Design. The NCHRP 9-38 research team developed a Microsoft Excel spreadsheet to solve the three-stage Weibull parameters, which produces similar results to the N3stage program.

Figures 4.6 and 4.7 show examples of the three-stage Weibull fit. This methodology provides a good fit to both

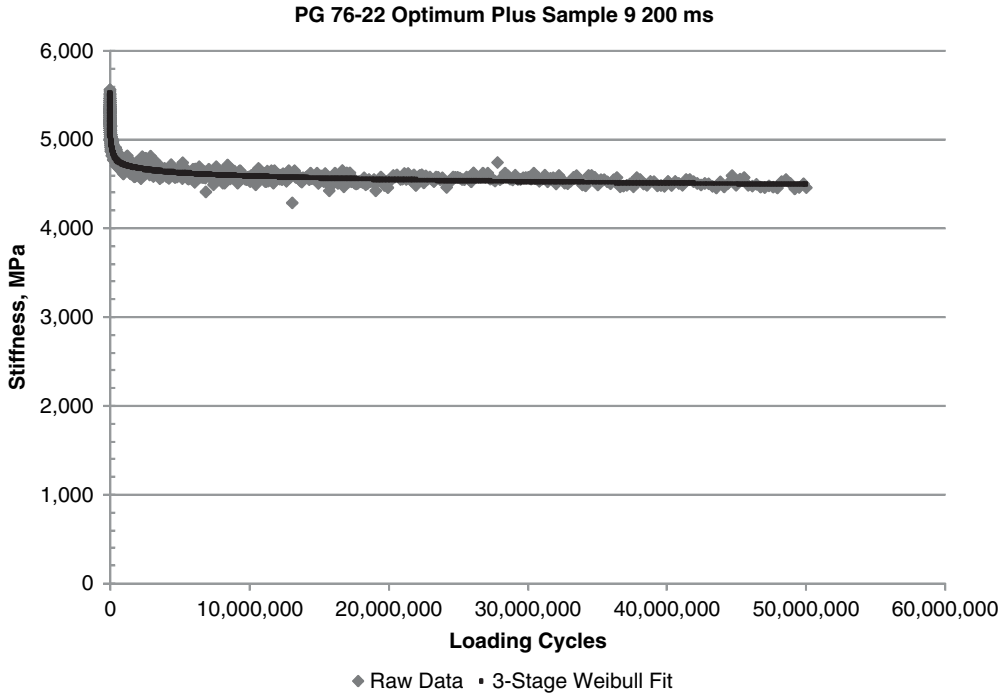

Figure 4.7. Three-stage Weibull fit to stiffness data.

normal and low strain fatigue data. In some cases, only one or two stages are fit, even if three stages are initially identified.

Ratio of Dissipated Energy Change (RDEC)

Dissipated energy is a measure of the energy that is lost to the material or altered through mechanical work, heat generation, or damage to the sample. Other researchers have used cumulative dissipated energy to define damage within a specimen, assuming that all of the dissipated energy is responsible for the damage. The approach suggested by Ghuzlan and Carpenter (*34*) considers that only a portion of the dissipated energy is responsible for actual damage.

Typically, three regions are observed in the RDEC analysis as shown in Figure 4.8. Region I represents the initial "settling" of the sample where the rate of change of dissipated energy decreases. In Region II, the rate of change of dissipated energy reaches a plateau, representing a period where the amount of damage occurring to the sample is constant. Finally, in Region III, sample instability begins as the rate of change of dissipated energy rapidly increases. A lower dissipated energy ratio (DER) plateau value implies that less damage is occurring per cycle. Therefore, a sample with a low DER plateau value would be expected to have a longer fatigue life than a sample with a high DER plateau value. Shen and Carpenter (*40*) refined this technique and suggested that the RDEC plateau value (PV) should be calculated at the number of cycles that produced 50% of the initial sample stiffness (N_f). A PV of 8.57E-9 was proposed by Shen and Carpenter as indicative of a long life pavement (*40*).

The RDEC analysis procedure is described in Appendix C, Proposed Standard Practice for Extrapolating Long-Life Beam Fatigue Tests Using the Ratio of Dissipated Energy Change (RDEC). RDEC is the ratio of dissipated energy change between two data points divided by the number of cycles between the two data points, that is, the average ratio of dissipated energy change per loading cycle. This is written as follows:

$$RDEC_a = \frac{DE_a - DE_b}{DE_a * (b - a)} \tag{13}$$

where,

$RDEC_a$ = the average ratio of dissipated energy change at cycle a, comparing to next cycle b;
a, b = load cycle a and b, respectively (the cycle count between cycle a and b for RDEC calculation will vary depending on the data acquisition software); and
DE_a, DE_b = the dissipated energy produced in load cycle a, and b, respectively.

The dissipated energy for each loading cycle is determined by measuring the area within the stress-strain hysteresis loop for each captured load pulse. This methodology is used by the IPC Global beam fatigue device used in the study by NCAT, Asphalt Institute, and the University of Illinois. Alternatively, the dissipated energy can be calculated according to Equation 14.

$$w_n = \pi \times \sigma_n \times \varepsilon_n \times \sin\delta_n \tag{14}$$

where,

σ_n = maximum tensile stress in cycle n, in kPa,
ε_n = maximum tensile strain in cycle n,
$\delta_n = 360 \times f \times s$,
f = loading frequency, Hz, and
s = time lag in seconds between peak load and peak deflection in seconds.

Due to testing noise, as shown in Figure 4.8, the raw dissipated energy data are not directly usable for calculating RDEC

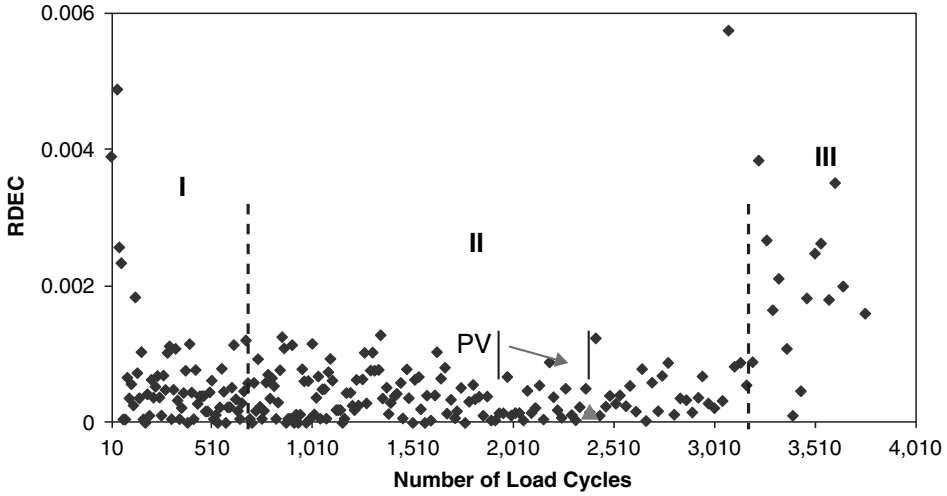

Figure 4.8. Typical RDEC versus loading cycles plot and the indication of PV.

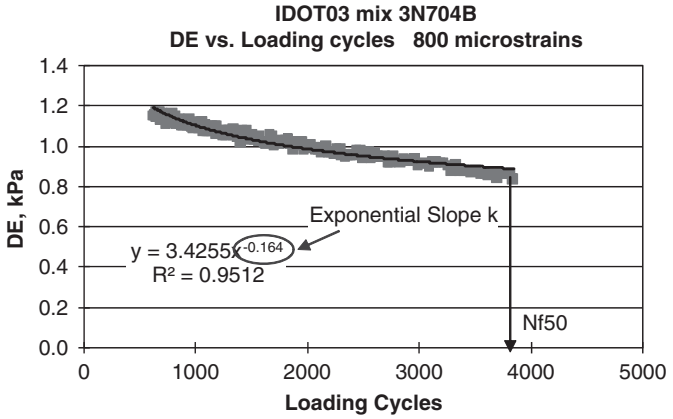

Figure 4.9. DE versus LC chart for one IDOT mix with fitted curve.

and PV. A curve fitting procedure is recommended to obtain the best fit equation for the dissipated energy-loading cycle data. It is assumed that the regression equation of dissipated energy-loading cycle relationship follows a power law relationship, Ax^f (as indicated in Figure 4.9). The key for the curve fitting process is to obtain a slope (in the power law relation plot) of the curve, f, which can best represent the original curve. In general, there are two rules for evaluating the goodness of the fitted curve: (1) a high R-square value, and (2) correct trend of the DE-LC curve. This is similar to the procedures described previously for fitting logarithmic or power models to the stiffness-loading cycle curves and is illustrated in Figure 4.10.

The average RDEC for an arbitrary 100 cycles at cycle a can be simply calculated using the following equation:

$$RDEC_a = \frac{1-\left(1+\frac{100}{a}\right)^f}{100} \quad (15)$$

where,

f = the slope from the regressed dissipated energy-loading cycle curve.

In the RDEC approach, PV is defined as the RDEC value at the 50% stiffness reduction failure point (Nf_{50}). Therefore, the PV value can be obtained using Equation 16.

$$PV = \frac{1-\left(1+\frac{100}{Nf_{50}}\right)^f}{100} \quad (16)$$

Here, the PV value depends only on the f factor of the regressed power law DE-LC curve and the defined failure point, Nf_{50}. For long-life tests, where Nf_{50} was not known, the stiffness-loading cycle curve first needed to be extrapolated to determine Nf_{50}, resulting in the calculation being based on a double extrapolation.

Using this approach, Shen and Carpenter (*40*) demonstrated a unique PV-Nf curve for all HMA mixes at normal strain/damage level testing, regardless of the testing condition, loading modes, and mixture types. The tests used for establishing this relationship at all normal testing were carried to or beyond the failure point (i.e., the Nf_{50} values are known). Also, using the results from long-term fatigue testing, Shen and Carpenter (*40*) demonstrated that the unique relation-

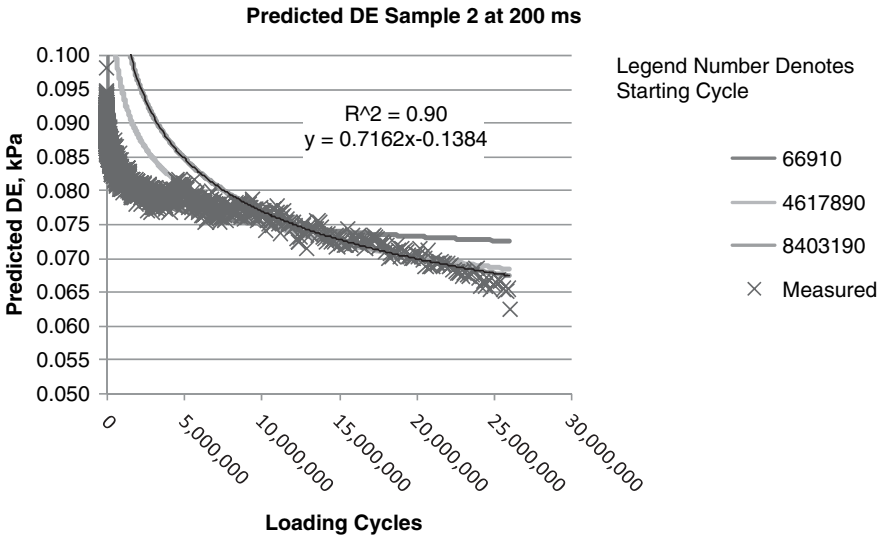

Figure 4.10. Dissipated energy versus loading cycle for raw data and various power models.

ship between PV-Nf is also valid for low strain testing. In other words, the PV-Nf relationship is unique for the whole loading range including both normal and low strain/damage level.

An error analysis was performed for two dissipated energy curve fitting routines using 19 Illinois DOT mixtures tested at low strain levels, and the results are presented in Figure 4.11. All the samples were tested to extended load repetitions (i.e., 5 to 30 million load repetitions). Hence, the Nf values obtained from the stiffness reduction curve are reasonable, and the comparison can be focused on the errors that could be involved due to fitting the DE-LC curve. Two PV-Nf lines are shown in Figure 4.11. One is with the PVs obtained from highest R^2 fitting of the dissipated energy-loading cycle curve; the other is with the PVs from visual fitting that represents the dissipated energy-loading cycle curve's best trend (especially the extension trend). They are closer at relatively higher PV (shorter fatigue life). With the decrease of PV (increase in fatigue life), the PV calculated from the highest R^2 fitting gives a greater value compared to the values obtained from visual fitting. For low strain testing, the segment that gives higher R^2 does not necessarily represent the real trend of the curve, which could induce error. Therefore, for low strain long fatigue testing, the "highest R^2 fitting" rule is not best suited. For most cases, the initial segment of the DE-LC curve has to be eliminated and only the later segment that gives a good extension trend of the curve should be used, since it is more representative for the actual long-term fatigue performance.

The unique PV-loading cycle curve is also illustrated in Figure 4.11. As illustrated in Appendix C, an alternative approach for extrapolating the fatigue life of a sample that does not fail is to plot the sample's RDEC versus loading cycle on a log-log plot and determine the intersection with the unique PV-Nf line.

Comparison of Fatigue Life Methods

This extended discussion on fatigue life extrapolation techniques is provided as an introduction to future methodologies for identifying the endurance limit. In this study, tests were conducted to a maximum of 50 million cycles in order to confirm the existence of the endurance limit. As noted previously, it takes approximately two months to complete a single test at this high number of cycles. This extended test time is not practical for routine determination of the endurance limit. One alternative to determine the strain level that corresponds to the endurance limit for a given mixture would be to conduct beam fatigue tests at a low strain level to a more limited number of cycles (perhaps less than 10 million or approximately 10 days) and extrapolate the data. Thus, a model would be fit to the stiffness versus loading cycle data and the number of cycles required to reach 50% of the initial stiffness would be extrapolated. A significant deviation from a log-log plot of strain versus cycles to failure would indicate the strain level corresponding to the endurance limit (this will be shown later in the section on Existence of

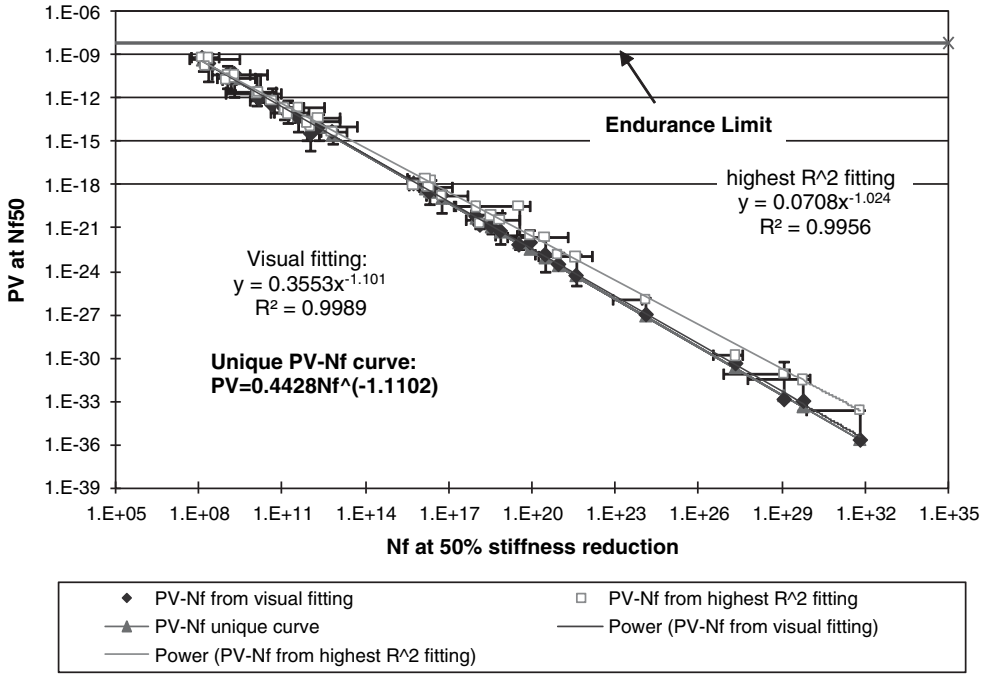

Figure 4.11. PV-Nf curve for IDOT03 mix at low strain with error bars indicated.

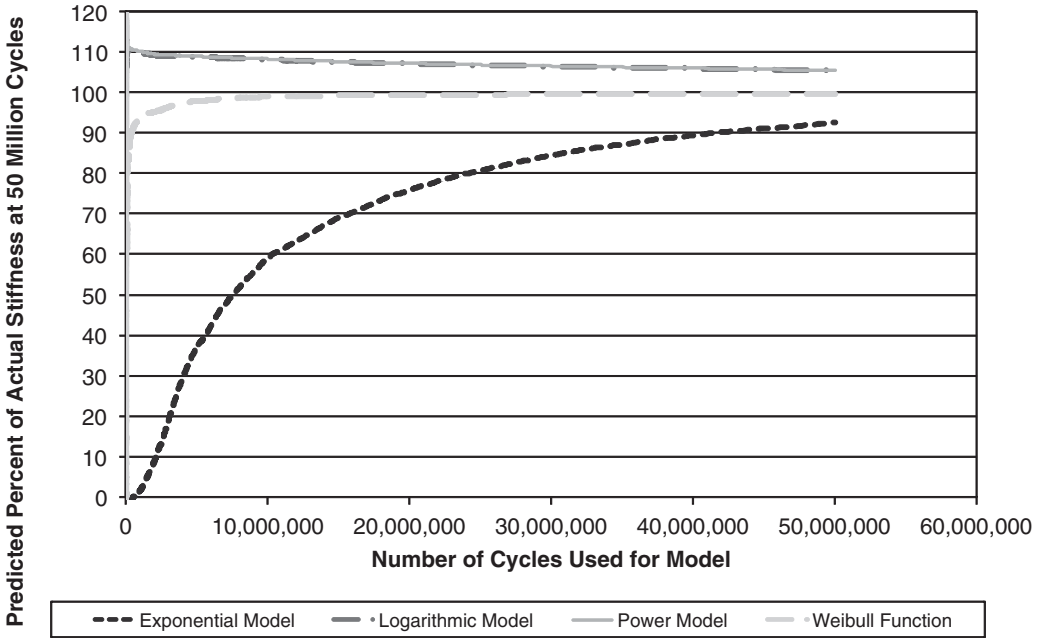

Figure 4.12. Convergence of extrapolated stiffness for PG 67-22 Sample 4.

the Endurance Limit). The two main requirements for this technique that need to be evaluated are (1) the appropriate form of the model and (2) the minimum number of cycles that need to be tested.

The samples tested at 100 ms for the PG 67-22 at optimum asphalt content were first used to evaluate the ability of the various models to predict the sample stiffness at 50 million cycles. Four models were considered: exponential (AASHTO T321), logarithmic, power, and Weibull function. All of the initial cycles were included when fitting the models. Figures 4.12 and 4.13 show the percentage of the actual measured stiffness at 50 million cycles for each of the models for PG 67-22 at optimum for Samples 4 and 13, respectively. The cycles shown in Figures 4.12 and 4.13 represent the total number of cycles (starting at the first cycle) used to fit the model. The stiffness at 50 million cycles extrapolated using that model

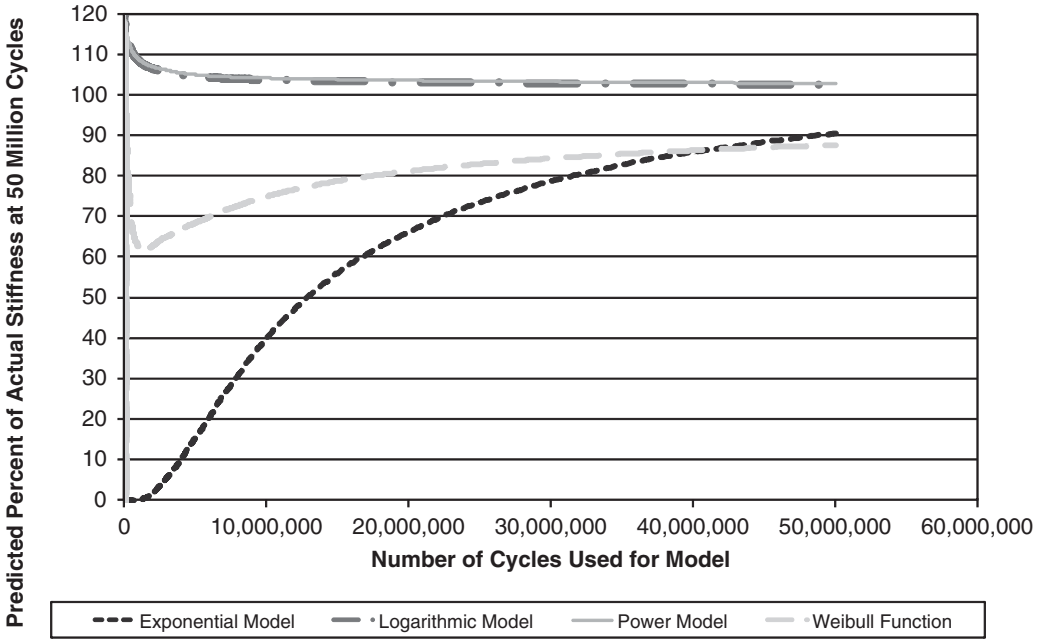

Figure 4.13. Convergence of extrapolated stiffness for PG 67-22 Sample 13.

is then shown as a percentage of the measured stiffness on the y-axis. For example, if Sample 4 would have been tested to 10 million cycles and a logarithmic model fit to the data, the extrapolated stiffness at 50 million cycles would be 108.2% of the measured stiffness at 50 million cycles.

Examination of Figures 4.12 and 4.13 show that the exponential model consistently underestimates the stiffness at 50 million cycles and is slow to converge on the measured stiffness (testing would need to be conducted to a high number of cycles to even approach the measured stiffness). This would suggest that the exponential model recommended by AASHTO T321 is not a good choice for extrapolating fatigue data.

The predicted stiffness values using the logarithmic and power models are basically the same in Figures 4.12 and 4.13. Both converge to a reasonable predicted stiffness within 10 million cycles. However, when all of the loading cycles are used, both overestimate the stiffness at 50 million cycles and, consequently, would overestimate the fatigue life. The single-stage Weibull function converges quickly and provides the most accurate results for Sample 4, but does a relatively poor job for Sample 13. Recall that the Weibull function for Sample 13 had the concave down shape in Figure 4.4.

The accuracy of the stiffness prediction is not the only factor which will affect the accuracy of the fatigue life extrapolation. The shape of the model will also have an effect. Logarithmic and power models can produce very flat slopes at high numbers of loading cycles that result in overestimation of the fatigue life (particularly if some of the initial cycles are not eliminated to better match the slope of stiffness versus loading cycles at a high number of loading cycles).

Five samples tested in Phase I had fatigue lives between 20 and 50 million cycles. These samples were used to evaluate the accuracy of the extrapolation techniques. Predictions were based on models developed using the first 4 million loading cycles and the first 10 million loading cycles. A previous study on the endurance limit by Peterson and Turner (*38*) extrapolated the fatigue life based on testing to 4 million cycles. Shen and Carpenter (*40*) extrapolated test results based on tests conducted to greater than 8 million cycles. Table 4.2 shows the fatigue life predictions for the five samples using six different extrapolation methods: exponential model, logarithmic model, power model, single-stage Weibull, three-stage Weibull, and RDEC.

The RDEC procedure consistently overestimates the samples' fatigue lives by three to seven orders of magnitude. For example, the actual fatigue life of Sample 2 of the PG 67-22 at optimum asphalt content is 2.60E+07 whereas the predicted fatigue life using the RDEC procedure for the first 10 million cycles is 3.08E+11. The power model also consistently overestimates fatigue life by two to seven orders of magnitude.

For the remaining methods, with the exception of the exponential model, the fatigue life of Sample 5 of the PG 67-22 at optimum asphalt content was overestimated by a larger degree than for the other samples. Sample 5 was tested at 170 ms. The logarithmic model overestimated the fatigue life of Sample 5 by five orders of magnitude, but the remaining four samples by one to two orders of magnitude. The three-stage Weibull model overestimated fatigue life of Sample 5 by three or four orders of magnitude based on the data from 4 million and 10 million loading cycles, respectively. However, for the remaining samples, the three-stage Weibull function overestimated fatigue life by zero to two orders of magnitude. Sample 23 of the same mix was also tested at 170 ms. It was tested to 60 million cycles without reaching 50% of its initial stiffness.

The exponential and single-stage Weibull function produced the most accurate fatigue life predictions. As shown in Figure 4.14, the exponential model consistently underestimates fatigue life. The fatigue life of points above the line of

Table 4.2. Comparison of fatigue life extrapolations.

Mix	Sample	Cycles Used for Extrapolation (Millions)	Actual	Exponential	Logarithmic	Power	Single-Stage Weibull	Three-Stage Weibull	RDEC
PG 67-22 Optimum	2	4	2.60E+07	7.89E+06	2.54E+09	3.80E+10	3.31E+07	1.41E+08	6.78E+11
		10		1.87E+07	2.83E+09	3.43E+10	5.59E+07	1.89E+08	3.08E+11
	21	4	2.08E+07	4.94E+06	4.84E+08	4.19E+09	1.44E+07	4.43E+07	5.53E+10
		10		9.88E+06	3.17E+08	1.78E+09	1.91E+07	5.04E+07	1.92E+09
	5	4	3.47E+07	1.27E+07	2.13E+12	2.15E+14	3.87E+08	7.23E+11	1.66E+14
		10		2.88E+07	2.27E+12	2.15E+14	7.24E+08	1.92E+10	8.02E+13
PG 67-22 Optimum Plus	4	4	3.90E+07	8.62E+06	5.57E+09	1.58E+11	3.11E+07	1.20E+09	2.26E+15
		10		1.84E+07	4.59E+09	2.97E+10	4.97E+07	3.39E+09	1.06E+11
PG 76-22 Optimum Plus	10	4	3.96E+07	7.69E+06	6.56E+08	7.16E+09	1.13E+07	3.28E+08	2.56E+12
		10		1.73E+07	7.77E+08	7.41E+09	2.01E+07	4.54E+08	1.71E+10

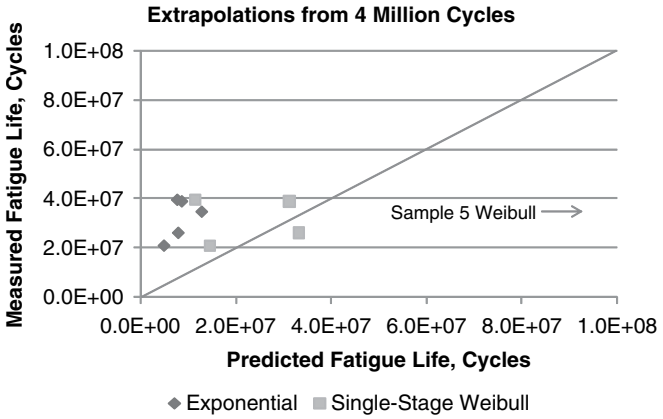

Figure 4.14. Comparison of exponential and single-stage Weibull extrapolations with measured fatigue lives.

equality is underestimated and below the line of equality is overestimated. The error is greater for larger extrapolations (e.g., testing to 10 million cycles for a sample with a fatigue life of 40 million cycles). The extrapolations for the single-stage Weibull model are distributed around the line of equality. As noted previously, the fatigue life for Sample 5 is significantly overestimated. However, the single-stage Weibull function appears to give the most reasonable extrapolation of fatigue test results.

When looking at the accuracy of fatigue predictions, it should be considered that strain versus fatigue life data typically is looked at on a log-log plot. The log of 26 million, the measured fatigue life for Sample 2, is 7.41, while the log of 56 million, the fatigue life estimated based on the first 10 million cycles using the single-stage Weibull function, is 7.75. This indicates that the two predictions are relatively close.

In summary, the Weibull functions were selected for extrapolating fatigue tests that did not fail within 50 million cycles or when the test was interrupted prior to failure (as occurred with Sample 6 of the PG 67-22 mix at optimum asphalt content). For long-life fatigue tests, at strain levels slightly above the endurance limit, the single-stage Weibull function appears to provide the most accurate extrapolation of fatigue life. The three-stage Weibull function, however, provides the best fit to the stiffness versus loading cycle data. Fatigue extrapolations from both methods are shown when discussing evidence of the endurance limit. Based on the results from this section, an AASHTO Standard Practice for Predicting the Endurance Limit of Hot Mix Asphalt (HMA) for Long-Life Pavement Design was developed and is presented in Appendix A. The draft format includes extrapolation techniques using both the single- and three-stage Weibull functions.

Existence of the Endurance Limit

Samples tested below the fatigue endurance limit are expected to have an essentially infinite fatigue life. As noted previously, testing was only conducted to 50 million cycles. Therefore, the failure point of these samples needed to be extrapolated. Two techniques were used to extrapolate the stiffness versus loading cycle data, the single- and three-stage Weibull functions. Additionally, the data were analyzed using the RDEC procedures to determine the plateau value. The following sections present the results from the testing and discuss each of the analyses. Tables 4.3 through 4.6 present the data collected in Phase I of the study.

Table 4.3. Granite 19.0 mm NMAS mix with PG 67-22 at optimum asphalt.

Beam ID	Air Voids, %	Initial Flexural Stiffness, MPa	Micro-Strain	Cycles Tested	Extrapolated Cycles to 50% Initial Stiffness		PV	Cycles to 50% Initial Stiffness	Average Cycles to Failure
					Single-Stage Weibull	Three-Stage Weibull			
18	6.6	5,175	800	6,000	NA	NA	3.66E-5	6,000	6,377
3	6.8	4,686	800	7,130	NA	NA	2.06E-5	7,130	
7	7.4	4,522	800	6,000	NA	NA	2.63E-5	6,000	
10	6.8	5,153	400	246,220	NA	NA	6.25E-7	246,220	252,136
46	7.0	5,239	400	57,000	NA	NA	2.24E-7	267,808[1]	
1	7.0	5,868	400	242,380	NA	NA	3.17E-7	242,380	
2	6.6	5,175	200	26,029,000	NA	NA	5.33E-9[4]	26,029,000	20,445,922
6	7.2	6,435	200	12,930,000	NA	NA	6.19E-9[4]	14,537,186[2]	
21	7.4	6,240	200	20,771,580	NA	NA	6.35E-9[4]	20,771,580	
5	6.7	4,519	170	34,724,500	NA	NA	2.30E-9[4]	34,724,500	69,362,250
23	6.8	5,645	170	60,000,000	1.04E+08	9.16E+07	5.37E-10[4]	1.04E+08[3]	
4	6.7	6,602	100	50,000,000	5.49E+09	5.52E+09	9.25E-15[4]	5.49E+09[3]	2.90E+09
13	7.4	5,059	100	50,000,000	3.00E+08	1.04E+11	6.37E-16[4]	3.00E+08[3]	

Notes:
[1]Failure extrapolated. Testing suspended at 58% of initial stiffness at 57,000 due to computer problem.
[2]Software froze, apparently due to error writing to network drive. Sample stiffness 3,439 MPa, at 53.4% of initial stiffness. Result extrapolated using linear regression of latter cycles.
[3]Results extrapolated using single-stage Weibull model.
[4]Less than 8.57E-9 proposed by Shen and Carpenter (*40*) as indicative of long-life pavement.

Table 4.4. Granite 19.0 mm NMAS mix with PG 76-22 at optimum asphalt.

Beam ID	Air Voids, %	Initial Flexural Stiffness, MPa	Micro-Strain	Cycles Tested	Extrapolated Cycles to 50% Initial Stiffness		PV	Cycles to 50% Initial Stiffness	Average Cycles to Failure
					Single-Stage Weibull	Three-Stage Weibull			
4	7.2	3,025	800	42,240	NA	NA	4.02E-06	42,240	26,160
7	6.7	5,445	800	10,080	NA	NA	1.58E-05	10,080	
2	7.1	4,191	400	3,609,470	NA	NA	1.66E-08	3,609,470	1,664,400
8	6.6	4,976	400	591,770	NA	NA	2.87E-07	591,770	
13	7.2	3,675	400	791,960	NA	NA	2.15E-07	791,960	
1	7.3	4637	250	14,837,450	NA	NA	3.30E-08	14,837,450	NA
11	6.8	4148	250	50,000,000	2.91E+09	1.31E+15	2.22E-18[2]	2.91E+09[1]	
5	6.7	4,460	200	50,000,000	2.75E+09	1.53E+11	0.00E+00[2]	2.75E+09[1]	2.72E+09
3	7.1	4,062	200	50,000,000	2.68E+09	2.61E+21	0.00E+00[2]	2.68E+09[1]	

Notes:
[1]Results extrapolated using single-stage Weibull model.
[2]Less than 8.57E-9 proposed by Shen and Carpenter (*40*) as indicative of long-life pavement.

Table 4.5. Granite 19.0 mm NMAS mix with PG 67-22 at optimum plus asphalt.

Beam ID	Air Voids, %	Initial Flexural Stiffness, MPa	Micro-Strain	Cycles Tested	Extrapolated Cycles to 50% Initial Stiffness		PV	Cycles to 50% Initial Stiffness	Average Cycles to Failure
					Single-Stage Weibull	Three-Stage Weibull			
Cox & Sons fixture in Interlaken Load Frame, except as noted									
8	3.0	5,054	800	15,464	NA	NA		15,464	24,982
14	3.2	5,306	800	34,500	NA	NA		34,500	
10	3.2	5,896	400	468,343	NA	NA		468,343	403,232
15	3.3	6,698	400	338,121	NA	NA		338,121	
9	3.4	6,094	200	10,000,000	24,944,621	1.14E+08		24,944,621[1]	62,310,044
4[2]	3.5	6,923	200	38,985,510	NA	NA		38,985,510	
1[3]	3.8	6,219	200	50,000,000	1.23E+08	9.95E+07		1.23E+08[1]	
IPC Global fatigue device									
6	4.7	6,862	800	5,570	NA	NA	4.17E-05	5,570	5,400
3	4.1	7,472	800	5,230	NA	NA	3.99E-05	5,230	
7	5.1	7,675	400	131,390	NA	NA	1.49E-06	131,390	94,615
4	4.9	7,653	400	57,840	NA	NA	6.26E-06	57,840	
2	4.7	7,512	200	3,584,740	NA	NA	1.58E-07	3,584,740	3,584,740
6a	3.3	8,605	100	15,350,090	5.81E+08	NA[4]	NA	5.81E+08[1]	5.81E+08

Notes:
[1]Results extrapolated using single-stage Weibull model.
[2]Testing conducted by Rutgers University on an IPC Global fatigue device.
[3]Tested on Asphalt Institute IPC Global fatigue device.
[4]No solution.

Table 4.6. Granite 19.0 mm NMAS mix with PG 76-22 at optimum plus asphalt.

Beam ID	Air Voids, %	Initial Flexural Stiffness, MPa	Micro-Strain	Cycles Tested	Extrapolated Cycles to 50% Initial Stiffness		PV	Cycles to 50% Initial Stiffness	Average Cycles to Failure
					Single-Stage Weibull	Three-Stage Weibull			
8	3.7	3,520	800	252,450	NA	NA	2.61E-07	252,450[1]	48,050
5	3.0	5,451	800	32,520	NA	NA	3.12E-06	32,520	
14	3.3	5,764	800	63,580	NA	NA	1.09E-06	63,580	
1	2.8	5,532	400	2,860,000	NA	NA	1.17E-08	2,860,000	6,257,500
4	3.0	5,532	400	9,655,000	NA	NA	2.05E-09[3]	9,655,000	
10	3.6	4,308	300	39,624,000	NA	NA	1.71E-09[3]	39,624,000	7.57E+07
2	3.5	5,427	300	8,811,810[4]	4.88E+7	5.63E+09	1.84E-13[3]	4.88E+7[2]	
12	3.5	4,105	300	20,080,750[4]	1.47E+8	2.46E+10	7.33E-17[3]	1.47E+8[2]	
11	4.0	5,162	300	50,000,000	6.75E+7	4.50E+09	1.25E-13[3]	6.75E+7[2]	
13	3.1	6,841	200	50,000,000	5.96E+9	6.79E+11	2.22E-18[3]	5.96E+9[2]	1.85E+10
9	3.1	5,609	200	50,000,000	3.10E+10	1.58E+16	0.00E+00[3]	3.10E+10[2]	

Notes:
[1]Not included in average.
[2]Results extrapolated using single-stage Weibull model.
[3]Less than 8.57E-9 proposed by Shen and Carpenter (*40*) as indicative of long-life pavement.
[4]Sample did not fail, extrapolated using single-stage Weibull model.

PG 67-22 Mix at Optimum Asphalt Content

The results for the PG 67-22 mix tested at optimum asphalt content were presented in Table 4.3. The PG 67-22 mix at optimum asphalt content was tested by NCAT. The extrapolations shown in Table 4.3 are based on the single- and three-stage Weibull functions, as well as the RDEC. Sample 23, tested at 170 ms, produced N_f of 1.04E+08 and 9.16E+07 using the single- and three-stage Weibull functions, respectively. Samples 4 and 13, tested at 100 ms produced extrapolated N_f using the single-stage Weibull function of 5.49E+09 and 3.00E+08, respectively. Although both of these numbers represent extraordinarily long fatigue lives, Table 4.3 indicates that Sample 13 would be expected to have a longer fatigue life. The single-stage Weibull function fits for Samples 4 and 13 was previously presented in Figure 4.4. As shown in Figure 4.4, the slope of the data decreases above approximately 1 million loading cycles, indicating less damage. The best fit line for the Weibull function for Sample 13 has a steeper slope, resulting in the prediction of a shorter fatigue life.

Tsai et al. (*57*) developed a three-stage Weibull function to more accurately model the changes in slope observed in the data. As discussed previously, three regions can be observed with the Weibull function. In the third region, damage can either increase rapidly—leading to failure—or decrease as observed for Sample 13. The three-stage Weibull results for Sample 13 are shown in Figures 4.15 and 4.16. The three-stage Weibull function resulted in N_f predictions of 5.52E+09 and 1.04E+11 for Samples 4 and 13, respectively.

Figure 4.17 shows a log-log plot of cycles to failure versus strain. For samples that did not fail within 50 million cycles, extrapolations are shown using single-stage Weibull, three-stage Weibull, and RDEC. The data from 800 through 170 ms were used to fit the regression line. A fatigue life of 60 million cycles was assigned to Sample 23, tested at 170 ms (the actual number of cycles tested). Ninety-five percent confidence limits are shown for the regression line and 95% prediction intervals are shown from 170 through 50 ms. Although the three-stage Weibull extrapolation of N_f for Samples 23 and 4 fall on the upper prediction limit, the fatigue life estimate at 100 ms for Sample 13 indicates a deviation from the log-log regression line, which in turn indicates the existence of an endurance limit between 100 and 170 ms.

Recall that 170 ms was selected to produce a beam fatigue life of 50 million cycles, or approximately 500 million load repetitions in the field. Based on Sample 23's deviation from the prediction limits in Figure 4.17, this strain level appears to be close to the endurance limit, but slightly high. N_f was substituted in the regression as the predictor for strain level and the regression re-run, resulting in Equation 17, as follows:

$$\varepsilon = 10^{3.54} \times (N)^{-0.170} \quad (17)$$

Ninety-five percent prediction limit, in terms of strain, was calculated for N = 50 million cycles. The lower prediction limit for Equation 17 at 50 million cycles was 151 ms.

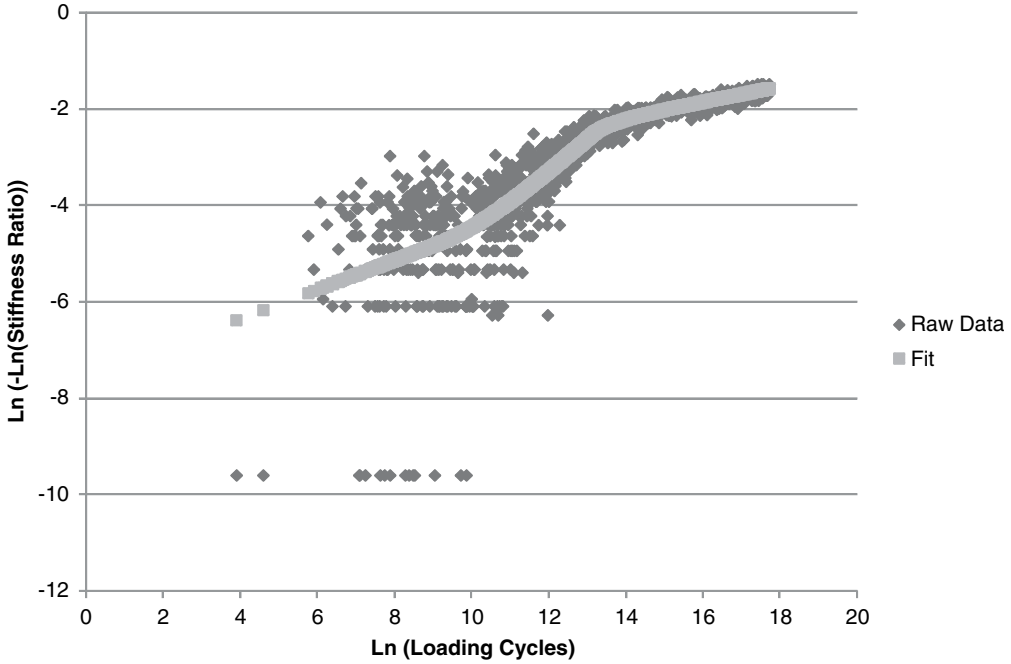

Figure 4.15. Three-stage Weibull function for Sample 13, PG 67-22 at optimum.

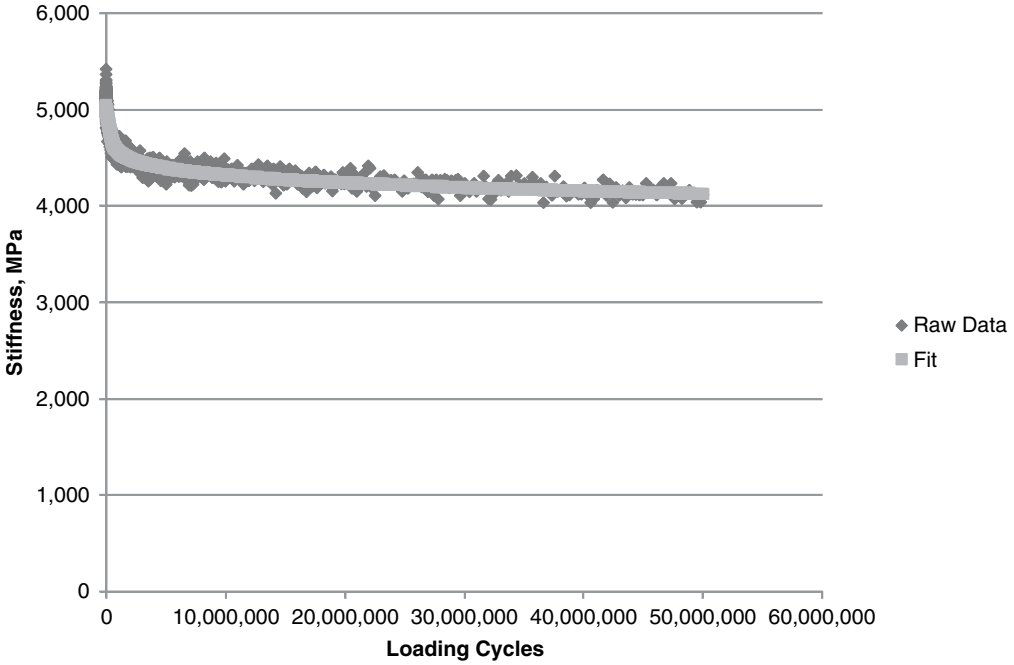

Figure 4.16. Three-stage Weibull fit for Sample 13, PG 67-22 at optimum.

By using the lower prediction limit, the strain level resulting in 50 million cycles should be below the endurance limit for the PG 67-22 mix at optimum asphalt content.

The RDEC plateau values were calculated for each of the PG 67-22 at optimum samples. The results are shown in Table 4.3. The samples tested at 200, 170, and 100 ms produce plateau values lower than the critical value, 8.57E-9 recommended by Shen and Carpenter (*40*) as indicative of long-life pavements. Although all three strain levels appear to provide a long fatigue life, 170 ms appears to be at, or slightly above, the endurance limit based on the other analyses. The recommended plateau value may not define the endurance limit, but rather a long fatigue life.

Figure 4.18 shows the relationship between cycles to failure and plateau value. The relationship for low strain tests developed by Shen and Carpenter (*40*) based on testing 602 beams

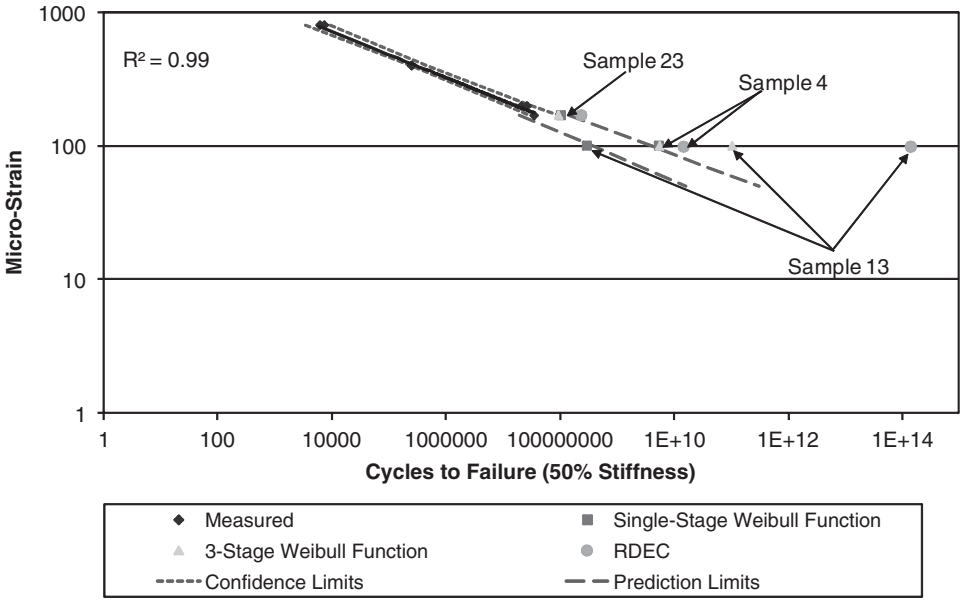

Figure 4.17. Cycles to failure versus strain for PG 67-22 at optimum.

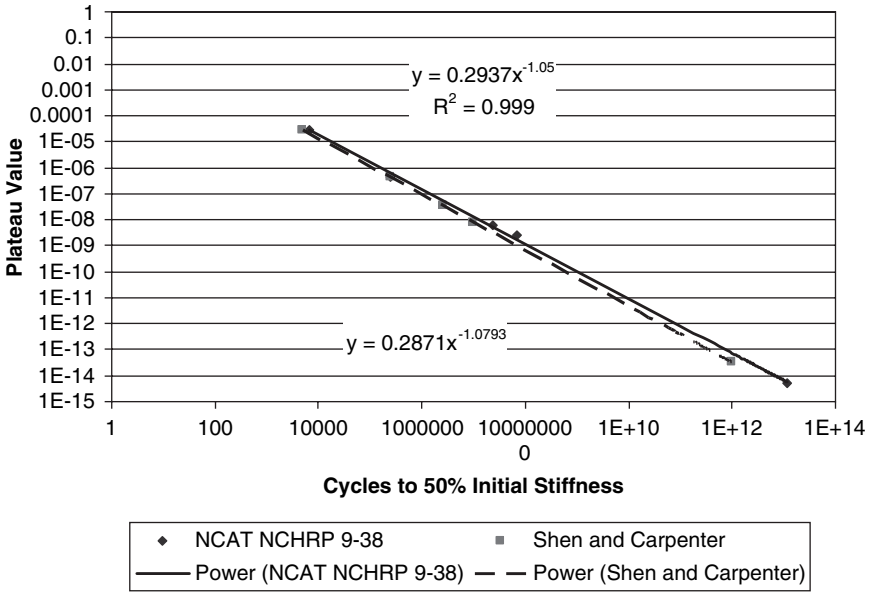

Figure 4.18. Cycles to failure versus plateau value.

is shown for comparison. The relationships are very similar. This would support Shen and Carpenter's proposal that there is one relationship between cycles to failure and plateau value for all mixes, regardless of the manner of testing.

PG 76-22 at Optimum Asphalt Content

The results for the PG 76-22 mix tested at optimum asphalt content were presented in Table 4.4. The PG 76-22 mix at optimum asphalt content was tested by NCAT. The extrapolations shown in Table 4.4 are based on the single-stage Weibull function. Extrapolations were also conducted using the three-stage Weibull function and RDEC. Sample 2 was evaluated as a potential outlier using the repeatability data developed in Phase II. The acceptable difference between two results is estimated to be 0.69 (on a log basis), while the difference between Sample 2 and Sample 13 is 0.66 on a log basis. This indicates that Sample 2 is within acceptable variation.

Sample 2 increased the variability of the data, producing an $R^2 = 0.92$ and resulting in larger prediction and confidence intervals (Figure 4.19). However, both points at 200 ms and one point at 250 ms indicate a deviation from the log-log plot

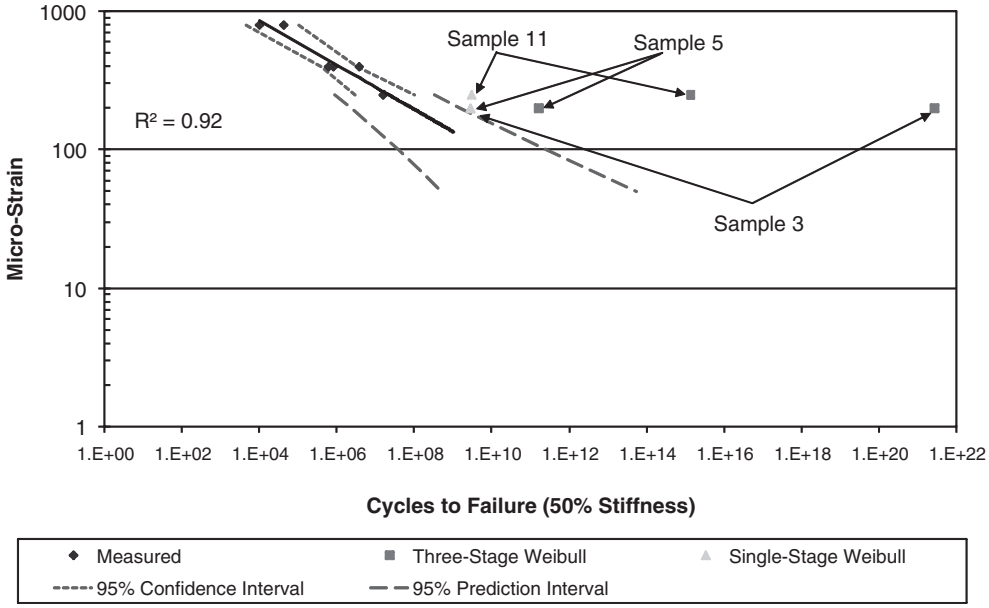

Figure 4.19. Cycles to failure versus strain for PG 76-22 at optimum.

of cycles to failure versus strain, indicative of the endurance limit. Similar to the PG 67-22 results at optimum, the regression was reversed to solve for the strain level that would produce 50 million and 100 million cycles. The lower 95% prediction interval indicated a strain level of 146 ms to produce 50 million cycles to failure. This strain level is slightly lower than that determined for the PG 67-22 at optimum even though the endurance limit appears to be at a higher value (between 200 and 250 ms). This is due to the increased variability in the testing.

One sample at 250 ms and both samples at 200 ms produced plateau values less than the critical value indicated by Shen and Carpenter to be indicative of long fatigue life.

PG 67-22 at Optimum Plus Asphalt Content

Testing for the PG 67-22 mix at optimum plus asphalt content was initially conducted on the Asphalt Institute's Interlaken servo-hydraulic frame using a Cox & Sons fixture. Due to problems with the Interlaken system, low-strain beams were later tested on IPC Global beam fatigue devices operated by both the Asphalt Institute and Rutgers University. Due to concerns about possible differences caused by the various machines, it was decided to retest the cells using the Asphalt Institute's IPC Global beam fatigue device. The initial results from the three machines and the retests using the IPC Global machine were presented in Table 4.5.

The fatigue lives for the retests are significantly shorter than for the original mix. A number of factors appear to contribute to this difference. The initial stiffness for the original set of beams averaged 6,027 MPa; the initial stiffness of the replacement beams averaged 7,435 MPa. The beams were prepared at air voids contents outside of the tolerance for the optimum plus target (3.3 ± 0.5%) and used NCAT's lab stock PG 67-22 binder instead of the dual graded PG 64/67-22 binder, which was used at the NCAT Test Track.

The SHRP A-404 surrogate fatigue model (Equation 18) (*18*) was used to assess whether the differences in initial stiffness and voids filled with asphalt (VFA) would tend to cause the degree of observed difference in the measured fatigue lives. VFA would be lower due to the higher air voids.

$$N_f = 2.738 \times 10^5 \exp^{0.077} VFA\left(\varepsilon_0\right)^{-3.624}\left(S_0''\right)^{-2.720} \quad (18)$$

where,

N_f = fatigue life,
VFA = voids filled with asphalt, percent,
ε_0 = initial strain, and
S_0'' = initial loss stiffness, psi.

Table 4.7 shows the predicted fatigue lives using Equation 18 and the actual and predicted percent difference between the two sets of beams. The SHRP A-404 surrogate fatigue equation fairly accurately predicts the percentage reduction in fatigue life at 800 ms (estimated 70% versus actual 78%). It underestimated the reduction at the lower strain levels. All of the fatigue lives predicted using the SHRP A-404 surrogate model are considerably lower than the measured values. Sensitivity analyses indicated that most of the effect was due to the increased initial stiffness. For the PG 76-22 mixes, initial stiffness increased with the lower air voids determined for the optimum plus samples. Comparisons between the asphalt content and gradation of randomly selected beams indicated no significant differences. There were also no differences in the environmental chamber temperature of measured stiffness of a plastic test beam to support the change in initial stiffness. Therefore, it is felt that the difference in initial stiffness must be attributed to the different binders used to produce the beams.

Figure 4.20 shows a log-log plot of cycles to failure versus strain. Sample 1 from the first set at 200 ms and Sample 6a from the second set at 100 ms show deviations indicative of the endurance limit from their respective best-fit lines. Based on the first data set, the 95% lower prediction interval for a fatigue life of 50 million cycles is 158 ms, which is essentially the same as that determined for the PG 67-22 at optimum (151 ms).

PG 76-22 at Optimum Plus Asphalt Content

The results for the PG 76-22 mix tested at optimum plus asphalt content were presented in Table 4.6. The PG 76-22

Table 4.7. Fatigue life predictions based on SHRP A-404 surrogate model.

Binder	Micro-Strain	Initial Stiffness, psi	VFA	Predicted N_f	Predicted Percent Reduction	Measured Percent Reduction
First Set	800	751,307	76	1,659	70	78
Second Set	800	1,039,502	72	504		
First Set	400	913,317	76	12,027	57	77
Second Set	400	1,111,587	72	5,180		
First Set	200	929,996	76	141,164	52	94
Second Set	200	1,089,540	72	67,442		

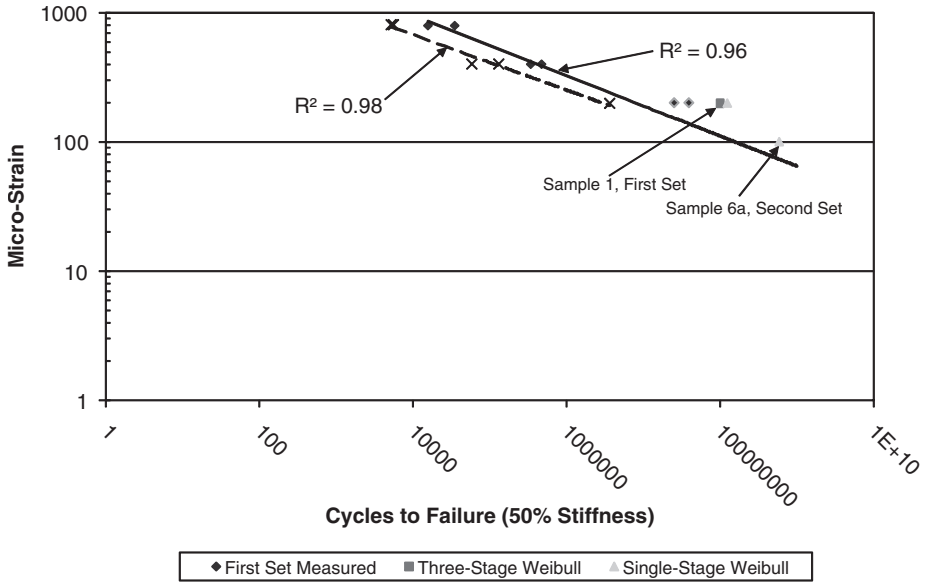

Figure 4.20. Cycles to failure versus strain for PG 67-22 at optimum plus.

mix at optimum asphalt content was tested by NCAT. The extrapolations shown in Table 4.6 are based on the single-stage Weibull function. Extrapolations also were conducted using the three-stage Weibull function and RDEC. Figure 4.21 shows the log-log plot of cycles to failure versus strain. Although a deviation from the regression line is first indicated at 300 ms, particularly for the three-stage Weibull and RDEC extrapolations, it is not clear until 200 ms. The 95% lower confidence limit for the endurance limit using the methodology described in Appendix A is 200 ms. This represents an increase as compared to both the PG 76-22 at optimum and PG 67-22 at optimum plus mixes.

Summary of Phase I Observations Regarding Endurance Limit

Clear indications of the endurance limit were shown for three of four mixes (not PG 67-22 at optimum plus). The strain level corresponding to the endurance limit appears to be mix dependent. Visually, the endurance limit appears to be more sensitive to binder properties than to asphalt content/air void content. An endurance limit (predicted value, not lower prediction interval) of approximately 170 ms was determined for the PG 67-22 mix at optimum asphalt content. The endurance limit for the PG 76-22 mixture appears to be on the order of

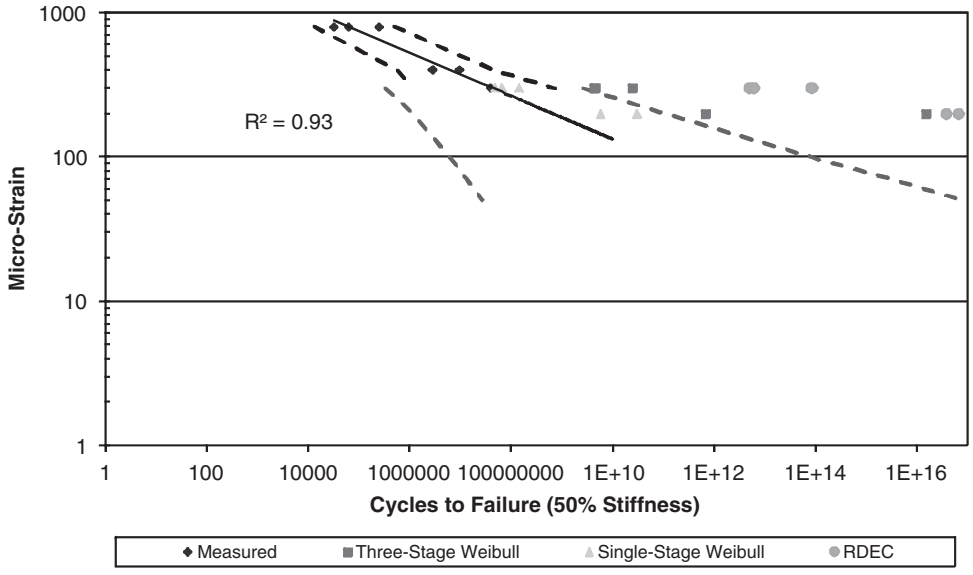

Figure 4.21. Cycles to failure versus strain for PG 76-22 at optimum plus.

Table 4.8. Granite 19.0 mm NMAS mix with PG 58-28 at optimum asphalt.

Sample	Air Voids, %	Initial Stiffness, MPa	Micro-Strain	Cycles Tested	Extrapolation Cycles to 50% Stiffness		Cycles to 50% Stiffness	Average Cycles to Failure
					Single-Stage Weibull	Three-Stage Weibull		
4	6.8	3,216	800	12,730	NA	NA	12,730	10,097
8	7.2	3,014	800	8,730	NA	NA	8,730	
9	7.0	2,974	800	8,830	NA	NA	8,830	
2	6.9	3,372	400	166,290	NA	NA	166,290	183,793
6	7.4	3,424	400	148,090	NA	NA	148,090	
7	7.4	3,424	400	237,000	NA	NA	237,000	
5	7	4,217	76	12,000,000	1.01E+09	1.11E+08	1.01E+09[1]	1.03E+09
15	7	4,332	76	12,000,000	1.57E+09	5.30E+09	1.57E+09[1]	
16	7	4,706	76	12,000,000	5.04E+08	4.39E+09	5.04E+08[1]	

Note:
[1]Extrapolated using single-stage Weibull model.

220 ms, and approximately 300 ms for the PG 76-22 at optimum plus. The plateau value criteria determined by Shen and Carpenter (*40*) appears to be indicative of very long fatigue life, but not necessarily the endurance limit.

The Weibull function appears to be the best technique for extrapolation of low strain stiffness results. One rapid technique for determining the endurance limit may be to test three replicates at each of two strain levels, nominally 800 and 400 ms and then fit a log-log relationship between cycles to failure and strain. Testing additional samples at normal strain levels would potentially reduce the estimate of the standard deviation and therefore increase the confidence in the prediction. The predicted endurance limit for the PG 76-22 mix at optimum asphalt content would most likely benefit from testing additional samples. The lower 95% prediction limit for a fatigue life of 50 million cycles appears to be reasonably close to the endurance limit. This technique was originally presented in the Proposed Standard Practice for Predicting the Endurance Limit of Hot Mix Asphalt (HMA) for Long-Life Pavements in Appendix A. This technique was used for the testing conducted in Phase II. Appendix A was later modified in an effort to obtain a more accurate estimate of the endurance limit.

Phase II Testing to Investigate Additional Binder Grades

Testing was conducted in Phase II to evaluate additional binder grades. The 19.0 mm NMAS granite test track mix was replicated using a true grade PG 64-22 and PG 58-28. Three beams were tested at 800 ms and three beams were tested at 400 ms for each mixture. The fatigue testing was conducted by NCAT. The endurance limit was estimated using the one-sided 95% lower prediction interval for a strain level corresponding to 50 million cycles according to the methodology described in Appendix A. The lower 95% prediction intervals were 82 and 75 ms, respectively, for the PG 58-28 and PG 64-22 mixtures. Confirmation tests for the endurance limit of the mixture using the PG 58-28 binder were carried out at 76 ms due to an error in the t-value used in determining the lower prediction limit. The tests should have been carried out at 82 ms. The test data is presented in Tables 4.8 and 4.9 and shown graphically in Figures 4.22 and 4.23.

For the PG 58-28 mixture, the single-stage Weibull extrapolations for the samples tested at 76 ms indicate fatigue lives that are longer than that predicted from the log-log regression,

Table 4.9. Granite 19.0 mm NMAS mix with PG 64-22 at optimum asphalt.

Sample	Air Voids, %	Initial Stiffness, MPa	Micro-Strain	Cycles Tested	Extrapolation Cycles to 50% Stiffness		Cycles to 50% Stiffness	Average Cycles to Failure
					Single-Stage Weibull	Three-Stage Weibull		
5	7.5	3,635	800	5,580	NA	NA	5,580	5,377
6	7.5	3,736	800	5,060	NA	NA	5,060	
8	7.5	4,234	800	5,490	NA	NA	5,490	
2	7.3	4,666	400	98,120	NA	NA	98,120	95,377
4	7.5	4,449	400	111,250	NA	NA	111,250	
9	7.4	4,227	400	76,760	NA	NA	76,760	
3	6.6	5,190	75	12,000,000	8.18E+10	1.08E+09	8.18E+10[1]	3.95E+10
7	6.7	4,667	75	12,000,000	3.64E+10	3.18E+08	3.64E+10[1]	
10	6.7	5,989	75	12,000,000	2.82E+08	2.82E+08	2.82E+08[1]	

Note:
[1]Extrapolated using single-stage Weibull model.

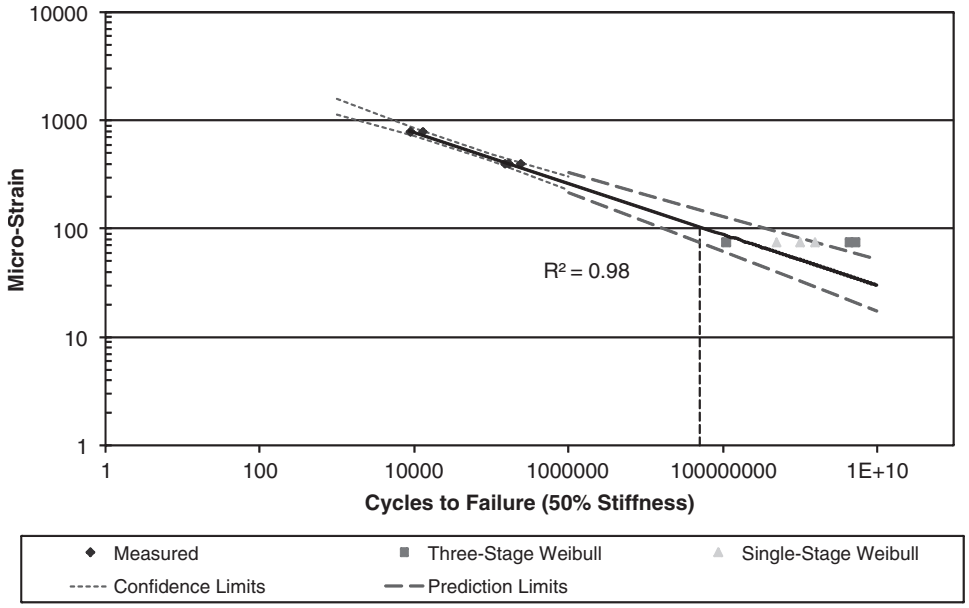

Figure 4.22. Cycles to failure versus strain for PG 58-28 at optimum asphalt content.

but within the prediction limits for the extrapolation. Two of the three-stage Weibull extrapolations exceed the prediction limits, but Sample 16 indicates a shorter fatigue life.

The single- and three-stage Weibull fatigue life extrapolations for the PG 64-22 mixture samples exceeded the fatigue lives estimated from the log-log plot of cycles to failure versus strain. The extrapolated fatigue lives also exceeded the prediction limits for the log-log regression line. This is a clear indication of the endurance limit.

In general, the predicted endurance limits for the PG 58-28 and PG 64-22 binders were lower than what might have been expected based on the Phase I testing. Historically, softer binders are believed to perform better in constant strain tests (see Table 2.1).

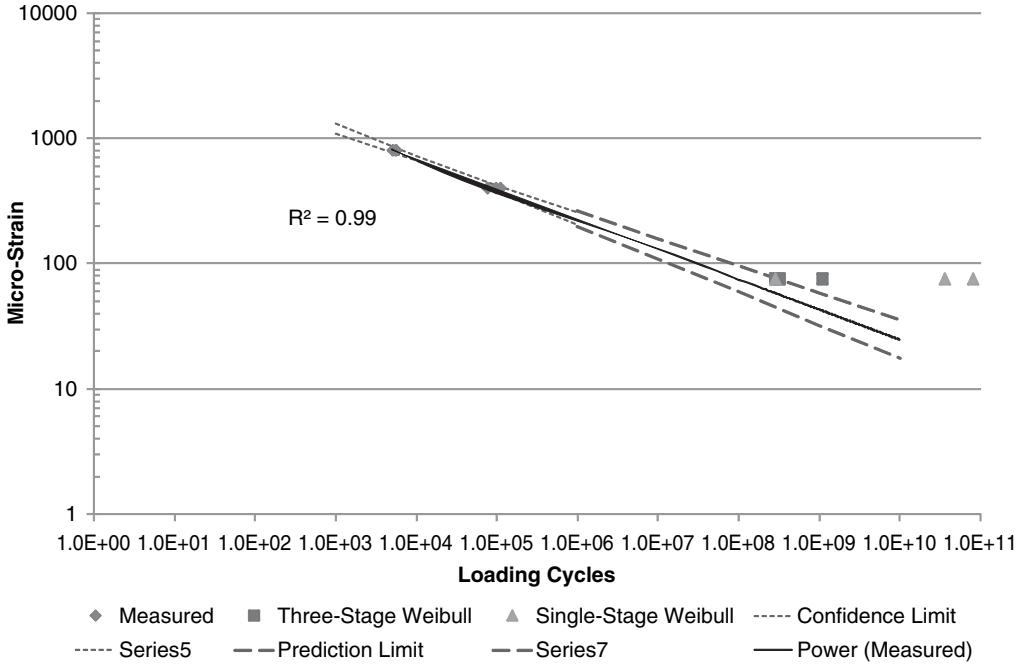

Figure 4.23. Cycles to failure versus strain for PG 64-22 at optimum asphalt content.

Estimate of Precision of Beam Fatigue Tests

In Phase II, a small-scale round-robin was conducted to develop precision estimates for the beam fatigue test and the extrapolation procedures. ASTM C802 recommends a minimum of 10 labs for a round-robin study. Due to the testing time commitments involved with beam fatigue testing, only five laboratories, three represented by the research team, and two volunteers, participated. The volunteer labs only tested one mix at three strain levels. The experimental matrix for the mini round-robin is shown in Table 4.10.

Variability is expected to consist of four components: materials, sample preparation, beam testing, and analysis. To minimize materials variability, NCAT prepared and batched all of the aggregates. SEM Materials and the University of California participated on a voluntary basis.

The directions provided for preparation of the test samples are presented in Appendix F. Each lab mixed and compacted their own beams for testing. The aggregate batches were randomized prior to shipping. In some cases, however, additional batches were required in order to obtain beams with the appropriate air void levels. The samples were short-term oven aged for 4 h at 275°F (135°C) according to AASHTO R30 prior to compaction. The range of equipment used to compact the beams included linear kneading compactors, vibratory compactors, and rolling wheel compactors.

Testing was conducted in accordance with the draft practice for the determination of the endurance limit, which has since been modified (Appendix A). Fatigue lives were also extrapolated using the logarithmic and RDEC described in Appendix C. Each lab first tested three beams each at 800 and 400 ms. Extrapolations were conducted using each lab's data to estimate the endurance limit. The average estimated endurance limit for all of the participating labs was determined. Using a single strain level for the endurance limit allowed repeatability and reproducibility calculations to be performed on the fatigue life extrapolations. Each lab then tested three beams at the average estimated endurance limit to 12 million cycles. Low strain beams were not tested for the PG 67-22 mix at optimum plus. The average estimated endurance limits were 151, 175, and 188 ms, respectively, for the PG 67-22 at optimum, PG 67-22 at optimum plus, and PG 76-22 at optimum asphalt content mixes. The strain levels used for the beams tested to evaluate the low strain extrapolations were 130 and 220 ms, respectively, for the PG 67-22 and PG 76-22 mixes at optimum asphalt content. The differences arose since not all labs had reported their data when the confirmation strain levels were selected.

The round-robin data were analyzed according to ASTM E691. When analyzing round-robin data, it is desirable to have a constant standard deviation or constant coefficient of variation at the various test (strain) levels. To achieve this, the precision estimates are based on the log base 10 of the actual test results. This is reasonable since fatigue transfer functions utilized in pavement design are logarithmic.

Three potential outliers were identified based on the h and k statistics utilized in ASTM E691. Only one outlier was removed from the data set, Lab 2's results for the PG 67-22 at optimum asphalt content samples tested at 120 ms and extrapolated using the logarithmic model.

The precision estimates, without the outlier, are presented in Tables 4.11 and 4.12 for the normal strain and extrapolated data, respectively. The complete data are presented in Appendix D. An examination of Table 4.11 suggests that the repeatability and reproducibility standard deviations for the normal strain tests are consistent for the different mixes and strain levels. Based on the data in Table 4.11, the log of two properly conducted tests by the same operator should not differ by more than 0.69 with 95% confidence. Similarly, the log of two properly conducted normal strain tests by two different laboratories should not differ by more than 0.89.

For the extrapolation methods shown in Table 4.12, the single-stage Weibull function produces the least variable results, followed by the logarithmic model. The RDEC procedure produces the most variable results. The use of the unique plateau value versus cycles to failure line proposed in Appendix C appeared to create erroneously low fatigue lives with one of the data sets and exceptionally long lives with one of the other lab's data. Based on the potential for overestimating fatigue life and the associated variability in calculation, the RDEC model is not recommended for extrapolating endurance limit data.

Table 4.10. Mini round-robin testing matrix.

Lab/Mix	PG 67-22 at Optimum	PG 67-22 at Optimum Plus	PG 76-22 at Optimum
NCAT	X	X	X
Asphalt Institute	X	X	X
University of Illinois	X	X	X
SEM Materials	X		
University of California	X		

Table 4.11. Summary of normal strain round-robin results.

Code	No. of Labs	Log of Average of All Labs	Standard Deviation between Log of Cell Averages (S_x)	Repeatability Standard Deviation (S_r)	Reproducibility Standard Deviation (S_R)	Between-Lab Standard Deviation of Log of Lab Means (S_L)	Within-Lab Coefficient of Variation, %	Between-Lab Coefficient of Variation, %
PG 67-22 Opt. at 800 ms	7	3.876	0.220	0.249	0.300	0.167	6.4	7.7
PG 67-22 Opt. at 400 ms	7	5.370	0.365	0.240	0.414	0.338	4.5	7.7
PG 76-22 Opt. at 800 ms	3	3.932	0.127	0.261	0.261	0.000	6.6	6.6
PG 76-22 Opt. at 400 ms	3	5.624	0.299	0.295	0.384	0.246	5.2	6.8
PG 67-22 Opt.+ at 800 ms	3	4.203	0.107	0.207	0.207	0.000	4.9	4.9
PG 67-22 Opt.+ at 400 ms	3	5.717	0.134	0.243	0.243	0.000	4.2	4.2
Pooled			0.234	0.248	0.318	0.164	5.4	6.8

Indirect Tensile Strength as a Surrogate for Endurance Limit Determination

Indirect Tensile Strength (IDT)—or, more correctly, the tensile strain at failure from the IDT test—was examined as a surrogate for beam fatigue tests to identify the fatigue endurance limit. The Asphalt-Aggregate Mixture Analysis System (AAMAS) used a mixture's resilient modulus and tensile strain at failure from the IDT test to assess fatigue resistance (*59*). In the AAMAS system, testing was conducted at the following three temperatures: 5°C, 25°C, and 40°C. The measured resilient modulus and tensile strain at failure were compared to the properties of a "standard" mix, the dense-graded mix used at the AASHO Road Test. Von Quintus (*personal communication*) suggested that long-life pavements be designed with tensile strains at the bottom of the asphalt layer that were < 1% of the tensile strain at failure. Maupin and Freeman (*9*) demonstrated satisfactory correlations between constant strain fatigue-life curves and indirect tensile test results.

Samples of the PG 67-22 mixtures at optimum and optimum plus asphalt content and PG 76-22 mixtures at optimum and optimum plus asphalt content were compacted in the Superpave Gyratory Compactor (SGC) for IDT testing to the same air void levels used for the beam fatigue tests. The samples were tested in the IDT at 25°C. Testing was conducted according to AASHTO T322. Tensile strain was calculated as described by Kim and Wen (*60*). Strain was calculated at 98% of the peak stress, and the results are shown in Figure 4.24 versus the predicted and 95% lower confidence limits for the endurance limit determined from the beam fatigue tests. From Figure 4.24, it is apparent the predicted and 95% lower confident interval for the endurance limit are approximately 5 and 3%, respectively, of the indirect tensile failure strain. However, although the indirect tensile test appears to be sensitive to the two different binders, it does not appear to be sensitive to binder content. This procedure appears to have some potential to predict the magnitude of the endurance limit. Additional work is necessary with a broader range of materials.

Table 4.12. Summary of round-robin extrapolations at the estimated endurance limit.

Code	Number of Labs	Log of Average of All Labs	Standard Deviation between Log of Cell Averages (S_x)	Repeatability Standard Deviation (S_r)	Reproducibility Standard Deviation (S_R)	Between-Lab Standard Deviation of Log of Lab Means (S_L)	Within-Lab Coefficient of Variation, %	Between-Lab Coefficient of Variation, %
Logarithmic								
PG 67-22 Opt. at 130 ms	5	10.609	1.642	1.322	1.965	1.454	12.5	18.5
PG 76-22 Opt. at 220 ms	3	8.209	0.441	1.207	1.207	0.000	14.7	14.7
Pooled			1.192	1.279	1.681	0.909	13.3	17.1
Weibull								
PG 67-22 Opt. at 130 ms	5	8.794	0.915	0.586	1.032	0.850	6.7	11.7
PG 76-22 Opt. at 220 ms	3	7.563	0.309	0.719	0.719	0.000	9.5	9.5
Pooled			0.688	0.636	0.915	0.531	7.7	10.9
RDEC								
PG 67-22 Opt. at 130 ms	4	10.275	3.421	2.341	3.919	3.143	22.8	38.1
PG 76-22 Opt. at 220 ms	3	9.607	0.967	2.151	2.151	0.000	22.4	22.4
Pooled			2.369	2.259	3.161	1.796	22.6	31.4

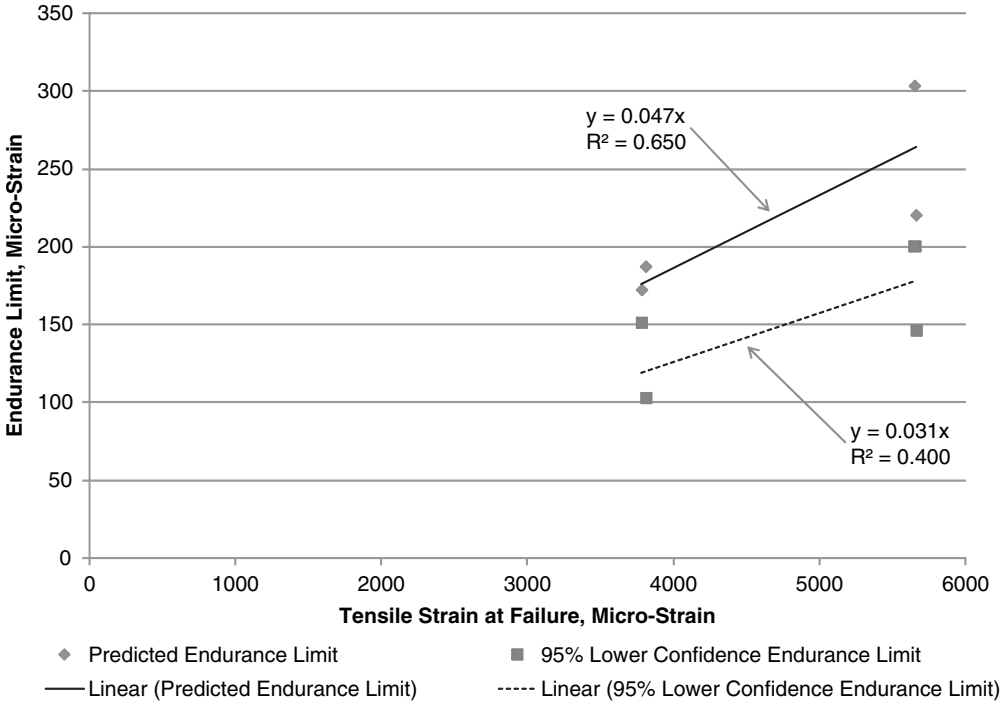

Figure 4.24. IDT tensile strain at failure versus beam fatigue endurance limit.

CHAPTER 5

Uniaxial Tension Results and Analyses

The testing performed at the University of New Hampshire (UNH) includes complex modulus, monotonic, and fatigue tests in uniaxial tension. Analysis of the data is done using viscoelastic and continuum damage mechanics principles to identify the fatigue endurance limit of the PG 67-22 optimum, PG 67-22 optimum plus, PG 76-22 optimum, and PG 76-22 optimum plus mixtures. Frequency sweeps at various temperatures are run to measure the complex dynamic modulus of each mix. The dynamic modulus and phase angle master curves are then constructed from these data and the relaxation master curve is obtained through linear viscoelastic conversion. The damage characteristic curve of each mix is obtained by running uniaxial monotonic tests to failure or by running constant amplitude fatigue tests to failure. The characteristic damage curve is used to predict the number of cycles to failure at different strain amplitudes to determine the fatigue endurance limit of the mixture.

Fatigue tests with increasing strain amplitude are run in uniaxial tension to directly identify the fatigue endurance of the mixtures. The testing and analysis procedures are described in the following sections, starting with the dynamic modulus tests, followed by monotonic tests, fatigue tests, and finally the prediction of endurance limit.

Test Specimens

A summary of the air void content and testing performed on each specimen at UNH is shown in Table 5.1. All test specimens were fabricated at NCAT using an SGC and shipped to UNH, where they were cut and cored to 75-mm diameter, 150-mm tall specimens. Steel plates were glued to the ends of the uniaxial specimens using plastic epoxy glue in a gluing jig designed to align the specimen vertically. Four LVDTs spaced 90° apart around the circumference of the specimen were attached to the surface of the specimen using a 100-mm gage length.

Dynamic Modulus and Phase Angle Master Curves

Uniaxial complex modulus tests were performed on at least three specimens from each mixture. The testing was done at the following five temperatures: −10°C, 0°C, 10°C, 20°C, and 30°C and at eight frequencies: 0.1, 0.2, 0.5, 1, 2, 5, 10, and 20 Hz.

The dynamic modulus and phase angle values at each frequency and temperature were calculated from stresses and LVDT measured strains. The individual dynamic modulus curves were shifted along the frequency axis to construct the dynamic modulus master curve using the time-temperature superposition principle. The reference temperature was selected as 20°C. The resulting master curve for dynamic modulus ($|E^*|$) is expressed by the following sigmoidal equation:

$$\log|E^*| = a + \frac{b}{1+\exp\left(-c - d\log f_r\right)} \tag{19}$$

where,

a, b, c, and d are positive regression coefficients.

The term f_r represents the reduced frequency, given by

$$\log f_r = \log f + \log a_T \tag{20}$$

where,

a_T is the shift factor which is a function of temperature and
f is the actual frequency at which the individual curves are obtained.

The solver function in Microsoft Excel is used to simultaneously determine the sigmoidal fit coefficients and the shift factors for the individual specimens using error minimization. An overall mixture master curve is determined by fitting the sigmoidal function in Equation 19 to all of the individual specimen master curves. Figures 5.1 through 5.4 show the individual and overall dynamic modulus master

Table 5.1. Summary of specimens and tests conducted.

Mix	Specimen No.	Air Voids % (After Core and Cut)	|E*| Test	Monotonic Test	Fatigue Test		Comments
					Constant Amplitude	Increasing Amplitude	
PG 67-22, Optimum	1	8.6					Broke during |E*| testing
	2	7.0	X				
	3	7.3					Broke during |E*| testing
	4	7.3	X				
	5	7.5	X				
	6	6.8	X				
	7	7.7	X				
	8	7.2	X				
	9	7.7	X				
	10	7.5	X				
	11	7.7	X	X			
	12	7.0					Broke during |E*| testing
	13	7.7	X	X			
	14	6.9			X		
	15	6.9				X	
	16	6.7			X		
	17	6.7				X	
	18	6.6				X	
PG 76-22, Optimum	1	6.5					Broke during |E*| testing
	2	6.9	X	X			
	3	6.1	X	X			
	4	7.0	X	X			
	5	6.2	X	X			
PG 67-22, Optimum+	1	2.2	X			X	
	2	1.5	X			X	
	3	2.2	X	X			Monotonic test data not usable
	4	1.3	X	X			
	5	2.1	X	X			
	6	3.6	X			X	
	7	3.6					Broke during |E*| testing
	8	2.7	X			X	
	9	3.0					Broke during |E*| testing
	10	3.0	X			X	
PG 76-22, Optimum+	1	1.5	X			X	
	2	1.3	X				
	3	1.9	X			X	
	4	1.2	X	X			
	5	1.0					Broke during |E*| testing
	6	3.1	X			X	
	7	3.2	X			X	
	8	2.7	X			X	
	9	3.7	X			X	
	10	2.8	X			X	

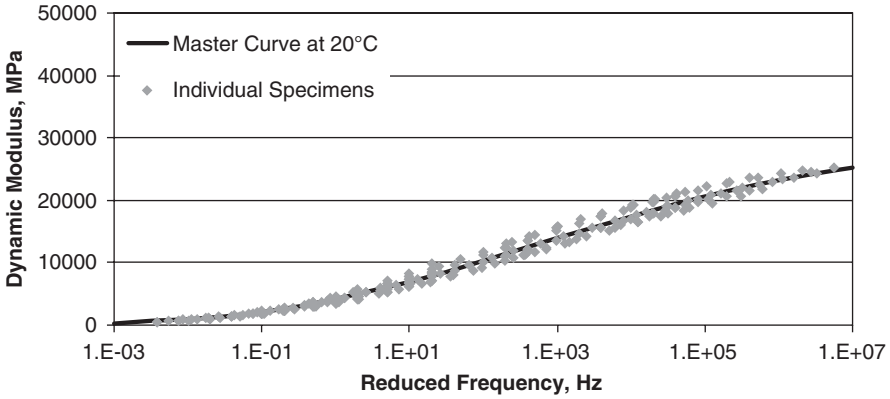

Figure 5.1. Dynamic modulus master curves for PG 67-22 optimum.

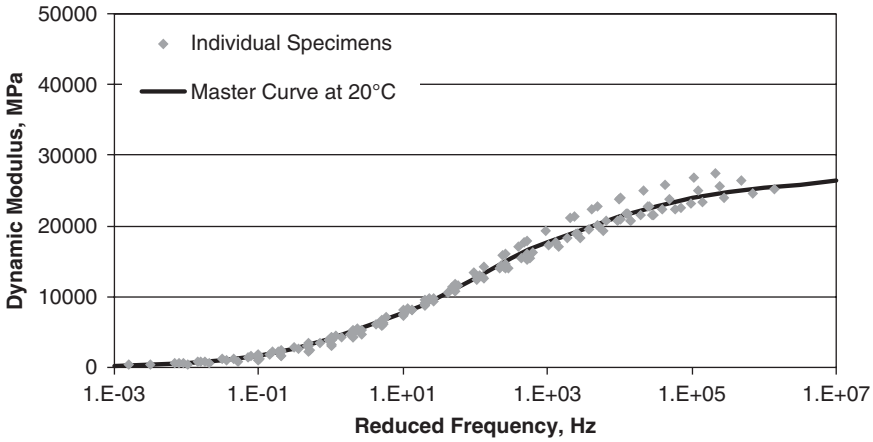

Figure 5.2. Dynamic modulus master curves for PG 76-22 optimum.

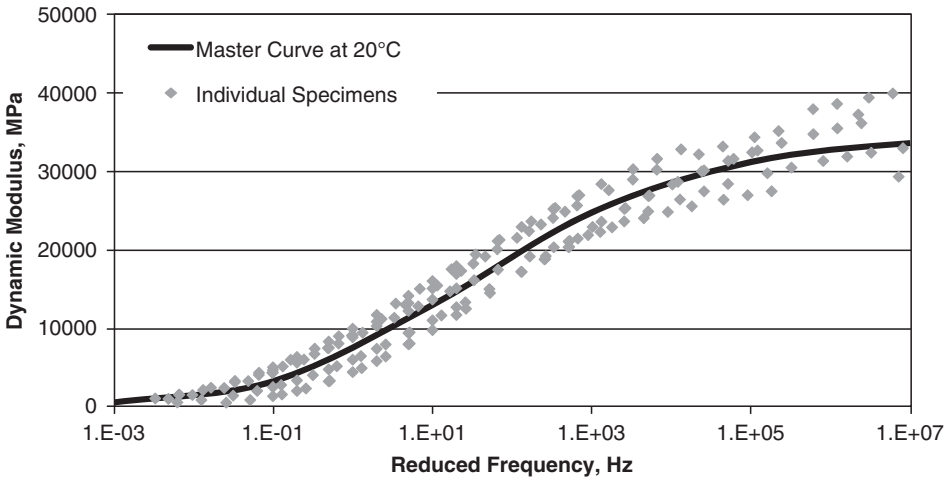

Figure 5.3. Dynamic modulus master curves for PG 67-22 optimum plus.

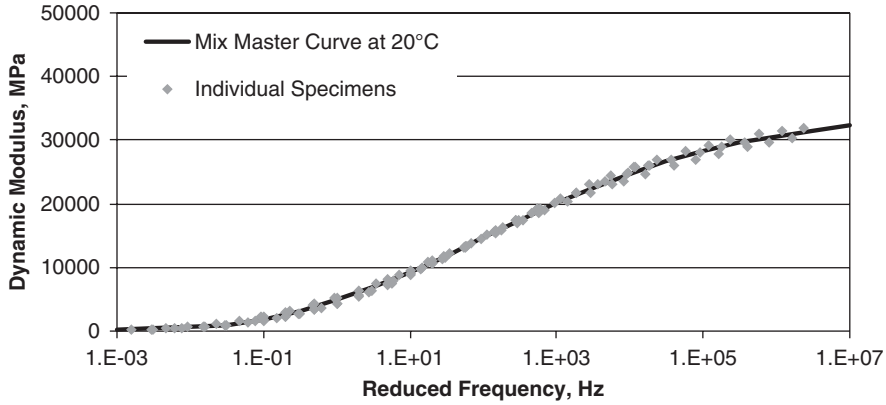

Figure 5.4. Dynamic modulus master curves for PG 76-22 optimum plus.

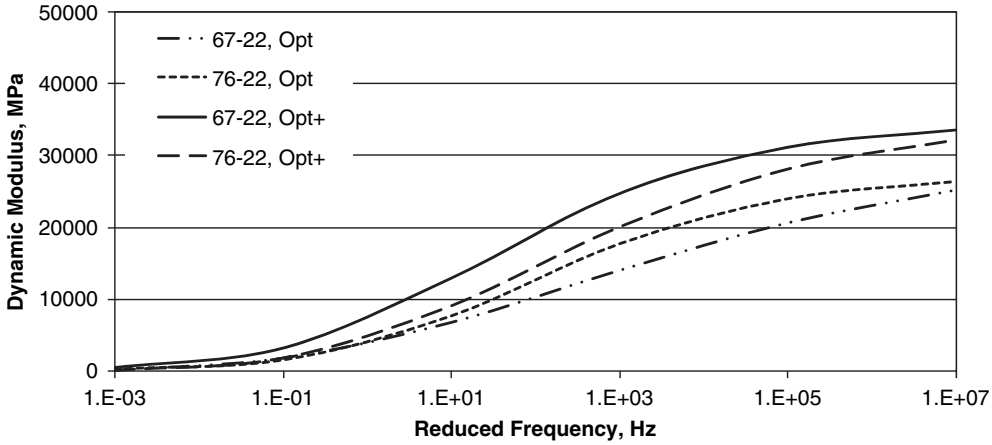

Figure 5.5. Dynamic modulus master curves for all mixes tested.

curves obtained for the four mixtures. Figure 5.5 shows the overall dynamic modulus curves (obtained from fit) for all four mixtures together.

The shift factors determined from the dynamic modulus master curves were then used to shift the individual phase angle curves at each temperature to obtain the phase angle master curve for each specimen. The phase angle master curves are fit with a sigmoidal function of the form in Equation 19. Figures 5.6 through 5.9 show the individual and overall phase angle master curves for individual mixtures. Figure 5.10 shows the overall phase angle master curves for all four mixtures together.

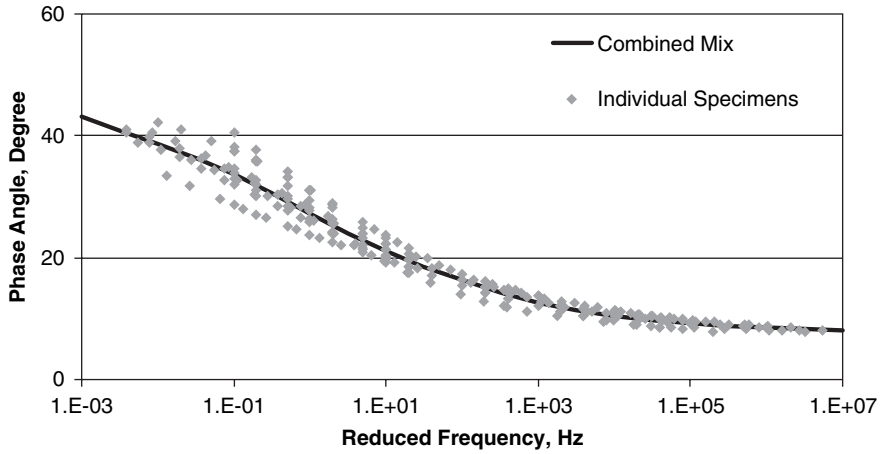

Figure 5.6. Phase angle master curves for PG 67-22 optimum.

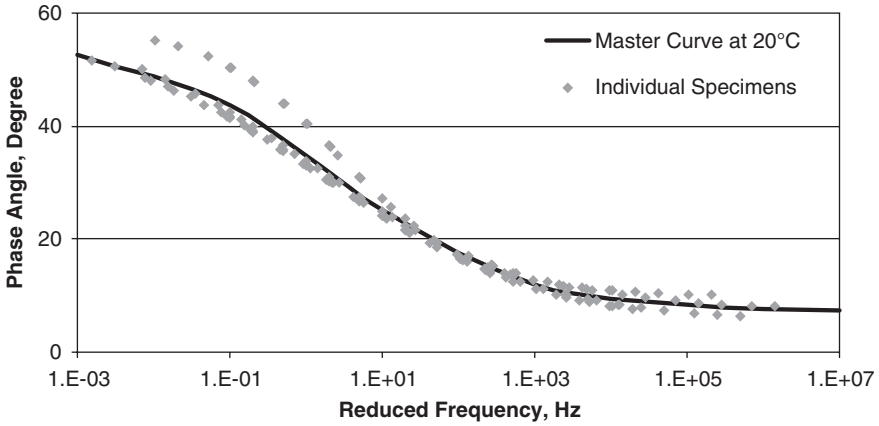

Figure 5.7. Phase angle master curves for PG 76-22 optimum.

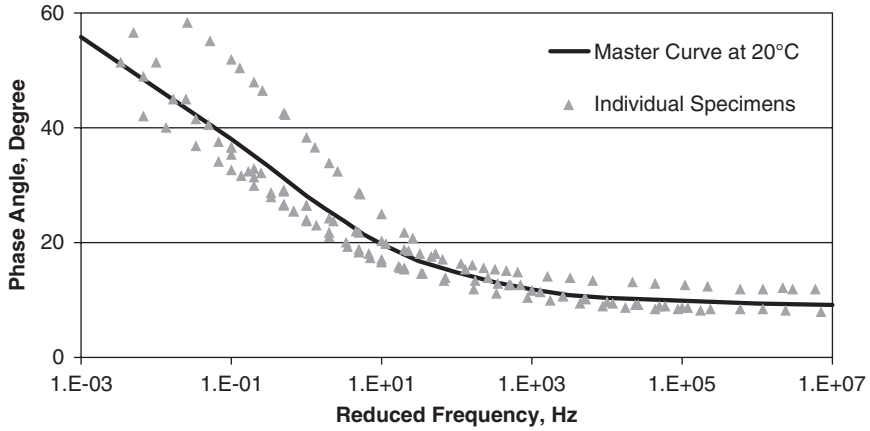

Figure 5.8. Phase angle master curves for PG 67-22 optimum plus.

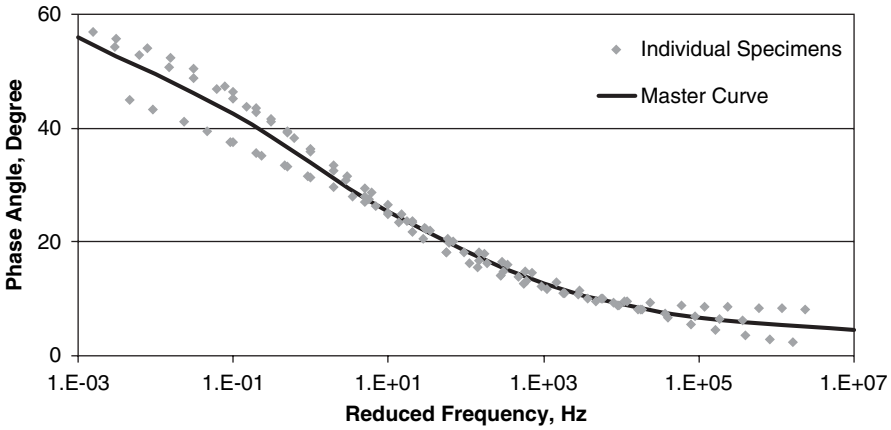

Figure 5.9. Phase angle master curves for PG 76-22 optimum plus.

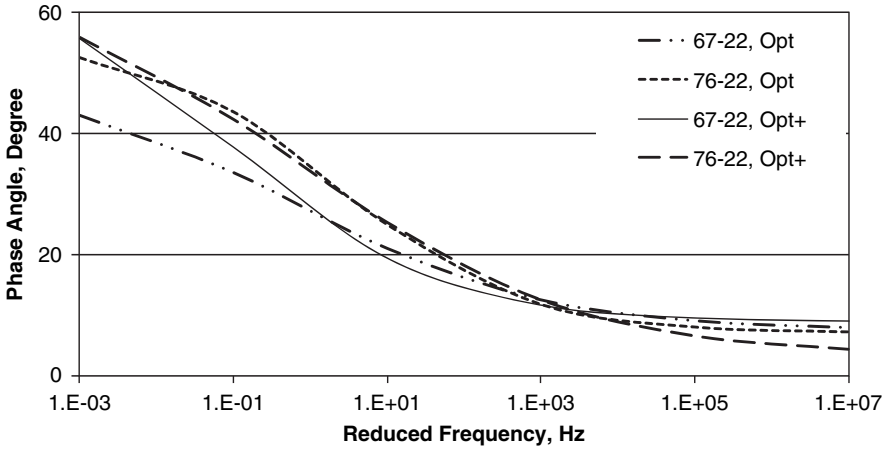

Figure 5.10. Phase angle master curves for all mixes tested.

Damage Characteristic Curve

The characteristic curve for a mixture describes the relationship between C, which is normalized pseudo stiffness calculated through viscoelastic theory, and S, which is the damage parameter calculated from continuum damage mechanics theory. Practically, C can be thought of as the material's integrity at any point in time and S as the level of damage over time. As the amount of damage in the material increases, the material integrity decreases. A mixture's characteristic curve can be constructed from monotonic or cyclic tests. The steps involved in the construction of the characteristic curves are described in Appendix E.

Monotonic Testing

Figures 5.11 through 5.14 show the characteristic curves obtained from on-specimen LVDTs for each individual mixture tested under monotonic loading. The individual specimen data are fit using both a generalized power model and an exponential model (*60, 61*), given in Equations 21 and 22, respectively.

$$C = 1 - C_{11}(S)^{C_{12}} \tag{21}$$

$$C = e^{-kS} \tag{22}$$

where,

C_{11}, C_{12}, and k are regression coefficients (hereafter referred to as damage curve coefficients) obtained by ordinary least squares technique.

The generalized power law does a better job fitting the actual data obtained from the tests. Figures 5.15(a) and (b) show the characteristic curve fits for all mixtures obtained using the generalized power model and exponential model, respectively. The behavior of the PG 76-22 optimum plus mixture appears to be significantly different from the other mixtures; the curve for this mixture only represents one specimen, so more testing

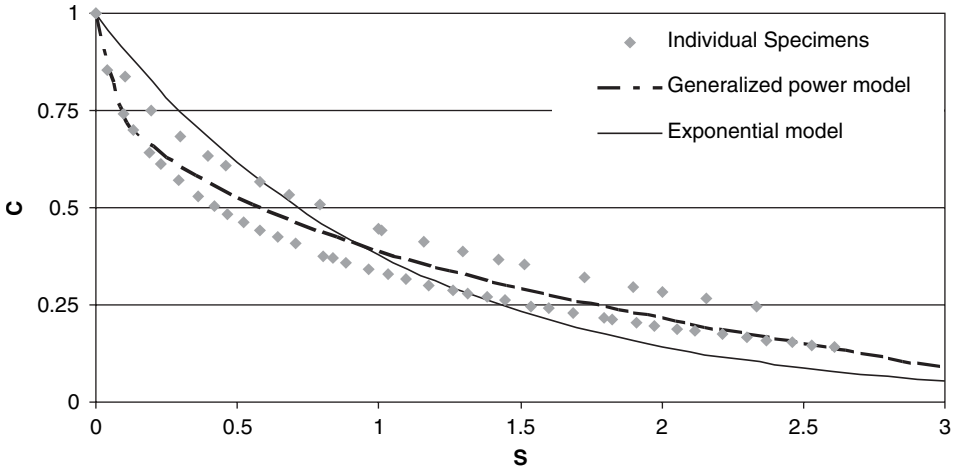

Figure 5.11. Characteristic curves using on-specimen LVDTs for different strain rates for PG 67-22 optimum.

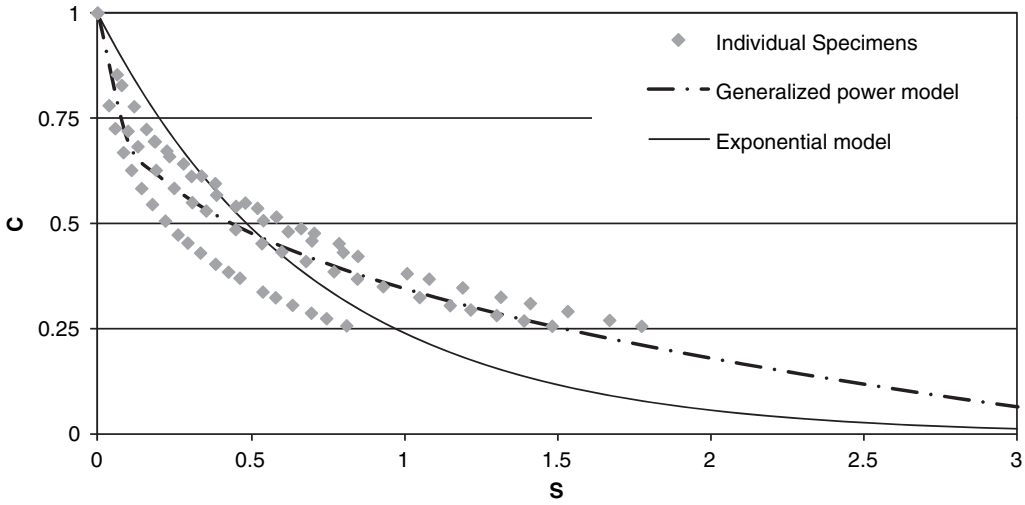

Figure 5.12. Characteristic curves using on-specimen LVDTs for PG 76-22 optimum.

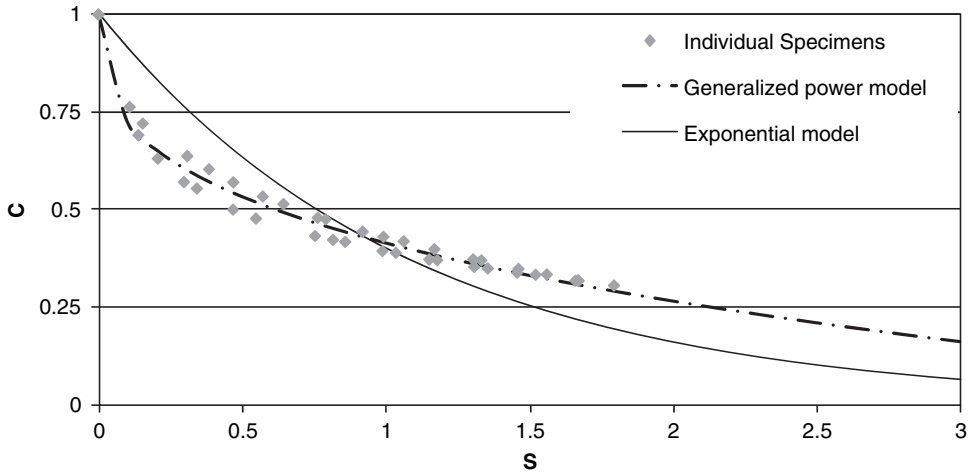

Figure 5.13. Characteristic curves using on-specimen LVDTs for PG 67-22 optimum plus.

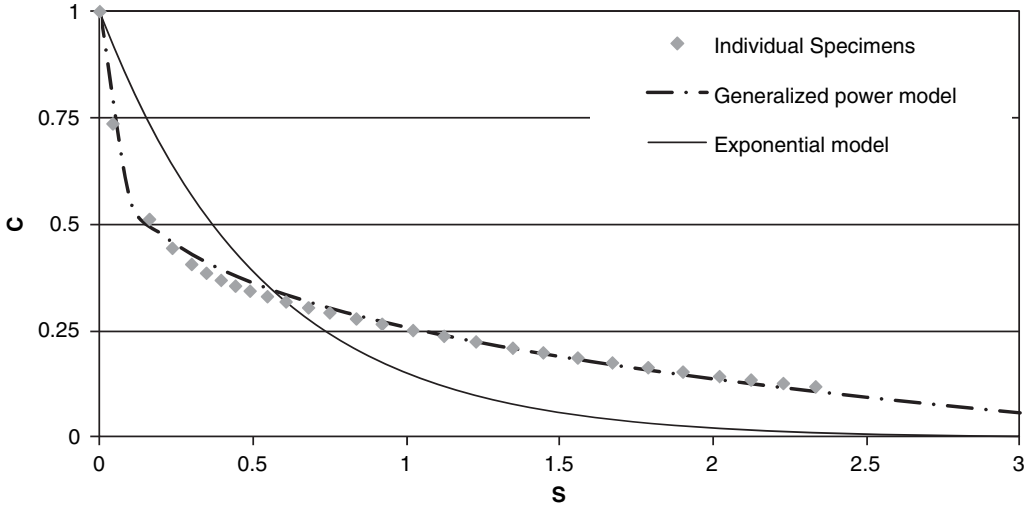

Figure 5.14. Characteristic curves using on-specimen LVDTs for PG 76-22 optimum plus.

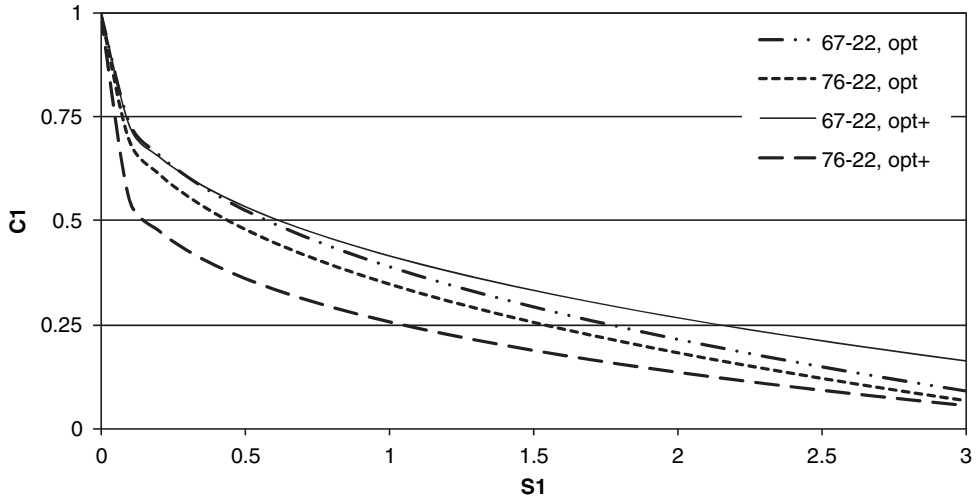

(a) Generalized power model

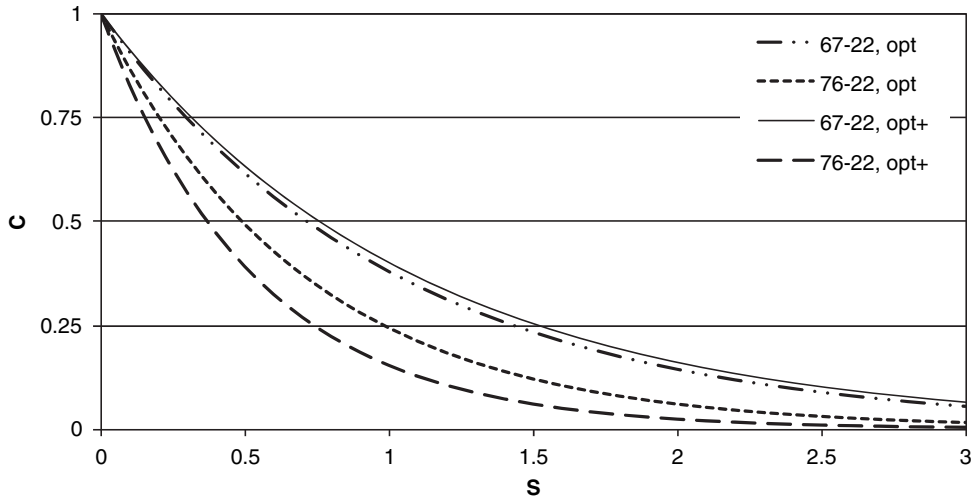

(b) Exponential model

Figure 5.15. Overall characteristic curves using on-specimen LVDTs for all mixtures tested under monotonic loading.

must be done to determine if this is representative behavior or a problem with the one test specimen.

Initially, specimens failed near the end plates during monotonic tests, which is likely due to the presence of high air void content at the ends of the specimens. The specimens were shortened by cutting more material from the top and bottom. This was successful in producing failure in the middle of the specimens. In addition to making shorter specimens, LVDTs were located plate to plate along with the on-specimen LVDTs during the monotonic tests (two on-specimen and two plate-to-plate LVDTs). The advantage of using the plate-to-plate LVDTs is that the material response can be captured even if the specimens fail outside the on-specimen LVDT gage length.

Monotonic tests performed at various strain rates can be used to investigate whether there is any significant effect of plasticity in the mixture behavior. If there is a significant portion of viscoplastic strain in the material response, the C versus S curves will be different for the various strain rates. Figures 5.16(a) and (b) show the C versus S curves at different strain rates measured using the on-specimen and plate-to-plate LVDTs, respectively. It can be seen from these figures that the curves for the various strain rates fall on top of each other except for the plate-to-plate curve for Specimen 10. There are some issues related to the strain data obtained from plate-to-plate LVDTs for this specimen. Thus, the data for the remaining specimens indicates that the effect of viscoplasticity in the monotonic test results is not significant.

Fatigue Testing

A total of five specimens of PG 67-22 optimum were tested under cyclic fatigue loading using four on-specimen LVDTs. The testing was performed at 20°C by controlling the cross-head displacements. Haversine waveforms were applied to the

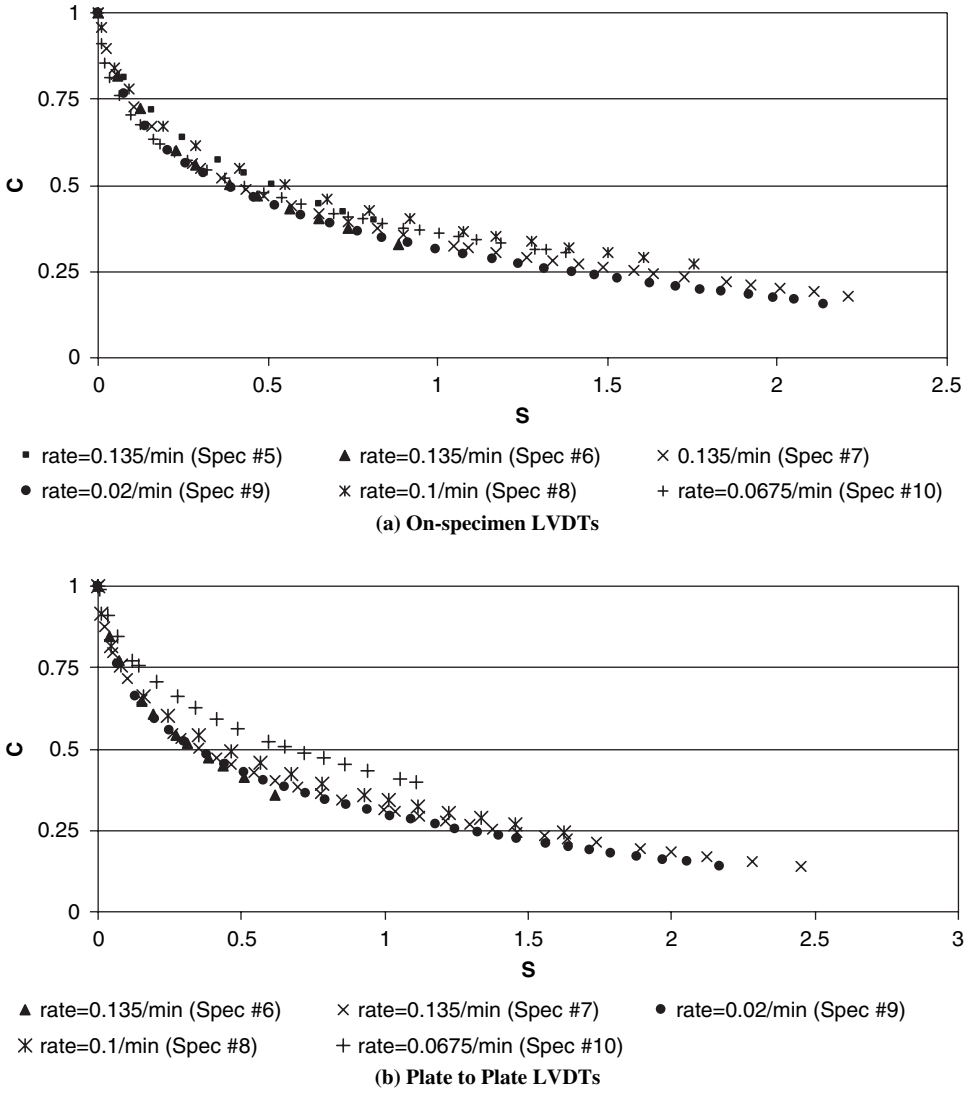

Figure 5.16. C versus S curves at different strain rates for PG 67-22 optimum specimens.

specimen until failure occurred. Table 5.2 summarizes the fatigue testing. Specimen 17 was the first specimen tested. The research team anticipated that the specimen would fail within 10,000 cycles, so the test was halted after about 26,000 cycles to determine what was happening. Due to machine compliance, the actual strains measured by the LVDTs were roughly one-quarter of the applied crosshead strain, so the strain amplitude was increased for subsequent tests.

The fatigue tests are neither controlled strain nor controlled stress tests, rather a mixed mode of loading occurs because the crosshead rate is controlled, but the on-specimen strains are used for analysis. Figures 5.17(a) and (b) show typical stress and strain history, respectively, recorded during a constant amplitude fatigue test. The load continuously decreases due to the development of damage, and decreases dramatically at failure. The mean strain increases continuously

Table 5.2. Summary of fatigue tests performed on PG 67-22 optimum specimens.

Specimen ID	Average On-Specimen LVDT Strain, ms	Crosshead Strain, ms	N_f	Comments
Specimen 14	242	1050	17,480	Failed in the middle
Specimen 15	254	1017	10,728	Failed in the middle
Specimen 16	n/a	n/a	n/a	Failed at first cycle
Specimen 17	134	1300	>26,687	Did not fail
Specimen 18	223	1017	1731	Failed near top end plate

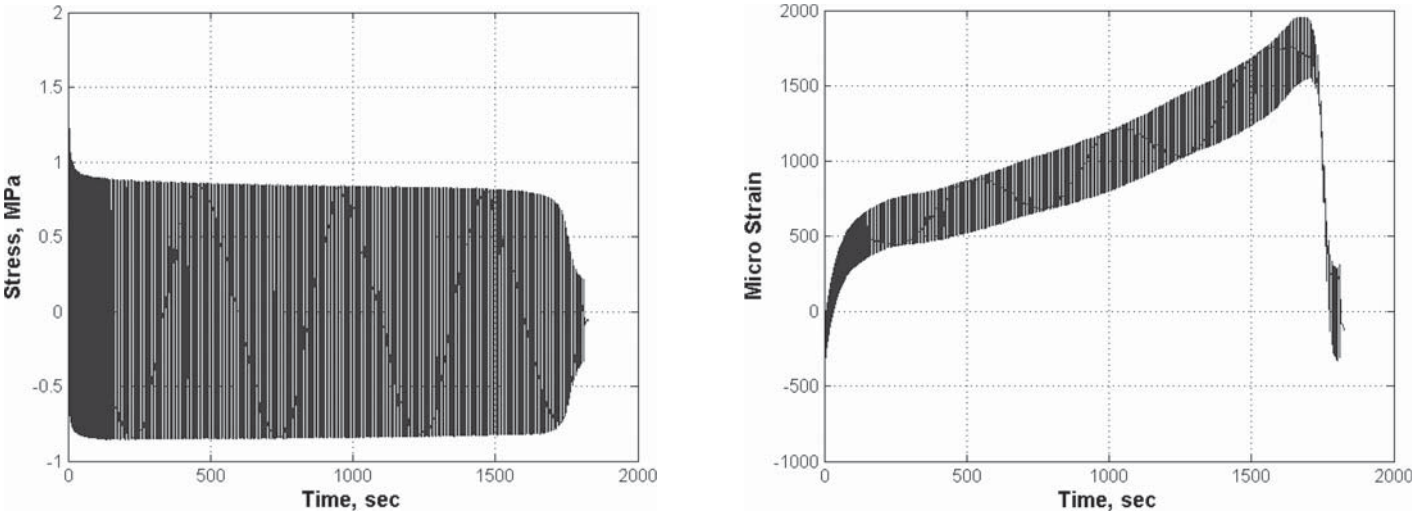

(a) Stress history (b) Strain history

Figure 5.17. Typical stress/strain history for constant amplitude uniaxial fatigue test.

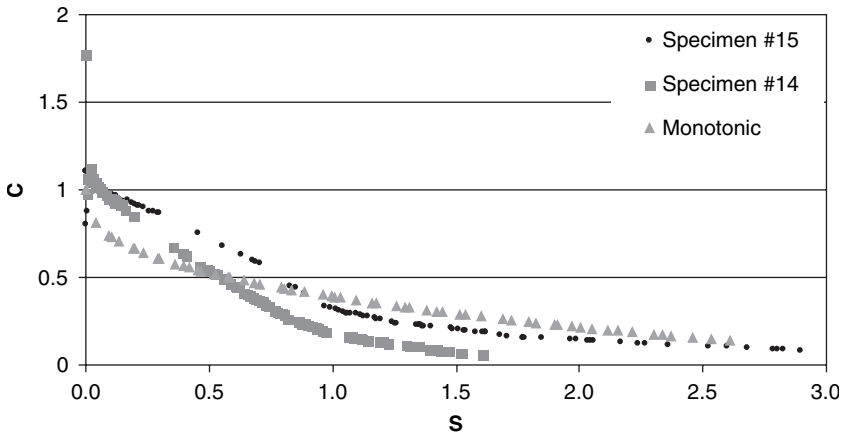

Figure 5.18. Comparison monotonic and cyclic curves for PG 67-22 optimum.

during the tests until failure, at which point the mean strain drops.

Figure 5.18 shows the characteristic curves constructed from both the fatigue and monotonic tests for the PG 67-22 optimum mixture. Previous research has shown better agreement between samples and between monotonic and cyclic tests (*32*).

Evaluation of Endurance Limit

Prediction from Characteristic Damage Curves

Once dynamic modulus, initial stiffness, testing frequency, and damage curve coefficients are known, the strain level required to sustain any number of design load repetitions can be predicted. Equations 23 and 24 can be used to find required strain level with generalized power law and exponential models, respectively (*60, 61*).

$$\varepsilon_0^{2\alpha} = \frac{fS^p}{p\left(0.125IC_{11}C_{12}\right)^{\alpha} N\left(|E^*|\right)^{2\alpha}} \quad (23)$$

$$\varepsilon_0^{2\alpha} = \frac{2^{\alpha} f\left[e^{-\alpha kS} - 1\right]}{\alpha I^{\alpha}\left(-k\right)^{1+\alpha} N\left(|E^*|\right)^{2\alpha}} \quad (24)$$

where,

ε_0 is the strain level required to sustain N number of load repetitions,
S is the damage parameter value at failure (measured from the damage characteristic curve for the mixture at the point where $C = 0.3$, identified in previous research [*32*]),
I is the initial pseudo stiffness,
$|E^*|$ is the dynamic modulus at testing frequency (f), and
α is the material constant, $p = 1 + (1 - C_{12})\alpha$.

Plots of strain level (ε_0) versus design load repetitions (N) obtained for individual asphalt mixtures are presented in

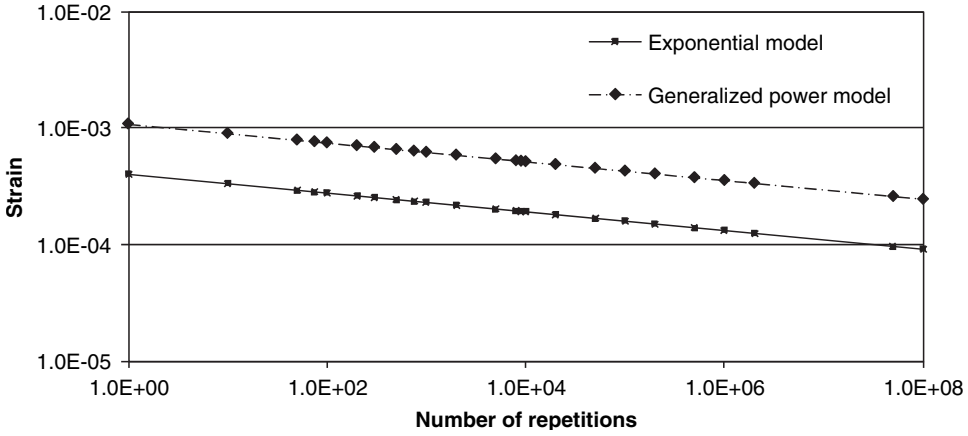

Figure 5.19. Plot of strain level versus load repetitions for PG 67-22 optimum.

Figures 5.19 through 5.22. A comparison of the relations of all mixtures together is presented Figures 5.23(a) and (b) for the generalized power law and exponential models, respectively.

The strain levels required to sustain 50 million cycles of repetitions for all mixtures are shown in Table 5.3 and presented graphically in Figure 5.24. The values obtained using the exponential model are much lower than those obtained from the generalized power law model. There is more confidence in the values from the generalized power law because this function fits the C-versus-S data for these mixtures better than the exponential function.

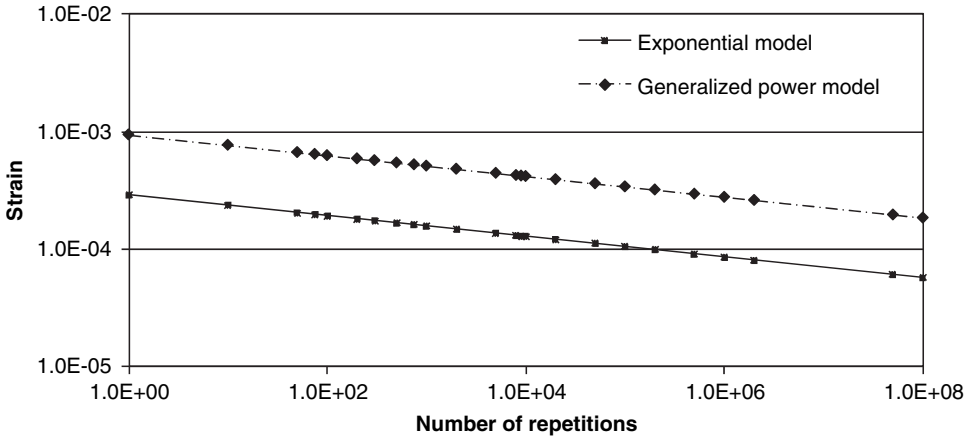

Figure 5.20. Plot of strain level versus load repetitions for PG 76-22 optimum.

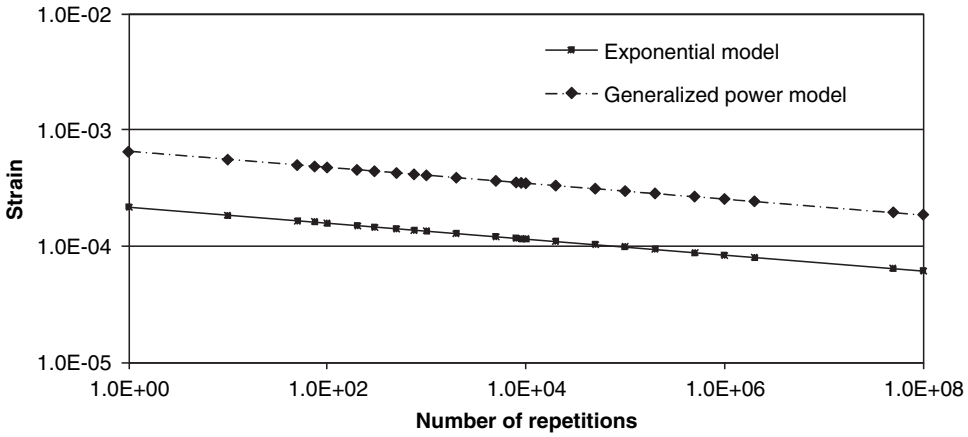

Figure 5.21. Plot of strain level versus load repetitions for PG 67-22 at optimum plus.

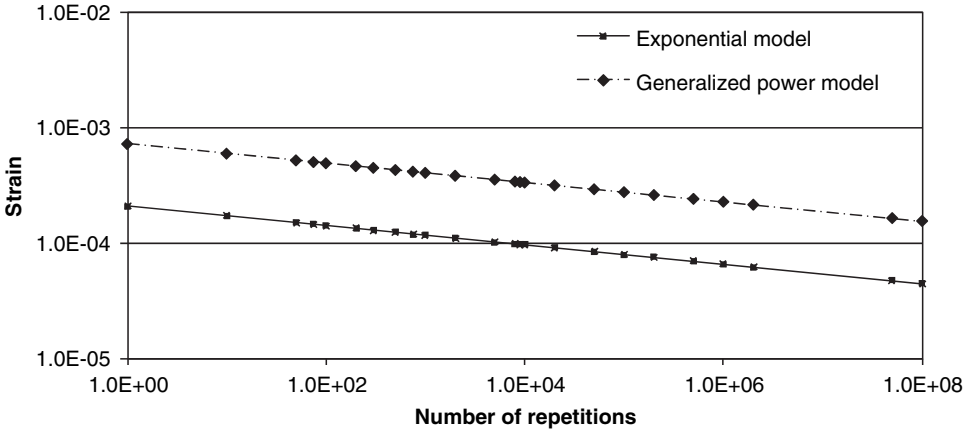

Figure 5.22. Plot of strain level versus load repetitions for PG 76-22 at optimum plus.

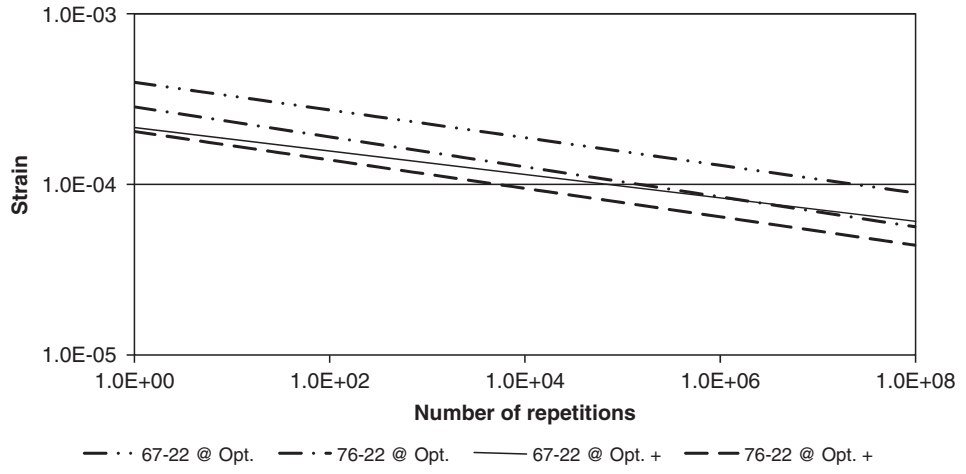

(a) Generalized power models

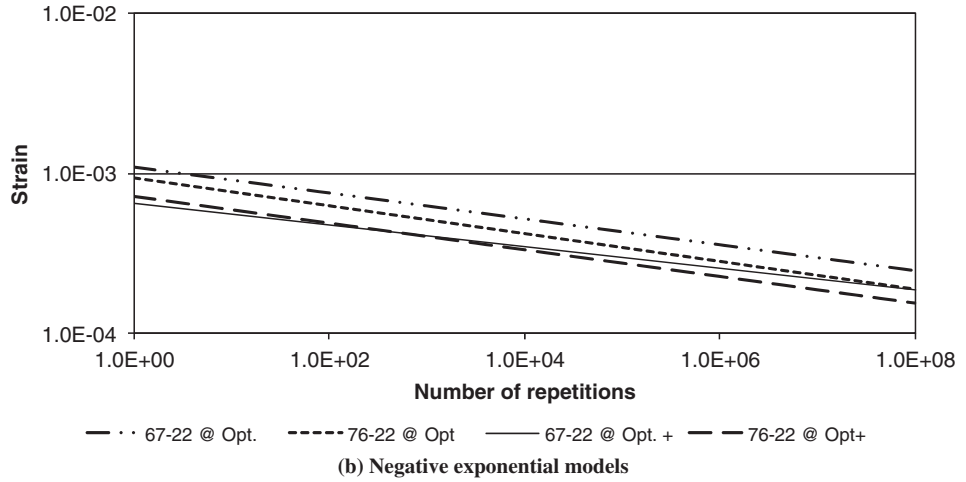

(b) Negative exponential models

Figure 5.23. Plot of strain level versus load repetitions LVDTs for all mixtures.

Table 5.3. Computed critical micro-strain to sustain 50 million cycles.

Damage Characteristic Curve Form	Asphalt Mixture Grade			
	67-22 Optimum	76-22 Optimum	67-22 Optimum+	76-22 Optimum+
Exponential model	96	70	64	47
Generalized power model	261	197	194	164

Increasing Strain Amplitude Test

This test consists of applying blocks of haversine loading to a uniaxial test specimen. Initially, a relatively low strain amplitude that is thought to be below the fatigue endurance limit is applied. Typically, this is close to the same amplitude at which dynamic modulus tests are performed. Approximately 10,000 cycles are applied at this amplitude to allow the specimen to reach steady-state response. The applied strain amplitude is then increased and 10,000 more cycles are applied. This procedure is continued until the specimen fails. Figures 5.25(a) and (b) show a typical load and strain history, respectively, recorded during an increasing amplitude fatigue test. It should be noted that, for this project, the crosshead displacement was controlled while the on-specimen LVDT measurements were used for strain analysis. Machine compliance made it difficult to precisely control the strain amplitude in the specimen at the different levels.

Concept of Pseudo Strain

The use of pseudo strain instead of engineering strain in constitutive analysis removes the hysteretic effect of viscoelasticity. For example, a plot of stress versus strain data obtained from a dynamic modulus test produces a hysteresis loop, as shown in Figure 5.26. The load levels applied during a dynamic modulus test are low enough not to induce damage, so the hysteresis loop is purely due to the viscoelastic response of the material. The hysteresis loop collapses when the pseudo strain is plotted versus the stress, as seen in Figure 5.27. If damage occurs in the material, a hysteresis loop will appear in the stress-pseudo strain plot.

The analysis of the increasing strain amplitude fatigue tests involves calculating the pseudo strain and then plotting pseudo strain versus stress at each strain amplitude to determine the strain level at which loops begin to appear. The presence of a loop in the stress-pseudo strain plot indicates that damage is occurring in the specimen. Figures 5.28 and 5.29 show the stress versus pseudo strain plots for PG 67-22 optimum plus and PG 76-22 optimum plus specimens, respectively. For the PG 67-22 optimum plus specimen, it is clear that there is no loop at the lowest strain amplitude, a loop appears to just be forming at the middle strain amplitude and a loop is definitely apparent at the highest strain amplitude. These two figures indicate that the fatigue endurance limit (strain level below which no damage is occurring) for this specimen is around 150 ms. For the PG 76-22 optimum plus specimen shown in Figure 5.29, the loop appears in the second load level, which is 245 ms. Hence, the fatigue endurance limit is somewhere between 93 and 245 ms. Table 5.4 summarizes the results of the increasing amplitude fatigue tests for all specimens tested. It should be noted that only three mixtures were subject to this test method.

The third column in Table 5.4 shows the bounds of the strain level at which loop formation was observed. For several specimens, the first level tested resulted in loop formation, so only an upper bound is reported. The specimen stiffness at 50 cycles and air void content are also shown in Table 5.4. From this information, it is evident that there are two groups of specimens for the 67-22 optimum plus and 76-22 optimum plus mixtures. The 67-22 optimum plus Specimens 1 and 2, and the 76-22 optimum plus Specimens 1 and 3, have lower air void contents and correspondingly higher stiffnesses and strain range at which loop formation occurs than the other specimens. Using engineering judgment, the

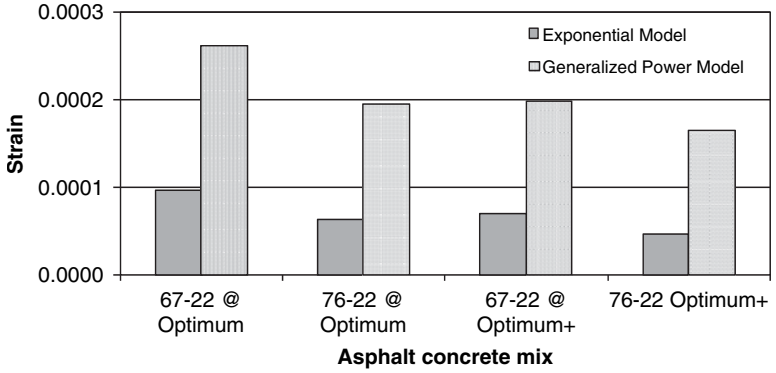

Figure 5.24. Comparison of critical strain to sustain 50 million cycles for all mixtures.

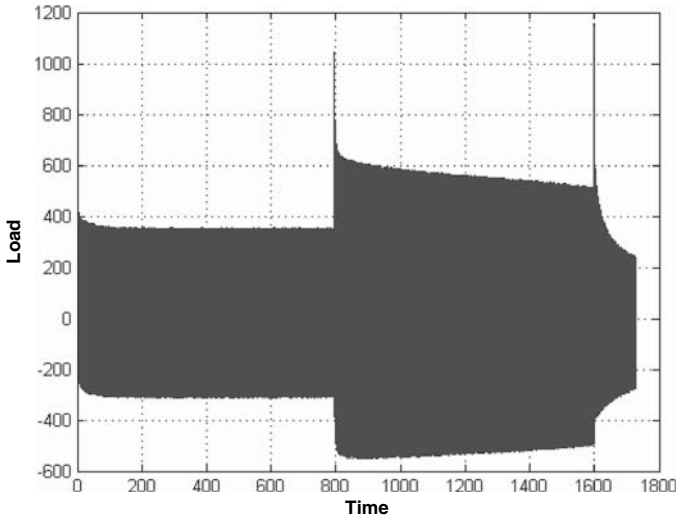

(a) Load History

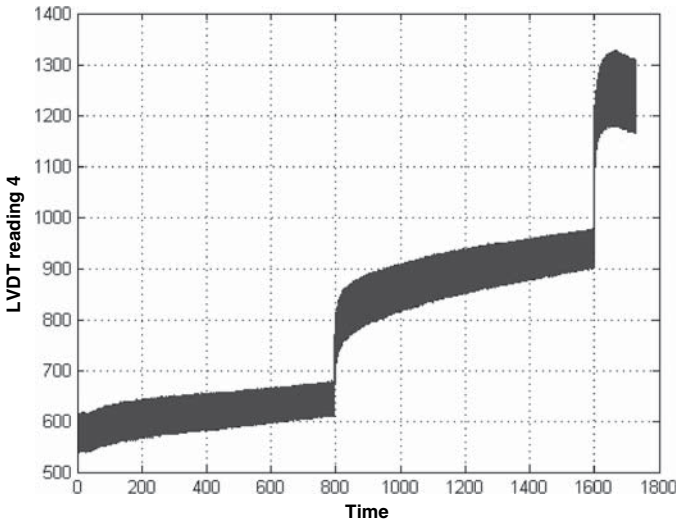

(b) Strain History

Figure 5.25. Typical stress/strain history for increasing amplitude uniaxial fatigue test.

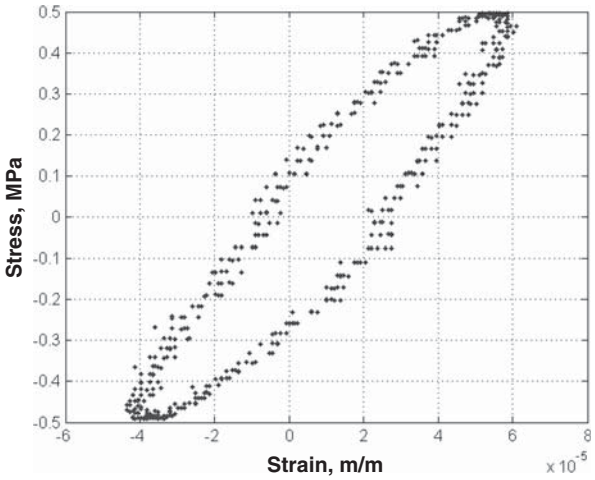

Figure 5.26. Stress versus strain plot for several cycles of loading.

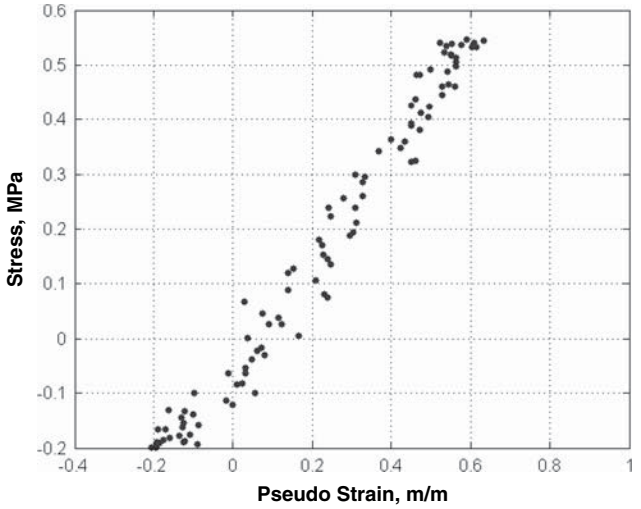

Figure 5.27. Stress versus pseudo strain plot for several cycles of loading.

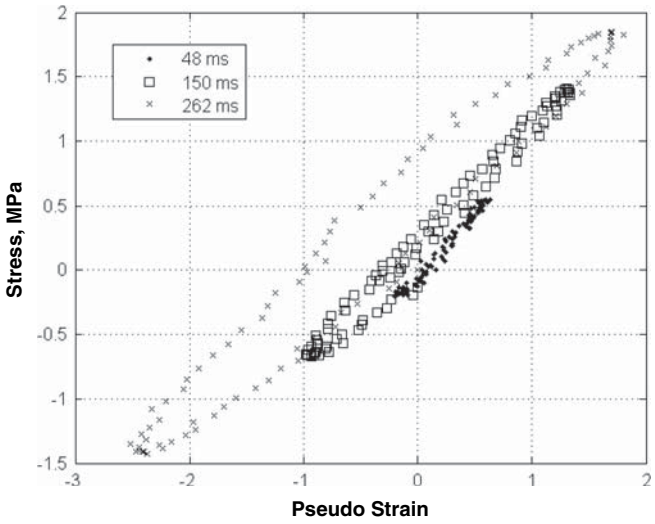

Figure 5.28. Stress versus pseudo strain plots for PG 67-22 optimum plus.

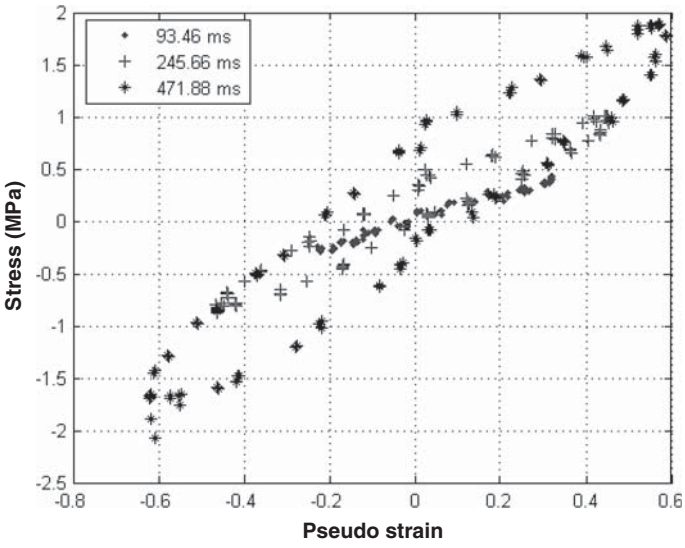

Figure 5.29. Stress versus pseudo strain plots for PG 76-22 optimum plus.

Table 5.4. Summary of increasing amplitude fatigue test data.

Mixture	Specimen Number	Loop Formation Strain Range	Stiffness @ 50th Cycle (MPa)	Air Voids, %	Estimated Endurance Limit
67-22 Opt	15	<181[1]	8955	6.9	~120
	17	107<LF<121	11594	6.7	
	18	<229[1]	7927	6.6	
67-22 Opt+	1	150<LF<262	14756	2.2	~250
	2	247<LF<345	17698	1.5	
	6	67<LF<82	7747	3.6	~150
	8	94<LF<147	9752	2.7	
	10	73<LF<155	10653	3.0	
76-22 Opt+	1	<236[1]	8997	1.5	~230
	3	<237[1]	8896	1.9	
	6	59<LF<125	11250	3.1	~115
	7	102<LF<225	7905	3.2	
	8	110<LF<123	9859	2.7	
	9	96<LF<240	6636	3.7	
	10	<131[1]	8868	2.8	

Note:
[1]Indicates loop formed at lowest strain level tested.

Table 5.5. Overall fatigue endurance limit summary.

Test Method		Estimated Fatigue Endurance Limit (ms)			
		PG 67-22 Optimum	PG 67-22 Optimum+	PG 76-22 Optimum	PG 76-22 Optimum+
C versus S Prediction	Generalized power law	261	194	197	164
	Exponential	96	64	70	47
Increasing Amplitude Fatigue Test	Low air void	120	250	Not tested	230
	High air void		150		115

estimated endurance limit values for the different mixtures are shown in the last column.

Summary of Endurance Limit Values

A summary of the fatigue endurance limit values determined from the different test methods is shown in Table 5.5. The estimated endurance limits for the different groups of specimens based on air void content are shown in the table. The C versus S prediction method does not follow expected trends with respect to increasing asphalt content. The increasing amplitude fatigue test shows an increase in endurance limit with an increase in asphalt content for the PG 67-22 mixtures. However, there is not much difference between the estimated endurance limits for the different asphalt grades.

The increasing amplitude fatigue test is promising and requires some continued research to refine the method. One of the main challenges in this test is controlling the strain amplitude measured on the specimen. It is difficult to do this by controlling the crosshead during the test because of machine compliance. The amount of compliance changes with different loading levels and is difficult to predict. There are several ways to mitigate this problem. The ideal solution is to control the test using the on-specimen LVDTs, however, great care must be taken in running tests on closed-loop systems in this way. Another alternative is to run load-controlled tests and determine the appropriate load levels by using the measured dynamic modulus and target strain amplitude.

A draft Proposed Standard Practice for Predicting the Endurance Limit of Hot Mix Asphalt (HMA) by Pseudo Strain Approach is presented in Appendix B.

CHAPTER 6

Examination of LTPP Database for Indications of an Endurance Limit

Introduction

Flexible pavements have traditionally been designed to limit load-related cracking. The more traffic, the thicker the HMA layer to limit the load-related cracks to some design limit. As noted, however, industry has been proposing the use of an endurance limit as a mixture property for HMA layers. The endurance limit is defined as the tensile strain below which no fracture or fatigue damage occurs and applies to cracks that initiate at the bottom of the HMA layer. Almost all design and analysis procedures that use the endurance limit concept assume that one value applies to all HMA mixtures and temperatures. Values that have been used vary from 65 to 120 ms.

This section of the report has three objectives: discuss the incorporation of the endurance limit design premise into mechanistic-empirical based pavement design procedures, confirm the reality and values suggested for the endurance limit, and recommend field studies to support use of this concept in the MEPDG software.

Including the Endurance Limit Design Premise into Mechanistic-Empirical-Based Pavement Design Procedures

All mechanistic-empirical pavement design procedures can be grouped into three types relative to wheel-load-induced cracking. These are as follows:

1. Design procedures that use the equivalent axle load and equivalent temperature concepts—The equivalent temperature is determined based on an annual or monthly basis. These procedures typically use the cumulative damage concept to determine the amount of fracture damage over the design period for each structure. The DAMA Program would fall within this category (*62*).
2. Design procedures that use the equivalent temperature concept but the axle load distribution for each axle type—These procedures also use the cumulative damage concept to determine the amount of fracture damage for each structure. The PerRoad Program would fall within this category (*63*).
3. Design procedures that calculate and use pavement temperatures at specific depths over some time interval, generally less than a month—These procedures typically use the incremental damage concept to determine the amount of fracture damage within specific time intervals and at specific depths within the pavement structure. The MEPDG would fall within this category (*64*).

The equivalent temperature concept simply defines one temperature for which the annual or seasonal damage equals the cumulative damage determined at monthly or more frequent intervals. The equivalent temperature is used to estimate the dynamic modulus for calculating the tensile strain at the bottom of the HMA layer on an annual or seasonal basis.

All M-E based design procedures, regardless of the group, use Miner's hypothesis to calculate fracture damage, and assume that wheel-load-related alligator cracks initiate at the bottom of the HMA layer and propagate to the surface with continued truck loadings, with the exception of the MEPDG. In addition, all M-E based design procedures use the maximum tensile strain at the bottom of the HMA layer as the pavement response parameter for calculating fracture damage and predicting the amount of alligator cracks. Those design procedures apply the endurance limit design premise in one of three methods, which are summarized as follows:

1. The introduction of the endurance limit design premise into those design procedures that use the equivalent temperature and equivalent axle load concepts is straight forward. Stated simply, the maximum tensile strain is calculated at the equivalent temperature and axle load and

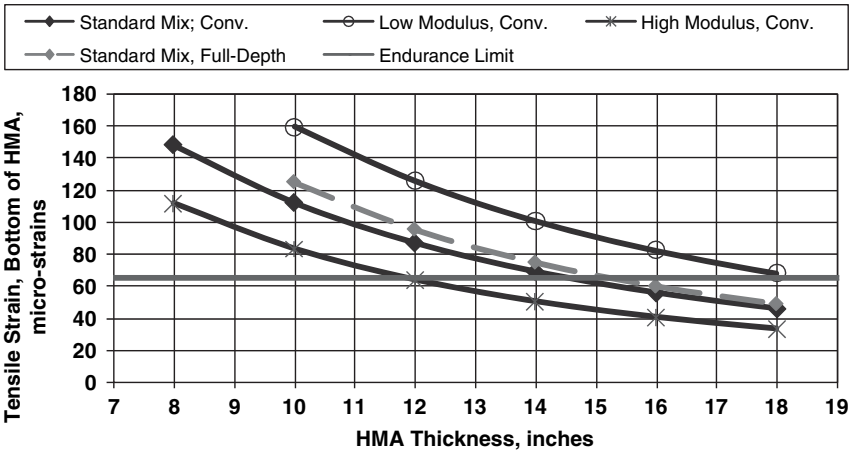

Figure 6.1. Tensile strains calculated for an 18-kip single-axle load for the equivalent annual temperature for different HMA mixtures.

compared to the endurance limit. The HMA layer thickness is simply determined for which the maximum tensile strain equals or is less than the endurance limit. Figure 6.1 illustrates the use of the endurance limit within this method.

2. The introduction of the endurance limit into those design procedures that use the equivalent temperature concept but use the actual axle load distribution is also fairly straight forward. The maximum tensile strain is calculated at the equivalent temperature for each axle load within the axle load distribution. The axle load distribution for each axle type is used to determine the probability of the tensile strain exceeding the endurance limit. The designer then considers that probability of exceeding that critical value in designing an HMA layer for which no fatigue damage would accumulate over time. Figure 6.2 illustrates the use of the endurance limit within this method. One concern with this method is that the higher loads result in significantly higher damage indices; an increase in axle load will result in an increase in damage to a power of about four. Thus, the probability of cracking is much higher than the probability of a specific tensile strain being exceeded.
3. Those design procedures that use the incremental damage concept establish a threshold value for the tensile strain, below which the fracture damage is assumed to be zero. In other words, the procedure simply ignores calculated tensile strains that are equal to or less than the value set as the endurance limit for determining the incremental damage within a specific time period and depth. Successive runs have been made with the MEPDG to determine the difference in calculated fracture damage with and without using the endurance limit as an HMA mixture property. Figures 6.3 and 6.4 illustrate the increasing

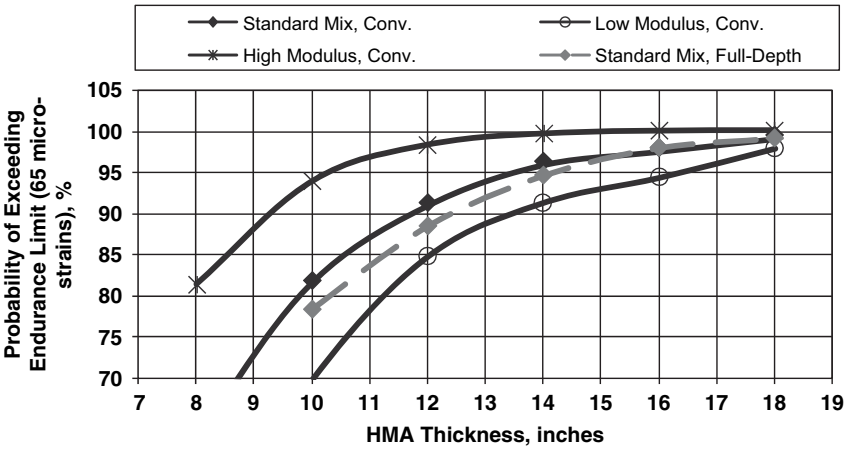

Figure 6.2. Probability of exceeding the endurance limit for different HMA mixtures using typical axle load distributions and seasonal temperatures.

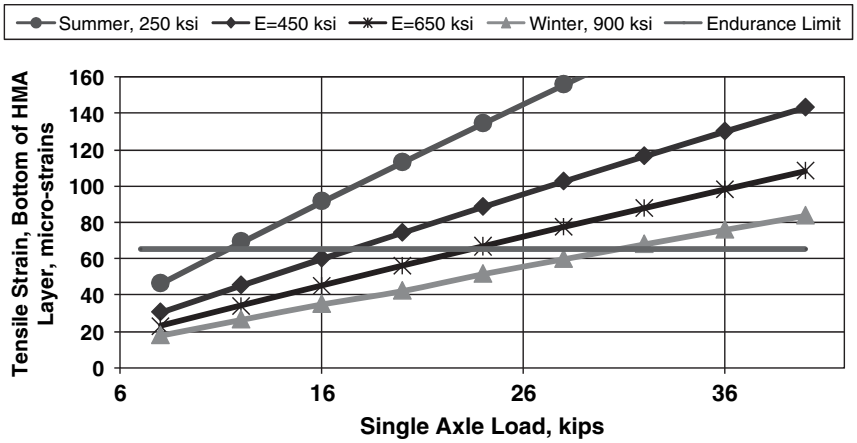

Figure 6.3. Increasing tensile strains for varying single-axle loads for different seasons or dynamic modulus within those seasons (HMA thickness equals 15 in.).

maximum tensile strains for varying single-axle loads for different dynamic modulus values and HMA thicknesses, respectively.

Version 0.9 of the MEPDG did not include the endurance limit design premise in the recalibration process of the design methodology or software. In other words, Version 0.9 assumes that any tensile strain in the HMA layer induces some facture damage. Two types of load-related cracking are predicted for designing flexible pavements in accordance with the MEPDG—alligator cracking and longitudinal cracking in the wheel path. Alligator cracking, the more common cracking distress used in design, is assumed to initiate at the bottom of the HMA layer. These cracks propagate to the surface with continued fracture damage accumulation. Longitudinal cracking in the wheel paths is assumed to initiate at the surface and propagate downward. The MEPDG assumes that both types of cracking are caused by load-induced tensile strains. That hypothesis, however, has yet to be confirmed.

As noted above, the new MEPDG uses an incremental damage index. Fracture damage is computed on a grid basis with depth for each month within the analysis or design period. Temperatures are computed with the Integrated Climatic Model at specific depth intervals for each hour of the day. These temperatures are then grouped into five averages at each depth interval for each month. The fatigue cracking (alligator cracking) equation is used to calculate the amount of fracture damage for each depth interval and month. The monthly damage indices are then summed over time to predict the area of fatigue cracking at each depth interval.

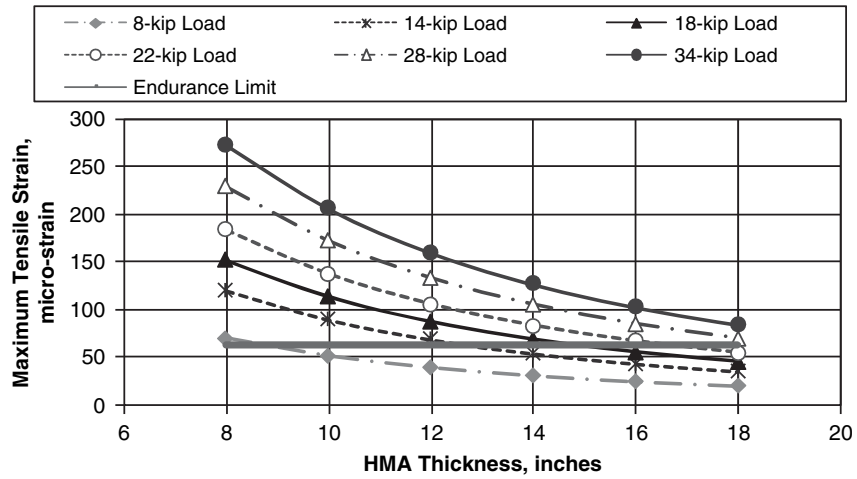

Figure 6.4. Increasing maximum tensile strains for varying single-axle loads for different HMA thicknesses (HMA dynamic modulus equals 450 ksi; equivalent annual modulus).

All design methods that accept the endurance limit design premise assume that the endurance limit is independent of the mixture and temperature. That endurance limit is the tensile strain below which no fracture damage occurs. If an endurance limit value was an input into the MEPDG or used within other M-E based design methods, the question becomes, what value should be used as the endurance limit? The purpose of this section is to use the LTPP database to try and answer three questions related to the endurance limit design premise, as follows:

1. Do field observations of alligator cracking support the existence of an endurance limit as an HMA mixture property?
2. If the field observations support the endurance limit theory or hypothesis, what is the tensile strain below which no more alligator cracking has been exhibited?
3. Is the endurance limit independent of mixture type and dynamic modulus?

Defining the Endurance Limit—A Survivability Analysis

A survivability analysis was used to try to answer the above questions using the LTPP database. The survivability analysis completed within this project is an expansion of work completed using the LTPP database in the mid-1990s. This section of the report describes the use of survival curves in determining the thickness or level of tensile strain at which only limited cracking has occurred over long periods of time.

Development and Application of Survival Curves

Survival or probability of failure analyses have been used for decades in actuarial sciences. They have also been used in the pavement industry to determine the expected service life of pavement structures for use in life cycle cost analysis, and to compare the mean and standard deviation of the expected service life for different design features and site factors in evaluating the adequacy of the design procedure (*65, 66*). Survival curves are uniquely useful because every point on the curve represents the probability that a given pavement section will be rehabilitated or exceed a specific level of distress.

Survival analysis is a statistical method for determining the distribution of lives or "Life Expectancy," as well as the occurrence of a specific distress for a subset of pavements. Since not all of the pavements included in the analysis have reached the end of their service life or a specific level of distress, mean values can not be used. The age or amount of alligator cracking and probability of occurrence are computed considering all sections in the subset using statistical techniques.

Survival curves are typically based on age but can also be based on traffic loadings or the probability of exceeding a specific level of distress. The age or condition at failure must be based on a clearly defined condition. Mathematical models are best fitted to the points in the survival curves to predict the probability of survival or failure as a function of age, thickness, cumulative traffic, or some other pavement feature. The general form of these models for use in life cycle cost analysis is as follows (*67, 68*):

$$\text{Probability of Failure} = \frac{a}{1+e^{b*(Age-c)}} + d \quad (25)$$

$$\text{Probability of Failure} = \frac{a}{1+e^{b*(ESAL-c)}} + d \quad (26)$$

where,

Failure = Existing pavement is overlaid or reconstructed, or a specified level of distress has been exceeded;
Age = Number of years since construction (new pavement or overlay);
ESAL = Cumulative equivalent single 18-kip axle loads since construction (new pavement or overlay), millions; and
a, b, c, d = Regression coefficients determined from the analysis.

The probability of survival is 1 minus the probability of failure. Optimization is typically used to determine the regression coefficients that best fit the survival points. A survival analysis also can be completed using a specific level of distress and pavement response value. In other words, the survival curves can be used to define the probability that a specific area of alligator cracking will be less than some specified amount for different HMA thicknesses or tensile strains at the bottom of the HMA layer.

It is important to note that survival curves for pavements are necessarily based on previously built designs, materials, construction, and maintenance. The data used to develop the survival rates or probability of failure represent typical construction, materials, mixture designs, and thicknesses that have been built by agencies within the past time period represented by the data. These can be defined as "benchmark" survival curves.

The reliability of a pavement depends on the length of time it has been in service and design features and site factors that are not properly accounted for in a thickness design procedure. Thus, the distribution of the time to failure of a pavement type or thickness level is of fundamental importance in reliability studies. A method used to characterize this distribution is the failure rate, or rate of occurrence, for a specific level of distress. The failure rate can be defined as follows.

If $f(t)$ is the probability density of the time to failure of a given pavement type and thickness, that is, the probability that the pavement will fail between times t and $t + \Delta t$ is given by $f(t)^* \Delta t$, then the probability that the pavement will fail on the interval from 0 to t is given by

$$F(t) = \int_0^t f(t)dx \tag{27}$$

The reliability function, expressing the probability that it survives to time t, is given by

$$R(t) = 1 - F(t) \tag{28}$$

Thus, the probability that the pavement will fail in the interval from t to $t + \Delta t$ is $F(t + \Delta t) - F(t)$, and the conditional probability of failure in this interval, given that the pavement survived to time t, is expressed by

$$\frac{F(t+\Delta t) - F(t)}{R(t)} \tag{29}$$

Dividing by Δt, one can obtain the average rate of failure in the interval from t to $t + \Delta t$, given that the pavement survived to time t by

$$\frac{F(t+\Delta t) - F(t)}{\Delta t}\left[\frac{1}{R(t)}\right] \tag{30}$$

For small Δt, one can get the failure rate, which is

$$Z(t) = \frac{f(t)}{R(t)} = \frac{f(t)}{1 - F(t)} \tag{31}$$

The failure rate is expressed in terms of the distribution of failure times. A typical failure rate curve is composed of three parts or can be grouped into three areas, as shown in Figure 6.5 and defined as follows:

1. The first part is characterized by a decreasing failure rate with time and is representative of the time period during which early failure or premature failures occur. This area or time typically represents pavements that were inadequately designed or built, using inferior materials.
2. The second part is characterized by a constant failure rate. A constant failure rate represents the time period when chance failures occur, or the failure occurs at random with pavement age. In some survival methods, this area is referred to as the useful life of a pavement.
3. The third part is characterized by an increasing failure rate with time. This area or time represents the reverse of the first part, and when failure is a result of multi-distresses as related to a combination of parameters over time (for example, exponential growth increases in traffic, past the design period from which thickness was determined).

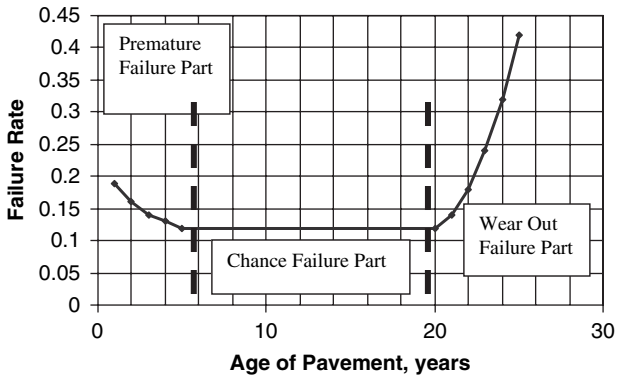

Figure 6.5. Typical failure rate relationship for pavement structures.

The failure rate can be determined by organizing the performance data in terms of the distribution of pavement age exceeding a critical level (failure) versus the distribution of age for those pavements exhibiting a value lower than the critical value. Figure 6.6 shows a typical probability of failure relationship from actual data included in the LTPP database for roughness measured on flexible pavements in the general pavement studies (GPS-1 and GPS-2) and special pavement studies (SPS-1) experiments. GPS-1 sections consist of HMA on granular base. GPS-2 sections consist of HMA on bituminous, hydraulic cement, lime, fly ash, or other pozzolan bound or stabilized base. SPS-1 sections are part of a strategic study of structural factors for flexible pavements.

Given the above definition of each part of the probability of failure relationship with time, the failure rate can be defined as

$$f(t) = Z(t)\left[e^{-\int_0^t Z(t)dx}\right] \tag{32}$$

Assuming that the failure rate is constant within the second part, and replacing $Z(t)$ with α, the distribution of failure times is an exponential distribution as shown below.

$$f(t) = \alpha\left[e^{-\alpha t}\right] \tag{33}$$

Many survival curves or, conversely, the probability of failure, are based on the above relationships and assumptions. Unfortunately, the failure rate within the second part is not usually constant, and the failure rates for the first and third parts are not inversely proportional to one another. For these

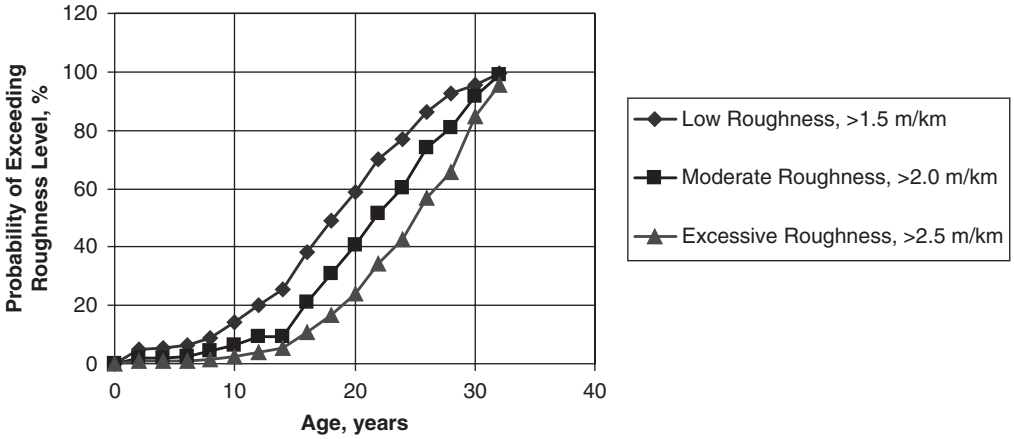

Figure 6.6. Illustration of results from a survivability analysis or probability of exceeding a critical roughness magnitude.

cases, which are typical for pavements, the failure rate can be estimated by the following relationship:

$$Z(t) = \alpha\beta(t)^{\beta-1} \tag{34}$$

Thus,

$$f(t) = \alpha\beta(t)^{\beta-1}\left[e^{-\alpha t^{\beta}}\right] \tag{35}$$

This density function is termed the Weibull distribution, and is typically used in failure analyses.

LTPP Database to Establish the Initial Survival Curve

A survivability analysis was completed by Von Quintus et al. for the Asphalt Pavement Alliance to determine the expected age for an amount of fatigue cracking that would result in rehabilitation of the roadway (*69*). The test sections used in the survival analysis were from the GPS-1 and GPS-2 experiments. Figure 6.7 shows the distribution of pavement age for the GPS-1 and GPS-2 test sections (LTPP database version 13.1/NT3.1 released in January 2002), and Figure 6.8 shows the number of test sections with different areas of alligator (fatigue) cracking. As shown in Figure 6.8, many of the LTPP test sections have no alligator cracking.

Figures 6.9 and 6.10 show the survival curves from the LTPP data for different levels of alligator cracking that would cause some type of rehabilitation activities. As shown, the average life (50% probability) to crack initiation and a low cracking amount (less than 10% of wheel-path area) is 19 and 23 years, respectively.

A similar survivability analysis was completed by Von Quintus in 1995 for a subset of the test sections included in the GPS-1 and GPS-2 experiments. The test sections were randomly selected from the LTPP program for the thicker

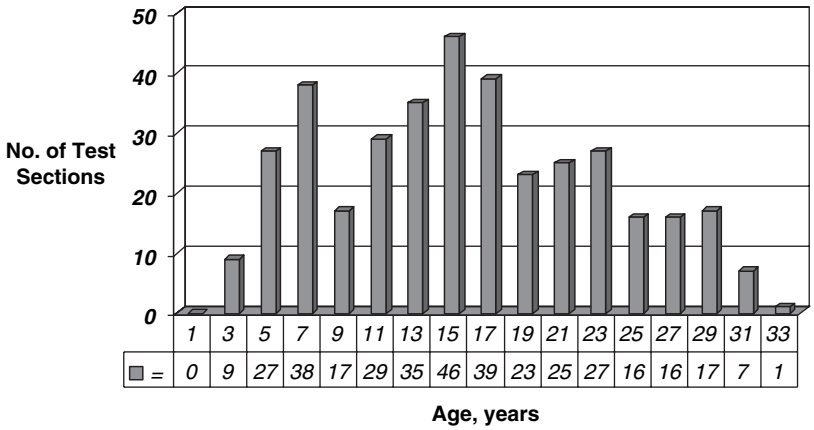

Figure 6.7. Frequency histogram of pavement age at the time of the distress survey for the LTPP GPS test sections included in the Asphalt Pavement Alliance study (69).

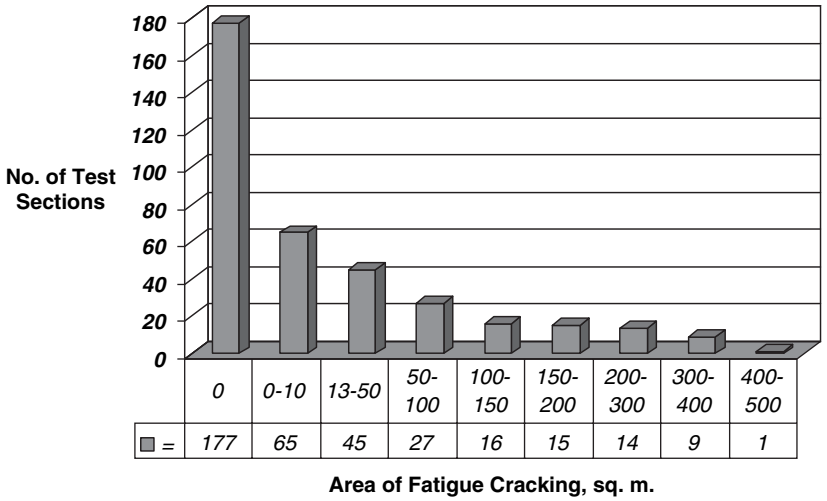

Figure 6.8. Histogram of the number of test sections with different levels of alligator cracking (69).

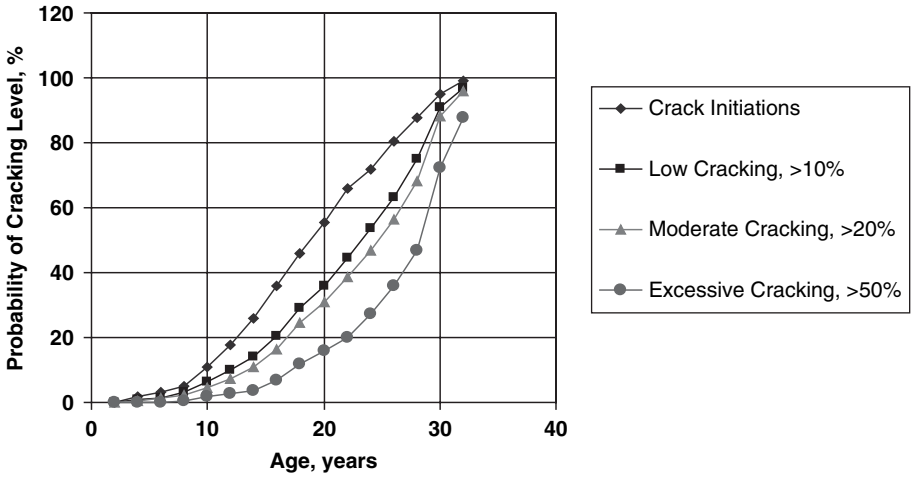

Figure 6.9. Graphical illustration of the probability of failure or exceeding a specified area of alligator cracking (69).

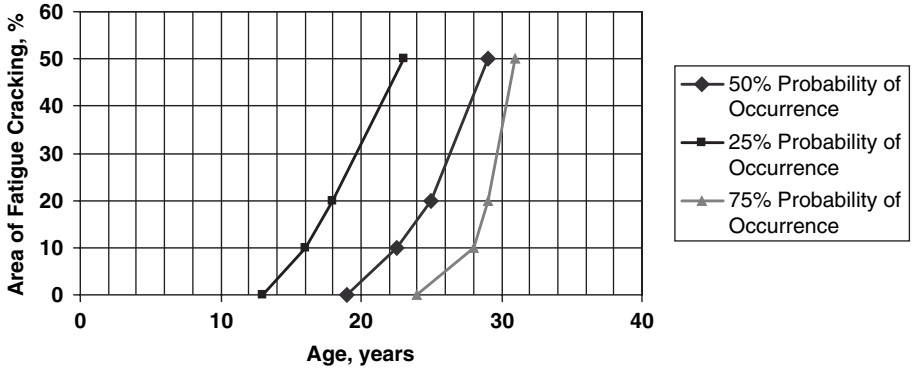

Figure 6.10. Probability of occurrence for alligator cracking (69).

HMA layers. This survivability analysis was completed to try to estimate a value for the endurance limit based on alligator cracking observations within the LTPP program, rather than just using values estimated from limited laboratory testing programs. This survival analysis was a desk-top study that has yet to be formally documented. The LTPP data were used to determine the probability of occurrence of different amounts of alligator cracking for different HMA thicknesses and tensile strains.

The EVERSTRESS Program was used to calculate the maximum tensile strain at the bottom of the HMA layer for each test section using the equivalent annual temperature and equivalent (18-kip) single-axle load concepts. The HMA modulus value used in the calculation of tensile strain was determined using the Witczak equation (*70*) based on volumetric data and physical properties of the HMA for the equivalent annual temperature. The modulus values for the other pavement and soil layers were based on resilient modulus testing performed in the laboratory. Figure 6.11 shows the survival curve from that limited study. A magnitude of 2% cracking was used in this initial survival analysis because of the measurement error in alligator cracking with time. A small measurement error could result in significant changes to this definition of the endurance limit. In summary, the endurance limit was determined to be 65 ms at a 95% confidence level for an 18-kip single-axle load applied to the pavement at the equivalent annual temperature for each LTPP site included in the analysis.

Preliminary Definition of the Endurance Limit as an HMA Mixture Property

The AAMAS project sponsored by NCHRP recommended use of the indirect tensile strength and modulus tests to estimate the fatigue strength/life of specific HMA mixtures (*59*). Figure 6.12 illustrates that relationship between HMA modulus and tensile strain at failure, where both properties are determined at 77°F (25°C). Points below the line in Figure 6.12 are assumed to have inferior fatigue properties, and those above the line exceed the fatigue strength/life of the standard mixture. Laboratory tests and field observations of alligator cracking have been used to check the validity of this relationship over time. More alligator cracking has been observed where the tensile strain at failure is less than that value from Figure 6.12 for a specific HMA modulus value based on the equivalent temperature concept.

Von Quintus used this relationship to estimate or define the endurance limit for different HMA mixtures as 1% of the tensile strain at failure measured in accordance with the test protocol from the AAMAS study (*59*). That definition has yet to be confirmed and validated.

Updated Survivability Analysis Using LTPP Data

The survivability analysis completed for this project included the same test sections from the 1995 study, plus additional test sections within the GPS-1, GPS-2, and SPS-1 experiments. A subset of the LTPP test sections was used, which was randomly selected to cover all environmental regions, soil types, and HMA thicknesses. The additional test sections used in the updated survivability analysis were from the GPS-1, GPS-2, and SPS-1 experiments—LTPP database version VR 2004.06, release 18.0 (2004). Figure 6.13 shows the distribution of HMA thickness for all test sections included in the updated survivability analysis.

Figure 6.14 shows the distribution of pavement age for the test sections with more than 10 in. of HMA that were used to update the survival curve (Figure 6.11). As shown, the age of 45% of the thicker test sections included in the updated study is greater than 15 years. Many of these additional test sections were from the SPS-1 experiment that was excluded from

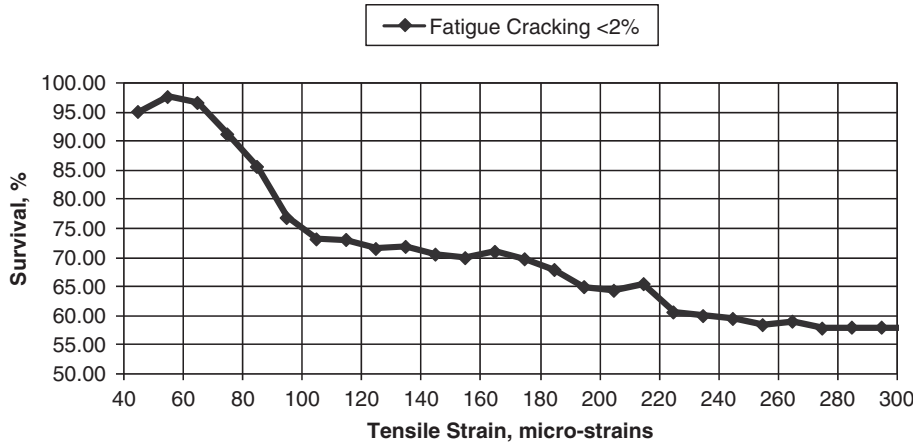

Figure 6.11. Survival curve for flexible pavements developed from data included in the LTPP GPS-1 and GPS-2 experiments (undocumented study, 1995).

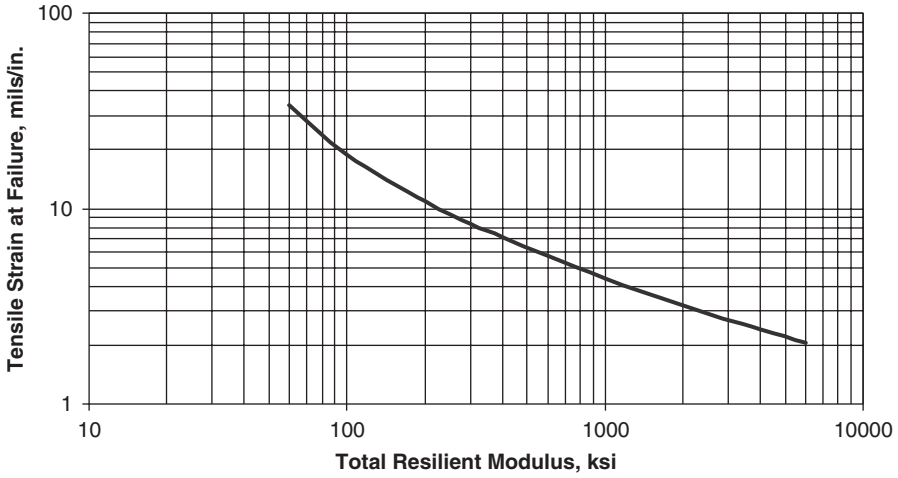

Note: ms and mils/in. are the same unit.

Figure 6.12. Relationship between modulus and tensile strain at failure to estimate the fatigue strength of HMA Mixtures at 77°F (25°C) (59).

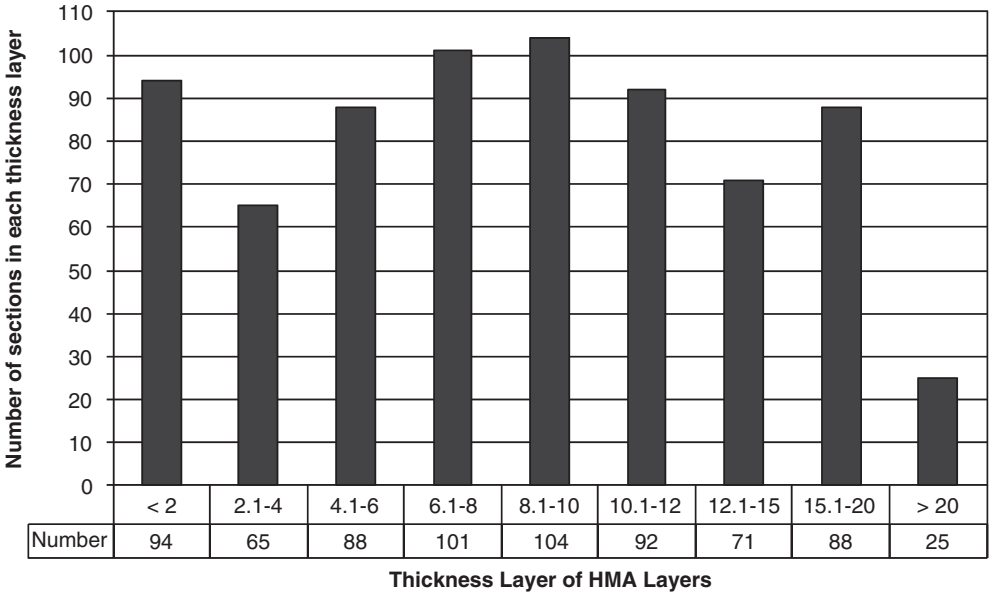

Figure 6.13. Distribution of HMA thickness for the test sections used in the updated survivability analysis.

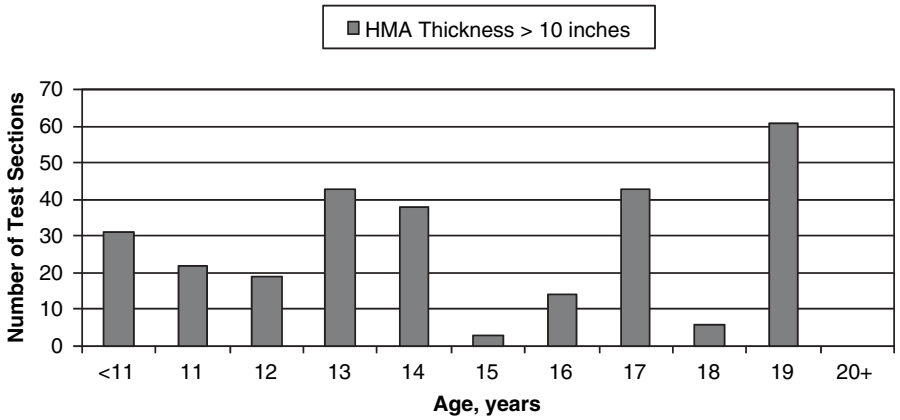

Figure 6.14. Distribution of age for those test sections with HMA layer thicknesses in excess of 10 in.

the initial study to estimate the endurance limit. The reason that the SPS-1 test sections were excluded from the study in 1995 is that most of the projects within the SPS-1 experiment were relatively new at that time.

The other important parameter in the survivability analysis is the truck traffic applied to each of these test sections. Without significant truck traffic, defining the endurance limit from field observations has limited meaning. Figure 6.15 shows the distribution of the cumulative number of 18-kip ESALs for the test sections included in the updated survivability study that have HMA thickness in excess of 10 in. The cumulative truck traffic for these thicker test sections is considered moderate traffic with most test sections having less than 15 million cumulative 18-kip ESALs.

In summary, the test sections with the thicker HMA layers are not new pavements (Figure 6.14), but do have truck traffic levels that are lower than what would be considered heavy truck traffic (Figure 6.15). This level of truck traffic is a concern to the definition established for the endurance limit. Much higher levels of truck traffic are needed to validate the endurance limit design premise with field observations and data.

HMA Thickness-Based Definition

The asphalt industry has proposed some maximum HMA thicknesses that are believed to be resistant to alligator cracking. The LTPP database was used to determine the level of HMA thickness at which none or little alligator cracking has been observed on HMA pavement surfaces. Figure 6.16 compares the amount of fatigue cracking (percent of wheel-path area) from the most recent distress survey and HMA thickness. As shown and expected, the test sections with thinner HMA layers generally have more fatigue cracking. However, there are an appreciable number of test sections with thicker HMA layers (15 in. or more) that have levels of fatigue cracking exceeding 5%.

Figure 6.17 compares the maximum tensile strain calculated for each section and HMA thickness. The modulus of the HMA layer was determined using the equivalent temperature concept for an 18-kip ESAL, as described previously for the original survivability analysis. As shown and expected, the tensile strains decrease with increasing HMA layer thickness. Figure 6.18 compares the maximum tensile strain at the bottom of the HMA layer and the amount of fatigue cracking observed on the LTPP test sections from the most recent distress survey included in the LTPP database. As shown and expected, the test sections with the lower tensile strains have less fatigue or alligator cracking.

Maximum Tensile-Strain-Based Definition

An updated survival curve to the one presented in Figure 6.11 was developed for the additional alligator cracking data and LTPP test sections. Figure 6.19 shows the results from the survival analysis for a range of fatigue cracking levels. The results from the updated survival analysis are significantly different from the 1995 desk-top study. In fact, the updated survival curve for the 1% and 2% alligator cracking levels would indicate that there is no endurance limit for these sections. The relationships shown in Figure 6.19 for the 1% and 2% cracking levels have a peak survival rate significantly less than 100% and then begin to decrease with lower tensile strain values.

Some of the GPS test sections that were without alligator cracks in 1995 now have some alligator cracks recorded in the LTPP database for the test sections with the thickest HMA layers. Possible reasons for the significant difference in results

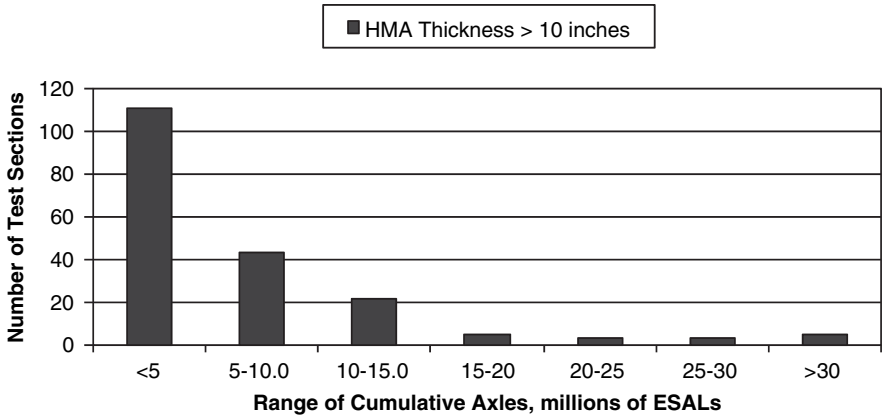

Figure 6.15. Distribution of cumulative equivalent single-axle loads for the test sections used in the survivability analysis with HMA layer thicknesses in excess of 10 in.

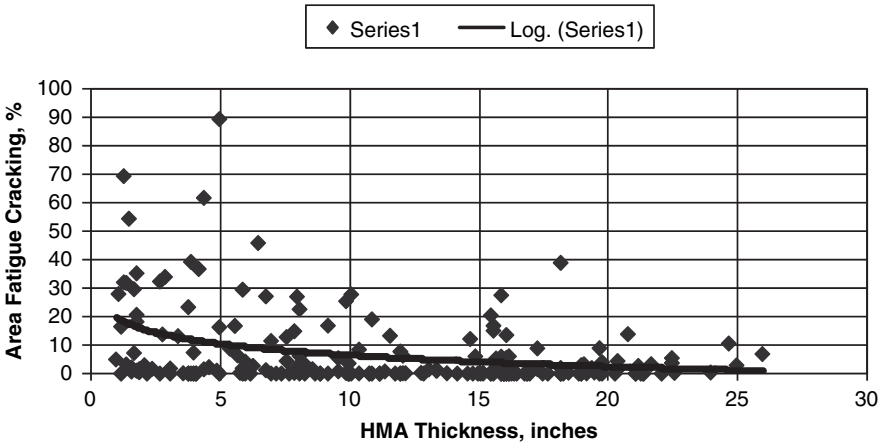

Figure 6.16. Comparison of area fatigue cracking (area alligator cracking based on a percent of wheel-path area) and HMA layer thickness.

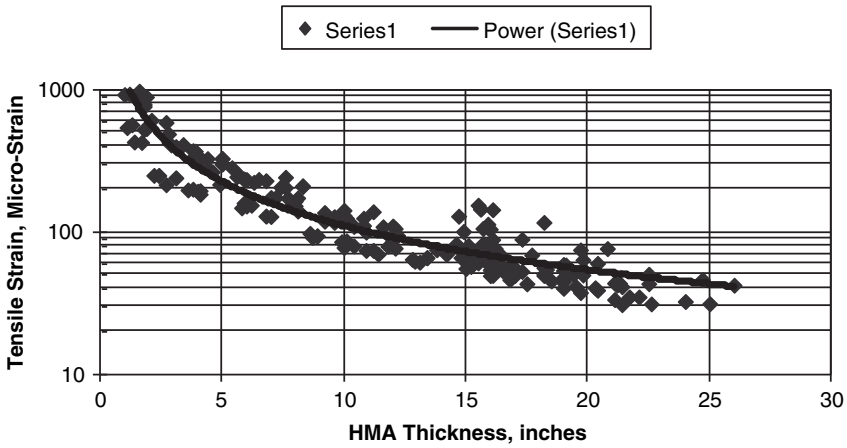

Figure 6.17. Comparison of the maximum tensile strain at the bottom of the HMA layer and HMA thickness.

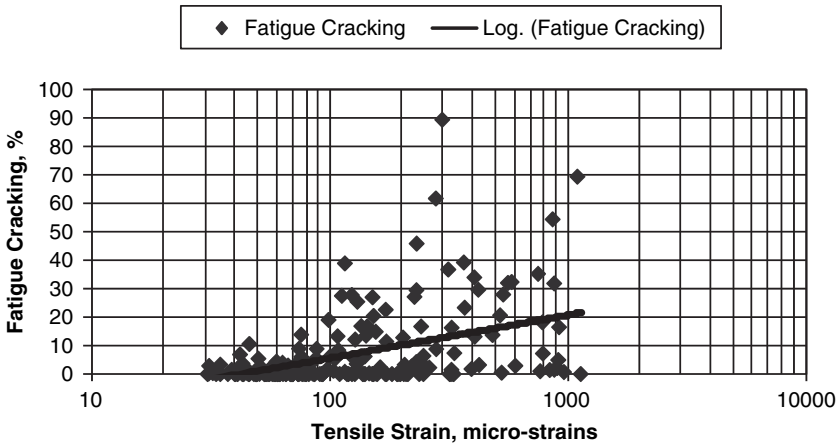

Figure 6.18. Comparison of the area fatigue cracking and maximum tensile strain computed at the bottom of the HMA layer.

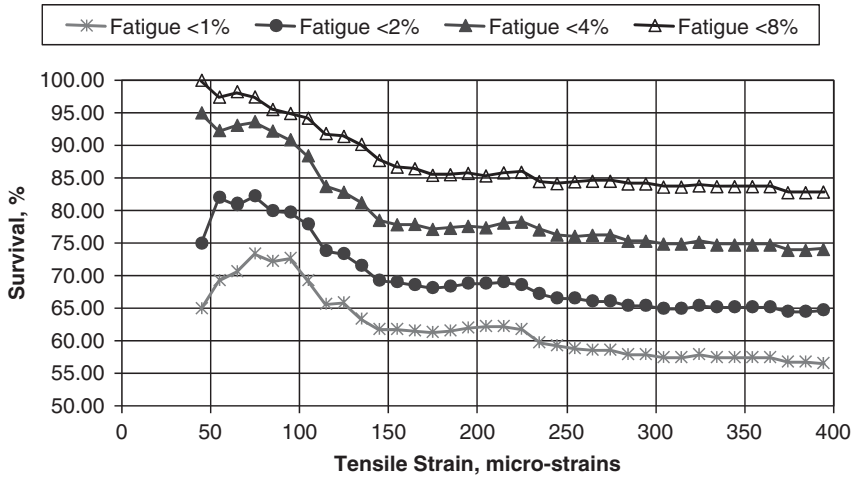

Figure 6.19. Survival curves based on the maximum tensile strain at the bottom of the HMA layers of flexible pavements included in the LTPP program.

or the survival curve from the one developed in 1995 are summarized as follows:

- The SPS-1 projects were added to the updated analysis. It is expected that including the SPS-1 projects did not cause this difference in findings, unless the fatigue cracking initiated from some other design-site feature that would have a higher probable occurrence within the SPS-1 test sections, as compared to the GPS sections. In addition, the study completed for the Asphalt Pavement Alliance concluded that there was a possibility that the GPS test sections selected by the individual agencies for the LTPP program are biased towards the better performing pavements. The SPS-1 projects were built during the LTPP program and would not be biased toward better performing pavements. It is expected that this is not the reason for the difference in survival curves.
- There was a change in the LTPP definition of longitudinal cracking in the wheel path. The change in definition definitely could have affected the updated survival curve. Many of the previously measured longitudinal cracks that are assumed to have initiated at the surface are now recorded as alligator cracking and are assumed to have initiated at the bottom of the HMA layer. The cracking maps and video distress data logs can be reviewed to segregate longitudinal cracks with crack deterioration along the edges from traditional alligator cracks. This evaluation process is time consuming. Figure 6.20 graphically presents the change in percentage of survival sections as a function for varying alligator cracking levels for different tensile strains at the bottom of

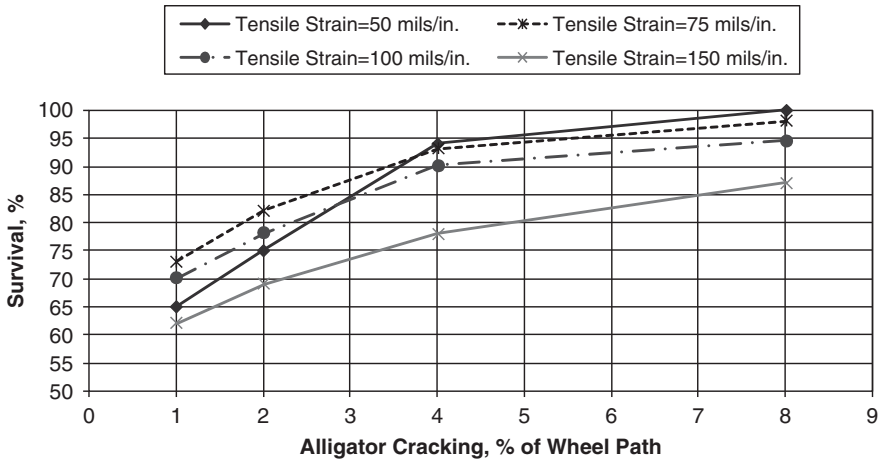

Figure 6.20. Percent survival of test sections for different levels of alligator cracking and tensile strain at the bottom of the HMA layer.

the HMA layer. As shown in Figure 6.20, the 150 ms (mils/in.) curve deviates from the other relationship. Errors in measuring small amounts of alligator cracking as well as a change in the definition for alligator cracking could have caused this anomaly. This indicates that other types of cracking may be included as fatigue cracks for pavements with strain levels of 100 ms or less at the bottom of the asphalt layer calculated using an equivalent annual temperature and 18-kip axle load. To determine the cause of the anomaly requires that forensic investigations be completed on these much thicker HMA sections to determine the cause of the recorded alligator cracking.

- The location where alligator cracks recorded in the LTPP database initiated are assumed. As noted above, alligator cracks are assumed to initiate at the bottom of the HMA layer and propagate to the surface. The validity of this assumption would have an effect on the survival curve. In addition, the maximum tensile strain at the bottom of the HMA layer was based on the assumption of full-bond between all HMA lifts. If partial bond exists between two lifts near the surface, load-related cracks can initiate at that location and propagate downward as well as upward. A full forensic investigation will be needed to determine the location of where these cracks, recorded in the LTPP data, initiated and the mechanism (debonding between adjacent HMA lifts) that resulted in those cracks.
- The initial and updated survivability analysis was performed assuming that stripping or moisture damage is not present within the HMA layer. Stripping and moisture damage were adequately identified during the initial sampling and coring program for the GPS test sections. For the SPS-1 projects, stripping or moisture damage may have occurred on some of the projects and resulted in premature alligator cracking for the thicker sections. This possible cause for the difference in findings can be resolved with forensic investigations.
- An additional reason or explanation for the difference in results is that there is no endurance limit for HMA mixtures.

In summary, it is still believed that the endurance limit is an HMA mixture property. Based on the results from the updated survival analysis, however, forensic investigations of the test sections with the thicker HMA layers are needed to confirm the location of crack initiation and other assumptions used noted above in the survivability analysis.

Affect of Polymer Modification on Field Performance

Von Quintus et al. (*71*) conducted a study to quantify the effects of polymer modification on pavement performance. Sites were selected from the LTPP database, NCAT Test Track, FHWA Accelerated Loading Facility (ALF), and a number of Canadian provinces and U.S. states with good records of performance and material properties. For each polymer modified section, a control mix or two to three unmodified sites were selected for comparison. The unmodified sections were termed *companion sites.*

The performance of the polymer modified asphalt (PMA) test sections and their companion sections was compared using a normalization technique that is based on computing damage indices for each test section. This normalization technique uses M-E models to reduce the effect from confounding factors between projects. The M-E performance prediction models were calibrated to local conditions using performance data from companion sections (without any additive or modifier in the HMA mixture). This local calibration procedure was used to estimate the true effect of PMA because of the variation and errors associated with the models selected for use.

Figure 6.21 presents a comparison of the fatigue cracking predicted using the locally calibrated fatigue cracking equation

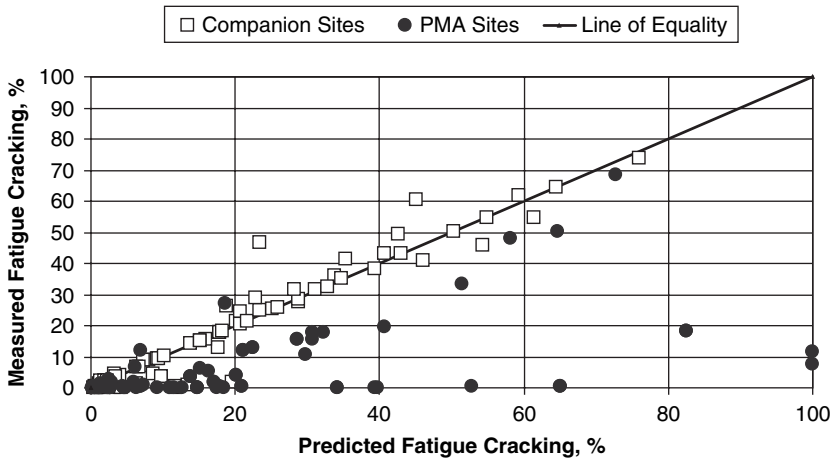

Figure 6.21. Comparison between the predicted and measured fatigue cracking for neat HMA and PMA mixtures (71).

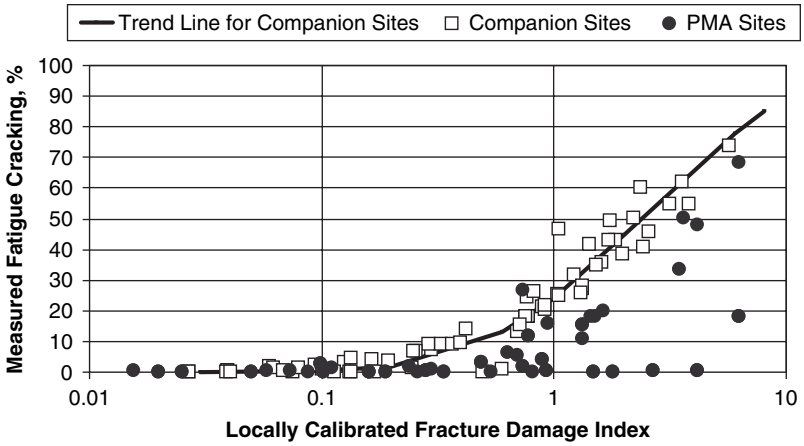

Figure 6.22. Comparison between the fracture damage index and measured fatigue cracking for neat HMA mixtures and PMA mixtures (71).

and that actually measured for the sites. The data for the unmodified sections fall along the line of equality, whereas the data for the polymer modified section indicate that the actual cracking is less than the predicted cracking. Figure 6.22 shows the damage index (DI) or ratio applied loads to allowable load before failure occurs versus measured fatigue cracking. Figure 6.22 also indicates that pavements constructed with PMA can withstand a larger percentage of their maximum load repetitions for a given level of cracking.

Both Figure 6.21 and 6.22 support the findings in Chapter 4 that indicate the polymer modified PG 76-22 should have a higher endurance limit. This also indicates that the endurance limit is mixture specific.

CHAPTER 7

Sensitivity of Pavement Thickness to the Endurance Limit

Summary of Predicted Endurance Limits

Estimates of the endurance limit were obtained from beam fatigue tests, uniaxial tension tests, and analysis of field performance. Table 7.1 summarizes the endurance limit predictions from the beam fatigue and uniaxial tension tests. An analysis of LTPP data, presented in Chapter 6, indicated an endurance limit of 65 ms. There appears to be good correlation between the beam fatigue estimates of the endurance limit determined in Phase I and those determined during the mini round-robin analysis. Based on the predicted values determined from testing at NCAT and the Asphalt Institute, stiffer high-temperature binder grades and optimum plus asphalt contents produce higher endurance limit values. The 95% lower prediction limit samples follow the same general trend. The prediction of the endurance limit from the round-robin data shows small differences based on binder grade and asphalt content.

The rankings from the uniaxial tension tests are the reverse of those determined from the beam fatigue tests. For the uniaxial tension tests, the PG 76-22 mixes generally result in lower estimates of the endurance limit. This appears to be the opposite of field experience with polymer modified binders, illustrated in Figures 6.21 and 6.22. There are a number of potential reasons for the differences observed between beam fatigue and uniaxial tension testing. There were very few uniaxial replicates tested, especially compared with the number of beams tested. In some cases, the trends are based on results from only one or two samples. Early in the uniaxial testing, there were a number of problems with end failures. Specimen fabrication was altered to reduce this problem. Finally, the modes of loading uniaxial and beam fatigue samples are different. To date, the basic research has not been completed to understand the differences between the modes of loading or how the stress state changes with damage. The state of stress in pavements is not completely understood either. More effort is needed prior to considering this approach.

Estimate of Shift Factors between Laboratory Tests and Field Performance

In Chapter 3, calculations were provided to show that the maximum expected load repetitions in a 40-year period is approximately 500 million. Then, using a shift factor of 10 between laboratory and field performance, a limit of 50 million cycles was determined for the laboratory beam fatigue testing. The selection of a shift factor of 10 was based on recommendations from SHRP (*46*). The structural sections from the 2003 NCAT Test Track provide an opportunity to verify the shift factors. Three methodologies were used to assess the shift factors for the 2003 NCAT Test Track structural sections: measured strains from in-place instrumentation, PerRoad, and the MEPDG.

The NCAT Test Track was initially constructed in 2000. All of the sections of the 2000 track consisted of 19 in. of HMA (15 in. of which were the same dense-graded mixes for all of the sections and the remaining 4 in. that were the experimental mixes that varied between sections), 5 in. of permeable asphalt-treated drainage layer, 6 in. of crushed aggregate base, and 12 in. of improved (AASHTO A-2) subgrade.

The 2003 NCAT Test Track cycle included eight structural sections. Three pavement sections were designed using the 1993 AASHTO Pavement Design Guide to carry approximately ⅓, ⅔, and the full 10 million ESAL loading (for that cycle). The design reliabilities are summarized in Table 7.2. The input parameters are summarized in Von Quintus (*72*).

The eight structural sections were selected to evaluate pavement sections designed for varying levels of traffic, polymer modified and unmodified or neat asphalt binders, stone matrix asphalt (SMA), and rich bottom layer. All eight sections were placed on 6 in. of granular base. The section layout is shown in Figure 7.1. The thin, medium, and thick pavement sections were constructed using both a neat PG 67-22 binder and a styrene-butadiene-styrene (SBS) polymer modified PG 76-22. The 19.0-mm NMAS base course was used for

Table 7.1. Summary of estimates of the endurance limit (ms).

Mix	Beam Fatigue		Beam Fatigue Round-Robin			Uniaxial C versus S		Uniaxial Increasing Amplitude	
	Predicted	95% Lower Confidence Limit	Predicted[1]	95% Lower Confidence Limit[2]	Average 95% Lower Confidence Limit[2]	Power Model	Exponential Model	Average for Loop Formation[3]	Average Lowest for Loop Formation[3]
PG 58-22	107	82	NA	NA	NA	NA	NA	NA	NA
PG 64-22	89	75	NA	NA	NA	NA	NA	NA	NA
PG 67-22	172	151	182	130	103	261	96	195	133
PG 67-22 Opt. +	184	158	176	141	121	194	64	223	150
PG 76-22	220	146	195	148	126	197	70	NA	NA
PG 76-22 Opt. +	303	200	NA	NA	NA	164	47	189	124

Notes:
[1]Calculated using the pooled data from the round-robin.
[2]Average of the 95% lower confidence limit calculated by each individual lab.
[3]Averages calculated based on individual specimen data not presented in Chapter 5.

Table 7.2. 2003 NCAT Test Track structural section design reliabilities (*72*).

Traffic	HMA, In.	Granular Base, In.	Fill[1], In.	Structural Number	Reliability at 10 Million ESALs
Full	9	6	15	6.2	92%
2/3	7	6	17	5.4	68%
1/3	5	6	19	4.6	30%

Note:
[1]Fill was placed from the top of the original improved subgrade to the bottom of the granular base to maintain the surface elevation of the structural sections with respect to the 2000 track.

the fatigue testing in this study with the same binders. For the seventh section, the 1-in. thick wearing course of the medium thickness design was replaced with SMA. SMA was also used as the wearing surface of the eighth section; in addition, the bottom 2 in. of the 19.0-mm base were replaced with a rich bottom layer containing an additional 0.5% asphalt (medium total thickness).

For the 2003 track, loading was provided by five triple-trailer trucks and one five-axle single trailer (FHWA Class 9 vehicle). A typical triple trailer is shown in Figure 7.2. For the triple trailer, the average steer axle weight was 10,680 lbs, the average weight of the tandem drive axles was 40,610 lbs, and the average weight of the single-axle trailer ranged from 20,550 to 21,010 lbs. For the five-axle single trailer, the steer axle weighed 11,550 lbs, the tandem drive axles weighed 33,850 lbs, and the tandem rear axles weighed 32,900 lbs (*73*). Hot tire inflation pressures were typically 105 psi.

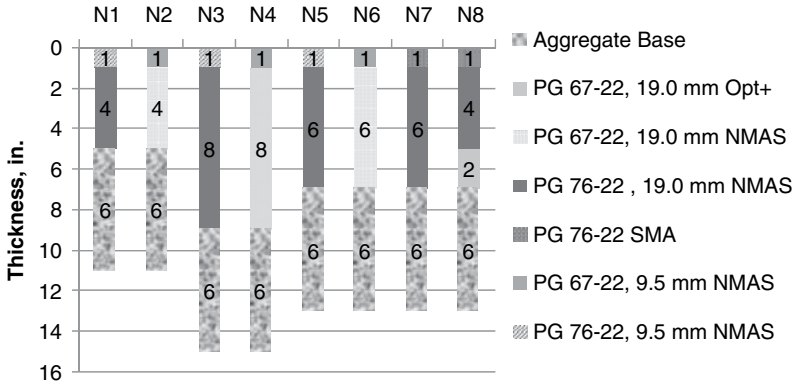

Figure 7.1. Layout of 2003 NCAT Test Track structural sections.

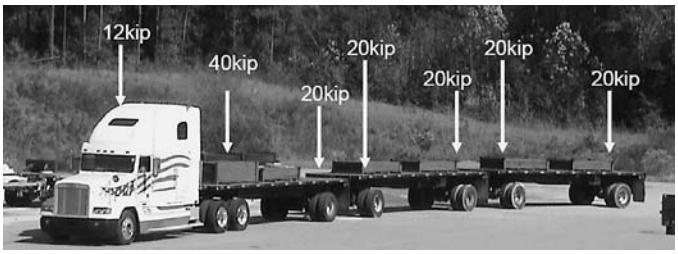

Figure 7.2. Typical triple-trailer weight distribution for 2003 NCAT Test Track (73).

Six of the eight structural sections developed some degree of fatigue cracking during the 2003 test track cycle (all but the 9-in. thick HMA sections N3 and N4). Three of the sections failed, with failure defined as fatigue cracking exceeding 20% of the total lane area (*73*). The MEPDG assumes cracking of 50% of the total lane area when damage equals 100% (*74*). The cracking data at failure and failure dates for Sections N1, N2, and N8 are shown in Table 7.3. The evolution, monitoring, and calculation of the crack areas are documented by Priest and Timm (*73*). The degree of cracking in Section N8, with the rich bottom layer, was unexpected, particularly when compared with the performance of Section N7. Willis and Timm (*75*) conducted a forensic evaluation that indicated slippage or debonding between the rich bottom layer and the overlying base layer. Cracking apparently began in the overlying layer.

Shift Factors Based on Measured Strain

The eight structural sections from the 2003 NCAT Test Track were instrumented to measure in situ strain in the asphalt, compressive stresses in the unbound layers, and moisture and temperature as a function of depth in the pavement structure (*72*). Temperature and moisture data were collected on an hourly basis throughout the two-year loading cycle. High-speed data (2,000 samples per second) from the asphalt strain gauges and unbound layer pressure cells were collected at least once a month for at least three truck passes for each section and weekly after cracking was initially observed. The layout of the instrumentation for each section is shown in Figure 7.3.

Based on the high-speed data acquisition, Priest and Timm (*73*) developed strain prediction models for each of the sections and the two loading configurations (triple trailer and five-axle single trailer). The regression model used a power relationship (Equation 36).

$$\varepsilon_t = \beta_1 T^{\beta_2} \quad (36)$$

where,

ε_t = horizontal tensile strain (ms),
T = mid-depth HMA temperature, °F, and
β_1 and β_2 = regression constants.

The regression constants are summarized in Tables 7.4 and 7.5. For Section N8, the data exhibited three different performance periods. Prior to April 20, 2004, the strain response appears to indicate that the layers were bonded. From April 20 to September 1, 2004, the strain response shifts, but maintains a power model relationship with temperature. After September 1, 2004, increasing strains, even with low mid-depth HMA temperatures, appear to indicate that cracks are propagating through the upper layers. Two separate models are shown in Table 7.4 with coefficients for traffic before and after the point when the bond appears to have failed.

A generic relationship for both the triple trailer and five-axle single trailer was developed for the sections as a function of thickness (*73*). The generic equation (37) was used to calculate the strains resulting from the five-axle single trailer for Section N1. Insufficient data were collected before N1 cracked to develop a specific model for Section N1. The surveyed HMA thickness of Section N1 was 4.8 in. A thickness of 5 in. was used for Section N8 after September 1, 2004 to represent debonding between the base and rich bottom layer.

$$\varepsilon_t = 2.1228T^{1.190} - 26.448t \quad (37)$$

where,

ε_t = horizontal tensile strain (ms),
T = mid-depth HMA temperature, °F, and
t = HMA thickness (in.).

The low-speed data acquisition system collected the average mid-depth HMA temperature for each section on an hourly basis. The numbers of laps by each triple trailer and five-axle single trailer truck were recorded for each hour. Both Priest (*76*) and Willis (*77*) developed spreadsheets to calculate the

Table 7.3. 2003 NCAT Test Track structural section failure data (*73*).

Section	Failure Date	Cracking, % of Total Lane	Cracking, % of Wheel Path
N1	6/14/2004	20.2	58.3
N2	7/19/2004	19.5	56.3
N8	8/15/2005	18.5	53.5

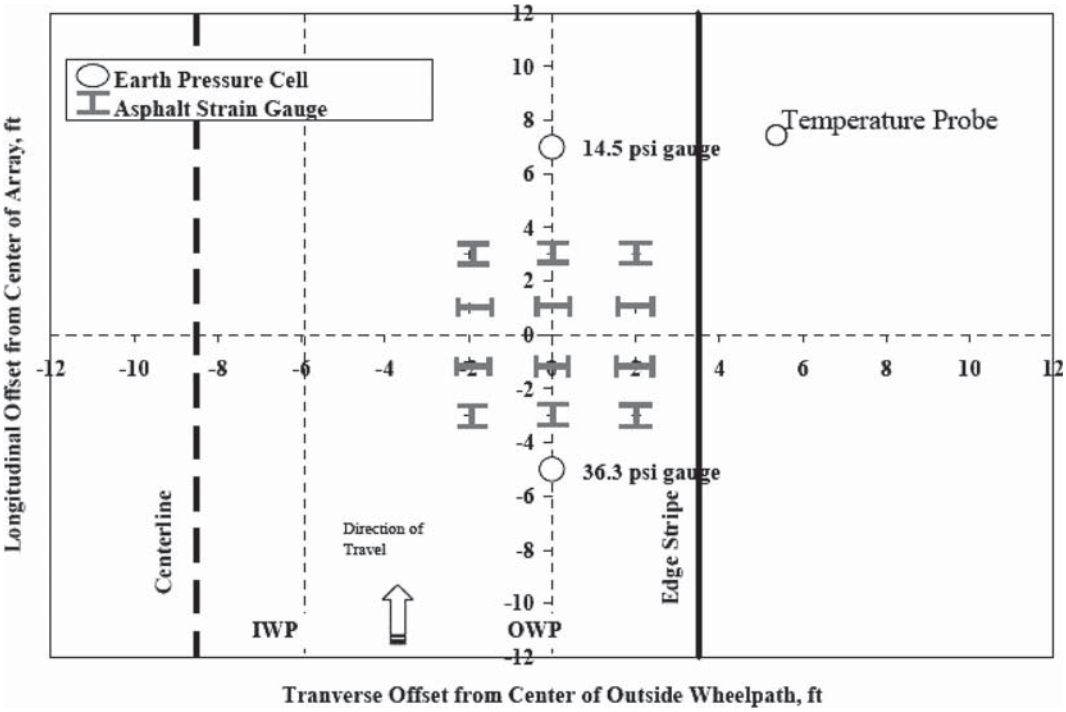

Figure 7.3. Typical gauge array for 2003 NCAT Test Track structural sections (72).

Table 7.4. Triple-trailer regression analyses for strain-temperature relationship (*73 [not N8]*).

Section	β_1	β_2	R^2
N1[1]	4.0439	1.066	0.76
N2	0.0005	3.081	0.88
N3	0.0508	1.899	0.91
N4	0.0211	2.086	0.82
N5	0.0109	2.291	0.88
N6	0.0132	2.293	0.81
N7	0.0022	2.652	0.71
N8 (prior 4/20/2004)	0.1487	1.556	0.90
N8 (4/20/2004 and after)	0.0926	1.824	0.81

[1]Limited data were available.

Table 7.5. Five-axle single-trailer regression analyses for strain-temperature relationship (*73 [not N8]*).

Section	β_1	β_2	R^2
N1	Insufficient data to perform regression		
N2	3.922E-05	3.579	0.871
N3	5.501E-03	2.332	0.773
N4	1.304E-03	2.632	0.773
N5	1.440E-04	3.185	0.887
N6	1.852E-02	2.155	0.881
N7	8.310E-04	2.796	0.821
N8 (prior to 9/1/2004)	1.170E-04	3.157	0.850

Table 7.6. Fatigue transfer function coefficients for 2003 NCAT Test Track 19.0-mm NMAS base mixes.

Mix	k_1	k_2	R^2
PG 67-22 Optimum	7.189E-15	5.782	0.99
PG 67-22 Optimum+	4.420E-09	4.107	0.98
PG 76-22 Optimum	4.663E-12	5.052	0.92

number of axle repetitions and respective strain for each hour of the 2003 NCAT Test Track loading cycles. Transfer functions were developed from the laboratory beam fatigue tests in the form of Equation 38, as follows:

$$N_f = \beta_1 \times k_1 \left(\frac{1}{\varepsilon_t}\right)^{k_2} \quad (38)$$

where,

N_f = number of load repetitions (cycles) to failure,
ε_t = tensile strain at the bottom of the HMA layer,
k_1 and k_2 = regression constants, and
β_1 = shift factor between laboratory and field performance (initially set at 1.0).

The regression constants for the 2003 NCAT Test Track 19.0-mm NMAS base mixes, based on the beam fatigue tests conducted as part of this study are shown in Table 7.6.

The incremental damage was calculated for each hour of loading by truck type (triple trailer or five-axle single trailer) using Miner's Hypothesis, shown in Equation 39, where failure is approached when the cumulative damage approaches 1.0 (*78*). The failure criterion was defined as fatigue cracking equal to 20% of the total lane area.

$$D = \sum_{i=1}^{n} D_i = \sum_{i=1}^{n} \frac{n_i}{N_{fi}} \quad (39)$$

where,

D = cumulative damage,
D_i = incremental damage for condition (in this case, repetitions of a given axle's load at a given HMA temperature over a given hour),
n_i = number of load applications at condition i, and
N_{fi} = allowable load applications to failure for condition i (in this case, determined using the laboratory fatigue transfer function shown in Equation 38 and Table 7.6).

Based on the observed level of cracking, Section N6 was assigned a cumulative damage factor of 0.7 after the application of 10 million ESALs at the end of the 2003 NCAT Test Track cycle (*73*). Willis (*77*) calculated strain for each hour based on the loading conditions using Equation 36 and the coefficients in Tables 7.4 and 7.5 based on the recorded mid-depth HMA temperature. The spreadsheets were modified to calculate N_i for each section, hour, and loading condition using Equation 38 and the coefficients in Table 7.6. The number of load repetitions of a given truck in each hour was divided by their respective N_i to determine the incremental damage. The cumulative damage, D, was determined by summing all the incremental damage according to Equation 39 until the date when failure occurred as identified in Table 7.3. For Section N6, the damage was summed until the end of the 2003 loading cycle (application of 10 million ESALs). The shift factor for each section, β_1, in Equation 38 was solved for using Microsoft Excel's Solver Function such that the cumulative damage, D, = 1.0 on the failure date. For Section N6, the shift factor was determined for D = 0.7 at the end of the loading cycles. The shift factors were determined with and without the inclusion of an endurance limit. The endurance limit represented by the lower limit of the 95% confidence interval was used in the calculations. The calculated shift factors between laboratory and field performance are summarized in Table 7.7. Based on the data in Table 7.7, the use of an endurance limit does not affect the shift factor for pavement sections likely to fail in fatigue.

Table 7.7. Calculated shift factors between laboratory and field performance based on measured strains.

Section	19.0-mm NMAS Base Mix	Shift Factor	Shift Factor with Endurance Limit
N1	PG 76-22 Optimum	4.24	4.24
N2	PG 67-22 Optimum	75.77	75.77
N6	PG 67-22 Optimum	38.00	38.00
N8	PG 67-22 Optimum+[1]	8.33	8.33

Note:
[1]Until debonding occurred, then PG 67-22 optimum.

Shift Factors Based on Calculated Strains Using M-E Design Programs

In Chapter 6, three classes of M-E pavement design programs were described, as follows:

1. Those that use equivalent axle loads and equivalent temperatures;
2. Those that use equivalent temperatures in the form of seasons and axle load distributions for each axle type; and
3. Those that use detailed temperature, load, and incremental damage calculations.

PerRoad is an example of the second type and the MEPDG is an example of the third type of pavement design program. Both programs were used to estimate shift factors between predicted and field performance.

The inputs used in the M-E design programs are described below. Where possible, the same inputs were used in both PerRoad and the MEPDG. Resilient modulus (M_r) values were calculated for both the subgrade and the granular base. Laboratory triaxial resilient modulus tests were performed on samples of both unbound materials according to the NCHRP 1-28A protocol by Burns, Cooley, Dennis, Inc. The multivariable, non-linear stress sensitivity model (Equation 40) recommended by the MEPDG was fit to the test data (*79, 80*). The model coefficients are shown in Table 7.8 for the subgrade and unbound granular base materials.

$$M_r = k_1 p_a \times \left(\frac{\theta}{p_a}\right)^{k_2} \times \left[\left(\frac{\tau_{oct}}{p_a}\right)+1\right]^{k_3} \quad (40)$$

where,

M_r = resilient modulus,
p_a = atmospheric pressure (14.696 psi),
θ = bulk stress = $\sigma_1 + \sigma_2 + \sigma_3 = \sigma_1 + 2\sigma_{x,y}$,
σ_1 = major principal stress = $\sigma_z + p_o$,
σ_2 = intermediate principal stress = σ_3 for M_r test on cylindrical specimen,
σ_3 = minor principal stress/confining pressure = $\sigma_{x,y} + k_o\,(p_o)$,
σ_z = vertical stress from wheel load(s) calculated using layered-elastic theory,
$\sigma_{x,y}$ = horizontal stress from wheel load(s) calculated using layered-elastic theory,
p_o = at-rest vertical pressure from overburden of paving layers above unbound layer or subgrade,
k_o = at-rest earth pressure coefficient,
τ_{oct} = octahedral shear stress = $\frac{1}{3}((\sigma_1 - \sigma_2)^2 + (\sigma_1 - \sigma_3)^2 + (\sigma_2 - \sigma_3)^2)^{1/2}$, and
k_1, k_2, k_3 = regression coefficients.

A design resilient modulus was calculated using Equation 40 for the pavement structures shown in Figure 7.1. Additional values were calculated for a 12-in. thick HMA section for use in sensitivity analyses to be described later in this chapter. The design values were calculated using an iterative process as described in the MEPDG (*80*). The wheel-load stresses were calculated for a 20,000-lb, single-axle load using WESLEA for Windows. Dynamic modulus values for the PG 67-22 and PG 76-22 mixes were calculated at a mean annual temperature of 74.3°F and 10 Hz frequency. The design resilient modulus values are summarized in Table 7.9. All of the design values matched the calculated values within 5%. The lower M_r values for the granular base were unexpected; however, they were consistent with previous laboratory testing conducted by the Alabama Department of Transportation (*81*) and back-calculated values from falling-weight deflectometer tests (*79*). Also, the subgrade consisted of a very angular material with good compactibility and strength.

Dynamic modulus testing was conducted on lab-compacted, field mixed material sampled from the 2003 NCAT Test Track by Purdue University. For the MEPDG, the dynamic modulus (E^*) results were used as Level 1 inputs. For PerRoad, a sigmoidal function, in the form recommended by the MEPDG (*82*), was fit to the experimental data. The E^* data are presented in Table 7.10 for the PG 67-22 and PG 76-22 19.0-mm NMAS base mixtures. The E^* master curves for the PG 67-22 and PG 76-22 mixtures are shown graphically in Figure 7.4. Observation of the data in Table 7.10 and Figure 7.4 suggests that the E^* values for the PG 67-22 and PG 76-22 mixtures are approximately equal.

The temperature data from the 2003 cycle of the NCAT Test Track were used for the PerRoad analysis. Figure 7.5 shows a frequency distribution of the air temperature data. The temperature corresponding to the 10th, 30th, 50th, 70th, and 90th percentiles of the frequency distribution were used to identify five "seasons" for the analysis. The air temperatures were converted to pavement temperatures at ⅓ of the HMA depth using Equation 41 (*7*). Dynamic modulus values were then calculated at 10 Hz for five temperatures determined from a frequency distribution of the pavement temperatures

Table 7.8. Unbound materials stress-sensitivity model coefficients (*79*).

Material	k_1	k_2	k_3	R^2
Granite Base	716.28	0.8468	-0.4632	0.93
Subgrade	1878.97	0.4067	-0.7897	0.42

Table 7.9. Design resilient modulus values for 2003 NCAT Test Track.

Section	Binder Grade	Total HMA Thickness, in.	Granular Base M_r, psi	Subgrade M_r, psi
N1	PG 76-22	5	17,500	26,000
N2	PG 67-22	5	17,500	26,000
N3	PG 67-22	9	12,000	18,000
N4	PG 76-22	9	12,000	18,000
N5	PG 76-22	7	14,000	21,000
N6	PG 67-22	7	14,000	21,000
Perpetual	PG 67-22	12	9,000	14,000
Perpetual	PG 76-22	12	9,000	14,000

experienced by the structural sections of the 2003 NCAT Test Track. The modulus values used for determining shift factors for the test track sections and subsequent sensitivity analyses are presented in Table 7.11.

$$MMPT = MMAT\left(1+\frac{1}{Z+4}\right)-\frac{34}{Z+4}+6 \quad (41)$$

where,

MMPT = mean monthly pavement temperature, °F,
MMAT = mean monthly air temperature, °F, and
Z = depth below surface at the upper third point of the layer, in.

For PerRoad, the load spectra were determined from the 2003 NCAT Test Track records. The average daily truck traffic in the design lane was 1,237 trucks. The triple trailers made up 88.5% of the truck traffic and the five-axle, single trailer comprised the remaining 11.5%. This results in 8,091 axle groups (or repetitions of an axle configuration) per day. The axle configurations had the following distribution: 15.3% steer axles (10,000–12,000 lbs); 67.7% single axles (20,000–22,000 lbs); and

Table 7.10. Dynamic modulus data of 2003 NCAT Test Track base mixtures (*after 81*).

Temperature, °F	Frequency, Hz	PG 76-22 Mixture			PG 67-22 Mixture		
		Avg. E*, psi	Std. Dev. E*, psi	COV, %	Avg. E*, psi	Std. Dev. E*, psi	COV, %
14	0.1	2,277,563	301,583	13.2%	2,298,485	192,823	8.4%
	0.5	2,725,367	337,116	12.4%	2,724,243	255,820	9.4%
	1	2,907,715	357,532	12.3%	2,897,164	276,114	9.5%
	5	3,304,176	410,690	12.4%	3,289,201	315,239	9.6%
	10	3,502,587	421,351	12.0%	3,421,801	320,689	9.4%
	25	3,689,759	450,429	12.2%	3,617,276	355,717	9.8%
40	0.1	1,153,195	203,310	17.6%	1,072,481	131,115	12.2%
	0.5	1,474,779	268,533	18.2%	1,395,625	157,677	11.3%
	1	1,623,189	300,838	18.5%	1,543,418	168,029	10.9%
	5	1,988,503	376,758	18.9%	1,920,335	188,822	9.8%
	10	2,148,479	421,027	19.6%	2,087,564	198,544	9.5%
	25	2,404,942	474,083	19.7%	2,327,093	210,715	9.1%
70	0.1	394,829	44,604	11.3%	378,875	67,659	17.9%
	0.5	565,357	71,916	12.7%	547,046	83,215	15.2%
	1	653,141	84,367	12.9%	643,423	88,274	13.7%
	5	913,955	125,840	13.8%	930,961	106,425	11.4%
	10	1,061,821	150,939	14.2%	1,064,722	116,677	11.0%
	25	1,243,734	184,064	14.8%	1,310,597	148,638	11.3%
100	0.1	151,383	15,348	10.1%	139,490	29,780	21.3%
	0.5	214,801	16,759	7.8%	197,650	38,716	19.6%
	1	254,106	17,495	6.9%	233,293	42,084	18.0%
	5	404,945	28,959	7.2%	359,657	57,351	15.9%
	10	507,342	34,227	6.7%	445,592	64,055	14.4%
	25	614,706	47,519	7.7%	574,095	105,440	18.4%
130	0.1	65,267	3,879	5.9%	63,055	6,364	10.1%
	0.5	83,832	5,467	6.5%	79,553	7,576	9.5%
	1	95,036	6,564	6.9%	89,815	9,182	10.2%
	5	142,898	4,857	3.4%	135,103	19,120	14.2%
	10	174,009	4,556	2.6%	167,845	25,931	15.4%
	25	218,137	16,623	7.6%	215,345	40,140	18.6%

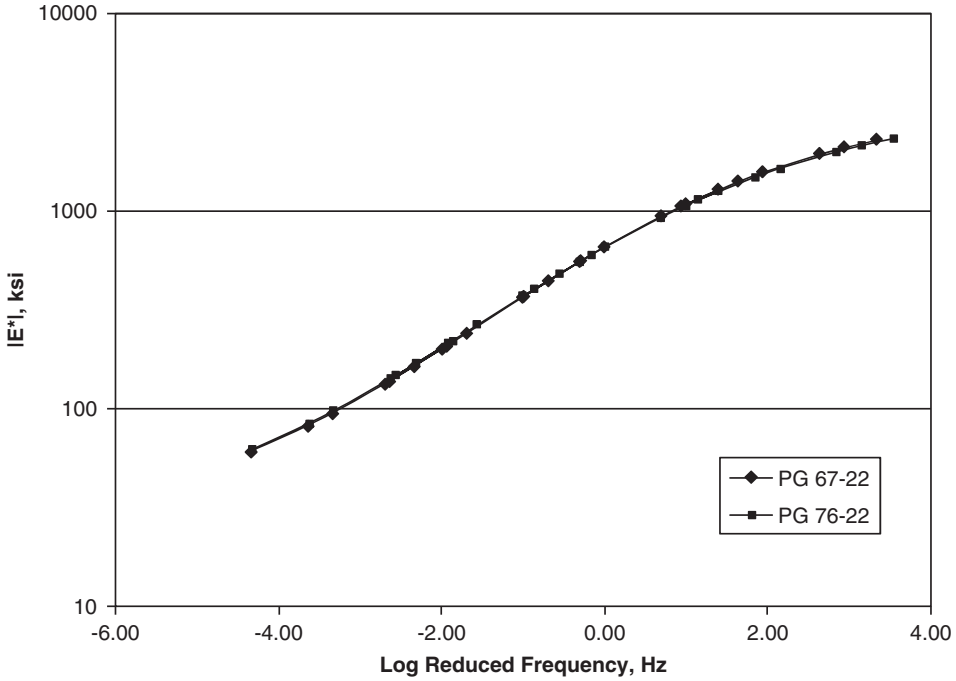

Figure 7.4. Master curves for PG 67-22 and PG 76-22 19.0-mm NMAS base mixtures at optimum asphalt content.

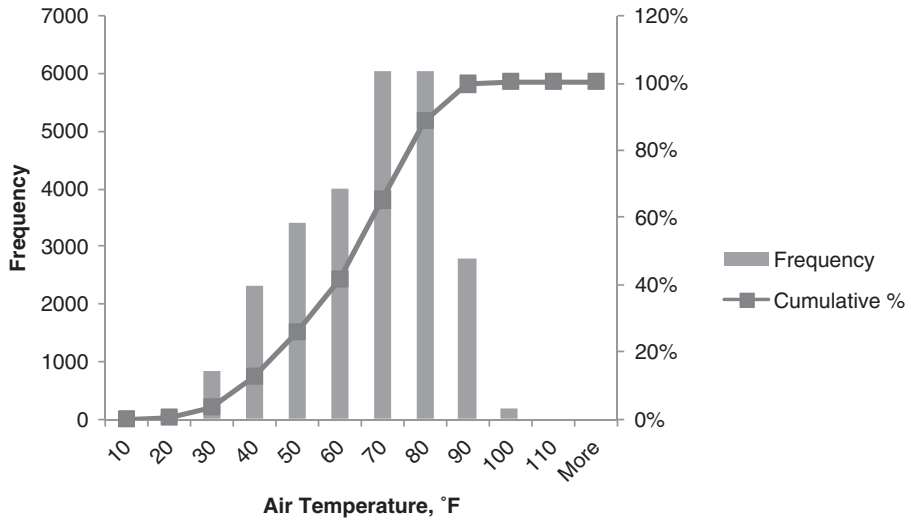

Figure 7.5. Frequency distribution of air temperature data for the 2003 NCAT Test Track.

Table 7.11. Summary of PerRoad E* inputs.

Season	Length, Weeks	20th Percentile Air Temperature, °F	Sections N1 and N2, 5 in. thick			Sections N3 and N4, 9 in. thick			Sections N5 and N6, 7 in. thick			Perpetual Section		
				E*, psi			E*, psi			E*, psi			E*, psi	
			MMPT, °F	PG 67-22	PG 76-22	MMPT, °F	PG 67-22	PG 76-22	MMPT, °F	PG 67-22	PG 76-22	MMPT, °F	PG 67-22	PG 76-22
Summer	9	80.6	94.8	158,401	168,421	93.3	166,643	177,089	94.0	162,895	173,149	89.6	187,724	199,180
Fall	12	72.2	84.9	219,579	232,367	83.7	229,303	242,454	84.2	224,897	237,886	80.8	252,532	266,478
Winter	10	37.1	43.6	770,325	798,342	43.5	772,034	800,051	43.6	771,269	799,286	44.0	765,289	793,302
Spring	11	53.2	62.6	501,586	526,939	61.9	509,352	534,864	62.2	505,866	531,307	60.9	522,602	548,371
Spring 2	10	65.5	77.1	286,911	301,854	76.0	297,443	312,652	76.5	292,685	307,775	73.8	320,829	336,568

Table 7.12. Shift factors from PerRoad analyses.

Section	Shift Factor Based on All Seasons	Shift Factor Neglecting Summer Season
N1	13.4	6.7
N2	45.0	19.2
N6	17.6	NA

NA = Not applicable because Section N6 went through two summer seasons.

17.0% tandem axles (20.6% of which were 32,000–34,000 lbs and 79.4% of which were 40,000–42,000 lbs). For the MEPDG, the triple-trailer trucks were modeled as FHWA Class 13 vehicles, neglecting the steer axle, and the five-axle single trailer truck was modeled as a Class 9 vehicle.

Shift factors were calculated using PerRoad for three sections: N1, N2, and N6. It was not felt that Section N8, with debonding occurring part way through the loading cycle, could be modeled with PerRoad. PerRoad runs a 5,000-cycle Monte Carlo simulation. The default variability was used for the modulus and thickness of the HMA and granular layers. Monte Carlo runs are distributed over the five seasons based on the number of weeks for each season and based on the distribution of axle loads. A resulting strain at the bottom of the HMA layer is output for each iteration of the Monte Carlo simulation. The strain was converted to damage per axle repetition using Equations 38 and 39 and the coefficients in Table 7.6 corresponding to the mixture used in a particular section. The average damage per axle repetition was calculated and multiplied by the total number of axle repetitions when the section failed or, in the case of Section N6, reached the end of the 2003 loading cycle. A shift factor was determined for the transfer function for a given section using Microsoft Excel Solver by minimizing the difference squared between the observed and calculated total damage. The shift factors are summarized in Table 7.12. Because Sections N1 and N2 did not go through a summer before they failed, the summer season data were removed and a new average damage and fatigue transfer function shift factor calculated. This shift factor is lower since higher strains (and hence more damage) were observed during the summer season.

An estimate of predicted cracking for the 2003 Test Track Sections was determined using the MEPDG (Version 1.0) and the nationally calibrated fatigue model (not the fatigue transfer functions developed as part of this research). The climate data were determined from the Enhanced Integrated Climatic Model using the test track's coordinates: latitude 32.36, longitude –85.18, elevation 630 ft, and depth to water table (on north tangent) of 12.5 ft. Three weather stations' data were used in the analysis: Columbus, GA; Troy, AL; and Montgomery, AL. The subgrade and granular base were modeled as Level 2 inputs. The M_r values are summarized in Table 7.9. The remaining granular base and subgrade inputs were taken from Taylor and Timm (*79*).

Level 1 inputs were used for the HMA. The entire HMA layer was modeled as the base material for simplicity (recall the surface layer is only 1-in. thick). The dynamic modulus results are summarized in Table 7.10. The binder properties are summarized in Table 7.13. The volumetric properties for specific sections were taken from Taylor and Timm (*79*). For the sensitivity analyses, described in the next section, the average volumetric properties were used, as follows:

- Air voids = 6%,
- Volume of effective binder = 10.5%, and
- Unit weight = 150.5 pcf.

Unless otherwise stated, the MEPDG default values were used for uncommon items, such as thermal properties.

Unlike PerRoad, the MEPDG does not output its raw layered elastic calculations. Therefore, a shift factor could not be calculated directly in the same manner as was done with PerRoad. The predicted cracking as a function of time is shown in Figure 7.6 for Section N1 and in Figure 7.7 for Sections N2 and N6. The MEPDG provides the predicted (50% reliability) bottom-up fatigue cracking, termed *maximum cracking*, and the predicted cracking at some level of reliability, in this case,

Table 7.13. 2003 NCAT Test Track binder properties for MEPDG.

Test Temperature, °F	PG 67-22		PG 76-22	
	G*, Pa	Delta, °	G*, Pa	Delta, °
136.4	13.610	73.2	--	--
147.2	6.125	76.7	6.597	65.9
158.0	2.832	80.0	3.683	67.3
168.8	--	--	2.057	69.1

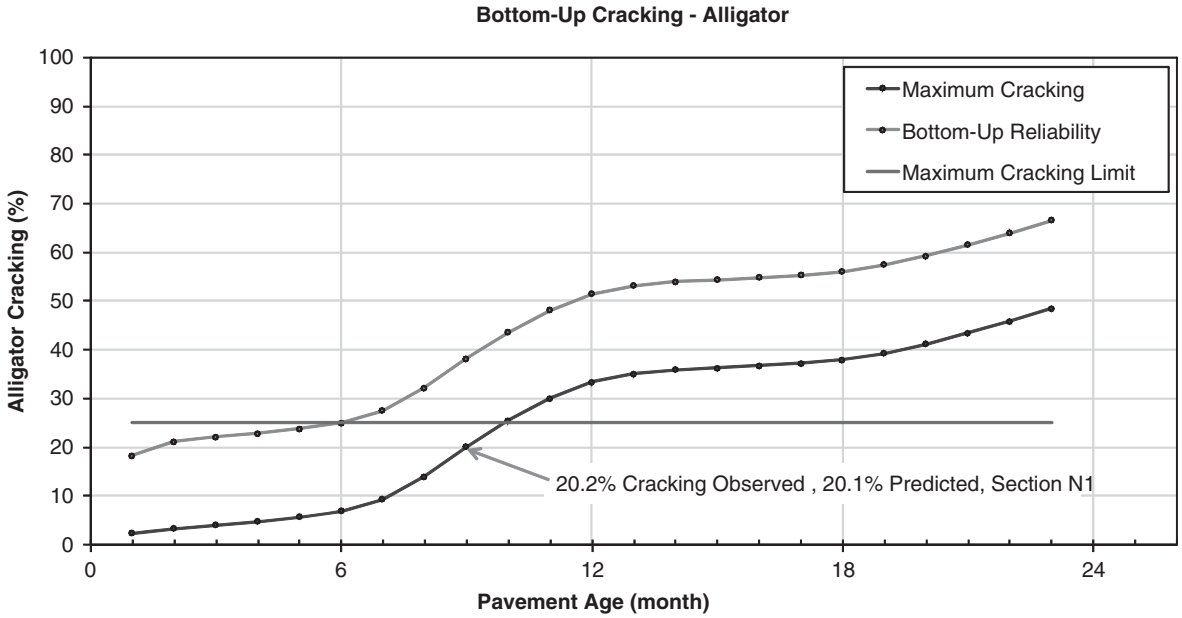

Figure 7.6. MEPDG predicted cracking for Section N1 (PG 76-22), 2003 NCAT Test Track.

90%, termed *bottom-up reliability* in Figures 7.6 and 7.7 (and in the MEPDG output). The MEPDG recommends reliabilities between 85% and 97% for urban interstate-type pavements and between 80 and 95% for rural interstate-type pavements (*83*). Observation of Figure 7.6 suggests that the maximum cracking (20.1%) closely approximates the observed cracking (20.2%) for Section N1 at the 2003 NCAT Test Track. However, the 90% reliability bottom-up cracking is significantly higher (38.2%). For Section N2, the observed cracking (19.5%) exceeded the maximum cracking (14.4%), but was again less than the 90% reliability cracking (32.5%).

In the MEPDG, damage is related to predicted cracking according to Equation 42 (*84*). Note that the minus sign between C_1 and C_2 in the equation in El-Basyouny and Witczak (*74*) is incorrect, and should be a plus sign as shown below.

$$FC = \left(\frac{6{,}000}{1+e^{C_1+C_2\times \mathrm{Log}\,D}}\right)\times\left(\frac{1}{60}\right) \qquad (42)$$

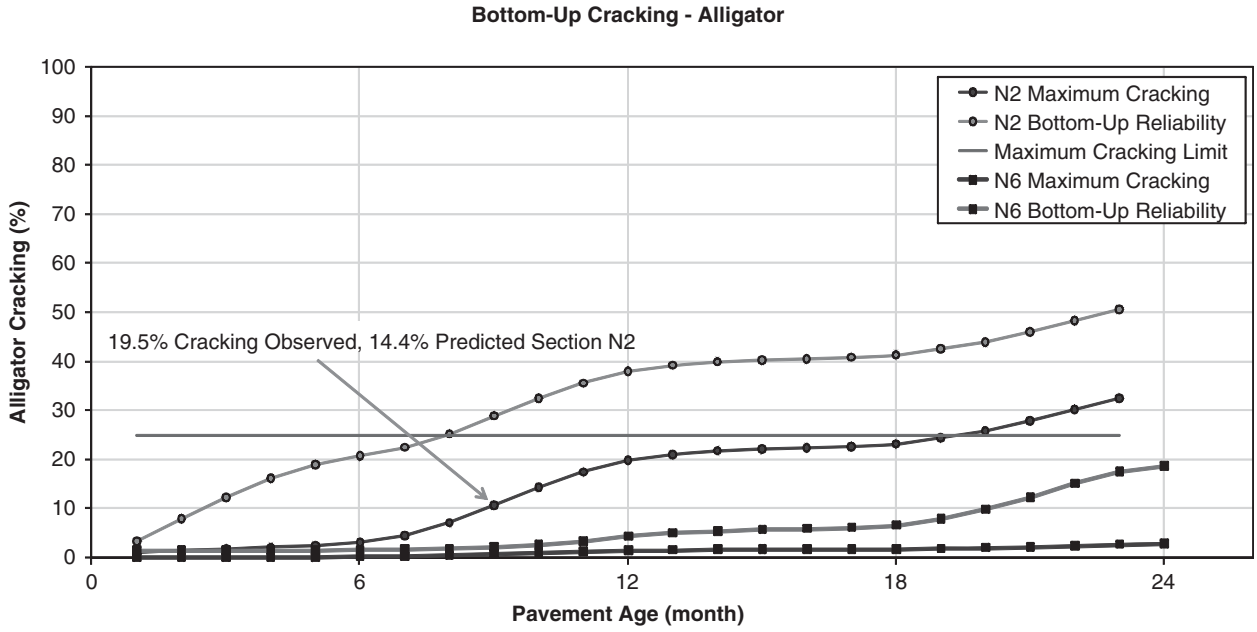

Figure 7.7. MEPDG predicted cracking for Sections N2 and N6 (PG 67-22), 2003 NCAT Test Track.

where,

FC = fatigue cracking (% of lane area),
$C_1 = 2 \times C_2$,
$C_2 = -2.40874 - 39.748 \text{ x } (1+h_{ac})^{-2.85609}$
h_{ac} = thickness of the HMA (in.),
D = cumulative theoretical fatigue damage, %.

Solving Equation 42 for a 5-in.-thick pavement, a cumulative damage of 0.294 (29.4%) corresponds to 20% cracking of the lane area. Considering the predicted cracking described above and back-calculating the corresponding cumulative damage, the shift factor would be approximately 1.0 for Section N1, and approximately 0.73 for Section N2.

Summary of Observed Shift Factors from 2003 NCAT Test Track Structural Sections

The observed shift factors based on the performance of the 2003 NCAT Test Track structural sections are summarized in Table 7.14. Based on the measured strains and the PerRoad analyses, the shift factor for the PG 67-22 mix at optimum asphalt content exceeds the assumed shift factor of 10.0. The shift factors for the PG 76-22 mix at optimum asphalt content, represented by Section N1, from both the measured strain and PerRoad analyses, are less than 10.0. The beam fatigue results for the PG 76-22 mix were variable, with some long fatigue lives observed at relatively high strain levels (see Table 4.4). This same variability resulted in a reduced 95% prediction limit of the endurance limit. The shift factor for Section N8, the PG 67-22 mix at optimum plus binder content, is slightly less than 10.0; however, this analysis was based on several assumptions regarding the measured strains once slippage between the layers occurred.

The fatigue equations developed from the laboratory testing were not used in the MEPDG, rather the NCHRP 1-37A calibrated fatigue models (*64*) were used. Based on these analyses, the MEPDG fatigue model reasonably predicts the observed cracking. However, design is based on the predicted cracking at some level of reliability being less than 25% area cracking. The 90% reliability cracking in Sections N1 and N2 exceeded the observed cracking by 91% and 68%, respectively.

In Chapter 3, a practical definition of a long-life or perpetual pavement is one able to withstand 500 million axle repetitions in a 40-year period without failing. A shift factor of 10 was assumed, resulting in a laboratory equivalent of 50 million repetitions. Based on the analyses in this section, a shift factor of 10 appears reasonable. Varying the shift factor when determining the endurance limit is not recommended.

Sensitivity of Mechanistic-Empirical Pavement Design Methods to the Endurance Limit

Four sensitivity analyses were conducted to assess the impact of the endurance limit on pavement design. The first analysis compared pavement design thicknesses using conventional and perpetual design procedures. The second analysis looked at the sensitivity of perpetual designs to the measured value of the endurance limit. The traffic and materials from the 2003 NCAT Test Track were used in the first two analyses. Since the NCAT Test Track used a limited range of axle weights, the third and fourth analyses were performed using the materials from the 2003 NCAT Test Track but the MEPDG's default truck traffic classification No. 1 for principal arterials. The third and fourth analyses repeated the first two analyses with a distribution of axle types and weights that are representative of typical traffic on a principal arterial.

NCAT Test Track Traffic

The 2003 NCAT Test Track pavement section was designed using three methodologies: 1993 AASHTO procedure, MEPDG Version 1.0, and PerRoad Version 3.3. The 1993 AASHTO design was conducted using a change in pavement serviceability index (PSI) = 1.2, design reliability = 95%, and an overall standard deviation = 0.45 for 200 million ESALs, the expected traffic over a 40-year period. The structural number was determined from the AASHTO design equation (*42*) numerically using the bisection method. Two design subgrade M_r values were used in the analysis, 5,500 psi used in the original design of the 2000 Track (*72*), and 14,000 psi, the value from Table 7.9 used in the perpetual designs. Layer coefficients

Table 7.14. Summary of observed shift factors.

Section	Measured Strain	PerRoad	MEPDG
N1	4.2	6.7	1.0
N2	75.8	19.2	0.73
N6	38.0	17.6	*
N8	8.3	NA	NA

Notes:
*Since the MEPDG bases failure on 20% cracking and this did not occur in Section N6, shift factor could not be calculated.
NA = Not applicable; no attempt was made to model debonding as part of this research.

of 0.14 and 0.44 were assigned to the granular base and HMA, respectively.

$$\log_{10} W_{18} = Z_R \times S_o + 9.36 \times \log_{10}(SN+1) - 20 + \frac{\log_{10}\left[\frac{\Delta PSI}{4.2-1.5}\right]}{0.40 + \frac{1094}{(SN+1)^{5.19}}} + 2.32 \times \log_{10} M_R - 8.07 \quad (43)$$

where,

W_{18} = the number of expected 18-kip ESALs in the design lane over the design life 200×10^6,
Z_R = the normal deviate associated with the chosen level of reliability, 90% = −1.28,
S_0 = materials standard deviation, 0.45,
SN = structural number,
ΔPSI = initial minus terminal serviceability, 1.2, and
M_R = effective soils resilient modulus, psi.

MEPDG analyses were performed using the inputs described previously. The three scenarios examined included 20-year and 40-year designs with 90% reliability of bottom-up cracking of less than 25% of the total lane area, and a 40-year perpetual analysis where the pavement thickness was selected to provide maximum damage and cracking = 0% at the end of 40 years.

The PerRoad analyses were performed using the inputs described previously. Both the MEPDG and PerRoad perpetual analyses used the respective one-sided 95% lower prediction limits of the endurance limit for the PG 67-22 (151 ms) and PG 76-22 (146 ms) mixes at optimum asphalt content determined in Phase I of this study. The design thickness was selected such that approximately 95% of the load applications were less than the endurance limit (*85*).

The results are summarized in Figure 7.8. All three MEPDG design thicknesses are less than that determined from the 1993 AASHTO Pavement Design Guide. Although the 20-year and perpetual MEPDG designs are the same thickness, the implications are significantly different. In the first case, at 90% reliability, bottom-up cracking over 20% of the lane area would be expected after 20 years; in the second case, no cracking would be expected after 40 years. This is further illustrated in Table 7.15 where pavement thickness was iterated in the MEPDG without specifying an endurance limit and the resulting damage determined. Thicknesses of 39 in. and 35 in. were required for the PG 67-22 and PG 76-22 mixes at optimum asphalt content to achieve predicted cracking performance similar to that achieved when an endurance limit was considered (for maximum cracking of 0% to be predicted at the end of 40 years). Some damage was predicted in all of the cases tested, including 1.45% bottom-up cracking at 90% reliability, which was predicted to occur in the first month of service.

It was expected that the PerRoad perpetual thickness would be less than that determined with the MEPDG. This expectation was based on the differences in the manner in which both programs handle pavement temperatures. For PerRoad, up to five seasons can be specified, with corresponding moduli for each season. Typically, this would be based on grouping average monthly temperature data. In this analysis, actual temperature data from the 2003 NCAT Test Track cycle were grouped and used in the analyses. This most likely resulted in higher temperatures being selected for the warmer season, which results in correspondingly lower design moduli. During PerRoad's Monte Carlo simulations, modulus is allowed to vary within a season based on a log-normal distribution. The default coefficient of variation used in this study is 30%. For the MEPDG, temperatures are predicted using the Enhanced Integrated Climatic Model on an hourly basis. They are then

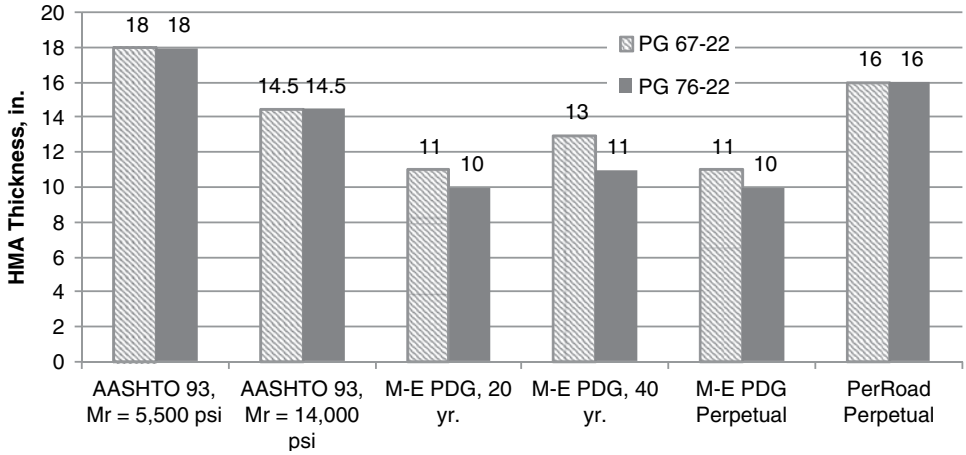

Figure 7.8. Comparison of pavement thicknesses from empirical, M-E, and perpetual design methodologies.

Table 7.15. Damage as a function of pavement thickness for the MEPDG with no endurance limit.

HMA Thickness, In.	PG 67-22 at Optimum			PG 76-22 at Optimum		
	Maximum Damage, %	Maximum Cracking, %	90% Reliability, Bottom-Up Cracking	Maximum Damage, %	Maximum Cracking, %	90% Reliability, Bottom-Up Cracking
10				11.5	9.07	27.18
11	14.5	11.4	29.51	6.57	5.28	23.29*
12	8.92	7.21	25.31			
13	5.67	4.61	22.45*			
15	2.47	1.99	6.52			
20	0.442	0.34	1.79	0.195	0.14	1.59
22				0.109	0.08	1.53
23				0.0838	0.06	1.51
25	0.112	0.08	1.53	0.0501	0.03	1.48
27				0.031	0.02	1.47
30	0.0352	0.02	1.47	0.0159	0.01	1.46
33	0.0191	0.01	1.46			
35	0.0132	0.01	1.46	0.00601	0*	1.45
37	0.00927	0.01	1.45			
38	0.00782	0.01	1.45			
39	0.00664	0*	1.45			
40	0.00564	0	1.45	0.00258	0	1.45
41	0.00481	0	1.45			
42	0.00413	0	1.45			
45	0.00264	0	1.45			

Note:
*Indicates minimum thickness with cracking less than 25% of total lane area at the end of the design life.

collected into five "bins" on a monthly basis for determination of layer moduli. This would be expected to result in higher temperatures occurring at some points during the year and, hence, lower moduli and higher strains.

A second difference that may have affected the MEPDG versus the PerRoad results is the way that the layers were subdivided for calculation purposes. For the PerRoad analysis, the HMA was treated as a single layer. The pavement temperature was calculated according to Equation 44 (*86*).

$$MMPT = 1.05 \times MMAT + 5 \quad (44)$$

where,

MMPT = mean monthly pavement temperature, °F and
MMAT = mean monthly air temperature, °F.

Equation 44 is representative of the average temperature of the HMA layer for pavement ≥ 10 in. thick. By comparison, the 10-in.-thick MEPDG section was subdivided (automatically) into seven layers, the top 0.5 in., the next 0.5 in., three 1.0-in. sublayers, a 4.0-in. sublayer and a bottom 2.0-in. sublayer. Pavement temperatures and corresponding moduli were calculated for each of these layers. The net result of this is that the temperature of the bottom 2-in. layer tends to be lower, resulting in a higher layer moduli, and, therefore, lower strains.

The second set of analyses examined the sensitivity of the MEPDG and PerRoad to the measured endurance limit using the NCAT Test Track traffic. Pavement design simulations were conducted using both the PG 67-22 and PG 76-22 mixes at optimum asphalt content, the previously described pavement design parameter, and three levels of the endurance limit: 70 ms, 100 ms, and the measured endurance limits (151 and 146 ms, respectively). The results, illustrated graphically in Figures 7.9 and 7.10 for the PG 67-22 and PG 76-22 mixes, respectively, indicate that the perpetual pavement design thickness is extremely sensitive to the measured endurance

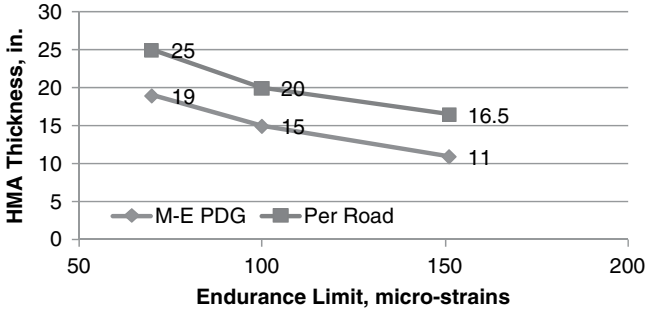

Figure 7.9. Sensitivity of pavement thickness to endurance limit for PG 67-22 mixes.

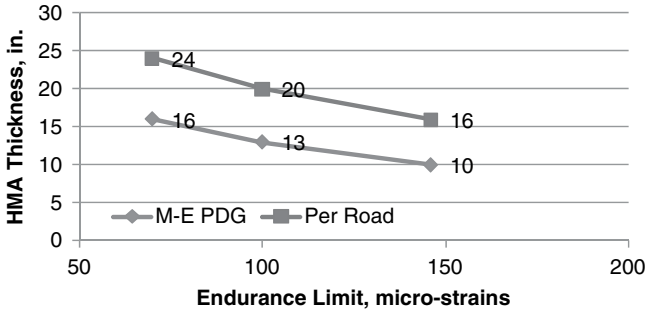

Figure 7.10. Sensitivity of pavement thickness to endurance limit for PG 76-22 mixes.

limit. The use of polymer modified PG 76-22 has a more substantial impact on pavement thickness with the MEPDG, as compared to PerRoad with the difference in thickness ranging between 1.0 and 3.0 in., depending on the endurance limit. Larger differences were observed with lower endurance limits.

Typical Principal Arterial Truck Traffic Classification

The third and fourth set of analyses examined the sensitivity of the MEPDG and PerRoad to the measured endurance limit using a normal load spectra that might be expected on a principal arterial. Pavement design simulations were conducted using the PG 67-22 mix at optimum asphalt content, the previously described pavement design parameters, and three levels of the endurance limit: 70 ms, 100 ms, and the measured (151 ms) endurance limit.

The MEPDG's Level 3 default truck traffic classification No. 1 and associated axle weight distributions for principal arterials were used for the load spectra. The MEPDG produces a file that records the accumulated ESALs on a monthly basis throughout the design life of the project. For the NCAT Test Track traffic, the MEPDG calculated 171,514,458 ESALs at the end of 40 years, assuming no growth. The average annual daily truck traffic (AADTT) was adjusted using the Level 3 default truck traffic classification No. 1 to produce a similar number of ESALs after 40 years (171,561,129). An AADTT of 21,833 with a 50% directional split, two lanes in each direction, and 90% of the trucks in the design lane were used for the calculations.

Traffic can be defined in PerRoad in two manners: FHWA vehicle class using default axle weight distributions or axle weight distribution by type (single, tandem, etc.). The MEPDG default truck traffic classification No. 1 was converted to the format used by PerRoad. The axle load configuration consisted of 9,824 axle groups per day in the design lane, of which 45.2% were single axles, 54.3% were tandem axles, and 0.5% were tridem axles. The load spectra for the three axle types are shown in Figure 7.11.

Figure 7.12 shows the sensitivity of the MEPDG and PerRoad to the measured endurance limit. Both the MEPDG and

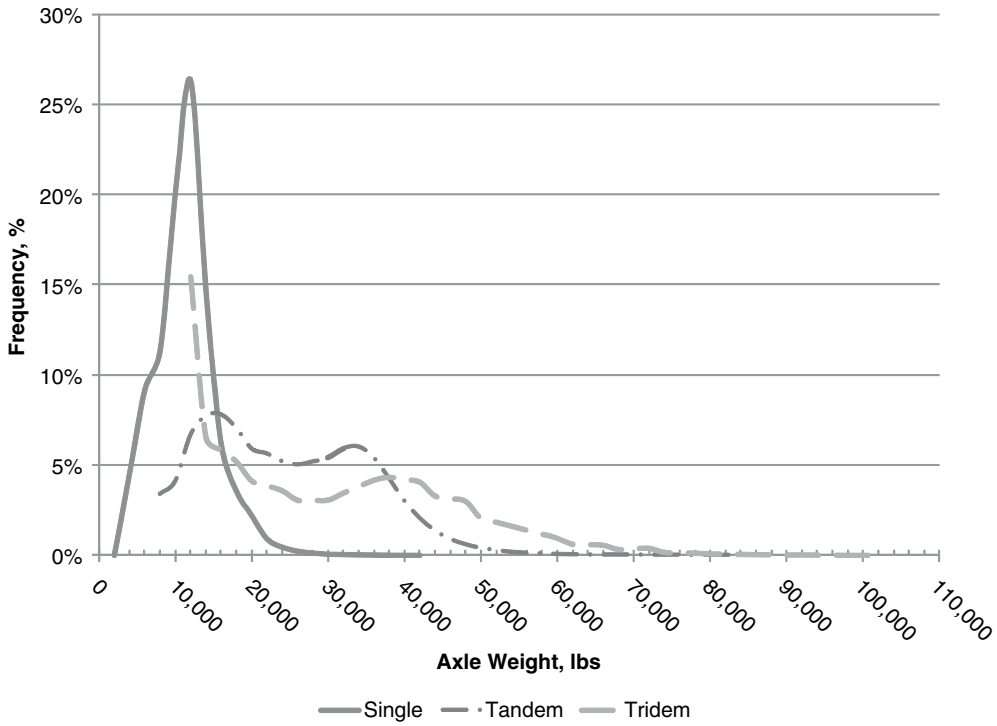

Figure 7.11. Axle weight distribution used in PerRoad.

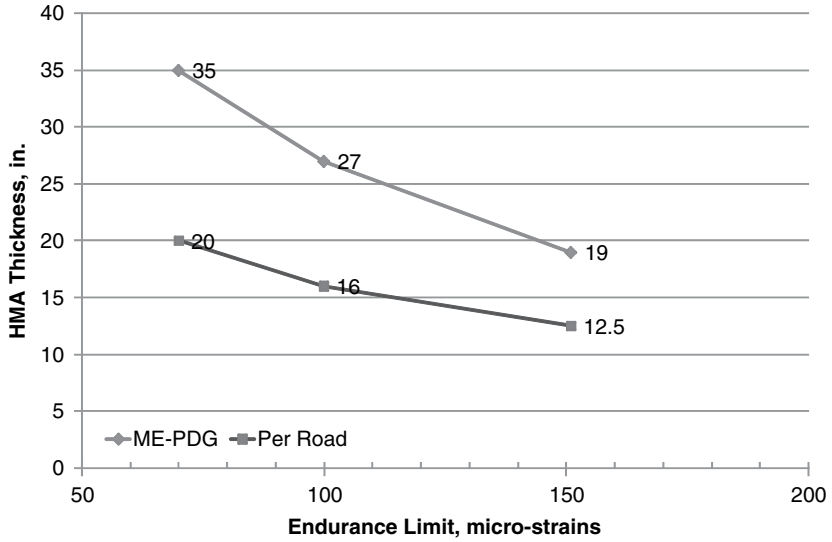

Figure 7.12. Sensitivity of pavement thickness to the endurance limit for typical axle distribution.

PerRoad are sensitive to changes in the measured endurance limit. For the MEPDG, a change in the endurance limit of 50 ms results in a change in pavement thickness of approximately 7 to 8 in. For PerRoad, a change in the endurance limit of 50 ms results in a change in pavement thickness of approximately 4 in. This sensitivity highlights the need to measure the endurance limit as accurately as possible.

Finally, design thicknesses were determined using the MEPDG and 1993 AASHTO Pavement Design Guide using design lives of both 20 and 40 years without considering an endurance limit. For the MEPDG, the thickness that resulted in at least 90% reliability against both bottom-up and top-down fatigue cracking was determined. Figure 7.13 shows a comparison of the conventional and perpetual design thicknesses.

The PerRoad perpetual design using the measured endurance limit of 151 ms is slightly less thick than the 40-year empirical design using the 1993 AASHTO Design Guide. The MEPDG thicknesses considering only fatigue cracking are similar to the PerRoad thickness. However, at an 11-in. pavement

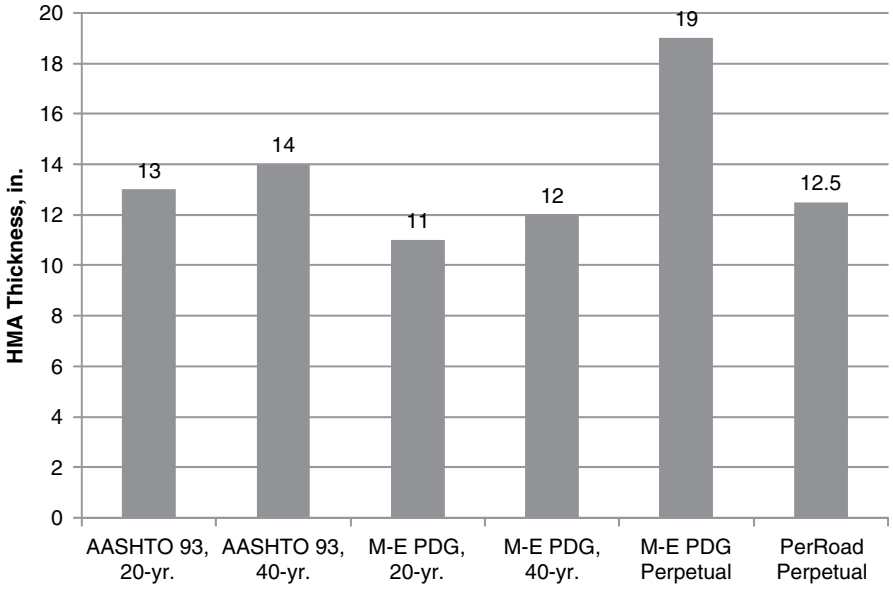

Figure 7.13. Comparison of pavement thicknesses from empirical, M-E, and perpetual design methodologies for typical axle distribution.

thickness, the 20-year MEPDG design fails the reliability criteria for terminal international roughness index (IRI), total pavement rutting, and HMA rutting. The HMA thickness must be increased to 14 in. to produce an acceptable reliability for terminal IRI. The HMA thickness must be increased to 30 in. to produce an acceptable reliability against total pavement rutting. The reliability for HMA rutting can not be achieved for this level of traffic in the NCAT Test Track's climate using a PG 67-22 binder. The perpetual thickness determined using the MEPDG is significantly thicker than that determined using PerRoad when considering a typical axle distribution.

Although the pavement thicknesses appear similar between conventional empirical or mechanistic designs and the perpetual pavement thickness determined using PerRoad, again the implications are very different. Based on the conventional MEPDG results, the 11-in. HMA pavement would be expected to have maximum cracking of 4.8% of the lane area after 20 years. The 90% reliability for bottom-up cracking is 22.72% of the lane area. Similarly, for the 12-in. pavement after 40 years, maximum bottom-up cracking was predicted at 5.9% with a 90% reliability of 23.99% of the lane area. Based on the conventional analysis, the pavement will have failed and be in need of reconstruction, whereas the perpetual analysis suggests that at a similar thickness there should be no bottom-up fatigue cracking after 40 years. This difference would have a significant effect on life-cycle cost analysis.

Summary of Sensitivity Analyses

The design thickness for a perpetual pavement is very sensitive to the measured endurance limit using both the MEPDG and PerRoad. Considering a typical traffic stream, a 50-ms change in the endurance limit resulted in a 7- to 8-in. or 4-in. change in HMA thickness, respectively, with the MEPDG and PerRoad. This sensitivity highlights the need for accurate determination of the endurance limit. To improve accuracy, the number of strain levels used to predict the endurance limit in Appendix A was increased from two to three with three replicates at each level from that used in Phase II of the study. Additional samples should reduce the standard error of the log-log regression and result in a smaller t-value when calculating the lower, one-sided prediction limit (endurance limit).

Again considering a normal traffic stream, the PerRoad perpetual design thickness was slightly less than that determined using the 1993 AASHTO Pavement Design Guide, and approximately the same as that required to satisfy the fatigue requirements of a 20- or 40-year MEPDG design (not considering the endurance limit). However, the predicted conditions of the pavement at the end of the design life are significantly different. At 90% reliability, the MEPDG would predict over 20% of the lane area to be cracked at the end of the design life whereas the perpetual pavements would not be expected to have any cracking. This significantly changes the required maintenance and rehabilitation requirements in a life-cycle cost analysis.

Considerations for Incorporating the Endurance Limit into M-E Design Procedures

In the preceding section, sensitivity analyses were presented demonstrating the affect of incorporating the endurance limit into two M-E programs, the MEPDG and PerRoad. Certainly the predicted performance from the MEPDG in terms of bottom-up cracking was improved compared to a conventional 20-year design. Using the experimentally determined endurance limits from this study, there was no increase in the design thickness determined using the MEPDG for a 20-year or perpetual design. The thicknesses determined, 11.0- and 10.0-in., respectively, for the PG 67-22 and PG 76-22 mixes at optimum asphalt content are consistent with Nunn's (*10*) recommendations that long-life pavements should range between 7.9 and 15.4 in. Further, Section N3 and N4 of the 2003 NCAT Test Track have now gone through two test track loading cycles without any observed fatigue cracking (*77*). This indicates that pavement thicknesses close to those designed as perpetual pavements (N3 and N4 are 9 in. thick) with the MEPDG are performing well after a fairly high number (20 million ESALs) of load applications. However, the sensitivity of the required pavement thickness to the measured endurance limit also has been demonstrated, as well as the apparent sensitivity to temperature as evidenced by the increased pavement thicknesses determined using PerRoad. Therefore, consideration should be given as to whether the endurance limit is really best represented by a single value, determined at a single temperature.

One hypothesis is that the fatigue endurance limit is driven, in part, by the ability of asphalt mixtures to heal. Healing occurs more readily at higher temperatures. Therefore, a mixture's fatigue capacity or endurance limit may be higher at higher temperatures. Testing was only conducted at a single temperature, 20°C, as part of this study. Tsai et al. (*87*) tested mixes at three temperatures, 10°C, 20°C, and 30°C, as part of a reflective-cracking study. A total of six samples was tested at each temperature, three each at two strain levels. The samples were compacted to 6% air voids (target). Five binders were tested: AR-4000, type G asphalt rubber (RAC-G), and three modified binders termed MB4, MB15, and MAC16. The endurance limit was predicted from published data included in Tsai et al. (*87*) using the procedure described in Appendix A. The results are shown in Table 7.16. Variations in the predicted endurance limit were observed both

Table 7.16. Predicted endurance limit as a function of test temperature.

Binder	Test Temperature, °C	Predicted Endurance Limit, ms	Lower 95% Prediction Limit, ms
AR-4000	10.2	101	39
	19.9	52	12
	30.4	105	80
RAC-G	10.3	130	91
	20.2	190	106
	30.0	183	124
MAC15	10.0	176	127
	20.0	255	178
	30.3	461	100
MB4	9.9	377	284
	20.5	394	230
	29.8	555	247
MB15	10.1	348	261
	20.0	215	135
	30.4	171	82

with changes in test temperature and binder. Three of the binders generally followed the expected trend of increasing endurance limit with increasing test temperature. In two of the cases, the predicted endurance followed the expected trend, while the 95% lower prediction limit was more variable, due to variability in the beam fatigue test results. For the RAC-G, the 95% lower prediction limit showed a trend of increasing endurance limit with increasing temperature. The MB15 binder indicated decreasing endurance limit with increasing temperature. The AR-4000 binder indicated its lowest endurance limit at 20°C.

Based on measured strains from the NCAT Test Track from sections that have not experienced fatigue cracking, Willis (*77*), proposed designing perpetual pavements based on a cumulative frequency distribution of allowable strains. A similar concept was initially proposed by Priest (*76*). The proposed upper bound for a cumulative frequency distribution of endurance limit strain is shown in Table 7.17 for Sections N3 and N4 of the NCAT Test Track. A cumulative frequency distribution defines the percentage of observed data below a given value. Based on Table 7.17, 50% of the in-service strain values should be less than 181 ms to prevent fatigue cracking. It should be

Table 7.17. Cumulative distribution of strain criteria for long-life pavements (*77*).

Percentile	Upper Bound Fatigue Limit	Maximum Fatigue Ratio
99	394	2.83
95	346	2.45
90	310	2.18
85	282	1.98
80	263	1.85
75	247	1.74
70	232	1.63
65	218	1.53
60	205	1.44
55	193	1.35
50	181	1.27
45	168	
40	155	
35	143	
30	132	
25	122	
20	112	
15	101	
10	90	
5	72	
1	49	

noted that the mean annual air temperature measured during the 2003 NCAT Test Track cycle was 65.5°F, which corresponds to a pavement temperature (based on Equation 44) of 73.8°F. This is greater than the 20°C (68.8°F) test temperature used for the beam fatigue tests. Hence, the fact that the 50% strain values are greater than the endurance limits measured for this study is not unexpected. Table 7.17 also presents strain ratios, which are ratios of the upper bound for the allowable strain at a given percentile to the measured endurance limits (151 ms and 146 ms for the PG 67-22 and PG 76-22 mixes, respectively) determined as part of this study. This offers an opportunity to adjust the distribution based on measured material properties.

Both concepts were developed based on observations that the cumulative frequency distribution of measured strains of sections that did and did not crack differed above the 55th percentile. It should be reiterated that these distributions are based on two sections for which bottom-up fatigue cracking has not been observed after the application of approximately 20 million ESALs. It is possible that fatigue cracking could occur with additional loading.

The last concept that needs to be considered in long-life pavement design is how different rates of loading may be accommodated. In addition to designing against damage from expected axle loads, frequency of application needs to be considered. Low volume roads may, in some cases, experience the same distribution of axle loads over time, but different frequencies of application. Infrequent load applications may offer more time for healing to occur and hence less accumulated damage. If load frequency is not considered, all perpetual pavements designed for the same distribution of axles on the same subgrade will have the same thickness.

CHAPTER 8

Conclusions and Recommendations

Conclusions

The following conclusions may be drawn based on the data presented to date:

- A practical definition of the endurance limit or long-life pavement would be a pavement able to withstand 500 million design load repetitions in a 40-year period.
- Several techniques can be used to evaluate beam fatigue data near the endurance limit. These include logarithmic extrapolation of the loading cycle versus stiffness curve, single- or three-stage Weibull model using the stiffness ratio, and ratio of dissipated energy change (RDEC). The single-stage Weibull model produced fairly accurate extrapolations that appear to be conservative. Extrapolations performed using the single-stage Weibull model resulted in the lowest variability in the mini round-robin. Therefore, the single-stage Weibull model is recommended for extrapolating low strain fatigue tests to confirm the existence of the endurance limit. In certain cases, the three-stage Weibull model may provide a better fit to the experimental data. Procedures for both methods are supplied in Appendix A.
- The data support the existence of an endurance limit for each of the six mixes tested. The 95% lower prediction limit varied from 75 to 200 ms.
- All of the estimated endurance limits were above 70 ms. An analysis of LTPP data indicated an endurance limit of 65 ms.
- On a log basis for normal strain fatigue tests, the repeatability (within-lab) standard deviation was determined to be 0.248 and the reproducibility (between-lab) standard deviation was determined to be 0.318. This results in within- and between-lab coefficients of variation of 5.4% and 6.8%, respectively.
- Uniaxial tension testing provides a promising technique. Results from the uniaxial tension test can be determined more quickly than beam fatigue tests, but the data are more complicated to analyze. There are difficulties controlling the strain that is actually applied to the sample being tested. Additional evaluation is needed to reconcile the difference between beam and uniaxial fatigue results, which produced trends for neat versus polymer modified binders that were the opposite of those determined with beam fatigue testing.
- Field observations, from the data discussed in Chapter 6 and from the NCAT Test Track, support the importance of good construction in addition to pavement thickness design and materials selection.
- Shift factors between laboratory and field performance, based on fatigue transfer functions developed as part of this research, ranged from 4.2 to 75.8.
- Pavement thicknesses for a perpetual design determined using the endurance limits measured as part of this study were consistent with thicknesses observed in previous studies of in-service pavements.
- The MEPDG and PerRoad perpetual design methodologies are sensitive to changes in the endurance limit.
- Considering a typical principal arterial traffic stream, the thickness of a perpetual pavement designed using PerRoad was similar to that determined using the 1993 AASHTO Pavement Design Guide or MEPDG (without the endurance limit) for a 20- or 40-year design life. The thickness of a perpetual pavement designed with the MEPDG was approximately 50% thicker. The predicted condition of the pavement at the end of 20 to 40 years was significantly different, with no cracking expected in the perpetual pavements versus over 20% of lane area cracking at 90% reliability (based on the MEPDG). Damage would also be expected based on a change in serviceability index of 1.2 for the 1993 AASHTO design procedure.

Recommendations

Recommendations from this study address the following five areas: (1) investigation of the endurance limit as a mixture property, (2) additional research and development to further the development of the uniaxial tension test, (3) field testing to investigate cracking observed in thicker LTPP sections that

appear to refute the existence of the endurance limit, (4) incorporation of the endurance limit into pavement design, and (5) cataloging endurance limit values.

Only a single gradation and two aggregate sources blended in a single mix were tested in this study. Further, only a single form of binder modification was evaluated. Table 2.1 presented the affect of a range of factors on fatigue life (*1*). Of these, binder stiffness and air void content were expected to have a larger affect than aggregate type and gradation. Differences were observed in the predicted endurance limit based on binder stiffness. The affect of binder content and in-place air voids was mixed. Few affects were observed for the PG 67-22, but a more pronounced affect was observed for the polymer modified PG 76-22. Additional evaluations should be conducted with a wider range of mixtures, binder types, and modified binders.

The samples tested in this study were short-term samples, oven aged for four hours at 275°F (135°C) according to AASHTO R30. No long-term aging was evaluated. Nunn (*10*) indicates that the stiffness of thick pavements increases with time. This should reduce the strain at the bottom of the asphalt layer. However, the endurance limit or strain "capacity" of the mix may decrease with increased oxidative aging and physical hardening. The affect of long-term aging on the endurance limit should be investigated.

Samples for the uniaxial tension test can be prepared on a gyratory compactor. Uniaxial tension testing is less time-consuming than beam fatigue testing. Therefore, this test method deserves additional development. Basic research should be conducted to better understand the stress states in uniaxial tension samples. Better techniques should be developed to control the strain experienced by the test sample.

Forensic investigations should be conducted on a stratified random sample of the thickest GPS-1, GPS-2, and SPS-1 pavements in the LTPP database that exhibit cracking, to determine the cause of that cracking.

For pavements designed using equivalent annual or equivalent seasonal temperatures, the use of a single value for the endurance limit appears to be reasonable. However, field data presented from the NCAT Test Track indicate that pavements can withstand a cumulative distribution of strains (which includes strain levels that exceed the mixtures' endurance limit, determined at a single temperature, as described in this study) and still exhibit perpetual behavior (*77*). Further, there is evidence that the endurance limit, determined from beam fatigue tests, varies as a function of temperature. Thus, future efforts to incorporate the endurance limit into the MEPDG should consider a distribution of acceptable strains or endurance limits that vary as a function of temperature.

Agencies should use Appendix A, Proposed AASHTO Practice for Beam Fatigue Testing, to determine catalogs of endurance limit values for typical mixes, binder grades, and binder sources. Only a single aggregate source and gradation were tested in this study. Therefore, it is difficult to assess the affect of those parameters on the endurance limit. Based on the literature review, these seem to be secondary factors. The endurance limit catalog should concentrate on mixes used at the bottom of the HMA layer where cracking initiates. An experimental plan should include the binder grades and types of modifiers the agency typically uses in the bottom-lift, laboratory compaction efforts (e.g., N_{design}) if historical experience indicates these different levels result in different optimum asphalt content, and major aggregate types. If the agency is considering the use of a rich-bottom layer, with or without polymer modified binder or a high-modulus base, they should also be included. Laboratory samples should be compacted to a density representative of the level typically achieved in the field.

References

1. Epps, J. A. and C. L. Monismith. "Fatigue of Asphalt Concrete Mixtures-Summary of Existing Information." *ASTM STP 508: Fatigue of Compacted Bituminous Aggregate Mixtures.* American Society for Testing and Materials, Coshocken, PA, 1972, pp. 19–45.
2. Tangella, S. C. S. R., J. Craus, J. A. Deacon, and C. L. Monismith. "Summary Report on Fatigue Response of Asphalt Mixtures." TM-UCB-A-003A-89-3, Strategic Highway Research Program, Project A-003-A, University of California, Berkley, CA, 1990.
3. Tayebali, A. A., J. A. Deacon, J. S. Coplantz, J. T. Harvey, and C. L. Monismith. "Fatigue Response of Asphalt-Aggregate Mixes: Part I Test Method Selection." SHRP A-404 Strategic Highway Research Program, National Research Council, Washington, DC, 1994.
4. Callister, W. D. Jr. *Materials Science and Engineering: An Introduction.* John Wiley & Sons, New York, 1985.
5. Barret, C. R., W. D. Nix, and A. S. Tetelman. *The Principles of Engineering Materials.* Prentice Hall, Englewood Cliffs, NJ, 1973.
6. Baladi, G. Y. and M. B. Snyder. "Highway Pavements." *Pavement Design,* Publication No. FHWA HI-90-027, Vol. II, Part III, National Highway Institute, Washington, DC, 1992.
7. Huang, Y. H. *Pavement Analysis and Design.* Prentice Hall, Upper Saddle River, NJ, 1993.
8. Monismith, C. L. and D. B. McLean. "Structural Design Considerations." In *Proceedings of the Association of Asphalt Paving Technologists,* Vol. 41, 1972.
9. Maupin, G. W. Jr. and J. R. Freeman Jr. "Simple Procedure for Fatigue Characterization of Bituminous Concrete." Final Report No. FHWA-RD-76-102, Federal Highway Administration, Washington, DC, 1976.
10. Nunn, M. "Long-life Flexible Roads." In *Proceedings of the 8th International Conference on Asphalt Pavements,* Vol. 1, University of Washington, Seattle, WA, August 1997, pp. 3–16.
11. Nishizawa, T., S. Shimeno, and M. Sekiguchi. "Fatigue Analysis of Asphalt Pavements with Thick Asphalt Mixture Layer." In *Proceedings of the 8th International Conference on Asphalt Pavements*, Vol. 2, University of Washington, Seattle, WA, August 1997, pp. 969–976.
12. Wu, Z., Z. Q. Siddique, and A. J. Gisi. "Kansas Turnpike—An Example of Long Lasting Asphalt Pavement." *Proceedings International Symposium on Design and Construction of Long Lasting Asphalt Pavements,* National Center for Asphalt Technology, Auburn, AL, 2004, pp. 857–876.
13. Mahoney, J. P. "Study of Long-Lasting Pavements in Washington State." In *Transportation Research Circular 503: Perpetual Bituminous Pavements,* Transportation Research Board, Washington, DC, 2001, pp. 88–95.
14. Newcomb, D. *APA 101: Perpetual Pavements: A Synthesis.* Asphalt Pavement Alliance, Lanham, MD, 2002.
15. Harvey, J. T. and B. W. Tsai. "Effects of Asphalt Content and Air Void Content on Mix Fatigue and Stiffness." In *Transportation Research Record No. 1543,* Transportation Research Board, Washington, DC, 1996, pp. 38–45.
16. Monismith, C. L. "Some Applications of Theory in the Design of Asphalt Pavements." *Fifth Annual Nevada Streets and Highway Conference,* University of Nevada, 1970.
17. Goodrich, J. L. "Asphalt and Polymer Modified Asphalt Properties Related to the Performance of Asphalt Concrete Mixes." In *Proceedings of Association of Asphalt Paving Technologists Technical Sessions,* Vol. 57, Williamsburg, VA, 1988, pp. 116–175.
18. Tayebali, A. A., J. A. Deacon, J. S. Coplantz, F. N. Finn. and C. L. Monismith. "Fatigue Response of Asphalt-Aggregate Mixes: Part II Extended Test Program." SHRP A-404 Strategic Highway Research Program, National Research Council, Washington, D.C. 1994.
19. Bahia, H. U., D. I. Hanson, M. Zeng, H. Zhai, M. A. Khatri, and R. M. Anderson. "Characterization of Modified Asphalt Binders in Superpave Mix Design." NCHRP Report 459, Transportation Research Board, National Research Council, Washington, DC, 2001, p. 95.
20. Monismith, C. L., F. Long, and J. T. Harvey. "California's Interstate-710 Rehabilitation: Mix and Structural Section Designs, Construction Specifications." *Journal of the Association of Asphalt Paving Technologists,* Vol. 70, Clearwater Beach, FL, 2001, pp. 762–799.
21. Lee, H. J., J. Y. Choi, Y. Zhao, and Y. R. Kim. "Laboratory Evaluation of the Effects of Aggregate Gradation and Binder Type on Performance of Asphalt Mixtures." In *Proceedings of the Ninth International Conference on Asphalt Pavements,* Copenhagen, Denmark. 2002.
22. Asphalt Pavement Alliance. "Determination of Threshold Strain Level for the Fatigue Endurance Limit in Asphalt Mixtures: Phase I." Asphalt Pavement Alliance, 2003.
23. Von Quintus, H. "Quantifications of the Effects of Polymer-Modified Asphalt for Reducing Pavement Distress." ER-215, Asphalt Institute, Lexington, KY 2004.
24. Harvey, J., C. Monismith, R. Hornjeff, M. Berjarano, B. W. Tsai, and V. Kannekanti. "Long-Life AC Pavements: A Discussion of Design and Construction Experience Based on California Experience." In *Proceedings of International Symposium on Design and Construction of Long Lasting Asphalt Pavements,* National Center for Asphalt Technology, Auburn, AL, 2004, pp. 285–333.
25. Harvey, J. T. and B. W. Tsai. "Effects of Asphalt Content and Air Void Content on Mix Fatigue and Stiffness." In *Transportation Research*

Record No. 1543, Transportation Research Board, Washington, DC, 1996, pp. 38–45.
26. Anderson, R. M. and R. Bentsen. "Influence of Voids in Mineral Aggregate (VMA) on the Mechanical Properties of Coarse and Fine Asphalt Mixtures." *Journal of the Association of Asphalt Paving Technologists,* Vol. 70, Clearwater Beach, FL, 2001, pp. 1–37.
27. Maupin, G. W. Jr. "Additional Asphalt to Increase the Durability of Virginia's Superpave Surface Mixes." VTRC 03-R15, Virginia Transportation Research Council, Charlottesville, VA, 2003.
28. Corte, J. F. "Development and Uses of Hard-Grade Asphalt and of High-Modulus Asphalt Mixtures in France." In *Transportation Research Circular 503: Perpetual Bituminous Pavements,* Transportation Research Board, Washington, DC, 2001, pp. 12–31.
29. Ferne, B. W. and M. Nunn. "The European Approach to Long Lasting Asphalt Pavements—A State of the Art Review by ELLPAG." *Proceedings International Symposium on Design and Construction of Long Lasting Asphalt Pavements,* National Center for Asphalt Technology, Auburn, AL, 2004, pp. 87–101.
30. Tayebali, A. A., J. A. Deacon, J. S. Coplantz, and C. L. Monismith. "Modeling Fatigue Response of Asphalt-Aggregate Mixtures." *Journal of Association of Asphalt Paving Technologists,* Vol. 62, Austin, TX, 1993, pp. 385–421.
31. Lee, H. J., J. Y. Choi, Y. Zhao, and Y. R. Kim. "Laboratory Evaluation of the Effects of Aggregate Gradation and Binder Type on Performance of Asphalt Mixtures." In *Proceedings of the Ninth International Conference on Asphalt Pavements,* Copenhagen, Denmark, 2002.
32. Daniel, J. S. and Y. R. Kim, "Development of a Simplified Fatigue Test and Analysis Procedure Using a Viscoelastic, Continuum Damage Model." *Journal of the Association of Asphalt Paving Technologists,* Vol. 71, 2002, pp. 619–645.
33. Chehab, G. R., Y. R. Kim, R. A. Schapery, M. W. Witczak, and R. Bonaquist. "Time-Temperature Superposition Principle for Asphalt Concrete Mixtures with Growing Damage in Tension State." *Journal of Association of Asphalt Paving Technologists,* Vol. 71, 2002, pp. 559–593.
34. Ghuzlan, K. and S. Carpenter. "Energy-Derived, Damage-Based Failure Criterion for Fatigue Testing." In *Transportation Research Record No. 1723,* Transportation Research Board, Washington, DC, 2000, pp. 141–149.
35. Rowe, G. M. "Performance of Asphalt Mixtures in the Trapezoidal Fatigue Test." *Journal of the Association of Asphalt Paving Technologists,* Vol. 62, Austin, TX, 1993, pp. 344–384.
36. Carpenter, S. H., K. A. Ghuzlan, and S. Shen. "A Fatigue Endurance Limit for Highway and Airport Pavements." In *Transportation Research Record No. 1832,* Transportation Research Board, Washington, DC, 2003, pp. 131–138.
37. Thompson, M. R. and S. H. Carpenter. "Design Principles for Long Lasting HMA Pavements." In *Proceedings of International Symposium on Design and Construction of Long Lasting Asphalt Pavements.* National Center for Asphalt Technology, Auburn, AL, 2004, pp. 365–384.
38. Peterson, R. L. and P. Turner. "Determination of Threshold Strain Level for Infinite Fatigue Life in Asphalt Mixtures." Interim Report for Asphalt Pavement Alliance, Asphalt Institute, Lexington, KY, 2002.
39. Peterson, R. L., P. Turner, M. Anderson, and M. Buncher. "Determination of Threshold Strain Level for Fatigue Endurance Limit in Asphalt Mixtures." In *Proceedings of International Symposium on Design and Construction of Long Lasting Asphalt Pavements,* National Center for Asphalt Technology, Auburn, AL, 2004, pp. 385–410.
40. Shen, S. and S. H. Carpenter. "Application of Dissipated Energy Concept in Fatigue Endurance Limit Testing." In *Transportation Research Record No. 1929,* Transportation Research Board, Washington, DC, 2005, pp. 165–173.
41. El-Basyouny, M. M. and M. Witczak. "Development of the Fatigue Cracking Models for the 2002 Design Guide." *Presented at 84th Annual Meeting of The Transportation Research Board*, Transportation Research Board, Washington, DC, 2005.
42. American Society for Testing and Materials. "Standard Practice for Statistical Analysis of Linear or Linearized Stress-Life (S-N) and Strain-Life (ε-N) Fatigue Data." E739-91, In *ASTM Standards on Precision and Bias for Various Applications,* Conshohocken, PA, 1992.
43. Harvey, J. T., J. A. Deacon, A. A. Tayebali, and R. B. Leahy. "A Reliability-Based Mix Design and Analysis System for Mitigating Fatigues Distress." In *Proceedings of the 8th International Conference on Asphalt Pavements,* Vol. 1. University of Washington, Seattle, WA, August 1997, pp. 301–323.
44. Savard, Y., M. Boutonnet, C. Mauduit, and N. Pouliot. "Comparison of Pavement Design Methods in France and Quebec." In *Proceedings of International Symposium on Design and Construction of Long Lasting Asphalt Pavements,* National Center for Asphalt Technology, Auburn, AL, 2004, pp. 153–198.
45. Deacon, J., J. Coplantz, F. Finn, and C. Monismith. "Temperature Considerations in Asphalt-Aggregate Mixture Analysis and Design." In *Transportation Research Record No. 1454,* Transportation Research Board, Washington, DC, 1994, pp. 97–112.
46. Leahy, R. B., R. G. Hicks, C. L. Monismith, and F. N. Finn. "Framework for Performance—Based Approach to Mix Design and Analysis." In *Proceedings of the Association of Asphalt Paving Technologists,* Vol. 64, Association of Asphalt Paving Technologists, Minneapolis, MN, 1995, pp. 431–473.
47. Pierce, L. M. and J. P. Mahoney. "Asphalt Concrete Overlay Design Case Studies." In *Transportation Research Record No. 1543,* Transportation Research Board, Washington, DC, 1996, pp. 3–9.
48. *Highway Capacity Manual.* Transportation Research Board, National Research Council, Washington, DC, 2000.
49. Timm, D. H. and A. L. Priest. "Dynamic Pavement Response Data Collection and Processing at the NCAT Test Track." NCAT Report 04-03, National Center for Asphalt Technology, Auburn University, Auburn, AL, June 2004.
50. University of Washington Civil Engineering Department. "Trucks and Buses." http://training.ce.washington.edu/WSDOT/Modules/04_design_parameters/trucks_buses.htm Accessed August 18, 2006.
51. Deacon, J. A., A. A. Tayebali, J. S. Coplantz, F. N. Finn, and C. L. Monismith. "Fatigue Response of Asphalt-Aggregate Mixes: Part III Mix Design and Analysis." SHRP A-404, Strategic Highway Research Program, National Research Council, Washington, DC, 1994.
52. American Association of State Highway and Transportation Officials. "Standard Specifications for Transportation Materials and Methods of Sampling and Testing: Part 2B: Tests," 25th ed., Washington, DC, 2005.
53. Rowe, G. M. and M. G. Bouldin. "Improved Techniques to Evaluate the Fatigue Resistance of Asphaltic Mixes." In *2nd Eurasphalt and Eurobitume Congress Barcelona 2000–Proceedings 0081,* UK.
54. Personal communication with S. Shen, January 2005.
55. Tsai, B. W., J. T. Harvey, and C. L. Monismith. "High Temperature Fatigue and Fatigue Damage Process of Aggregate-Asphalt Mixes." *Journal of the Association of Asphalt Paving Technologists,* Vol. 71, 2002, pp. 345–385.
56. Tsai, B.W. "High Temperature Fatigue and Fatigue Damage Process of Aggregate-Asphalt Mixes." Report to California Department of Transportation, Pavement Research Center, Institute of Transportation Studies, University of California, Berkley, CA,
57. Tsai, B. W., J. T. Harvey, and C. L. Monismith. "Using the Three-Stage Weibull Equation and Tree-Based Model to Characterize the

Mix Fatigue Damage Process." In *Transportation Research Record No. 1929,* Transportation Research Board, Washington, DC, 2005, pp. 227–237.
58. Tsai, B. W., V. N. Kannekanti, and J. T. Harvey. "Application of Genetic Algorithm in Asphalt Pavement Design." In *Transportation Research Record No. 1891,* Transportation Research Board, Washington, DC, 2004, pp. 112–120.
59. Von Quintus, Harold L., J. A. Scherocman, C. S. Hughes, and T. W. Kennedy. "Asphalt-Aggregate Mixture Analysis System: AAMAS." NCHRP Report No. 338, National Cooperative Highway Research Program, National Research Council, Washington, DC, March 1991.
60. Kim, Y. R. and H. Wen. "Fracture Energy from Indirect Tension Testing." *Journal of the Association of Asphalt Paving Technologists,* Vol. 71, Colorado Springs, CO, 2002, pp. 779–793.
61. Christensen, D.W. and R.F. Bonaquist. "Practical Application of Continuum Damage Theory to Fatigue Phenomena in Asphalt Concrete Mixtures." *Journal of the Association of Asphalt Paving Technologists,* Vol. 74, 2005, pp. 963–1002.
62. Computer Program DAMA (CP-1/1991 Revision). "Pavement Structural Analysis Using Multi-Layered Elastic Theory." Asphalt Institute, Lexington, KY, 1991.
63. Timm, D. H. *Computer Program PerRoad.* Version 3.3, Auburn University, February 2008.
64. Applied Research Associates and Arizona State University. "Computer Program Mechanistic Empirical Pavement Design Guide Version 1.003." May 2007.
65. Gharaibeh, N. G. and M. I. Darter. "Longevity of Highway Pavements In Illinois—2000 Update." Final Report FHWA-IL-UI-283, Illinois Department of Transportation, Springfield, Illinois, 2002.
66. Gharaibeh, N. G. and M. I. Darter. "Probabilistic Analysis of Highway Pavement Life for Illinois." In *Transportation Research Record No. 1823,* Transportation Research Board, Washington, DC, 2003, pp. 111–120.
67. Smith, K. L., N. G. Gharaibeh, M. I. Darter, H. L. Von Quintus, B. Killingsworth, R. Barton, and K. Kobia, "Review of Life Cycle Costing Analysis Procedures" (in Ontario), Final Report prepared for the Ministry of Transportation of Ontario, Toronto, Ontario, Canada, 1998.
68. Bradbury, A., T. Kazmierowski, K. L. Smith, and H. L. Von Quintus. "Life Cycle Costing of Freeway Pavements in Ontario." Paper presented at the 79th Annual Meeting of the Transportation Research Board, Washington, DC, 2000.
69. Von Quintus, H. L., J. Mallela, and J. Jiang. "Expected Service Life and Performance Characteristics of HMA Pavements in LTPP." Final Report 5672-2/1, Applied Research Associates, Inc., prepared for the Asphalt Pavement Alliance, June 2004.
70. Fonseca, O. A. and M. W. Witczak. "A Predictive Methodology for the Dynamic Modulus of In-Place Aged Asphalt Mixtures." *Journal of the Association of Asphalt Paving Technologists,* Vol. 65, 1996, pp. 532–567.
71. Von Quintus, H. L., J. Mallela, and J. Jiang. "Quantification of the Effects of Polymer-Modified Asphalt for Reducing Pavement Distress." Final Report No. 5504-2/2, Applied Research Associates, Inc., prepared for the Asphalt Institute, October 2004.
72. Timm, D. H., A. L. Priest, and T. V. McEwen. "Design and Instrumentation of the Structural Pavement Experiment at the NCAT Test Track." NCAT Report 04-01, Auburn, AL, April 2004.
73. Priest, A. L. and D. H. Timm. "Methodology and Calibration of Fatigue Transfer Functions for Mechanistic-Empirical Flexible Pavement Design." NCAT Report 06-03, Auburn, AL, December 2006.
74. El-Basyouny, M. M. and M. Witczak. "Calibration of Alligator Fatigue Cracking Model for 2002 Design Guide." In *Transportation Research Record No. 1919,* Transportation Research Board, National Academies, Washington, DC, 2005, pp. 77–86.
75. Willis, J. R. and D. H. Timm. "Forensic Investigation of a Rich-Bottom Pavement." NCAT Report 06-04, Auburn, AL, December 2006.
76. Priest, A. L. "Calibration of Fatigue Transfer Functions for Mechanistic-Empirical Pavement Design." Master's Thesis. Auburn University, Auburn, AL, 2005.
77. Willis, J. R. "Field-Based Strain Thresholds for Flexible Perpetual Pavement Design." Doctoral Dissertation. Auburn University, Auburn, AL, 2008.
78. Miner, M. A. "Estimation of Fatigue Life with Particular Emphasis on Cumulative Damage." *Metal Fatigue,* Sines and Waisman, eds., McGraw Hill, Inc., New York, 1959, pp. 278–89.
79. Taylor, A. J. and D. H. Timm. "Mechanistic Characterization of Resilient Moduli for Unbound Pavement Layer Materials." NCAT Report 09-06, Auburn, AL, 2009.
80. ARA, Inc. *Guide for Mechanistic-Empirical Design of New and Rehabilitated Pavement Structures.* Final Report, Part 2: Design Inputs, "Chapter 1: Subgrade/Foundation Design Inputs," NCHRP, Transportation Research Board, Washington, DC, 2004.
81. Timm, D. H. and A. L. Priest. "Material Properties of the 2003 NCAT Test Track Structural Study." NCAT Report 06-01, Auburn, AL, 2006.
82. ARA, Inc. "Guide for Mechanistic-Empirical Design of New and Rehabilitated Pavement Structures." Final Report, Part 2 Design Inputs, Chapter 2: Subgrade/Foundation Design Inputs, NCHRP, Transportation Research Board, Washington, DC, 2004.
83. ARA, Inc. "Guide for Mechanistic-Empirical Design of New and Rehabilitated Pavement Structures." Final Report, Part 1 Introduction, Chapter 2: Background, Scope, and Overview.
84. ARA, Inc., "Guide for Mechanistic-Empirical Design of New and Rehabilitated Pavement Structures." Final Report, Appendix II-1: Calibration of Fatigue Cracking Models for Flexible Pavements.
85. Newcomb, D. E. "A Guide to PerRoad 2.4 for PerRoad Perpetual Pavement Software." *Asphalt Pavement Alliance,* 2004.
86. Yoder, E. J. and M. W. Witczak. *Principles of Pavement Design,* 2nd Ed., John Wiley & Sons, New York, 1975.
87. Tsai, B. W., D. Jones, J. T. Harvey, and C. L. Monismith. "Reflective Cracking Study: First-Level Report on Laboratory Fatigue Testing." Research Report UCPRC-RR-2006-08, Institute of Transportation Studies, University of California, Davis, 2008.

APPENDIX A

Proposed Standard Practice for Predicting the Endurance Limit of Hot Mix Asphalt (HMA) for Long-Life Pavement Design

AASHTO Designation: PP XX-XX

1. Scope

1.1 This practice describes methodology for predicting the endurance limit for hot mix asphalt for long-life pavement design.

1.2 *This standard may involve hazardous materials, operations, and equipment. This standard does not purport to address all of the safety problems associated with its use. It is the responsibility of the user of this procedure to establish appropriate safety and health practices and to determine the applicability of regulatory limitations prior to its use.*

---

2. Referenced Documents

2.1 *AASHTO Standards*

- T 321, Determining the Fatigue Life of Compacted Hot-Mix Asphalt (HMA) Subjected to Repeated Flexural Bending.
- R 30, Mixture Conditioning of Hot Mix Asphalt (HMA)

2.2 *Other Publications*

- NCHRP 9-38, "Endurance Limit of Hot Mix Asphalt Mixtures to Prevent Fatigue Cracking in Flexible Pavements," Draft Final Report.

---

3. Terminology

3.1 *Endurance limit* – the strain level, at a given temperature, below which no bottom-up fatigue damage occurs in the HMA.

3.2 *Long-Life Pavement Design* – a pavement designed to last a minimum of forty years without bottom-up fatigue failure, or need for structural strengthening.

3.3 *Normal strain levels* – strain levels where failure (50 percent of initial stiffness) occurs in less than 12 million cycles. For tests conducted at 20°C, strain levels of 300 microstrain or greater generally meet this requirement.

3.4 *Low Strain levels* – strain levels where failure (50 percent of initial stiffness) does not occur by 12 million cycles. The failure point of low strain tests generally needs to be extrapolated by one of the methods described in this document.

4. Summary of Practice

4.1 This practice describes the analysis needed to determine the endurance limit for hot-mix asphalt concrete mixtures. It involves collecting beam fatigue test data at specified strain rates, predicting the endurance limit based on a log-log extrapolation, and then running tests at the predicted strain level to confirm endurance limit behavior. Since the tests conducted at the predicted strain level should not fail, the failure point is extrapolated from the test data by use of one of several different techniques to confirm the endurance limit of the asphalt mixture.

5. Significance and Use

5.1 The endurance limit can be used during pavement design to determine a pavement thickness which will prevent bottom-up fatigue cracking.

6. Apparatus

6.1 *Specimen Fabrication Equipment* – Equipment for fabricating beam fatigue test specimens as described in AASHTO T 321, Determining the Fatigue Life of Compacted Hot-Mix Asphalt (HMA) Subjected to Repeated Flexural Bending.

6.2 *Beam Fatigue Test System* – Equipment for testing beam fatigue samples as described in AASHTO T 321, Determining the Fatigue Life of Compacted Hot-Mix Asphalt (HMA) Subjected to Repeated Flexural Bending.

6.3 *Analysis Software* – Data is collected during the test using a data acquisition system described in section 6.2. Data analysis can be conducted using a spreadsheet program, or a variety of statistical packages.

7. Hazards

7.1 This practice and associated standards involve handling of hot asphalt binder, aggregates and asphalt mixtures. It also includes the use of sawing and coring machinery and servo-hydraulic or pneumatic testing equipment. Use standard safety precautions, equipment, and clothing when handling hot materials and operating machinery.

8. Standardization

8.1 Items associated with this practice that require calibration are included in the documents referenced in Section 2. Refer to the pertinent section of the referenced documents for information concerning calibration.

9. Beam Fatigue Test Data

9.1 *Test Specimen Fabrication*

9.1.1 Prepare at least twelve test specimens to the target air void content in accordance with AASHTO T 321. Samples should be short-term oven aged according to AASHTO R 30 for four hours at 135°C prior to compaction. The target air void content should be representative of that expected to be obtained in the field. A target air void content of 7 percent was used for mixes produced at optimum asphalt content in the NCHRP 9-38 research. A reduced air void content would be expected for optimum plus or so-called rich-bottom type mixes.

Note 1 – A reasonable air void tolerance for test specimen fabrication is ± 0.5 %.

Note 2 – The following are estimated based on a limited round robin. The coefficient of variation of the log (base 10) of the fatigue life of a properly conducted beam fatigue tests at normal strain levels is 5.4 and 6.8 percent, respectively, for within- and between-lab variability. The difference between the logs of the fatigue lives (log sample 1 – log sample 2) of two properly conducted test should not exceed 0.69 for a single operator or 0.89 between two labs.

9.2 *Testing Conditions*

9.2.1 Separate the test specimens into four groups with approximately equal air voids. Determine the number of cycles to failure (50 percent of initial stiffness) of each specimen in one group using the beam fatigue test system at a strain level of 700 micro-strain. Determine the number of cycles to failure in a second group at a strain level of 500 micro-strain. Determine the number of cycles to failure in the third group at a strain level of 300 micro-strain. The test results at the normal strain level should not be extrapolated; all nine sample should be tested to failure.

Note 3 – The original research, including round robin testing, was based on testing three samples each at 800 and 400 micro strain. Additional samples were added to improve the estimation of the endurance limit due to the sensitivity of pavement thickness to the endurance limit.

9.3 *Beam Fatigue Data Summary to Predict Endurance Limit*

9.3.1 Transform the data by taking the log (base 10) of both the micro-strain levels and cycles to failure. Research has shown that the log-log transformation of the data from tests conducted at normal strain levels (above the endurance limit) produce a straight line. Perform a simple linear regression on the transformed data using fatigue life as a predictor for micro-strain level. Using the regression coefficients determined from the regression analysis, determine the micro-strain level corresponding to a fatigue life of log 50,000,000 cycles = 7.69897. Designate this value y_o. Calculate the one-sided lower 95% prediction interval according to Equation 1.

$$\text{Lower Prediction Limit} = \hat{y}_o - t_\alpha s\sqrt{1+\frac{1}{n}+\frac{\left(x_o-\bar{x}\right)^2}{S_{xx}}} \quad (1)$$

where:

t_α = value of t distribution for $n - 2$ degrees of freedom = 1.89458 for $n = 9$ with $\alpha = 0.05\%$,

s = estimate of standard deviation from the regression analysis, also referred to in Microsoft Excel as the standard error,
n = number of samples = 9,
$S_{xx} = \sum_{i=1}^{n} (x_i - \bar{x})^2$ (Note: log of fatigue lives),
x_0 = log 50,000,000 = 7.69897,
$\bar{x}$ = average of the fatigue life results determined in 9.2.1.

Note 4 – A simple spreadsheet has been developed to perform the calculations described above.

9.3.2 Conduct the beam fatigue test at the strain level corresponding to the 95% one-sided lower prediction limit for a fatigue life of 50,000,000 cycles to 10,000,000 cycles. Research has shown that tests conducted to a minimum of 10,000,000 cycles can extrapolate to estimate long-life fatigue lives.

10. Data Analysis to Extrapolate Long-life Fatigue Tests

Beam fatigue tests conducted at low strain levels are unlikely to fail in a reasonable number of cycles. This is particularly true for tests conducted at the 95% one-sided lower prediction limit for the endurance limit determined in section 9.3.1. In order to confirm the existence of the endurance limit, the test data needs to be extrapolated to predict a failure point. This section provides three procedures for extrapolating the beam fatigue failure point for low-strain tests.

10.1 *Data Extrapolation Using the Single-Stage Weibull Survivor Function*

10.1.1 General Form. The general form of the Weibull Survivor function is shown as Equation 2:

$$R(t) = \exp\left[-\left(\frac{t-\delta}{\theta-\delta} \right)^{\gamma} \right] \tag{2}$$

where:
$R(t)$ = the reliability at time t where t might be time or another life parameter such as loading cycles,
γ = the slope,
δ = the minimum life, and
θ = the characteristic life.

10.1.2 Simplified Form. A specialized case of the Weibull function assumes the minimum life, δ, equals zero. Therefore, the hazard function would equal $1/\gamma$, which simplifies Equation 2 into Equation 3. Since the beam fatigue loading cycles are applied at a constant frequency of 10 Hz, the loading cycles, n, can be substituted for time, *t*.

$$S(n) = \exp(-\lambda \times n^{\gamma}) \tag{3}$$

where:
$S(t)$ = probability of survival until time t,
n = number of loading cycles,
λ = scale parameter (intercept),
γ = shape parameter (slope).

10.1.3 Final Form. The stiffness ratio (SR) is used to characterize fatigue damage. The stiffness ratio is the stiffness measured at cycle n, divided by the initial stiffness, determined at the 50th cycle. Tsai reports that at a given cycle n, the beam being tested has a probability of survival past cycle n equal to the stiffness ratio times 100 percent. Thus, $SR(n)$ can be substituted for $S(t)$. Equation 4 allows the scale and shape parameters for laboratory beam fatigue data to be determined by linear regression.

$$\ln(-\ln(SR)) = \ln(\lambda) + \gamma \times \ln(n) \quad (4)$$

10.1.4 Plot the left-hand side of Equation 4 versus the natural logarithm of the number of cycles, n so a straight line regression can be determined. If the measured stiffness at a given number of cycles is greater than the initial stiffness, e.g. SR > 1.0, ln(-ln(SR)) cannot be computed. Eliminate these data from the regression analysis. Using the shape (slope) and scale (intercept) parameters determined from the simple linear regression, solve Equation 4 for n which produces an SR of 0.5. This can be readily done using a solver function or by trial and error in a spreadsheet. This value of n is the extrapolated fatigue life for 50 percent initial stiffness.

10.1.5 The endurance limit is confirmed by the divergence of the test data below the regression line at a high number of cycles. Figure 1 illustrates this divergence.

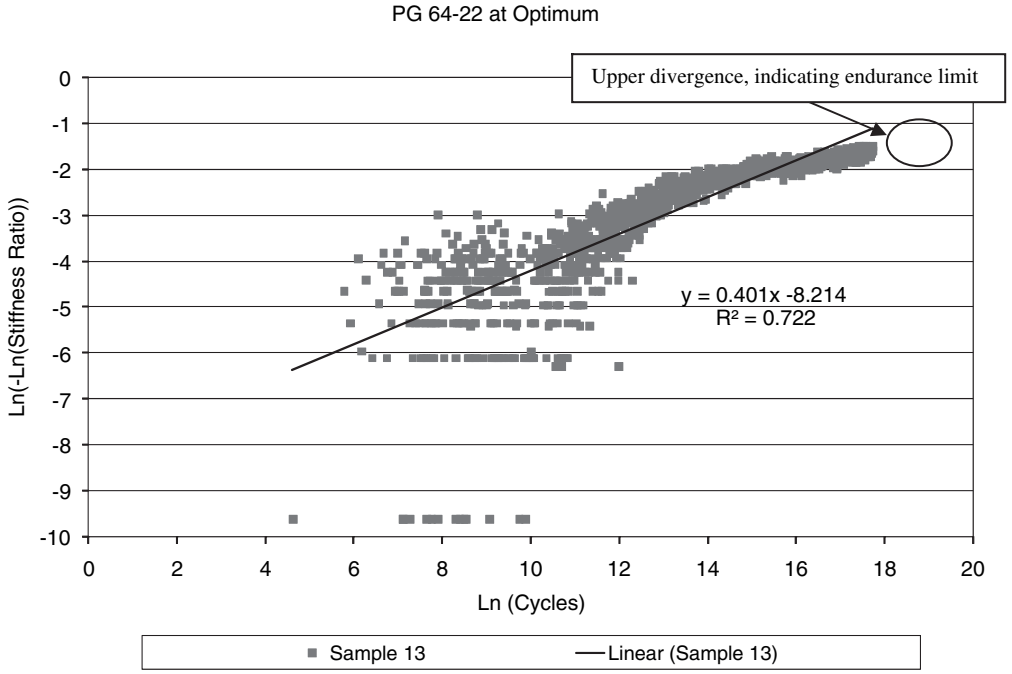

Figure 1. Weibull functions.

10.2 *Data Extrapolation Using Three-Stage Weibull Survivor Function*

10.2.1 To improve upon the accuracy of the single-stage Weibull function, Tsai et al. (*2*) developed a methodology for fitting a three-stage Weibull curve. Tsai et al. (*2*) theorized that a plot of loading cycles versus stiffness ratio could be divided into three stages: initial heating and temperature equilibrium, crack initiation, and crack propagation. In the case of low strain tests (below the endurance limit), the third stage does not appear to represent crack propagation, but rather concave down stage with a reduced rate of damage.

In most cases, low strain fatigue tests can be most accurately extrapolated using the single-stage Weibull function. However, in some cases, there are three distinct slopes to the transformed data, in which case the three-stage Weibull function may be used to provide a better estimate of the fatigue life.

10.2.2 First, plot the data as described in Section 10.1.4. Visually examine the data to determine three stages, determined by groups of data exhibiting distinct slopes. Assign a data series to each group of data, representing a single slope. Perform a linear regression on the transformed data for each stage. The regression coefficients become seed values for either a compiled Fortran program or Microsoft Excel spreadsheet solution. An example is shown in Figure 2.

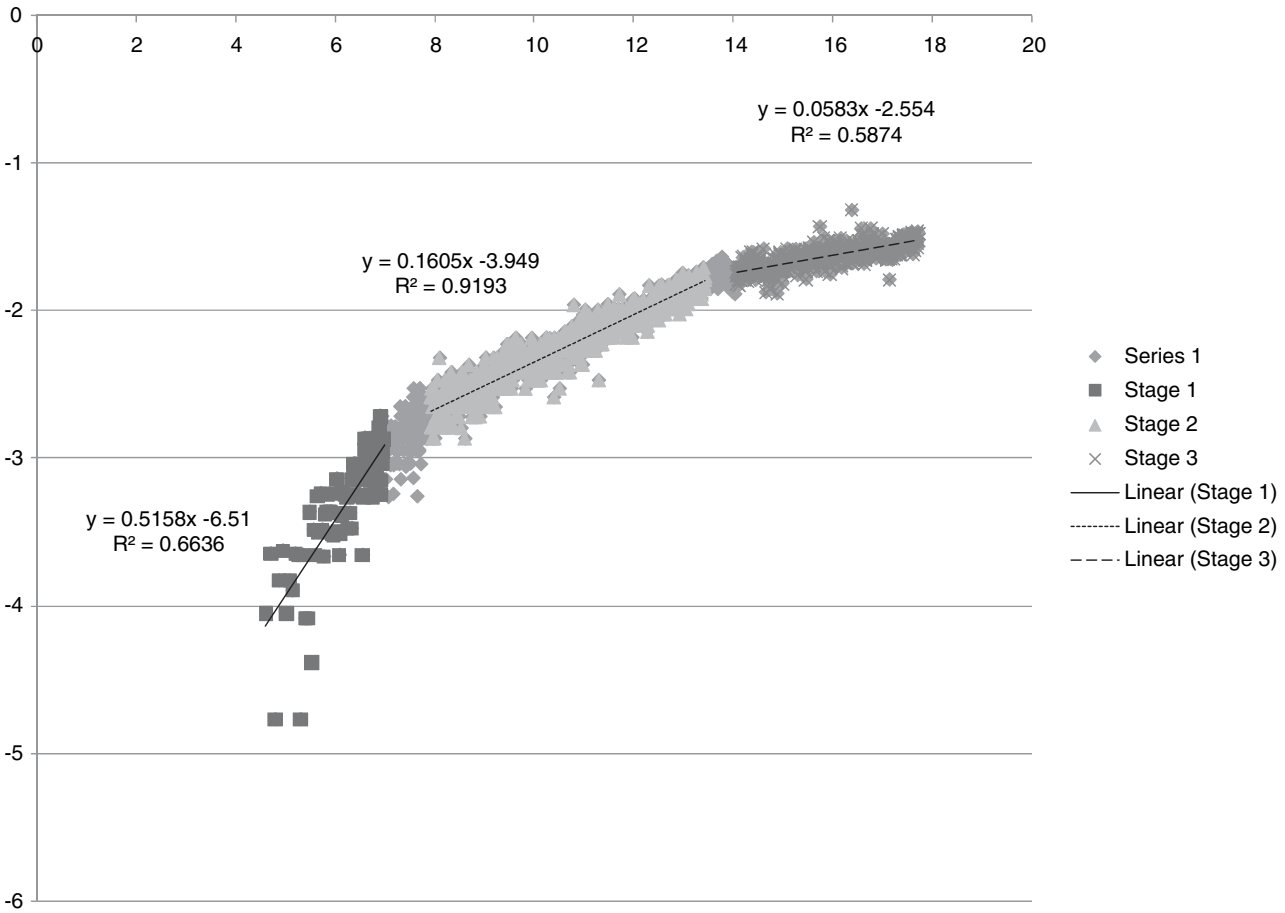

Figure 2. Estimation of three Weibull stages by inspection.

10.2.3 A Weibull function is fit to each of these stages as shown in Equation 5:

$$SR_1 = e^{\left(-\alpha_1 \times n^{\beta_1}\right)} \quad \text{for } 0 \le n < n_1 \tag{5}$$

$$SR_2 = e^{\left(-\alpha_2 \times (n-\gamma_1)^{\beta_2}\right)} \quad \text{for } n_1 \le n < n_2$$

$$SR_3 = e^{\left(-\alpha_3 \times (n-\gamma_2)^{\beta_3}\right)} \quad \text{for } n_2 \le n < n_3$$

10.2.4 Coefficients α_1, α_2, α_3, β_1, β_2, β_3, n_1, and n_2 are illustrated in Figure 3. Using a series of mathematical manipulations (*2*), n_1, γ_1, n_2, and γ_2 can be calculated sequentially as follows:

$$n_1 = \left[\frac{\alpha_2}{\alpha_1} \times \left(\frac{\beta_2}{\beta_1}\right)^{\beta_2}\right]^{\frac{1}{\beta_2 - \beta_1}} \tag{6}$$

$$\gamma_1 = \left[1 - \frac{\beta_2}{\beta_1}\right] \times n_1 \tag{7}$$

$$n_2 = \gamma_1 + \left[\frac{\alpha_3}{\alpha_2} \times \left(\frac{\beta_3}{\beta_2}\right)^{\beta_3}\right]^{\frac{1}{\beta_2 - \beta_3}} \tag{8}$$

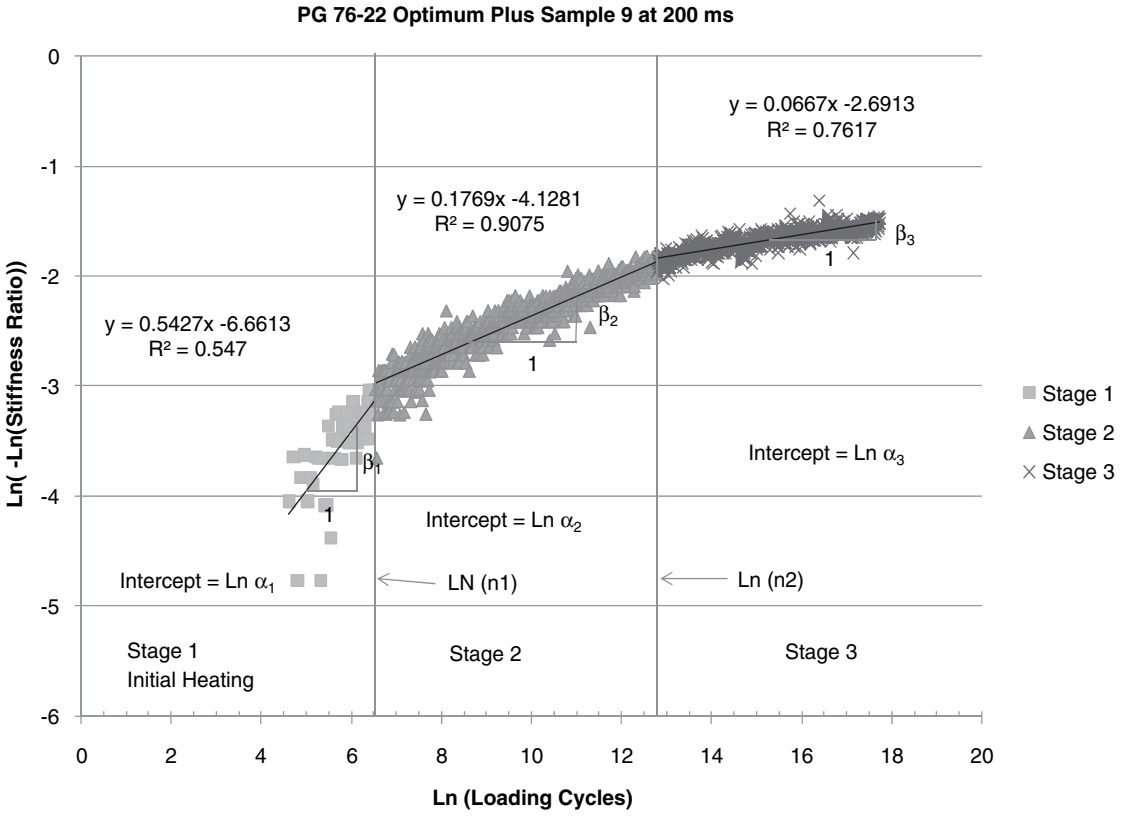

Figure 3. Three-stage Weibull curve definitions.

$$\gamma_2 = \left(1 - \frac{\beta_3}{\beta_2}\right) \times n_2 + \frac{\beta_3}{\beta_2} \times \gamma_1 \quad (9)$$

10.2.4 The trial values for α_1, α_2, α_3, β_1, β_2, β_3 and he test data are entered into a FORTRAN program, N3stage.exe, developed by Tsai or into a spreadsheet developed as part of NCHRP 9-38. N3stage.exe provides a robust solution, but can take up to 45 minutes to run. The spreadsheet uses Microsoft Excel's Solver Function and takes less than a moment, but in a few cases does not identify a solution. The N3stage.exe program can be obtained from: BWTsai@Berkeley.edu

10.2.5 Using the results from the NStage3.exe program or NCHRP 9-38 spreadsheet, the predicted fatigue life can be calculated according to Equation 10.

$$N_f = e^{\left((\ln(-\ln(0.5)) - \ln\left(\frac{\alpha_3}{\beta_3}\right)\right)} + \gamma_2 \quad (10)$$

11. Report

11.1 For each sample, report the following:

11.1.1 Sample air voids

11.1.2 Test Temperature

11.1.3 Initial flexural stiffness (measured at 50 cycles)

11.1.4 Normal Strain Tests

11.1.4.1 Micro-strain level

11.1.4.2 Number of cycles (measured) to 50 percent of initial stiffness

11.1.5 Low Strain Tests

11.1.5.1 Method of Extrapolation

11.1.5.2 Equation used for extrapolation and R^2 value for equation

11.1.5.3 Extrapolated fatigue life N_f for 50 percent of initial stiffness

11.1.6 Endurance Limit

11.1.6.1 Log-Log plot of data with cycles to failure on *x*-axis and micro-strain on *y*-axis.

11.1.6.2 Best-fit regression line/equation of normal-strain data should be included on graph.

11.1.6.3 Predicted endurance limit from normal-strain regression with N_f = 50,000,000 cycles

11.1.6.4 Lower one-sided 95 percent confidence interval for micro-strain level corresponding to N_f = 50,000,000 cycles, termed predicted endurance limit.

12. Keywords

12.1 Beam fatigue, endurance limit, long-life pavement

13. References

13.1 Tsai, B-W, "High Temperature Fatigue and Fatigue Damage Process of Aggregate-Asphalt Mixes." Report to California Department of Transportation, Pavement Research Center, Institute of Transportation Studies, University of California at Berkeley.

13.2 Tsai, B.-W., J. T. Harvey, and C. L. Monismith. "Using the Three-Stage Weibull Equation and Tree-Based Model to Characterize the Mix Fatigue Damage Process." In Transportation Research Record No. 1929, Transportation Research Board, Washington, DC, 2005, Pp 227-237.

APPENDIX B

Proposed Standard Practice for Predicting the Endurance Limit of Hot Mix Asphalt (HMA) by Pseudo Strain Approach

AASHTO Designation: PP XX-XX

1. Scope

1.1 This practice describes methodology for predicting the endurance limit for hot mix asphalt for long-life pavement design by pseudo strain approach.

1.2 *This standard may involve hazardous materials, operations, and equipment. This standard does not purport to address all of the safety problems associated with its use. It is the responsibility of the user of this procedure to establish appropriate safety and health practices and to determine the applicability of regulatory limitations prior to its use.*

---

2. Referenced Documents

2.1 *AASHTO Standards*

- PP XX-XX, Preparation of Cylindrical Performance Test Specimens Using the Superpave Gyratory Compactor
- PP XX-XX, Determining the Dynamic Modulus and Flow Number for Hot Mix Asphalt (HMA) Using the Simple Performance Test System
- PP XX-XX, Developing Dynamic Modulus Master Curves for Hot-Mix Asphalt Concrete Using the Simple Performance Test System

2.2 *Other Publications*

- Equipment Specification for the Simple Performance Test System, Version 2.0, Prepared for National Cooperative Highway Research Program (NCHRP), March 26, 2004.

---

3. Terminology

3.1 *Dynamic Modulus* – $|E^*|$, the absolute value of the complex modulus calculated by dividing the peak-to-peak stress by the peak-to-peak strain for a material subjected to a sinusoidal loading.

3.2 *Phase Angle* – δ, the angle in degrees between a sinusoidally applied stress and the resulting strain in a controlled-stress test.

3.3 *Endurance limit* – the strain level, at a given temperature, below which no fatigue damage occurs in the HMA.

4. Summary of Practice

4.1 This practice describes the analysis needed to determine the endurance limit for hot-mix asphalt concrete mixtures by pseudo strain approach. It involves testing continuous cyclic fatigue test data of cylindrical asphalt concrete.

5. Significance and Use

5.1 The endurance limit can be used during pavement design to determine a pavement thickness which will prevent fatigue cracking.

6. Apparatus

Specimen Fabrication Equipment – Equipment for fabricating cylindrical test specimens as described in AASHTO PP XX-XX, Preparation of Cylindrical Performance Test Specimens Using the Superpave Gyratory Compactor.

6.1 Specimen Fabrication Equipment – Equipment for fabricating cylindrical test specimens as described in PP XX-XX, Preparation of Cylindrical Performance Test Specimens Using the Superpave Gyratory Compactor.

6.2 *Dynamic Modulus Test System* – A dynamic test system meeting the requirements of Equipment Specification for the Simple Performance Test System, Version 2.0

6.3 *Conditioning Chamber* – An environmental chamber for conditioning the test specimens to the desired testing temperature. The environmental chamber shall be capable of controlling the temperature of the specimen over a temperature range from 4 to 60°C (39 to 140°F) to an accuracy of ± 0.5°C (1°F). The chamber shall be large enough to accommodate the number of specimens to be tested plus a dummy specimen with a temperature sensor mounted at the center for temperature verification.

6.4 *Analysis Software* – Software capable of handling numerical approaches like numerical integration and nonlinear optimization. Data analysis can be conducted using a spreadsheet program, or a variety of scientific computation packages like MATLAB, Lab View.

7. Hazards

7.1 This practice and associated standards involve handling of hot asphalt binder, aggregates and asphalt mixtures. It also includes the use of sawing and coring machinery and servo-hydraulic or pneumatic testing equipment. Use standard safety precautions, equipment, and clothing when handling hot materials and operating machinery.

8. Standardization

8.1 Items associated with this practice that require calibration are included in the documents referenced in Section 2. Refer to the pertinent section of the referenced documents for information concerning calibration.

9. Test Specimen

9.1 *Compaction* – Prepare at least three test specimens to the target air void content and aging condition in accordance with AASHTO PP XX-XX, Preparation of Cylindrical Performance Test Specimens Using the Superpave Gyratory Compactor (SGC). The target air void content should be representative of that expected to be obtained in the field.

Note 1 – A reasonable air void tolerance for test specimen fabrication is ± 0.5 %.

Note 2 – The coefficient of variation for properly conducted fatigue tests has not yet been determined

9.2 *Preparation* – Core the cylinders from gyratory compacted specimens and cut the ends of cylinders thus obtained to ensure uniform air void content. Check the cylinder for its geometry and axis alignment.

Note 3 – A reasonable diameter tolerance for test specimen is ± 1 mm.

9.3 *Gluing* – Clean the cored sample using compressed air and modified alcohol so that the dust particles over the surface are totally removed. Apply glue on the ends of the cleaned specimen. Place end plate over the specimen end and press against one another by hand. Repeat same procedure for another end also. Mount the specimen along with end plates on gluing jig and make adjustments such that cylinder axis is aligned with that of end plates. Place dead weight on gluing jig so that endplates are pressed against specimen. Remove the excess glue (if any) and leave the specimen for sufficient curing.

Note 4 – Process of gluing end plates to test specimen shall be completed well within initial setting time of glue.

10. Testing

10.1 *Dynamic Modulus*

10.1.1 Conduct dynamic modulus test in tension over a range of temperature and frequencies using three specimens in accordance with AASHTO PP XX-XX, Determining the Dynamic Modulus and Flow Number for Hot Mix Asphalt (HMA) Using the Simple Performance Test System.

Note 5 – Applied loads should be within linear elastic limits of asphalt concrete (this can be guaranteed when observed strain is less than 75 microns).

Note 6 – As flow number is not used in test practice described in this document, flow number part of AASHTO PP XX-XX guidelines should be ignored.

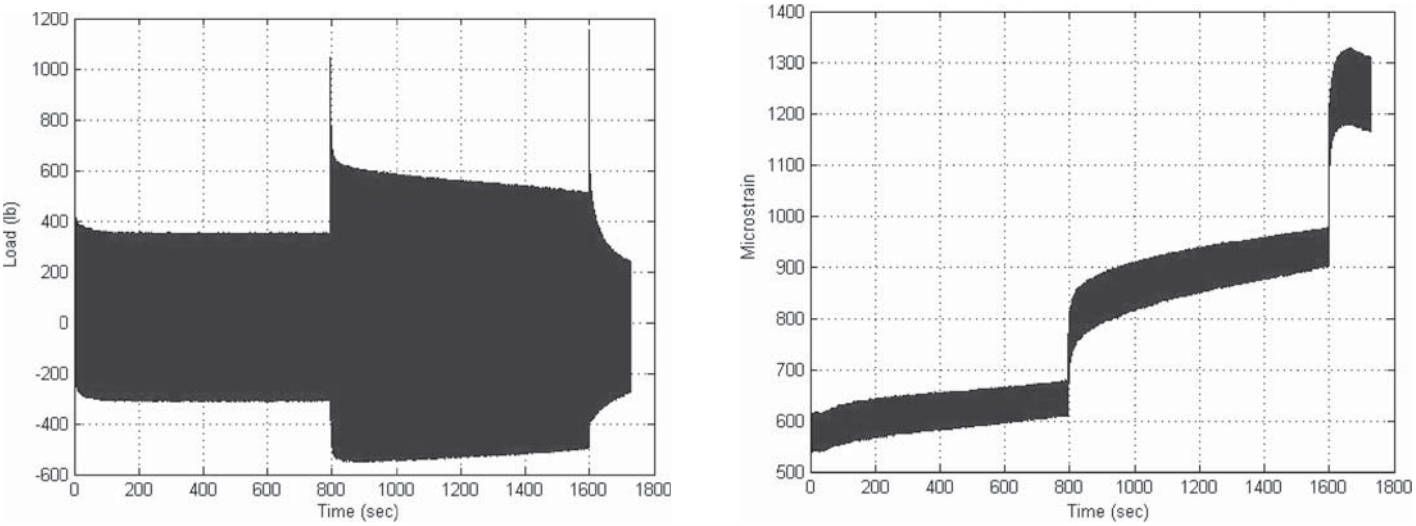

(a) Load History **(b) Strain History**

Figure 1. Typical stress/strain history for increasing amplitude uniaxial fatigue test.

10.2 *Increasing Strain Amplitude Test*

10.2.1 Conduct increasing strain amplitude fatigue test on other three specimens until failure starting from low strain amplitude at constant temperature (usually 20 C). A good starting strain amplitude value is that at which dynamic modulus tests are conducted. Around 10,000 cycles are applied at this amplitude to get steady state response. Applied strain amplitude is then increased and 10,000 more cycles are applied. This process shall be repeated at increasing strain amplitude level successively until specimen fails.

Note 7 – Mounting of LVDT's and load cells shall be similar to that of dynamic modulus determination (refer 10.1).

Note 8 – Temperature at which fatigue test is conducted shall be henceforth referred as reference temperature.

Typical plots of load and strain histories for an increasing amplitude fatigue test are given in Figure 1a and 1b respectively.

11. Calculations

11.1 *Dynamic Modulus Mastercurve Construction*

11.1.1 Using data previously obtained dynamic modulus data (refer 10.1), construct dynamic modulus master curves at reference temperature for individual specimens. General form of the dynamic modulus master curve is given in Equation 1.

$$\log|E^*| = \delta + \frac{(Max - \delta)}{1 + e^{\beta + \gamma\left\{\log\omega + \frac{\Delta E_a}{19.14714}\left[\left(\frac{1}{T}\right) - \left(\frac{1}{T_r}\right)\right]\right\}}} \quad (1)$$

where:

$|E^*|$ = dynamic modulus, MPa
ω_r = reduced frequency, Hz
Max = limiting maximum modulus, MPa
T_r = reference temperature, °K
T = test temperature, °K
ΔE_a = activation energy (treated as a fitting parameter)
δ, β, and γ = fitting parameters.

11.2 *Relaxation Modulus Prediction*

11.2.1 Using dynamic modulus ($|E^*|$) and phase angle (ω_r) data (refer 10.1), obtain relaxation modulus for each specimen using following relations.

$$E'(\omega_r) = |E^*(\omega_r)|\cos(\phi(\omega_r))$$

$$E(t_r) = \frac{1}{\lambda'}E'(\omega_r), \omega_r = \frac{0.08}{t_r}$$

$$\lambda' = \Gamma(1-n)\cos\left(\frac{n\pi}{2}\right)$$

$$n = \frac{d\log E'(\omega)}{d\log\omega}$$

where:

$|E'(\omega_r)|$ = storage modulus,
t_r = reduced time,
Γ = gamma function,
n = slope of $\log(E'(\omega))$ versus $\log(\omega)$ obtained at each point of reduced frequency.

11.2.2 Fit Prony series for relaxation modulus values obtained previously (refer 11.2.1). General expression for relaxation modulus as Prony series is given by Equation 2.

$$E(t) = E_\infty + \sum_n E_n \exp\left(-\frac{t}{\rho_n}\right) \tag{2}$$

where:

E_∞ = Relaxation modulus as $t \to \infty$,
E_n = Prony series coefficients,
ρ_n = Relaxation time.

11.3 *Calculation of Pseudo Strain*

11.3.1 Using time history of strain (using data obtained in 10.2) and predicted relaxation modulus (refer 11.2), calculate pseudo strains for entire strain history for each specimen. Equation 2 shall be used for calculating pseudostrains at reference temperature.

$$\varepsilon_R(t) = \frac{1}{E_R}\int_0^t E(t-\tau)\frac{d\varepsilon}{d\tau}d\tau \tag{3}$$

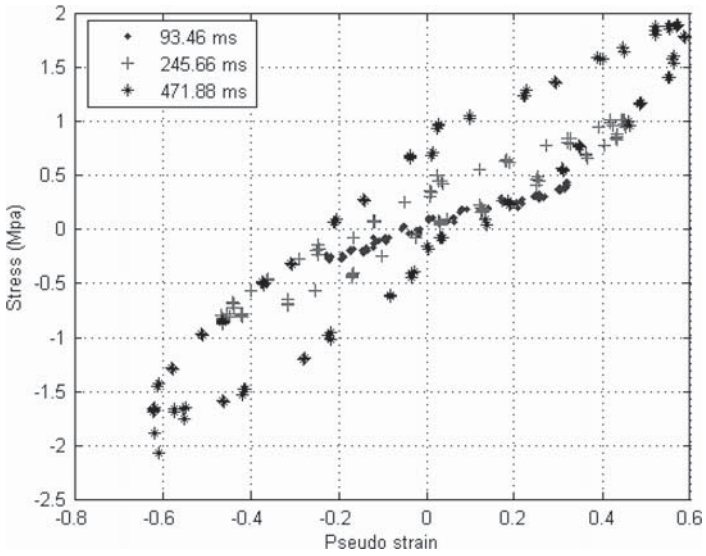

Figure 2. Cross plot of Stress vs. Pseudo strain.

where:

E_R = reference modulus (usually chosen as unity), MPa

$E(t)$ = relaxation modulus, MPa

ε = measured strain

11.3.2 Crossplot stress vs. pseudo strain and check for formation of hysteretic loop. This shall be started from lowest level of strain amplitude. Note down the strain level at which hysteresis loop appears for first time. Also calculate average value of strain level at which hysteresis loop forms. Typical plot comparing stress vs. pseudo strain before and after damage is presented in Figure 2.

Note 6 – The loop is observed in cross plot of stress vs. pseudo strain if the damage has occurred.

12. Report

12.1 For each specimen, report the following

12.1.1 Sample air voids

12.2 For each mix, report the following

12.2.1 Reference Temperature

12.2.2 Dynamic modulus master curve coefficients

12.2.3 Strain level at which hysteresis loop appears for first time in cross plot of stress vs. pseudo strain

12.2.4 Average strain level for loop formation

13. Keywords

13.1 Fatigue, Viscoelastic Continuum damage, Endurance limit

APPENDIX C

Proposed Standard Practice for Extrapolating Long-Life Beam Fatigue Tests Using the Ratio of Dissipated Energy Change (RDEC)

AASHTO Designation: PP XX-XX

1. Scope

1.1 This practice describes methodology for extrapolating long-life Beam Fatigue Tests Using the RDEC

1.2 *This standard may involve hazardous materials, operations, and equipment. This standard does not purport to address all of the safety problems associated with its use. It is the responsibility of the user of this procedure to establish appropriate safety and health practices and to determine the applicability of regulatory limitations prior to its use.*

---

2. Referenced Documents

2.1 *AASHTO Standards*

- T 321, Determining the Fatigue Life of Compacted Hot-Mix Asphalt (HMA) Subjected to Repeated Flexural Bending.

2.2 *Other Publications*

- NCHRP 9-38, "Endurance Limit of Hot Mix Asphalt Mixtures to Prevent Fatigue Cracking in Flexible Pavements," Draft Final Report.

---

3. Terminology

3.1 *Normal strain levels* – strain levels where failure (50 percent of initial stiffness) occurs in less than 12 million cycles. For tests conducted at 20 °C, strain levels of 300 microstrain or greater generally meet this requirement.

3.2 *Low Strain levels* – strain levels where failure (50 percent of initial stiffness) does not occur by 12 million cycles. The failure point of low strain tests generally needs to be extrapolated by one of the methods described in this document.

---

4. Summary of Practice

4.1 This practice describes the analysis needed to extrapolate the failure point of long-life beam fatigue tests that are not tested to failure (50 percent reduction in initial stiffness).

5. Significance and Use

5.1 The extrapolation procedure can be used to estimate the failure point of fatigue tests which do not fail in a reasonable amount of loading cycles (<12,000,000).

6. Apparatus

6.1 *Specimen Fabrication Equipment* – Equipment for fabricating beam fatigue test specimens as described in AASHTO T 321, Determining the Fatigue Life of Compacted Hot-Mix Asphalt (HMA) Subjected to Repeated Flexural Bending.

6.2 *Beam Fatigue Test System* – Equipment for testing beam fatigue samples as described in AASHTO T 321, Determining the Fatigue Life of Compacted Hot-Mix Asphalt (HMA) Subjected to Repeated Flexural Bending.

6.3 *Analysis Software* – Data is collected during the test using a data acquisition system described in section 6.2. Data analysis can be conducted using a spreadsheet program or variety of statistical packages.

7. Hazards

7.1 This practice and associated standards involve handling of hot asphalt binder, aggregates and asphalt mixtures. It also includes the use of sawing and coring machinery and servo-hydraulic or pneumatic testing equipment. Use standard safety precautions, equipment, and clothing when handling hot materials and operating machinery.

8. Standardization

8.1 Items associated with this practice that require calibration are included in the documents referenced in Section 2. Refer to the pertinent section of the referenced documents for information concerning calibration.

9. Beam Fatigue Test Data

9.1 *Test Specimen Fabrication*

9.1.1 Prepare test specimens to the target air void content and aging condition in accordance with AASHTO T 321. The target air void content should be representative of that expected to be obtained in the field. A target air void content of 7 percent was used for mixes produced at optimum asphalt content in the NCHRP 9-38 research. A reduced air void content would be expected for optimum plus or so-called rich-bottom type mixes.

Note 1 – A reasonable air void tolerance for test specimen fabrication is ± 0.5 %.

9.2 *Testing Conditions*

9.2.1 Samples tested to a minimum of 10 million cycles, which have not reached 50 percent of initial stiffness, may be extrapolated to determine a failure point as described in the following section.

10. Data Analysis to Extrapolate Long-life Fatigue Test Using RDEC

Beam fatigue tests conducted at low strain levels are unlikely to fail in a reasonable number of cycles.

10.1 *Ratio of Dissipated Energy Change (RDEC)*

10.1.1 PV calculation for normal strain testing

10.1.1.1 Determine the number of loading cycles, N_f, to failure from testing.

10.1.1.2 Obtain a dissipated energy (kPa) vs. loading cycle (DE-LC) relationship. Obtain a best fit equation for the DE-LC data, using a power law relationship. From the best fit equation, record the slope, f, of the curve, that can best represent the original curve. Figure 1 illustrates a DE-LC fitted curve.

10.1.1.3 Calculate RDEC. By definition, RDEC is the ratio of dissipated energy change between two loading cycles by the number between the cycles, that is, the average ratio of dissipated energy change per loading cycles, as seen in Equation 1.

$$\mathrm{RDEC}_a = \frac{\mathrm{DE}_a - \mathrm{DE}_b}{\mathrm{DE}_a * (b - a)} \tag{1}$$

where,

RDEC_a = the average ratio of dissipated energy change at cycle a, comparing to next cycle b;

a, b = load cycle a and b, respectively. The typical cycle count between cycle a and b for RDEC calculation is 100, i.e., $b - a = 100$;

DE_a, DE_b = the dissipated energy (kPa) produced in load cycle a, and b, respectively.

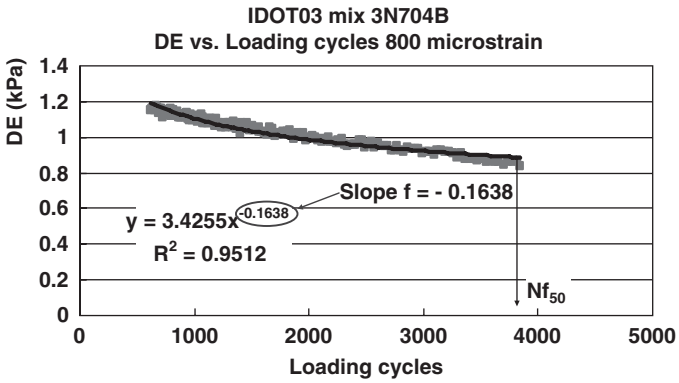

Figure 1. DE vs. LC chart with fitted curve.

10.1.1.4 The average RDEC for an arbitrary 100 cycles at cycle 'a' can be simply calculated using Equation 2.

$$\mathrm{RDEC}_a = \frac{1-\left(1+\frac{100}{a}\right)^f}{100} \tag{2}$$

where,
f = the slope from the regressed DE-LC curve

10.1.1.5 Calculate the plateau value (PV). The PV is defined as the RDEC value at the number of cycles equal to the failure point (Nf_{50}). Failure is defined as a 50 percent reduction in initial stiffness, with the initial stiffness being determined at the 50th loading cycle. The PV is determined using Equation 3.

$$\mathrm{PV} = \frac{1-\left(1+\frac{100}{Nf_{50}}\right)^f}{100} \tag{3}$$

where,
f = the slope from the regressed DE-LC curve (kPa/cycle)
Nf_{50} = 50% stiffness reduction failure point

10.1.2 PV calculation for low strain testing

10.1.2.1 Plot the DE-LC data and fit the DE-LC curve using the power law relationship. Obtain the f factor of the curve.

10.1.2.2 To achieve the best curve fit, it is recommended to eliminate the initial segment of the DE-LC curve, but use the later part to ensure the fitted curve visually best represents the curve's outspread trend. The fitted segment should not be less than ¼ of the total testing length to avoid being misleading.

10.1.2.3 Calculate RDEC at each loading cycle using Equation 2, where f is given by the fitted DE-LC curve. Plot the RDEC-LC curve (log-log).

10.1.2.4 Plot the unique PV-N_f curve as shown by Equation 4 on the same chart

$$\mathrm{PV} = 0.4428 Nf_{50}^{-1.1102} \tag{4}$$

10.1.2.5 Extend the RDEC-LC curve until it crosses the unique PV-Nf curve. The intersection point of these two curves produces: $y = \mathrm{PV}$, $x = Nf_{50}$

10.1.2.6 For $|f| < 0.25$ (which is the case for most fitted DE-LC curves from fatigue testing), calculate PV and Nf_{50} using equations 5 and 6, respectively.

Note: Figure 2 illustrates the fatigue life prediction using the RDEC approach at low strain testing.

$$\mathrm{PV} = \frac{1-\left(1+\frac{100}{Nf_{50}}\right)^f}{100} \approx -\frac{f}{Nf_{50}} \tag{5}$$

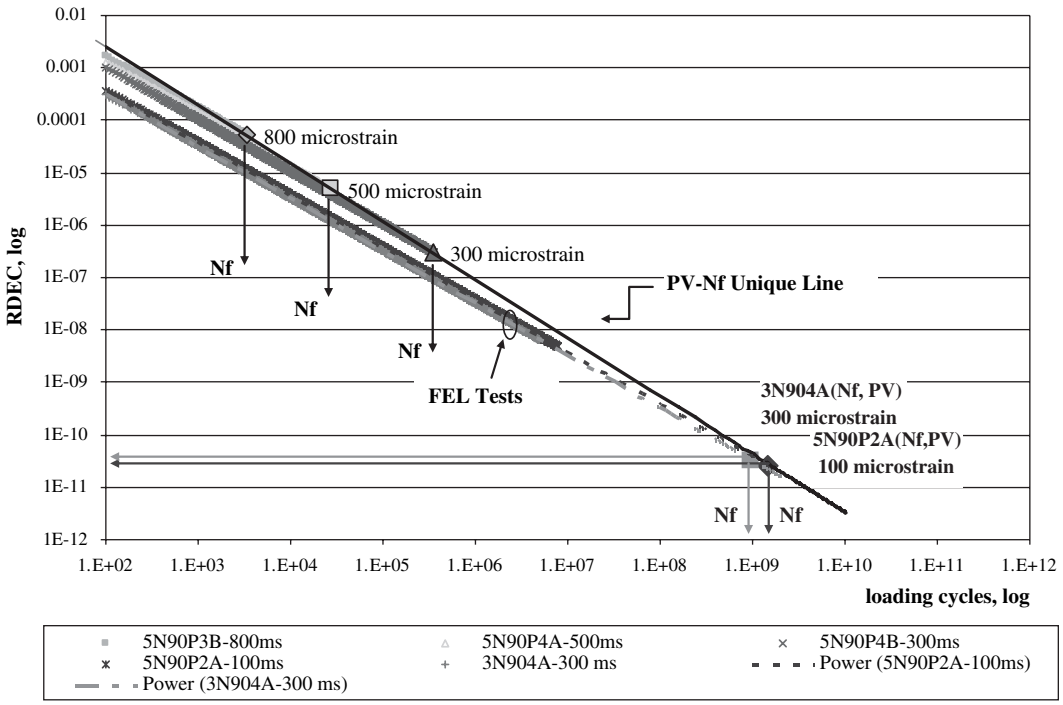

Figure 2. Fatigue life prediction using RDEC approach.

$$Nf_{50} = \left(\frac{-f}{0.4428} \right)^{-9.0744} \tag{6}$$

11. Report

11.1 For each sample, report the following:

11.1.1 Sample air voids

11.1.2 Test Temperature

11.1.3 Initial flexural stiffness (measured at 50 cycles)

11.1.4 Method of Extrapolation

11.1.5.1 Equation used for extrapolation and R^2 value for equation

11.1.5.2 Extrapolated fatigue life *Nf* for 50 percent of initial stiffness

12. Keywords

12.1 Beam fatigue, long-life

13. References

13.1 Shen, S. and S. H. Carpenter. "Application of Dissipated Energy Concept in Fatigue Endurance Limit Testing" In Transportation Research Record 1929, Transportation Research Board, Washington, DC, 2005, Pp 165-173.

APPENDIX D

NCHRP 9-38 Beam Fatigue

Fatigue Life

LAB	MATERIAL A (PG 67-22 Opt. 800 ms)							
	1	2	3	Avg.	Std. Dev.	Variance	h	k
1	3.13	3.66	3.72	3.50	0.324	0.105	-1.69	1.30
2	3.82	3.68	3.97	3.82	0.146	0.021	-0.25	0.58
3	3.89	3.99	3.42	3.77	0.305	0.093	-0.50	1.22
4	4.26	3.93	4.26	4.15	0.191	0.037	1.24	0.77
5	4.09	3.95	4.06	4.03	0.073	0.005	0.72	0.29
6	3.78	3.85	3.78	3.80	0.043	0.002	-0.33	0.17
7	4.39	4.18	3.59	4.06	0.415	0.172	0.82	1.66

Average of all Labs	3.876		
Std. Dev. Between Cell Averages (S_x)	0.220		
Repeatability Standard Deviation (S_r)	0.249		
Reproducibility Standard Deviation (S_R)	0.300		
Between Lab Standard Deviation of Lab Means(S_L)	0.167		
Pooled within lab variance (S_A^2)	0.062	(Components of variance)	W/L
Between Lab Variance of Lab Means(S_L^2)	0.028	(Components of variance)	B/L
W/L Variance	0.062		
B/L Variance	0.090		
h critical = 2.05	k critical = 2.03		

LAB	MATERIAL B (PG 67-22 Opt. 400 ms)							
	1	2	3	Avg.	Std. Dev.	Variance	h	k
1	5.49	5.60	5.43	5.51	0.087	0.008	0.38	0.36
2	4.68	4.94	5.06	4.89	0.196	0.038	-1.30	0.81
3	5.50	5.64	5.58	5.58	0.070	0.005	0.56	0.29
4	5.99	5.76	6.10	5.95	0.174	0.030	1.60	0.72
5	5.35	4.59	4.95	4.97	0.381	0.145	-1.11	1.59
6	5.39	5.43	5.38	5.40	0.023	0.001	0.09	0.10
7	5.57	4.81	5.49	5.29	0.421	0.177	-0.22	1.75

Average of all Labs	5.370		
Std. Dev. Between Cell Averages (S_x)	0.365		
Repeatability Standard Deviation (S_r)	0.240		
Reproducibility Standard Deviation (S_R)	0.414		
Between Lab Standard Deviation of Lab Means(S_L)	0.338		
Pooled within lab variance (S_A^2)	0.058		
Between Lab Variance of Lab Means(S_L^2)	0.114		
W/L Variance	0.058		
B/L Variance	0.172		
h critical = 2.05	k critical = 2.03		

LAB	MATERIAL C (PG 67-22 120 ms Logarithmic)							
	1	2	3	Avg.	Std. Dev.	Variance	h	k
1	9.92	7.60	7.24	8.25	1.453	2.110	-1.44	1.10
2	21.92	10.55	21.62				1.64	2.07
3	10.13	10.80	11.63	10.85	0.751	0.564	0.15	0.57
4	12.88	10.90	12.25	12.01	1.012	1.024	0.86	0.77
5	9.52	13.15	11.29	11.32	1.814	3.290	0.43	1.37

Average of all Labs		10.609
Std. Dev. Between Cell Averages (S_x)		1.642
Repeatability Standard Deviation (S_r)		1.322
Reproducibility Standard Deviation (S_R)		1.965
Between Lab Standard Deviation of Lab Means(S_L)		1.454
Pooled within lab variance (S_A^2)		1.747
Between Lab Variance of Lab Means(S_L^2)		2.114
W/L Variance		1.747
B/L Variance		3.861
h critical =	1.74 k critical =	1.92

Lab 2's data excluded as outlier

LAB	MATERIAL C (PG 67-22 120 ms Weibull)							
	1	2	3	Avg.	Std. Dev.	Variance	h	k
1	8.04	7.68	7.34	7.69	0.350	0.123	-1.21	0.60
2	10.49	9.31	10.22	10.01	0.620	0.385	1.33	1.06
3	7.84	8.25	8.40	8.16	0.292	0.085	-0.69	0.50
4	9.36	8.63	9.91	9.30	0.640	0.409	0.55	1.09
5	7.83	9.26	9.33	8.81	0.844	0.713	0.02	1.44

Average of all Labs		8.794
Std. Dev. Between Cell Averages (S_x)		0.915
Repeatability Standard Deviation (S_r)		0.586
Reproducibility Standard Deviation (S_R)		1.032
Between Lab Standard Deviation of Lab Means(S_L)		0.850
Pooled within lab variance (S_A^2)		0.343
Between Lab Variance of Lab Means(S_L^2)		0.723
W/L Variance		0.343
B/L Variance		1.066
h critical =	1.74 k critical =	1.92

LAB	MATERIAL C (PG 67-22 120 ms RDEC)							
	1	2	3	Avg.	Std. Dev.	Variance	h	k
1	9.76	3.82	2.18	5.26	3.988	15.908	-1.47	1.70
2	13.73	9.81	13.43	12.32	2.177	4.740	0.60	0.93
3	11.57	13.29	12.85	12.57	0.892	0.795	0.67	0.38
4								
5	10.65	11.74	10.47	10.95	0.690	0.476	0.20	0.29

Average of all Labs	10.275	
Std. Dev. Between Cell Averages (S_x)	3.421	
Repeatability Standard Deviation (S_r)	2.341	
Reproducibility Standard Deviation (S_R)	3.919	
Between Lab Standard Deviation of Lab Means(S_L)	3.143	
Pooled within lab variance (S_A^2)	5.480	
Between Lab Variance of Lab Means(S_L^2)	9.875	
W/L Variance	5.480	
B/L Variance	15.355	
h critical = 1.49	k critical = 1.82	

RDEC could not be calculated with dissipated energy data provided by Lab 4

LAB	MATERIAL A (PG 76-22 800 ms)							
	1	2	3	Avg.	Std. Dev.	Variance	h	k
1	3.66	3.77	4.30	3.91	0.343	0.117	-0.17	1.31
2	4.30	3.87	4.04	4.07	0.218	0.048	1.07	0.84
3	3.87	3.60	3.98	3.82	0.197	0.039	-0.90	0.76

Average of all Labs	3.932	
Std. Dev. Between Cell Averages (S_x)	0.127	
Repeatability Standard Deviation (S_r)	0.261	
Reproducibility Standard Deviation (S_R)	0.261	
Between Lab Standard Deviation of Lab Means(S_L)	0.000	
Pooled within lab variance (S_A^2)	0.068	(Components of variance) W/L
Between Lab Variance of Lab Means(S_L^2)	0.000	(Components of variance) B/L
W/L Variance	0.068	
B/L Variance	0.068	
h critical = 1.15	k critical = 1.67	

LAB	MATERIAL B (PG 76-22 400 ms)							
	1	2	3	Avg.	Std. Dev.	Variance	h	k
1	5.88	5.50	5.85	5.74	0.207	0.043	0.40	0.70
2	5.57	4.91	5.37	5.28	0.336	0.113	-1.14	1.14
3	5.51	6.16	5.86	5.84	0.324	0.105	0.74	1.10

Average of all Labs	5.624	
Std. Dev. Between Cell Averages (S_x)	0.299	
Repeatability Standard Deviation (S_r)	0.295	
Reproducibility Standard Deviation (S_R)	0.384	
Between Lab Standard Deviation of Lab Means(S_L)	0.246	
Pooled within lab variance (S_A^2)	0.087	(Components of variance) W/L
Between Lab Variance of Lab Means(S_L^2)	0.060	(Components of variance) B/L
W/L Variance	0.087	
B/L Variance	0.147	
h critical = 1.15	k critical = 1.67	

LAB	MATERIAL C (PG 67-22 220 ms Logarithmic)							
	1	2	3	Avg.	Std. Dev.	Variance	h	k
1	7.64	9.29	9.00	8.64	0.883	0.779	0.98	0.73
2	9.39	7.06		8.22	1.644	2.702	0.03	1.36
3	6.67	8.23	8.38	7.76	0.944	0.891	-1.02	0.78

Average of all Labs	8.209	
Std. Dev. Between Cell Averages (S_x)	0.441	
Repeatability Standard Deviation (S_r)	1.207	
Reproducibility Standard Deviation (S_R)	1.207	
Between Lab Standard Deviation of Lab Means(S_L)	0.000	
Pooled within lab variance (S_A^2)	1.458	(Components of variance) W/L
Between Lab Variance of Lab Means(S_L^2)	0.000	(Components of variance) B/L
W/L Variance	1.458	
B/L Variance	1.458	
h critical = 1.15	k critical = 1.67	

LAB	MATERIAL C (PG 67-22 220 ms Weibull)							
	1	2	3	Avg.	Std. Dev.	Variance	h	k
1	7.42	7.49	7.45	7.45	0.034	0.001	-0.36	0.05
2	8.76	7.06		7.91	1.204	1.451	1.13	1.68
3	6.99	7.37	7.61	7.32	0.314	0.099	-0.77	0.44

Average of all Labs	7.563	
Std. Dev. Between Cell Averages (S_x)	0.309	
Repeatability Standard Deviation (S_r)	0.719	
Reproducibility Standard Deviation (S_R)	0.719	
Between Lab Standard Deviation of Lab Means(S_L)	0.000	
Pooled within lab variance (S_A^2)	0.517	(Components of variance) W/L
Between Lab Variance of Lab Means(S_L^2)	0.000	(Components of variance) B/L
W/L Variance	0.517	
B/L Variance	0.517	
h critical = 1.15	k critical = 1.67	

LAB	MATERIAL C (PG 67-22 220 ms RDEC)							
	1	2	3	Avg.	Std. Dev.	Variance	h	k
1	6.86	11.59	11.29	9.91	2.647	7.007	0.32	1.23
2	9.99	7.06		8.53	2.071	4.290	-1.12	0.96
3	8.54	11.47	11.14	10.39	1.606	2.578	0.80	0.75

Average of all Labs	9.607		
Std. Dev. Between Cell Averages (S_x)	0.967		
Repeatability Standard Deviation (S_r)	2.151		
Reproducibility Standard Deviation (S_R)	2.151		
Between Lab Standard Deviation of Lab Means(S_L)	0.000		
Pooled within lab variance (S_A^2)	4.625	(Components of variance)	W/L
Between Lab Variance of Lab Means(S_L^2)	0.000	(Components of variance)	B/L
W/L Variance	4.625		
B/L Variance	4.625		
h critical = 1.15	k critical = 1.67		

LAB	MATERIAL A (PG 67-22 Opt.+ 800 ms)							
	1	2	3	Avg.	Std. Dev.	Variance	h	k
1	3.88	4.42	4.12	4.14	0.268	0.072	-0.57	1.30
2	4.31	4.55	4.12	4.33	0.216	0.047	1.15	1.05
3	4.16	4.04	4.23	4.14	0.097	0.009	-0.58	0.47

Average of all Labs	4.203		
Std. Dev. Between Cell Averages (S_x)	0.107		
Repeatability Standard Deviation (S_r)	0.207		
Reproducibility Standard Deviation (S_R)	0.207		
Between Lab Standard Deviation of Lab Means(S_L)	0.000		
Pooled within lab variance (S_A^2)	0.043	(Components of variance)	W/L
Between Lab Variance of Lab Means(S_L^2)	0.000	(Components of variance)	B/L
W/L Variance	0.043		
B/L Variance	0.043		
h critical = 1.15	k critical = 1.67		

LAB	MATERIAL B (PG 67-22 Opt.+ 400 ms)							
	1	2	3	Avg.	Std. Dev.	Variance	h	k
1	5.60	5.97	6.04	5.87	0.239	0.057	1.14	0.98
2	5.94	5.34	5.59	5.62	0.303	0.092	-0.72	1.25
3	5.75	5.47	5.77	5.66	0.167	0.028	-0.42	0.69

Average of all Labs	5.717		
Std. Dev. Between Cell Averages (S_x)	0.134		
Repeatability Standard Deviation (S_r)	0.243		
Reproducibility Standard Deviation (S_R)	0.243		
Between Lab Standard Deviation of Lab Means(S_L)	0.000		
Pooled within lab variance (S_A^2)	0.059		
Between Lab Variance of Lab Means(S_L^2)	0.000		
W/L Variance	0.059		
B/L Variance	0.059		
h critical = 1.15	k critical = 1.67		

APPENDIX E

Construction of Characteristic Curve

Determination of the Relaxation Modulus

Construction of the damage characteristic curve requires the calculation of pseudo strains, which in turn require the relaxation modulus, E(t), of the mixture. The relaxation modulus is difficult to measure directly in the laboratory and is therefore determined from the dynamic modulus master curve using linear viscoelastic theory. The relaxation modulus is expressed as the Prony series:

$$E(t) = E_\infty + \sum_n E_n \exp\left(-\frac{t}{\rho_n}\right) \tag{1}$$

Where E_∞ is the value of $E(t)$ as $t \to \infty$, E_n are Prony series coefficients and ρ_n are relaxation times. To obtain the Prony series expression of relaxation modulus from dynamic modulus, the first step is to determine the storage modulus master curve using:

$$E'(\omega_r) = |E^*(\omega_r)|\cos(\varphi(\omega_r)) \tag{2}$$

Where $|E'(\omega_r)|$ is the storage modulus, φ is the phase angle and ω_r is the reduced frequency in rad/sec. The relaxation modulus curve of each specimen is obtained from the storage modulus master curve by applying the following relation:

$$E(t_r) = \frac{1}{\lambda'} E'(\omega_r), \omega_r = \frac{0.08}{t_r}$$
$$\lambda' = \Gamma(1-n)\cos\left(\frac{n\pi}{2}\right) \tag{3}$$
$$n = \frac{d\log E'(\omega)}{d\log\omega}$$

Where t_r is the reduced time, Γ is the gamma function and n is the slope of $\log(E'(\omega))$ versus $\log(\omega)$ curve which is obtained at each point of reduced frequency.

Once the relaxation modulus is obtained from the storage modulus, the Prony series coefficients in Equation 1 are obtained through the following steps.

First, Equation 1 is rewritten in matrix form as:

$$\{A\} = [B]\{C\}$$
$$A_j = E(t_j) - E_\infty$$
$$B_{jk} = \exp\left(-\frac{t_j}{\rho_k}\right) \tag{4}$$
$$C_j = E_j$$
$$j = 1, 2, \ldots, N$$

Where the relaxation times t_j are chosen at decade intervals along time axis and N is the number of data points used. The MATLAB optimization toolbox is used to obtain the solution for E_j with the following constraint:

$$\min_C \frac{1}{2}\|[B]\{C\} - \{A\}\|_2^2, \text{such that, } \{C\} \geq 0 \tag{5}$$

which provides positive values of E_j. The prony series representations of the relaxation modulus for the four mixtures are shown in Figure E1.

Monotonic Characteristic Curves

Pseudo Strain Calculation

Monotonic tests (constant crosshead) at 20°C are performed on specimens at various crosshead strain rates. The pseudo strains are calculated using the strains measured from the on-specimen LVDTs. Figure E2 shows the typical stress, crosshead strain, and LVDT strain as a function of time for a monotonic test.

The pseudo strain is defined as:

$$\varepsilon_R(t) = \frac{1}{E_R}\int_0^t E(t-\tau)\frac{d\varepsilon}{d\tau}d\tau \tag{6}$$

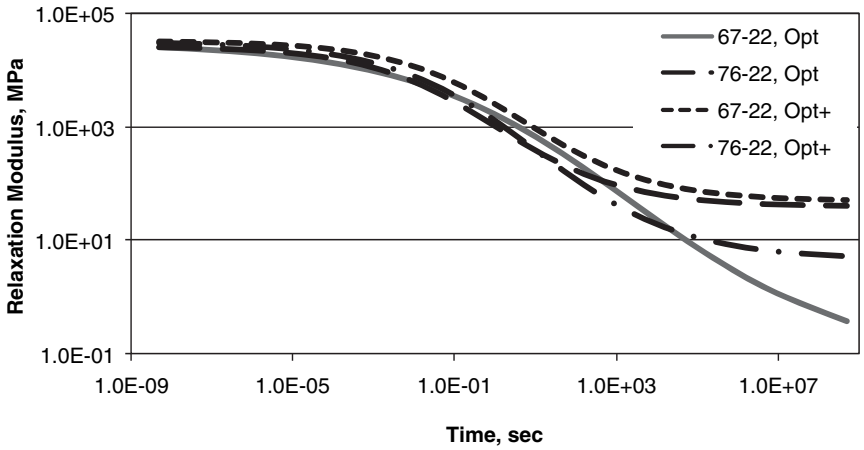

Figure E1. Relaxation modulus curves for all four mixtures.

where E_R is the reference modulus (which is chosen as unity), $E(t)$ is the relaxation modulus obtained from storage modulus and expressed as Prony series and ε is the on-specimen LVDT strain observed under monotonic tests. The above integration is evaluated numerically over the strain range up to the time of failure. The strain history is discritized into N number of small segments with time increment Δt and Equation 1 is substituted in Equation 6, resulting in the following form of numerical integration scheme:

$$\varepsilon_R(t) = \sum_{j=1}^{N+1} c_i E(u)\Big|_{t-t_j}^{t-t_{j-1}}, t_0 = 0, t_{N+1} = t$$
$$E(u) = E_\infty u - \sum_j E_j \rho_j \exp\left(-\frac{u}{\rho_j}\right) \quad (7)$$

Calculation of Pseudo Stiffness (C) and Damage Parameter (S)

The pseudo stiffness, C, is defined as:

$$C1(t) = \frac{\sigma(t)}{\varepsilon_R(t)} \quad (8)$$

where $\sigma(t)$ is the stress history. The damage parameter, S, is obtained from the following equation:

$$S1(t) = \sum_j \left(\frac{1}{2}(\varepsilon_{R,j})^2 (C_{j-1} - C_j)\right)^{\frac{\alpha}{1+\alpha}} (t_j - t_{j-1})^{\frac{1}{1+\alpha}} \quad (9)$$

where I is the initial pseudo stiffness and $\alpha = 1 + \frac{1}{m}$, where m is the slope of the linear portion of the relaxation curve. The damage characteristic curve is obtained by plotting the damage parameter versus the pseudo stiffness.

Fatigue Characteristic Curves

The following steps are used to construct the characteristic curve for the fatigue tests.

Step 1: Calculate Average Strain

The strain history is decomposed into the mean strain and cyclic strain components for analysis. The average strain is calculated for each cycle from each LVDT. The individual

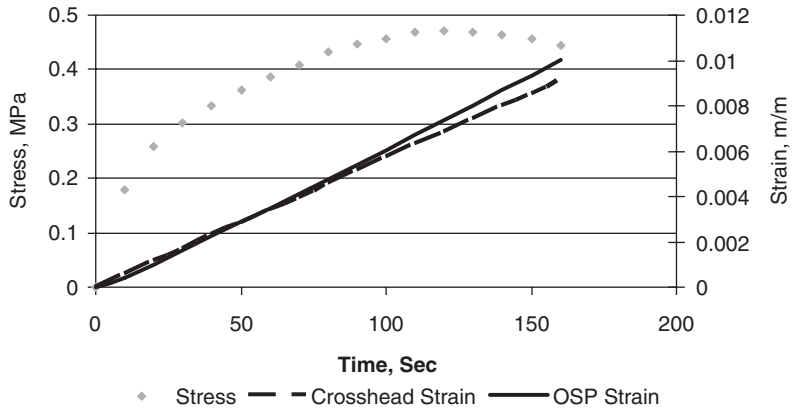

Figure E2. Stress and strain histories for a typical monotonic test.

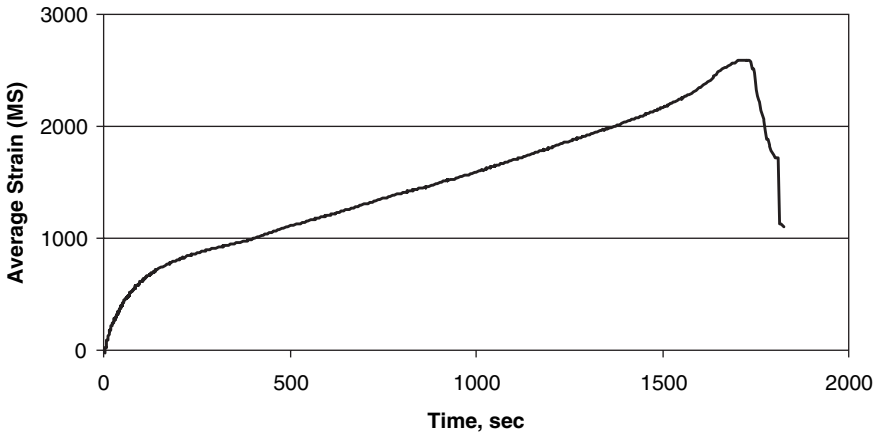

Figure E3. Mean strain for a PG 67-22 at optimum specimen.

strains recorded by different LVDTs are then averaged to determine the mean strain history for the specimen. Figure E3 shows the mean strain during a constant amplitude fatigue test for a PG 67-22 optimum specimen.

Step 2: Calculate Initial Pseudo Stiffness

Initial pseudo strain is needed to determine the initial pseudo stiffness, which is used to calculate the normalized pseudo stiffness for the entire fatigue test. Strains captured during the first loading cycle are used to calculate the initial pseudo strains in that cycle using Equation 6. The initial pseudo stiffness is calculated as the slope of the initial linear portion of the stress-vs-pseudo strain plot. Figure E4 demonstrates the calculation of the initial pseudo stiffness for a particular specimen.

Step 3: Calculate Mean Pseudo Strain

The mean strains determined in Step 1 are used to calculate the corresponding pseudo strains using the methodology described for the monotonic tests.

Step 4: Calculate Cyclic Pseudo Strain

The cyclic strain is determined by subtracting the mean strain from total strain. The cyclic strain is then fit using the following equation:

$$\varepsilon_{cy}(t) = p + q\cos(\omega t + \varphi) \tag{10}$$

where, p, q, ω and φ are regression constants. The cyclic pseudo strains are calculated using:

$$\varepsilon_{cy}^{R}(t) = q|E^*|\cos(\omega t + \varphi) \tag{11}$$

where, $|E^*|$ is the dynamic modulus of the mix at test temperature and frequency.

Step 5: Calculate Maximum Pseudo Strain in Each Cycle

The maximum pseudo strains for each cycle after the first cycle are calculated by adding the maximum cyclic pseudo strain in each cycle to the corresponding mean pseudo

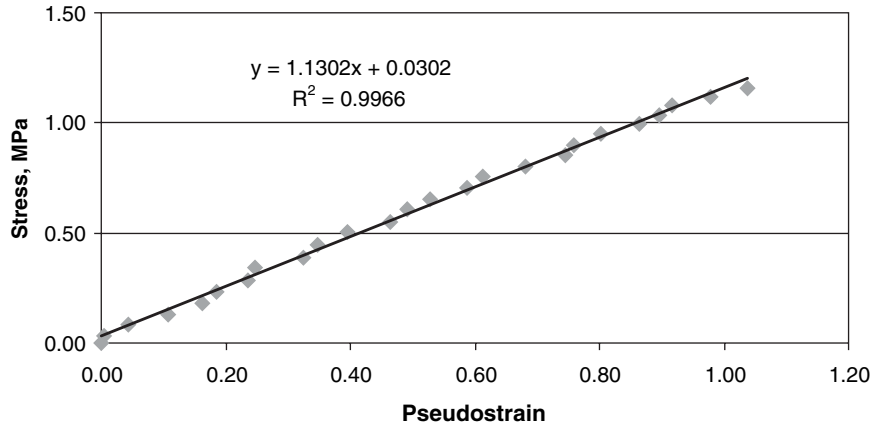

Figure E4. Determination of initial pseudo stiffness.

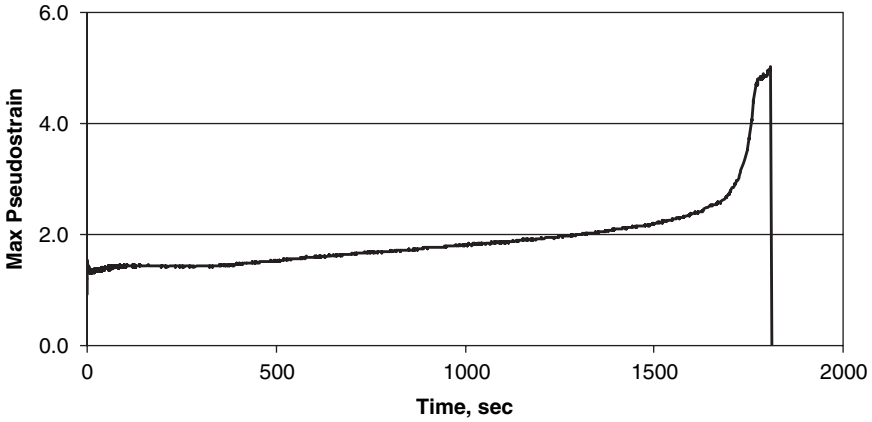

Figure E5. Typical plot of maximum pseudo strain versus time.

strain value. Figure E5 shows the variation of the maximum pseudo strain over the course of a typical constant amplitude fatigue test.

Step 6: Calculate Pseudo Stiffness

The pseudo stiffness is defined as:

$$S^R = \frac{\sigma}{\varepsilon^R} \tag{12}$$

For the first cycle, pseudo stiffness is calculated at each point along the loading path. The secant pseudo stiffness is calculated for subsequent cycles to represent the change in slope of the stress- pseudo strain loops:

$$S^R = \frac{\sigma_{max}}{\varepsilon^R_{max}} \tag{13}$$

where ε^R_{max} is the maximum pseudo strain in a cycle and σ_{max} is the stress corresponding to ε^R_{max}.

Step 7: Calculate Normalized Pseudo Stiffness

The normalized pseudo stiffness, *C,* is calculated as:

$$C = \frac{S^R}{I} \tag{14}$$

where, I is the initial pseudo stiffness, calculated in Step 2.

Step 8: Calculate Damage Parameter

The damage parameter, *S,* is calculated by using the following equations:

$$S(t) = \sum_{i=1}^{N}\left[\frac{1}{2} I\left(\varepsilon^R\right)^2\left(C_{i-1} - C_i\right)\right]^{\frac{\alpha}{1+\alpha}}\left(t_i - t_{i-1}\right)^{\frac{1}{1+\alpha}} \tag{15a}$$

$$S(t) = \sum_{i=1}^{N}\left[\frac{1}{2} I\left(\varepsilon^R_{max}\right)^2\left(C_{i-1} - C_i\right)\right]^{\frac{\alpha}{1+\alpha}}\left(\frac{t_i - t_{i-1}}{x}\right)^{\frac{1}{1+\alpha}} \tag{15b}$$

Equation 15*a* is used to calculate *S* during first loading cycle and Equation 15*b* is used during the rest of the loading cycles until failure. The parameter *x* is the fraction of the total stress-vs-strain cycle during which damage can grow. This is that portion of the loading curve where tensile stress occurs. To determine *x,* plots of the stress-vs-strain curves are examined. From Figures E6 and E7, it can be seen that an appropriate value for *x* is 4.0 (tensile stress on the loading portion of the curve is approximately ¼ of the whole loop).

Step 9: C-vs-S Characteristic Curve

The characteristic curve is constructed by cross-plotting C and S. An example is shown in Figure E8.

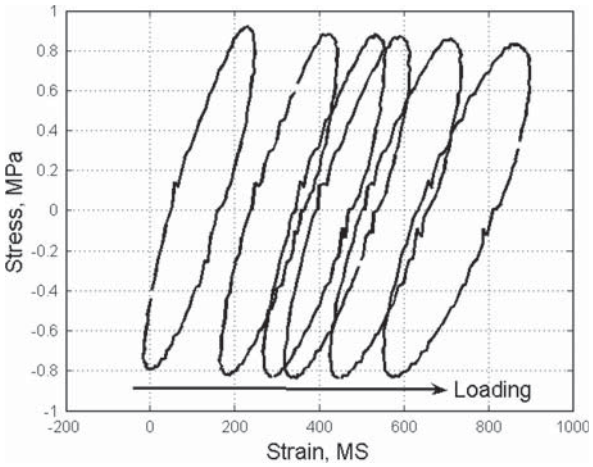

Figure E6. Stress-vs-strain plots for specimen No. 14.

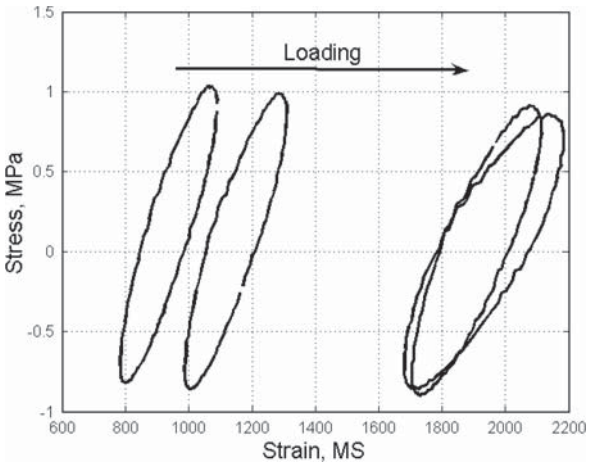

Figure E7. Stress-vs-strain plots for specimen no. 15.

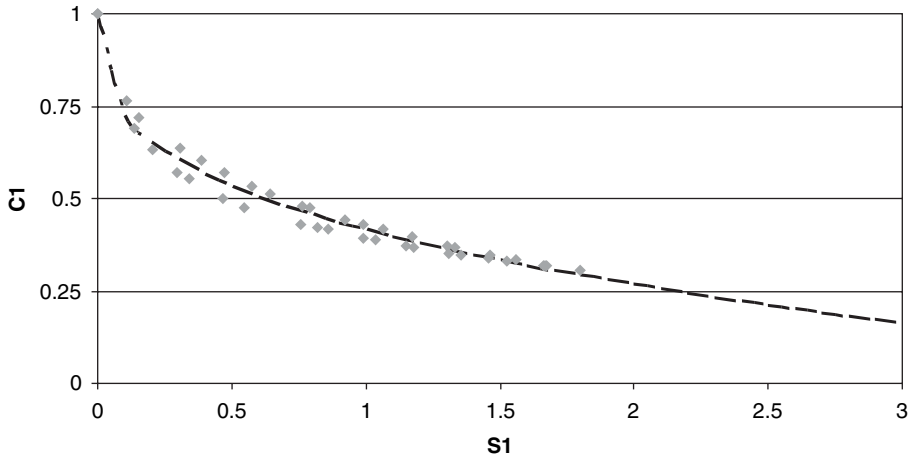

Figure E8. Example characteristic curve.

APPENDIX F

NCHRP 9-38 Beam Fatigue Round Robin

The beam fatigue testing conducted to date indicates that there is an endurance limit for hot mix asphalt (HMA). Techniques have been developed to identify the endurance limit using beam fatigue testing. One concern is that there is no precision statement for AASHTO T321, the beam fatigue test. A full round robin is beyond the scope of this study. However, a mini-round robin should provide an indication of the variability of beam fatigue testing and of the determination of the endurance limit. The round robin will encompass: sample preparation, beam fatigue testing, calculations to assess the endurance limit. Three techniques will be used to analyze the beam fatigue results: single-stage Weibull function, logarithmic extrapolation, and ratio of dissipated energy. The following describes the sample preparation and testing. A second document will be sent at a later date, which will describe the data analysis.

The mixes included in the study and the labs testing each mix are shown in Table 1. The mixes are the same mixes used previously in the NCHRP 9-38 study and are based on the lower layers of the structural sections of the 2003 NCAT Test Track.

Optimum asphalt content for both mixes is 4.5 percent by total weight of mix. The optimum plus asphalt content is 5.2 percent by total weight of mix.

Directions for Preparation of Samples

1. Each aggregate "batch" of material consists of two parts "A" and "B." The aggregate batches were randomized before shipping to the individual labs. To make one complete batch, an "A" and "B" can should be dry mixed. The combined aggregate weight should be 8,776 grams.
2. Therefore, 413.5 grams of binder should be mixed with one batch for the optimum asphalt content samples and 481.4 grams of asphalt for the optimum plus samples. The mixing temperatures are: 350°F for the PG 64-22 and 350°F for the PG 76-22.
3. After mixing, the batch should be split to the size required for your compaction device. We use the following formula for estimating the target sample weight for compaction:

$$\text{Target Weight} = (\text{Target Density} - \text{Correction Factor}) \div 100 \times G_{mm} \times \text{Compacted Sample Volume}$$

where,

Target Density = 93%,

Correction Factor = 2.5 accounts for surface voids and the fact that the center of a compacted sample tends to be denser,

G_{mm} = 2.586,

Compacted Sample Volume = length x width x height in cm^3 = (for us) 7.78 × 39.8 × 11.25 = 3483 cm^3.

Please contact us if we did not supply a large enough sample for your mold. If the initial sample does not produce 7 ± 0.5 percent air voids, this number may need to be adjusted. **The target density for the optimum plus mix is 96.7 percent.**

4. The mix should then be aged for four hours at 275°F (135 °C) according to AASHTO R30.
5. The sample should then be compacted using your in-house procedure. Vary the compaction effort to achieve the predetermined volume. Normally this means compacting to a specified height.
6. After the sample has cooled, it is a good idea to bulk the sample according to AASHTO T166 before sawing the sample to the test dimensions. This will be used, if necessary, to adjust the mass of future samples to achieve the correct air voids.
7. Use a wet saw to cut the compacted beam to 380 ± 6 mm in length, 63 ± 6 mm in width, and 50 ± 6 mm in height.
8. Determine the mass under water and SSD mass according to AASHTO T166. Dry the sample in front of a fan to

Table 1. Testing matrix.

Lab/Mix	PG 64-22 at Optimum	PG 64-22 at Optimum Plus	PG 76-22 at Optimum
NCAT	X	X	X
Asphalt Institute	X	X	X
University of Illinois	X	X	X
VA Transportation Research Council	X		
SEM Materials	X		
University of California	X		

a constant mass to determine the dry mass. Calculate the sample density and air voids using a $G_{mm} = 2.586$. If the air voids for the optimum asphalt content samples are not 7 ± 0.5 percent or the air voids of the optimum plus samples are not 3.3 ± 0.5 percent, the sample density is not in tolerance and a new sample must be made. Evaluate whether the sample mass should be adjusted. We normally adjusted by multiplying the dry mass in step 6 by the desired density divided by the measured density.

9. Is the sample is not going to be tested within 5 days, wrap the sample in plastic wrap and store it in a freezer.
10. Condition the sample to 20.0 ± 0.5°C for two hours. Samples that have been frozen should be allowed to thaw at room temperature for 16 hours prior to conditioning.
11. Test the sample according to AASHTO T321
    a. Test three samples at 800 micro-strain
    b. Test three samples at 400 micro-strain
12. Plot the results on a log-log graph and fit a regression line. This would be a power model in excel (Figure 1).

    You can then solve: $Y = 2E + 19(x)^{-5.3087}$ for 50,000,000 cycles.

    Recall that $x^{-5.3087}=1/x^{5.3087}$, then $x = \sqrt[5.3087]{\frac{2E+19}{50{,}000{,}000}}$ = 153 *micro-strain*

    You can also avoid the algebra and solve this using a least-squares procedure and solver in Excel.

13. Test three beams at the strain value predicted to give 50,000,000 cycles, in this example 153 micro-strain. Tentatively, we would like all of the labs to use the same strain level. Once you determine the strain level for 50,000,000 cycles in Step 12, please contact Brian Prowell. These sets of beams should be tested to a maximum of 12 million cycles. Later instruction will describe the procedure to extrapolate the data and confirm the identification of the endurance limit.

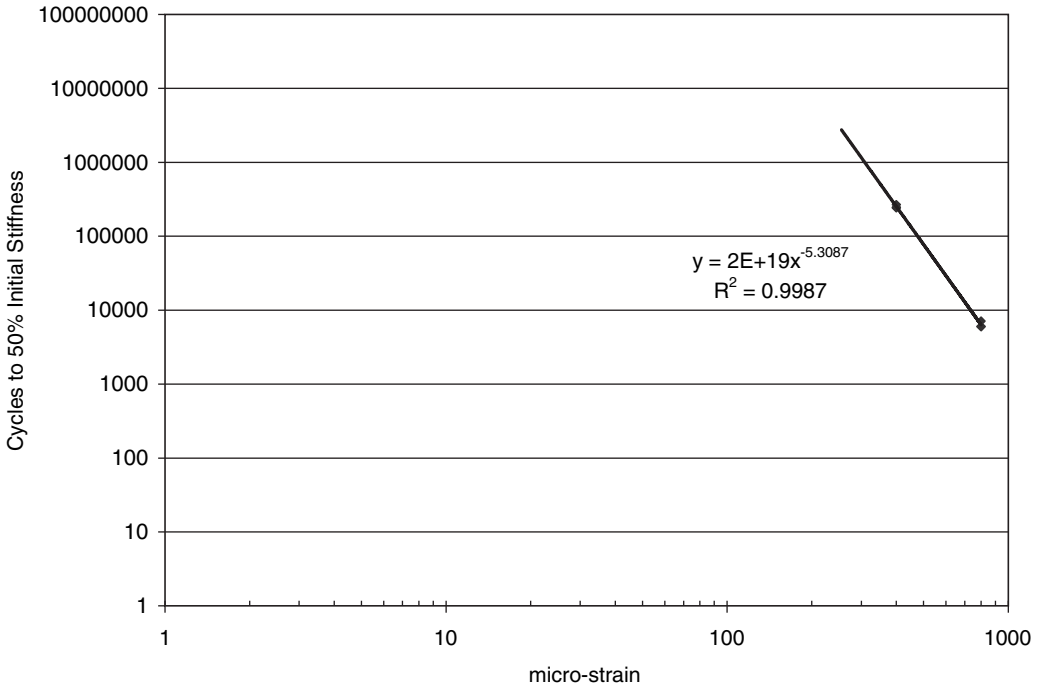

Figure 1. Log-log plot of strain versus cycles to failure.

Abbreviations and acronyms used without definitions in TRB publications:

AAAE	American Association of Airport Executives
AASHO	American Association of State Highway Officials
AASHTO	American Association of State Highway and Transportation Officials
ACI–NA	Airports Council International–North America
ACRP	Airport Cooperative Research Program
ADA	Americans with Disabilities Act
APTA	American Public Transportation Association
ASCE	American Society of Civil Engineers
ASME	American Society of Mechanical Engineers
ASTM	American Society for Testing and Materials
ATA	Air Transport Association
ATA	American Trucking Associations
CTAA	Community Transportation Association of America
CTBSSP	Commercial Truck and Bus Safety Synthesis Program
DHS	Department of Homeland Security
DOE	Department of Energy
EPA	Environmental Protection Agency
FAA	Federal Aviation Administration
FHWA	Federal Highway Administration
FMCSA	Federal Motor Carrier Safety Administration
FRA	Federal Railroad Administration
FTA	Federal Transit Administration
HMCRP	Hazardous Materials Cooperative Research Program
IEEE	Institute of Electrical and Electronics Engineers
ISTEA	Intermodal Surface Transportation Efficiency Act of 1991
ITE	Institute of Transportation Engineers
NASA	National Aeronautics and Space Administration
NASAO	National Association of State Aviation Officials
NCFRP	National Cooperative Freight Research Program
NCHRP	National Cooperative Highway Research Program
NHTSA	National Highway Traffic Safety Administration
NTSB	National Transportation Safety Board
PHMSA	Pipeline and Hazardous Materials Safety Administration
RITA	Research and Innovative Technology Administration
SAE	Society of Automotive Engineers
SAFETEA-LU	Safe, Accountable, Flexible, Efficient Transportation Equity Act: A Legacy for Users (2005)
TCRP	Transit Cooperative Research Program
TEA-21	Transportation Equity Act for the 21st Century (1998)
TRB	Transportation Research Board
TSA	Transportation Security Administration
U.S.DOT	United States Department of Transportation